DISCOVERING GENES RESPONSIBLE FOR KIDNEY DISEASES

by

Joseph Ly

A thesis submitted in conformity with the requirements

for the degree of Doctor of Philosophy

Department of Medicine

University of Toronto

Discovering genes responsible for kidney diseases.

Doctor of Philosophy, 2013

Joseph Ly, Department of Medicine, University of Toronto.

Abstract:

With the completion of the human genome project, researchers are now poised to discover new functions of the numerous genes identified. This is particularly important to our understanding of their role in maintaining normal physiology and in disease states, thereby guiding the discovery of novel therapeutic targets.

Method: In collaboration with the Center for Modeling Human Disease, forward genetics using *N-ethyl-N-nitrosourea* mutagenesis was undertaken. A mutant with renal glucosuria and cystic kidneys was found on a dominant screen and further characterized. Genome-wide association was performed using a which was followed by whole-exome next-generation re-sequencing, for identification of causative mutation(s).

Results I: A novel nonsense mutation in the *Slc5a2* gene, leading to the loss of normal functioning Sglt2 proteins, the major sodium glucose co-

transporter in the renal tubules, is causative to the renal glucosuria observed. Homozygous mutants with induced diabetes exhibit better overall glycemic control, but have an exaggerated mortality rate (70% in homozygous mutants versus 10% in wild-type controls at 20 weeks of diabetes).

Results II: We have identified a point mutation in *Samd9l* that causes cystic kidney phenotype. Homozygous mutants do not survive beyond P0. Glomerulocysts are present in most of the P0 homozygous mutants. They also manifest “kinked” tail and disoriented inner ear hair cells, phenotypes suggestive of planar cell polarity defects. Immunoprecipitation reveals potential interaction with E3 ubiquitin ligase Stub1, whose substrate is P53. Surprisingly, we observe lower protein levels of P53 and its downstream effector P21 in whole kidney lysates from homozygous mutants compared to their wild-type littermates.

Summary: Taken together, two new mouse models of kidney diseases are generated by ENU mutagenesis. The first mouse model has deficient sglt2 expression. The second mouse model of cystic kidney phenotype suggests the involvement of ubiquitination of cell cycle proteins in the pathogenesis of cystic kidney diseases, a novel pathway in cystogenesis.

Acknowledgements

I would like to extend my sincere gratitude to my supervisor and my mentor, Dr. Susan Quaggin, who has taken tremendous interest in my career development. From her, I learned that research calls for patience, diligence, accuracy, constantly considering potential pitfalls, well planning and organization, precision, and a positive attitude in times of difficulty. To a certain extent, research does reflect the ups and downs of life and I view it as a life lesson where I have the opportunity to learn science and learn to be a productive and tenacious member of the society. I would also like to thank my committee members, Dr. Lucy Osborne and Dr. York Pei, who not only are extremely generous with their time, they have also been an incredible resource. I am indebted for their generosity and selflessness. In addition, I am fortunate to be working in a lab full of gracious individuals who are more than willing to help and share their expertise including Jin Li, Vera Eremina, Marina Lunyova, Yoshiro Maezawa, Tuncer Onay, Stephan Heinen, Ben Thomson, Davide Cina, Karen Sison, and Marie Jeansson. I would also like to acknowledgement the help of my supervisor's collaborators including Dr. Bonventre, Dr. Schnermann, Dr. Harrison; the Samuel Lunenfeld Research Institute; the Nagy Lab; the Pawson Lab, especially Dr. Jin and Dr. Scott; the Drucker Lab; the Pelletier Lab; and the McNeil Lab. I am also indebted to Dragana, Sue's administrative assistant, who has made it possible for numerous seemingly impossible administrative tasks. I am very grateful for IMS, UT Clinician Investigator Program, and the University of Toronto in providing such an unparalleled educative experience. I wish to thank the Krescent Program, CIHR, and TD for their generous financial support. I also wish to thank the SMH division of Nephrology for their endless moral support and mentoring beyond my post-graduate clinical training. I am thankful for my wonderful examiners Dr. McNeil, Dr. Rogers, and Dr. Coffman for their time and interest in my project. Finally, my heartfelt gratitude to my family and friends, who not only have tremendous patience on me, but also encourage me, love me and see me through

the completion of this chapter of my life. I thank God for loving me and giving me opportunities to learn, enrich and enjoy my life.

Table of Contents

List of Tables

Chapter 1

Chapter 3

Chapter 4

Supplementary

List of Figures

Chapter 1

Chapter 3

Chapter 4

Supplementary

List of Abbreviations

ACCORD	Action to Control Cardiovascular Risk in Diabetes
ADPKD	Autosomal dominant polycystic kidney disease
ADVANCE	Action in Diabetes and Vascular Disease
AFLP	Amplified fragment length polymorphism
Ahi1	Abelson helper integration site 1
Akt	Protein kinase B
AmiRNA	Artificial micro-RNA
ANOVA	Analysis of variance
APC	Adenomatous polyposis coli
APKC	Atypical protein kinase C
ARE	AU-rich element
ARPKD	Autosomal recessive polycystic kidney disease
B6	C57BL/6J
BBS	Bardet-Biedl syndrome
Bicc1/bpk	Bicaudal C homolog 1
Bp	Basepair
BSA	Bovine serum albumin
β-TrCP	transductin repeat-containing protein
C3H	C3H/HeJ
Cas	CRISPR-associated
CBC	Cilium basal body complex
CC	Collaborative cross
Ccnd1	Cyclin D1
Cd2ap	CD2-associated protein
Cdc42	Cell division cycle 42
CK1	Casein kinase 1
CLL	Chronic lymphocytic leukemia
CM	Centimorgan

CMHD	Center for Modeling Human Disease
CPEB1	CPE-binding protein
CRISPR	Clustered regularly interspaced short palindromic repeat
CrRNA	CRISPR-derived RNA
DAPI	4',6-diamidino-2-phenylindole
Daxx	Death domain-associated protein
Dgo	Diego
Dlg	Disc Large
dNTP	Deoxynucleotide triphosphate
Ds	Dachsous
DSB	Double strand break
Dsh	Dishevelled
EDTA	Ethylenediaminetetraacetic acid
EMMA	Efficient mixed-model association
EMT	Epithelial-mesencyhmal transition
ENU	N-ethyl-N-nitrosourea
ES	Embryonic stem
ESRD	End-stage renal disease
FACS	Fluorescence activated cell sorting
Fat4	FAT tumor suppressor homolog 4
FITC	Fluorescein isothiocyanate
Fmi	Flamingo
Fy	Fuzzy
Fz	Frizzled
Gadd45a	Growth arrest and DNA-damage-inducible 45 alpha
GCKD	Glomerulocystic kidney disease
GFP	Green fluorescent protein
GFR	Glomerular filtration rate
GIP	Glucose-dependant insulinotropic polypeptide
Gli1/2/3	GLI-Kruppel family member 1/2/3

GLP-1	Glucagon-like peptide-1
Glis2/3	GLIS family zinc finger-2/3
Glut	Glucose transporter
GOF	Gain-of-function
GSK3β	Glycogen synthase kinase-3β
GWAS	Genome-wide association studies
H&E	Hematoxylin and eosin
HDL	High-density lipoprotein
HEK	Human embryonic kidney
Het	Heterozygous
HgbA1c	hemoglobin A1C
HIVAN	HIV associated nephropathy
HMDP	Hybrid Mouse Diversity Panel
HNF1α	HNF1 homeobox A
HNF1β	Hepatocyte Nuclear Factor 1β
Hprt	Hypoxanthine guanine phosphoribosyl transferase
Ift88	Intraflagellar transport 88
In	Inturned
Indel	Insertion/deletion
INF-γ	Interferon gamma
Inpp5e	Inositol polyphosphate-5-phsophatase E
IP	Intraperitoneal
IRF-1	Interferon-regulatory-factor-1
Jade-1	PHD finger protein 17
Jak2	Janus kinase 2
Jcpk	Juvenille congenital polycystic kidney disease
Jnk	C-Jun N-terminal kinase
Kap3	Kinesin-associated protein 3
Kif3a	Kinesin family member 3a
KIM1	Kidney injury molecule 1

KO	Knockout
Lama5	Laminin, alpha 5
Lef	Lymphoid-enhancer factor
Lgl	Lethal Giant Larvae
LRP	Lipoprotein receptor-related protein
Mb	Megabase
MCKD	Medullary cystic kidney disease
MGI	Mouse Genome Informatics
Mkks	Mckusick-Kaufman syndrome
MODY	Mature onset diabetes of the young
MOPED	Model organism protein expression database
MORM	Mental retardation, truncal obesity, retinal dystrophy, and micropenis
MTOR	Mammalian target of rapamycin
MTORC1/2	Mammalian target of rapamycin complex 1/2
Mut/MT	Homozygous mutant
Mx1	Myxovirus resistance 1
NCBI	National Center for Biotechnology Information
NGAL	Neutrophil gelatinase-associated lipocalin
NIDDK	National Institute of Diabetes and Digestive and Kidney Diseases
Noxa	Phorbol-12-myristate-13-acetate-induced protein 1
NPHP	Nephronophthisis
OCT	Optimal cutting temperature
OFD	oro-facial digital
Orpk	Oak Ridge polycystic kidney disease
PAS	Periodic acid-Schiff
PBS	Phosphate buffered saline
PC1/2	Polycystin-1/2
PCP	Planar cell polarity
Pk	Prickle
PKD	Polycystic kidney disease

Pkhd1	Polycystic kidney and hepatic disease 1
PFA	Paraformaldehyde
Ptf1a	Pancreas specific transcription factor, 1a
Puma	BCL2 binding component 3
QTL	Quantitative trait loci
RAPD	Random amplified polymorphic DNA
RhoA	Ras homolog gene family, member A
RISC	RNA-induced silencing complex
RtTA	Tet-On Advanced transactivator
Runx1	Runt-related transcription factor 1
Scc	Squamous cell carcinoma
Scrib	Scribbled homolog
Sfn	Stratifin
Sglt	Sodium/glucose cotransporter
SgRNA	Single-guide RNA
Shh	Sonic hedgehog
ShRNA	Short hairpin RNA
SIADH	Syndrome of inappropriate anti-diuretic hormone
Siah-1	Seven in absentia 1
SiRNA	Short-interfering RNA
Slc5a2	Solute carrier family 5, member 2
Slc16a12	Solute carrier family 16, member 12
Smit1	Solute carrier family 5, member 3
Snai1	Snail homologue 1
SNGFR	Single nephron GFR
SNP	Short nucleotide polymorphism
SP	Sweet Pee
SPO11	SPO11 meiotic protein covalently bound to DSB homolog
Sry	Sex determining region of chromosome Y
STS	Sequence-tagged site

Stub1	STIP1 homology and U-box containing protein E3 ubiquitin ligase
STZ	Streptozotocin
TCAG	The Center for Applied Genomics
TCF	T-cell factor
Tcf7l2	Transcription factor 7 like 2, T cell specific, HMG box
Tet1-3	Tet methylcytosine dioxygenase 1-3
THP	Tamm-Horsfall protein
TNF-α	Tumor necrosis factor alpha
TracrRNA	Trans-activating crRNA
TRF	Tandem Rpeat Finders
TRDB	Tandem Repeat Data Base
TSC	Tuberous sclerosis complex
UB	Ureteric bud
UCSC	University of California, Santa Cruz
Umod	Uromodulin
URAT	Urate transporter
UTR	Untranslated region
Uty	Ubiquitously transcribed tetratricopeptide repeat gene, Y chromosome
VADT	Veterans Administration Diabetes Trial
Vangl2	Vang-like 2
VEGF	Vascular endothelial growth factor
Vegfr	Vegf-receptor
WHO	World Health Organization
Wnt	Wingless-related MMTV integration site
WT	Wild-type
Wwtr1	WW domain containing transcription regulator 1

Chapter 1 Forward and reverse genetics strategies to study kidney development, function and disease

1 Abstract

The mouse is the most widely used model organism to study gene function in the kidney *in vivo*. Here we review recent advances in technologies to manipulate the mouse genome and gene function to study renal biology. We discuss strengths and weaknesses of the approaches and provide examples in which they have been used to address renal questions. In addition, we provide a summary of the available resources of mouse tools and gene-targeting consortia.

Although conventional gene-targeting and spontaneous genetic mutations in mice have provided great insights into kidney function over several decades, the addition of powerful renal-specific gene-targeting tools and the advent of RNA technologies to manipulate gene function *in vivo* allow investigators to address research questions more precisely in the laboratory. Together with the establishment of multiple international consortia to target all the genes in the mouse genome and the development of gene trap and *N*-ethyl-*N*-nitrosourea resources, genetic manipulation in mice has become more efficient.

In summary, the availability of newer technologies and tremendous resources for mouse strains and reagents ensure that the mouse will remain a key model organism to study renal function.

2 Introduction

The house mouse has inarguably become one of the most important model animals in modern genetics owing to the high degree of similarity between the mouse and human genomes, and the ever-expanding techniques developed in genetic manipulation of the mouse. Over 90% of the mouse and human genomes can be partitioned into regions of conserved synteny and about 350 segments of which are shared between the two(1). Furthermore, about 99% of the mouse genes have a human homolog(1). The mouse and humans share many basic biological, physiological, anatomical and metabolic pathways. These features allow us to use the mouse, as a mammalian model, to study critical conserved genetic pathways and functions that are shared in humans. Furthermore, the availability of inbred strains makes it ideal to the attribute phenotypes to genotype based on a homogenous genetic background. With the development of tools to manipulate the mouse genome, where gene expressions can be “switched” on and off, precisely in a temporal and cell-type specific manner, disruptions in gene function, which caused embryonic lethality in the past can now be examined. Together with the wealth of information available upon the completion of the Mouse Genome Project consisting of 2.5-Gb mouse genome sequence, which aimed to sequence the genomes of 17 key mouse strains, and the availability of reagents such as antibodies for immunostaining and breakthrough technologies such as next-generation re-sequencing in parallel, we are heralding into an exciting post-genomic era poised to discover new gene functions in health and in disease. The mouse was the second mammal to be sequenced as part of the Human Genome Project, informatics was then analyzed by the Mouse Genome Sequencing Consortium(2). Maps of single-nucleotide polymorphisms (SNPs) containing over 340,000 SNPs have been generated. A wealth of information including and not limited to actual genomic sequence, comparative genomics, mutation data, phenotype information, gene-expression data, DNA methylation and histone modification, and protein structure etc., is carefully curated and stored in repositories freely available to researchers. The next imminent challenge is to annotate functions to these genes, which typically involves changing expression pattern. Although space limitations

preclude a comprehensive overview of all approaches used in mice, we aim to provide an update on the most popular approaches, including both forward and reverse genetic strategies.

3 Forward genetics approach

One of the most effective experimental approaches to examine gene function is to create and analyze mutants. Mutations can be generated by targeting a specific gene, also known as reverse genetics, or by inducing random mutations without knowing what the actual gene(s) is mutated, also known as forward genetics.

The combination of embryonic stem cells technology(3) and the use of these cultured cells to recolonize the mouse germ line(4) led to the generation of the first knockout mouse in 1987. Since then, there is an explosion of mouse models with targeted gene mutations. Despite the success of this approach, it inherently has a few limitations. First, the gene chosen has likely been previously ascribed to certain disease of interest and gene targeting allows more in depth analysis by varying gene dosages or expression patterns. It is rarely used to discover functions of an unknown gene. Second, the process of gene targeting itself is labor intensive and it takes years to generate and validate a transgenic mousseline(5). Third, each targeting experiment generates one type of allele, and most often leads to overt outcome (such as knockout). For the purpose of using mouse models for human diseases, these experiments fall short in generating mutations that lead to more subtle effects that are seen in most human diseases especially those that involve complex multiple genes such as diabetes.

In contrast, forward genetics compliment reverse genetics and afford several unique advantages. Forward genetics uses large-scale high-throughput mutagenesis and can generate numerous mutations in one experiment and this leads to producing mutants much more rapidly than reverse genetics. This property is of particular value in attempting to assign gene functions to about 25,000 genes in the mouse genome.

Furthermore, since the knowledge of the gene(s) mutated is not known a priori, forward genetic screens represent an unbiased approach to identify genes responsible for a phenotype and is ideal to discover new genetic functions and pathways. Two common forward genetics tools, namely chemical mutagenesis with *N*-ethyl-*N*-nitrosourea (ENU) and gene trap approaches are discussed below.

3.1 ENU mutagenesis

ENU is the most commonly used chemical mutagen in large-scale mouse mutagenesis projects. ENU induces point mutations in the genomic DNA at a frequency of 1×10^{-3} per locus that is 100-fold higher than the estimated baseline spontaneous mutation rate(6). Although both autosomal dominant and recessive screens may be designed(7, 8), the majority of large ENU consortia have focused on dominant screens, as the breeding schemes are easier (reviewed by Nguyen *et al.*(9), Figure 1). The key strategy includes different starting mouse strains for the mutagenized male harboring mutations in the spermatogonial stem cells and the wild-type female mate; offspring are then systematically screened for phenotypes of interest and heritability confirmed through backcrossing. To identify renal phenotypes, the screens may include urine biochemistry to detect proteinuria, hematuria and glycosuria, anatomical studies to detect hydronephrosis, dysplasia or cysts and blood chemistry. In large-scale projects, high-throughput screens are necessary, whereas smaller, enhanced screens might permit more sensitive assays, such as MRIs, timed dissections and so on, at the expense of higher cost.

The success of ENU mutagenesis is also determined by the ease in identification of the causative genetic mutation, and, to this end, newer technologies such as targeted genomic enrichment(10) and whole exome next-generation resequencing have replaced older and more cumbersome approaches based on mismatch detection using nuclease(11, 12), Mu transposase(13) or intercalating dye(12). Further, the cost of sequencing a mouse exome has recently been reduced to as little as $1500 (http://www.tcag.ca/dnaSequencingSynthesis.html)

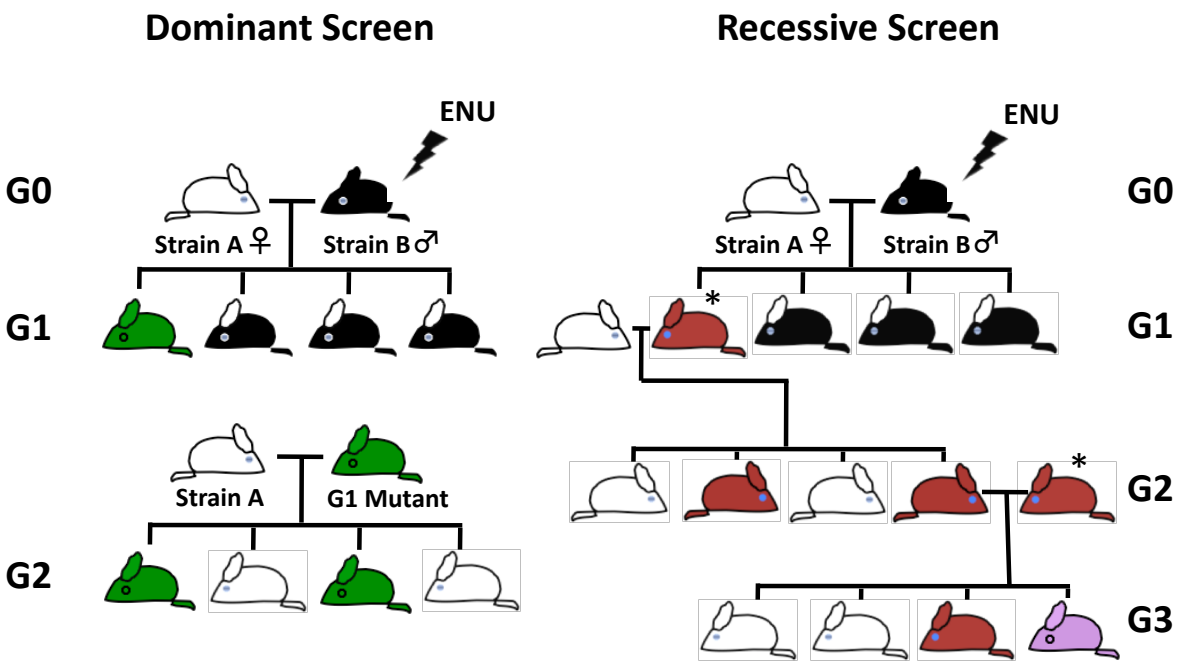

Figure 1 Breeding strategies for *N*-ethyl-*N*-nitrosourea-dominant and *N*-ethyl-*N*-nitrosourea-recessive screen.

For simplified illustration, only one gene mutation causing a variant phenotype is considered in each scenario. Breeding between a wild-type strain A female with a mutagenized strain B male produces G1 litter with an assortment of mutations. Each G1 mouse is screened and if an interesting phenotypic variant is identified (green mouse), it is then backcrossed with wild-type strain A. A mutation that causes dominant or near-dominant phenotype should yield G2 litters with close to 50% expressing the original variant phenotype. Alternatively, G1 may harbor a recessive mutation (red color). These G1 mice are individually backcrossed with wild-type strain A to produce G2. When the mouse harboring a recessive mutation is intercrossed with the founder G1 (*), around 25% of the G3 progeny will express a common variant phenotype (pink). Heritability of this phenotype is validated by crossing the affected G3 (pink) to wild-type strain A. G4 litters are then intercrossed and should replicate the phenotype in 25% of G5 progeny. ENU, *N*-ethyl-*N*-nitrosourea.

Recent successes that have employed autosomal dominant ENU screens for renal disease include identification of Catweasel(14) and Sweet Pee(15). Catweasel results from a hypomorphic missense mutation in the *Six1* gene that is associated with Branchio-oto-renal syndrome (*OMIM* #113650), an autosomal dominant genetic disorder characterized by hearing impairment and malformations in the kidney and the urinary tract. Homozygous Catweasel mutants exhibit hypoplastic kidneys and other severe renal phenotypes. Sweet Pee results from a nonsense mutation in exon 4 of the *Slc5a2* gene that encodes the major sodium glucose cotransporter (Sglt2) in the proximal tubule. The mutant was identified through a simple urine dipstick screen for glucose. The *Slc5a2* mutation results in low-level glycosuria in heterozygotes and high-level persistent glycosuria in homozygotes. This mouse is a model of benign familial glycosuria (*OMIM* #182381) and also provides a model to understand toxicities associated with SGLT2 inhibitors that are mostly on phase III trials for patients with type II diabetes. In fact, one of this first-in-class SGLT2 inhibitors, canagliflozin, has just received approval by the US Food and Drug Administration in March 2013. The Sweet Pee model suggested a higher rate of urinary tract infections, which is now reported as the most frequent side effect of this class of medications(16-18).

Although dominant screens are yielding important mutants, other renal diseases such as heritable forms of nephrotic syndrome, are more likely to occur as recessive diseases. One approach to identify these genes is to perform a smaller, recessive ENU screen on a genetically susceptible background strain. For example, to identify genes important in glomerular function and disease, it would be possible to perform mutagenesis in males that are bred to female mice that are haplo-insufficient for a critical glomerular gene (e.g. *Cd2ap*)(19).

The advantages of an ENU approach include the following: it is a high-throughput, unbiased technique, which generates phenotypes that mimic human diseases more closely than conventional knockouts, as many human disease-causing mutations are point mutations rather than large gene deletions. Worldwide, there are a large number

of ongoing ENU initiatives, which are listed in Table 1 (see review(20)) and are freely available to academic researchers.

Mutagenesis program	Website
MRC Harwell ENU Mutagenesis	www.mut.har.mrc.ac.uk/
Jax-HLBS: Mouse Heart, Lung, Blood, And Sleep Disorder Centre	http://pga.jax.org
Jax-Neuroscience Mutagenesis Facility	http://nmf.jax.org
Jax-Reproductive Genomics	http://reprogenomics.jax.org/index.html
Munich ENU Project	www.helmholtzmuenchen.de/en/ieg/group-genome-project/enu-screen/index.html
Mouse Functional Genomics Research Group, RIKEN GSC	www.gsc.riken.go.jp/Mouse/
Center for Modeling Human Disease	http://www.cmhd.ca/s (Toronto Centre for Phenogenomics, Toronto, Ontario, Canada)
Academia Sinica Mouse Mutagenesis Program	http://mmp.sinica.edu.tw/mmp/english/
Australian Phenomics Facility	http://www.apf.edu.au/
Baylor College of Medicine Mouse Mutagenesis for Development Defects	http://www.mouse-genome.bcm.tmc.edu/ENU/MutagenesisProj.asp
RIKEN ENU Mouse Mutagenesis	http://www.brc.riken.go.jp/lab/gsc/mouse/Mutant/serach.htm
Tennessee Mouse Genome Consortium Neuromutagenesis Project	http://www.tnmouse.org/neuromutagenesis/
Scripps Research Institute Mutagenetix	http://mutagenetix.scripps.edu/home.cfm
Sloan-Kettering Institute Mouse Project	http://mouse.mskcc.org/

Table 1 Summary of international *N*-ethyl-*N*-nitrosourea mutagenesis programs. Data extracted from reference 19.

3.2 Gene trapping

Gene trapping is another high-throughput mutagenesis strategy that complements the ENU approach. Genes are tagged for sequence retrieval by insertional mutagenesis, generating hundreds of different mutations from a single electroporation or viral infection(21). A `trap' vector is randomly introduced into the genome of mouse embryonic stem cells. The vector consists of a `promoterless' selectable gene cassette flanked by a splice acceptor. Only vectors that have been trapped and express the selection marker under an endogenous gene promoter will survive. When inserted into an intron of an expressing gene, transcription of the exons 3' to the cassette will form a truncated fusion transcript with cassette which contains a polyadenylation sequence for premature termination. One major drawback to this approach for kidney researchers is the fact that a gene must be expressed in an embryonic stem cell to be picked up. Thus, genes that are kidney specific may be missed. Regardless, there are now a number of sequenced `trapped' genes that have been deposited in freely accessible databases. It is possible to search the database, find your gene of interest and order the targeted embryonic stem cell or, sometimes, the mouse over the phone. Database links are provided in Table 2 (http://www.genetrap.org/).

Gene Trap programs	Website
BayGenomics	http://baygenomics.ucsf.edu/
Centre for Modeling Human Disease	http://www.cmhd.ca/genetrap/index.html (Toronto Centre for Phenogenomics, Toronto, Ontario, Canada)
Embryonic Stem Cell Database	http://EScells.ca
European Conditional Mouse Mutagenesis	http://www.eucomm.org/
Exchangeable Gene Trap Clones	http://egtc.jp/action/main/index
German Gene Trap Consortium	http://tikus.gsf.de/
RIKEN BioResource Center	http://www.brc.riken.jp/lab/animal/en/
Sanger Institute Gene Trap Resource	http://www.sanger.ac.uk/resources/mouse/sigtr/
Soriano Lab Gene Trap Database	http://research.mssm.edu/soriano/lab/Soriano_lab.html
Texas Institute for Genomic Medicine (TIGM)	http://www.tigm.org/
TIGEM-IRBM Gene Trap	http://genetrap.tigem.it/public/index.php

Table 2 International Gene Trap Consortia

4 Reverse gene-targeting approaches

Reverse gene-targeting approaches begin with a known gene of interest. Conventional gene-targeting and newer RNA-based methods are discussed below.

4.1 General advances

In conventional knockouts, a critical portion of the gene is altered/removed in embryonic stem cells, resulting in a null allele or nonfunctional protein. Stem cells carrying the altered gene are transferred to pseudopregnant females and are capable of generating the entire embryo proper (reviewed in(22)). The major drawback for studying genes in the kidney with this approach is the fact that deletion of a gene in embryonic stem cells may result in early embryonic lethality, precluding analysis of its role in kidney development or function, as this organ develops relatively late in gestation. In recent years, cell-specific knockout technologies have provided greater insight for renal research.

Cre-loxP and Flp-FRT are the two most widely used recombinases that recognize specific short DNA sequences and cleave the DNA backbone, exchange the two DNA strands and rejoin them(23). Other recombinases include the Dre-Rox system found in the bacteriophage D6, and the ϕC31 integrase(24), but they have not been as widely used. Conditional recombinases can be expressed in specific renal cell types based on the promoter chosen (Table 3)(25-48). Furthermore, systems that permit temporal regulation of gene function may be added on top of this cell specificity, permitting genetic manipulation in developing or mature kidneys. The most commonly used temporal regulatory systems depend upon a `tet' operon element in the targeting construct; the addition of a tetracycline derivative to the drinking water or food of a transgenic mouse results in induction of transgene expression in tet-on systems and loss of gene function in tet-off systems(49). The next most commonly used system utilizes the estrogen receptor T2 element, which uses tamoxifen to modulate gene expression(50). Benefits to the tamoxifen approach include the fact that both cell and temporal regulatory components are combined in a single transgene, whereas many

tetracycline-based systems are bitransgenic (which translates to more breeding). However, tamoxifen causes embryonic defects, whereas tetracycline derivatives may be given to developing and adult mice, permitting analysis over a wide range of time points(51).

Promoter	Renal expression	Extrarenal expression	References
Kidney androgen promoter 2	Proximal tubules	Brain	[25]
g-Glutamyl transpeptidase	Cortical tubules	None	[26]
Sodium glucose cotransporter	Proximal tubules	None	[27]
PEPCK	Proximal tubules	Liver	[28]
Aquaporin-2	Principal cells of collecting duct	Testis, vas deferens	[29]
Hox-B7	Collecting ducts, ureteric bud, Wolffian bud, ureter	Spinal cord, dorsal root ganglia	[30]
Ksp-cadherin	Renal tubules, collecting ducts, ureteric bud, Wolffian duct, mesonephros	Müllerian duct	[31]
Tamm-Horsfall protein	Thick ascending limbs of loops of Henle	Testis, brain	[32]
Nephrin	Podocytes	Brain	[33,34]
Podocin	Podocytes	None	[35]
Renin	Juxtaglomerular	Adrenal gland,	[36]

	cells, afferent arterioles	testis, sympathetic ganglia and so on	
Foxd1	Stromal cells	Not characterized	[37]
Six2	Cap mesenchyme	Anterior cranial base	[38,39]
Pax3	Metanephric mesenchyme	Neural tube, neural crest	[40,41]
Pax2	Metanephric mesenchyme, UB	Inner ear, midbrain, cerebellum, olfactory bulb	[42]
Cited1	Cap mesenchyme	Melanocytes	[43,44]
Pax8	Proximal, distal tubule and collecting duct (tet-on system)	Thyroid	[45,46]
Pod1/Tcf21	Metanephric mesenchyme, cap mesenchyme, podocytes, stromal cells	Epicardium, lung mesenchyme, gonad, spleen, adrenal gland	[47]

Table 3 Summary of kidney promoters available lines(25).

4.2 Cell-specific tools for targeting the kidney

Compared with a decade ago, the number of tools available to drive gene expression in specific cell populations within the kidney has expanded greatly(25). However, it is important to note that robust tools are still lacking for some clinically important cell populations such as: glomerular endothelial cells and renal interstitial cells. It is also important to remember that driver lines, particularly if they were generated as random integrant transgenes, may lose their recombinase ability over time. Thus, it is essential that any researcher using these tools re-evaluate the excision

abilities within their own lab. This is not trivial and requires analysis of reporter strains, but also, most importantly, requires analysis of recombination of the gene of interest. Cre-driver and Flp-driver may vary in their ability to cause recombination from locus to locus; thus, robust excision of a reporter gene may not translate to robust excision of any other gene. When reporting negative phenotypes, it is necessary to confirm genomic excision in the cell of interest that often requires isolation of specific cell populations by FACS analysis and Southern blot analysis.

4.3 Fate mapping in the kidney

Some of the most exciting and hotly debated topics in nephrology have utilized Cre-driver transgenic mouse strains to tag-specific cell lineages within the developing and mature kidney. Such an approach allowed investigators to identify and characterize a stem-like population within the developing metanephros; the subset of metanephric mesenchyme that expresses *Six2* has the potential to give rise to all epithelial cell lineages in the nephron down to the distal tubule and these cells have the ability for self-renewal(39). Parietal epithelial-specific Cre strains led to the identification of a `progenitor niche' in Bowman's capsule that contains cells that may differentiate into podocytes, even in the adult glomerulus(39, 51, 52).

In the setting of renal fibrosis, newer Cre-driver strains and more robust reporter lines that tag epithelial cell lineages with fluorescent markers raised questions about the abilities of tubular epithelial cells to undergo mesenchymal transition *in vivo* during renal fibrogenesis(38). Although lineage tags are advertised as being `permanent', it is important to realize that reporter gene expression may or may not be permanent, depending on the context (reviewed in (53)). Thus, although sometimes results might appear to be `black and white', careful interpretation is required(54).

4.4 Gene recombination systems: temporal and spatial targeting in the kidney

In addition to lineage-tracing experiments, temporal and cell-specific deletions have been widely employed to study all aspects of renal function, development and disease (Figure 2). Recent cell-specific knockouts in the kidney have identified roles

for autophagy(55) and insulin signaling in podocytes(56) and planar cell polarity in tubular cyst formation(57) and characterized the mechanism of action of calcineurin inhibitors in the treatment of nephrotic syndromes(58). Recently, more studies have included multiple Cre-driver strains or have added temporal control to the deletion strategies, permitting more extensive characterization of a gene's function. Such an elegant approach was used to explore the role of *Pkd2* in the formation of renal and extra-renal cysts(59). In addition, global postnatal deletion of the major vascular endothelial growth factor (VEGF) receptor (*Vegfr2*/*Flk1*/*Kdr*) from mice demonstrated that specific vascular beds including the glomerulus are exquisitely dependent upon VEGF signaling for maintenance of endothelial integrity. In the same study, deletion of the *Vegfr* from nonendothelial cell types, such as the podocyte, confirm that paracrine VEGF signaling against the flow of urinary filtrate dominates in mature glomeruli. It is important to realize that adult temporal knockouts often require four transgenes, which translates to a minimum of 2 years of breeding, but payoffs can be large once the colony is established.

Although Flp recombinases have not been as widely used for genetic targeting experiments as Cre-mediated gene recombination, Goldberg *et al*.(60) reported the generation of a podocyte-specific Flp recombinase-driver mouse strain. They performed an elegant study in which they deleted the *Lama5* using Cre-loxP technology. In parallel, they were able to re-establish expression in podocytes alone, using Flp recombinase. They showed that podocyte-expressed *Lama5* is critical and sufficient for glomerular barrier integrity. Combining both Flp and Cre recombinase systems allows one to design sophisticated experiments to switch genes on and off in more than one compartment or at different time points. This approach has been used widely in the nervous system (Math1-cre and hβact-Flp) and will likely be used more frequently in the kidney(61).

4.5 CRISPR/Cas-mediated genome engineering

It is more common than not that targeting multiple genes are required with the advancement in the precision of genome editing as discussed above, to study epistatic gene interaction, or to investigate the functions of gene family members with redundant functions. The conventional strategy involves complex breeding scheme between different transgenic lines. The major limitations of this strategy include high cost, significant time commitment, not all transgenes are readily available, and low efficiency especially when three or more transgenes are required. Very often, expansion of breeding colony is required in order to obtain a reasonable number of animals with all the desired transgenes and further increasing the costs of the experiment.

Wang et al(62) has recently published the use of type II bacterial CRISPR (clustered regularly interspaced short palindromic repeat)/Cas (CRISPR-associated) system for multiplex genome editing. CRISPR are essential RNA-based adaptive immune system that recognizes foreign nucleic acids utilized by bacteria and archea(63). They were first described in 1987(64) in the genome of *E. coli* characterized by a series of 29-nucleotide repeats separated with unique 32-nucleotide spacer sequences, which were later identified to be of viral and plasmid origin(65-67). It is now known that the CRISPR loci contain a series of repeats that are between 20 to 50 base pairs which can be variable in sequence, length and number of repeat-spacer units from one locus to another(68, 69). When bacteria encounter foreign virus or plasmid, a short segment of DNA from the invading agent is incorporated at the leader end of the CRISPR locus(70, 71). The transcription of CRISPR loci, and subsequent processing of the primary transcript into short CRISPR-derived RNAs (crRNAs), together with Cas proteins and trans-activating crRNA (tracrRNA) form ribonucleoprotein complexes that specifically detect and destroy foreign nucleic acid targets(72-74). Type II CRISPR systems consists of four Cas genes including Cas9 which has been shown to be critical for CRISPR RNA processing and target destruction(70, 71, 75). Of note, Cas9 endonuclease by itself can induce sequence-specific double strand break (DSB) in vitro with a synthetic single-guide RNA (sgRNA) made of crRNA and tacrRNA(74). The successful usage of this system to target single

genes has been demonstrated in human cells, zebrafish, and mice(76-78). With that, Wang et al(62) attempted to take advantage of this system for multiplexing and successfully targeted five genes with sgRNAs specific for *Tet1*, *Tet2*, *Tet3*, *Sry*, and *Uty* with a Cas9 expressing plasmid into ES cells. Ten percent of the 96 cones were shown to carry mutations in eight alleles of the five genes(62). The same group also successfully targeted two genes, *Tet1* and *Tet2*, and generated double mutant mice with co-injection of *Tet1* and *Tet2* sgRNAs and Cas9 mRNA into zygotes. Of the 144 embryos transferred, 31 pups were born and 22 mice carried targeted mutations at all four alleles. Finally, this system can also introduce specific changes in the sequence, rather than random insertion or deletion, by co-injecting single-stranded oligonucleotides with designed point mutations into the target genes along with sgRNAs and Cas9 mRNA. There are a few issues that require further investigation including the potential of off targeting and the efficacy in alteration of larger sequences such as inserting loxP sites. Nonetheless, the CRISPR/Cas genome editing system offers a new technology to target multiple genes simultaneously.

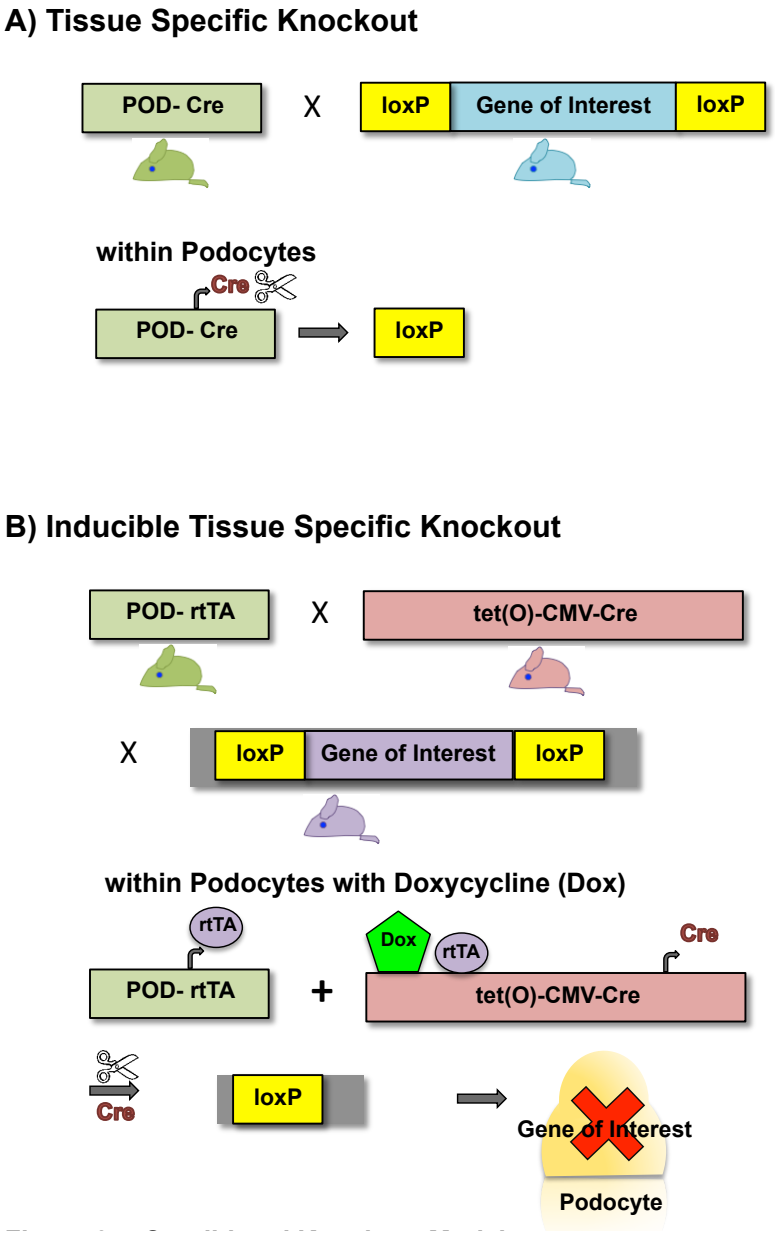

Figure 2 Conditional knockout models

(A) Podocyte-specific knockout of a gene of interest. In this example, the gene of interest is flanked by two loxP sequences. Within podocytes, podocyte-specific promoter (POD) drives the expression of the molecular scissor Cre recombinase, which causes excision of the *floxed* gene. (B) Inducible podocyte-specific knockout. In this model, Cre recombinase is activated within podocytes with POD driven rtTA and doxycline and excises the *floxed* gene (between two loxP sequences)

4.6 Gain-of-function transgenics

Discussion has focused on inactivation of gene function; however, gain-of-function (GOF) transgenics continue to be widely used(79). One of the benefits of GOF transgenics compared with knockouts is the speed of production; mice may be studied in the first or second generation and founder mice are produced more rapidly than knockouts. However, overexpression of proteins may result in mislocalization of the protein and off-target toxicities. Increased levels of protein within a cell may cause problems unrelated to the gene product. Thus, although they can be very useful, investigators must be careful to consider these effects when interpreting their data. Addition of temporal control that permits transient overexpression, may limit some of these issues.

4.8 RNA-base approaches

Limitations to the methods listed above include the following: the irreversibility of genetic alteration (except in the case of inducible GOF transgenes) and the length of time required to generate the mouse of interest. Despite the drawbacks, a major benefit to these approaches includes the robust genetic alteration that can be demonstrated experimentally without a doubt. In recent years, identification of RNAs that regulate endogenous gene expression has allowed development of reversible, efficient and scalable alternative options.

There are three major types of RNA species that are used to manipulate gene expression in mice. These include siRNA (small interfering RNA), shRNA (short hairpin RNA) and amiRNA (artificial microRNA). The differences are outlined in Figure 3A. Small interfering RNAs directly target transcription and translation, ultimately knocking down the protein encoded by the gene of interest. They do not require additional processing by the host cell and the effect is transient. In mouse models, siRNAs have been used to knockdown gene expression through direct tail vein injection. The challenges are obtaining robust and specific knockdown. Shamporter delivery system that targets podocytes was developed to try and enhance the effect(80). Wan *et al.*(81)

used this approach to demonstrate a protective effect of suppressing the inhibitory κB-kinase subunit in ischemia-reperfusion acute kidney injury.

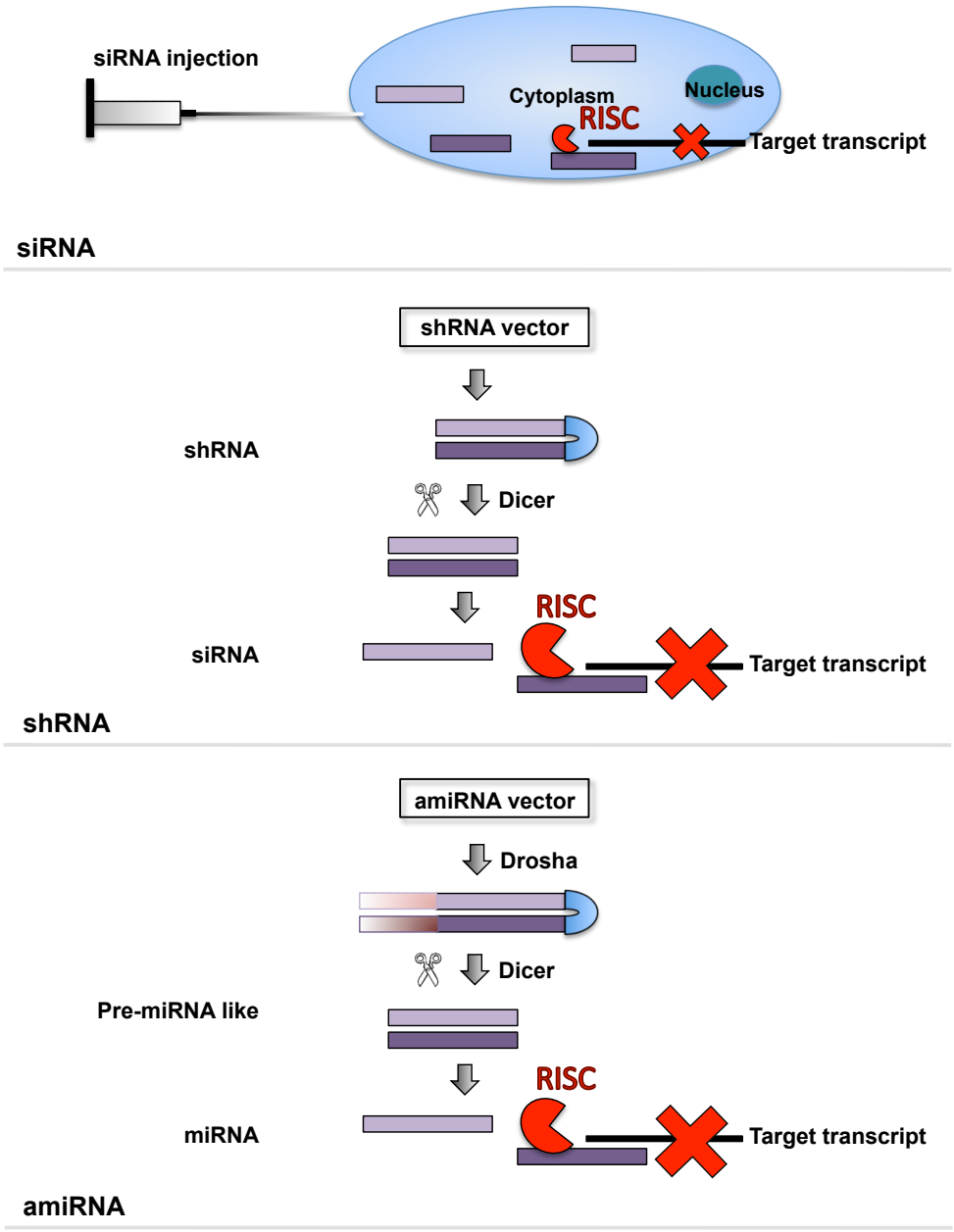

Figure 3A Comparisons between siRNA, shRNA, and amiRNA

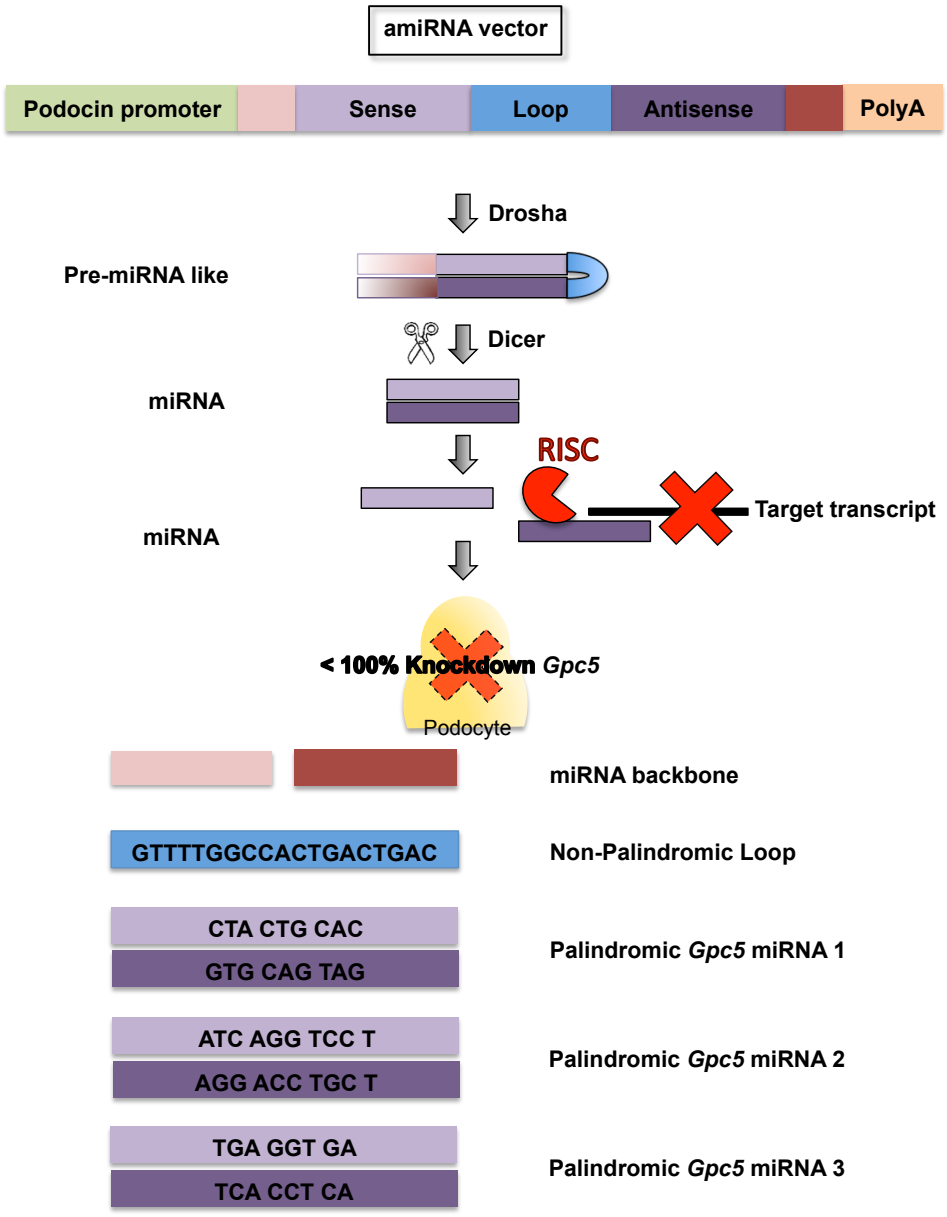

Figure 3B Glipican5 MicroRNA construct

Figure 3 Three major types of RNA and Glipican5 miRNA construct. (A) Comparison between siRNA, shRNA and amiRNA. Drosha is a Class2 RNase III enzyme that initiates the processing of miRNA. Dicer is an endoribonuclease in the RNase II family that cleaves double-stranded RNA into short double-stranded RNA fragments. The RNA-induced silencing complex (RISC) degrades target messenger RNA. (B) Glipican5 (*Gpc5*) construct is composed of podocin promoter, sequence modifications of endogenous miRNA backbone containing three different primary miRNA sequences with sequence complementary to *Gpc5* and a thymidine kinase polyadenylation sequence. Endogenous nuclear RNase III Drosha cleaves primary transcripts or pri-miRNAs and releases pre-miRNA, which is then processed in the cytoplasm by Dicer to form mature miRNAs. Mature miRNAs then interact with RNA-induced silencing complex, RISC, to cleave complementary RNA transcript and/or interrupt translation. This leads to knockdown of *Gpc5* in podocytes.

In contrast, shRNA are vector based and transcribed in the nucleus by the host cell; they require processing by Dicer, an endogenous endoribonuclease, before they can interact with the RNA-induced silencing complex (RISC). Thus, permanent expression of the shRNA can be achieved through standard embryonic stem or transgenic targeting approaches. In the kidney, this approach was used to demonstrate a role of nonselective cation channel Nr3a in modulating aquaporin 2 expression by direct renal artery injection(82). Both constitutive and conditional shRNA expression can be achieved(83). Recently, an inducible system using Tet-on to “switch on” the expression of shRNA for *Vegf-A* upon exposure to doxycycline, specifically in podocytes with podocin driving rtTA expression, successfully knockdown the expression of Vegf-A to about 20%(84). When these mice were induced in adulthood, they developed renal failure and proteinuria with associated mesangiolysis, microaneurisms, endothelial swelling, glomerular basement membrane lamination, and podocyte effacement(84).

Artificial microRNAs are similar to shRNA as described above. Both share the common feature of a vector-based delivery, requiring production of an intermediate transcript for cellular processing before they can participate in RNA interference. However, amiRNA specifically refers to shRNA embedded in a natural microRNA backbone to enhance its processing and shuttling from the nuclear compartment to the cytoplasm, wherein it exerts its action. It is possible to drive these amiRNAs with tissue-specific promoters as was recently done to demonstrate a role for *Gpc5* in glomerular function in mice and to provide supporting evidence that this gene, recently identified in a GWAS study of idiopathic nephrotic syndrome, is biologically important (Figure 3B)(85).

The ability to scale-up gene knockdown approaches is appealing. To this end, Premsrirut *et al.*(86) reported in *Cell*, a strategy to rapidly target (via Flp recombinase) any shRNA of interest into the *Col1a1* locus of embryonic stem cells. Doxycycline control and a GFP reporter are added features in the shRNA vector. Upon addition of doxycycline (the mouse must also carry an rtTA-driver of choice such as the ubiquitous rosa-rtTA), expression of shRNA occurs and can be followed by GFP fluorescence. Although the *Col1a1* and rosa-rtTA expression domains may not be first choice for kidney studies, the authors did show robust expression in kidneys(although specific cell types were not analyzed). Future studies may adopt this system for specific cell populations in the kidney using other rtTA-drivers and `anchored' genomic loci to insert the shRNA.

Some drawbacks or facts to be considered with RNA approaches are as follows: gene knockdown is not complete, off-target effects may occur due to knockdown of other genes and nonspecific toxicity of high levels of shRNA have been reported. Thus, although attractive, they will not replace more conventional strategies, but provide a complementary approach.

5 Other genetic systems

For sake of space limitations, other approaches such as congenic breeding to identify susceptible genes(87), zinc nucleases, nongenetic targeting systems such as nanoparticles and microbubble technology and tetraploid and chimeric strategies were not discussed. Some have yielded exciting insights into renal disease such as HIVAN(88). References for interested readers are supplied(79, 89-98).

6 Conclusion

As outlined above, the mouse is a powerful model system to study all aspects of kidney biology from development to physiology to adult diseases. The availability of phenotyping centers (including fetal ultrasound, MRIs, etc.) allows in-depth analysis of many biologic processes. Conventional gene-targeting strategies have provided great insight into kidney function; however, the development of high-throughput mutagenesis screens, and more refined tools that add spatial and temporal control to genetic regulation, allow more precise and comprehensive dissection of a gene's function. A number of international consortia and resources for targeted embryonic stem cell lines, mice and Cre-driver strains now exist, permitting researchers to generate their mouse model over the `phone'. Finally, RNA-based strategies are likely to become more and more widely used as a complementary system to DNA-based strategies. Taken together, these exciting advances guarantee that the mouse will remain a favored model system for years to come.

7 References

1. Guenet, J.L. 2005. The mouse genome. *Genome research* 15:1729-1740.
2. Waterston, R.H., Lindblad-Toh, K., Birney, E., Rogers, J., Abril, J.F., Agarwal, P., Agarwala, R., Ainscough, R., Alexandersson, M., An, P., et al. 2002. Initial sequencing and comparative analysis of the mouse genome. *Nature* 420:520-562.
3. Evans, M.J., and Kaufman, M.H. 1981. Establishment in culture of pluripotential cells from mouse embryos. *Nature* 292:154-156.
4. Bradley, A., Evans, M., Kaufman, M.H., and Robertson, E. 1984. Formation of germ-line chimaeras from embryo-derived teratocarcinoma cell lines. *Nature* 309:255-256.
5. Capecchi, M.R. 2005. Gene targeting in mice: functional analysis of the mammalian genome for the twenty-first century. *Nature reviews. Genetics* 6:507-512.
6. Justice, M.J., Noveroske, J.K., Weber, J.S., Zheng, B., and Bradley, A. 1999. Mouse ENU mutagenesis. *Hum Mol Genet* 8:1955-1963.
7. Hughes, M.R., Anderson, N., Maltby, S., Wong, J., Berberovic, Z., Birkenmeier, C.S., Haddon, D.J., Garcha, K., Flenniken, A., Osborne, L.R., et al. 2011. A novel ENU-generated truncation mutation lacking the spectrin-binding and C-terminal regulatory domains of Ank1 models severe hemolytic hereditary spherocytosis. *Experimental hematology* 39:305-320, 320 e301-302.
8. Rathkolb, B., Tran, T.V., Klempt, M., Hrabe de Angelis, M., Wanke, R., Wolf, E., and Aigner, B. 2005. Large-scale albuminuria screen for nephropathy models in chemically induced mouse mutants. *Nephron. Experimental nephrology* 100:e143-149.
9. Nguyen, N., Judd, L.M., Kalantzis, A., Whittle, B., Giraud, A.S., and van Driel, I.R. 2011. Random mutagenesis of the mouse genome: a strategy for discovering gene function and the molecular basis of disease. *American journal of physiology. Gastrointestinal and liver physiology* 300:G1-11.
10. Nijman, I.J., Mokry, M., van Boxtel, R., Toonen, P., de Bruijn, E., and Cuppen, E. Mutation discovery by targeted genomic enrichment of multiplexed barcoded samples. *Nat Methods* 7:913-915.
11. Mitani, N., Niwa, Y., and Okamoto, Y. 2007. Surveyor nuclease-based detection of p53 gene mutations in haematological malignancy. *Ann Clin Biochem* 44:557-559.
12. Gady, A.L., Hermans, F.W., Van de Wal, M.H., van Loo, E.N., Visser, R.G., and Bachem, C.W. 2009. Implementation of two high through-put techniques in a novel application: detecting point mutations in large EMS mutated plant populations. *Plant Methods* 5:13.
13. Yanagihara, K., and Mizuuchi, K. 2002. Mismatch-targeted transposition of Mu: a new strategy to map genetic polymorphism. *Proc Natl Acad Sci U S A* 99:11317-11321.
14. Bosman, E.A., Quint, E., Fuchs, H., Hrabe de Angelis, M., and Steel, K.P. 2009. Catweasel mice: a novel role for Six1 in sensory patch development and a model for branchio-oto-renal syndrome. *Dev Biol* 328:285-296.

15. Ly, J.P., Onay, T., Sison, K., Sivaskandarajah, G., Sabbisetti, V., Li, L., Bonventre, J.V., Flenniken, A., Paragas, N., Barasch, J.M., et al. The Sweet Pee model for Sglt2 mutation. *J Am Soc Nephrol* 22:113-123.
16. Nicolle, L.E., Capuano, G., Ways, K., and Usiskin, K. 2012. Effect of canagliflozin, a sodium glucose co-transporter 2 (SGLT2) inhibitor, on bacteriuria and urinary tract infection in subjects with type 2 diabetes enrolled in a 12-week, phase 2 study. *Current medical research and opinion* 28:1167-1171.
17. Bailey, C.J., Gross, J.L., Pieters, A., Bastien, A., and List, J.F. 2010. Effect of dapagliflozin in patients with type 2 diabetes who have inadequate glycaemic control with metformin: a randomised, double-blind, placebo-controlled trial. *Lancet* 375:2223-2233.
18. Musso, G., Gambino, R., Cassader, M., and Pagano, G. 2012. A novel approach to control hyperglycemia in type 2 diabetes: sodium glucose co-transport (SGLT) inhibitors: systematic review and meta-analysis of randomized trials. *Annals of medicine* 44:375-393.
19. Huber, T.B., Kwoh, C., Wu, H., Asanuma, K., Godel, M., Hartleben, B., Blumer, K.J., Miner, J.H., Mundel, P., and Shaw, A.S. 2006. Bigenic mouse models of focal segmental glomerulosclerosis involving pairwise interaction of CD2AP, Fyn, and synaptopodin. *The Journal of clinical investigation* 116:1337-1345.
20. Gondo, Y., Fukumura, R., Murata, T., and Makino, S. ENU-based gene-driven mutagenesis in the mouse: a next-generation gene-targeting system. *Exp Anim* 59:537-548.
21. Bradley, A. 2002. Mining the mouse genome. *Nature* 420:512-514.
22. Guan, C., Ye, C., Yang, X., and Gao, J. 2010. A review of current large-scale mouse knockout efforts. *Genesis* 48:73-85.
23. Grindley, N., Whiteson, KL & Rice, PA. 2006. Mechanisms of site-specific recombination. *Annu Rev Biochem* 75:567-605.
24. Sclimenti, C., Thyagarajan, B & Calos, MP. 2001. Directed evolution of a recombinase for improved genomic integration at a native human sequence. *Nucleic Acids Res* 30:2299-2306.
25. Maezawa Y, K.J., Quaggin S. 2012. *Embryology of the kidney*. Philadelphia: Saunders
26. Lavoie, J.L., Lake-Bruse, K.D., and Sigmund, C.D. 2004. Increased blood pressure in transgenic mice expressing both human renin and angiotensinogen in the renal proximal tubule. *Am J Physiol Renal Physiol* 286:F965-971.
27. Sepulveda, A.R., Huang, S.L., Lebovitz, R.M., and Lieberman, M.W. 1997. A 346-base pair region of the mouse gamma-glutamyl transpeptidase type II promoter contains sufficient cis-acting elements for kidney-restricted expression in transgenic mice. *The Journal of biological chemistry* 272:11959-11967.
28. Rubera, I., Poujeol, C., Bertin, G., Hasseine, L., Counillon, L., Poujeol, P., and Tauc, M. 2004. Specific Cre/Lox recombination in the mouse proximal tubule. *Journal of the American Society of Nephrology : JASN* 15:2050-2056.
29. Rankin, E.B., Tomaszewski, J.E., and Haase, V.H. 2006. Renal cyst development in mice with conditional inactivation of the von Hippel-Lindau tumor suppressor. *Cancer research* 66:2576-2583.
30. Nelson, R.D., Stricklett, P., Gustafson, C., Stevens, A., Ausiello, D., Brown, D., and Kohan, D.E. 1998. Expression of an AQP2 Cre recombinase transgene in

kidney and male reproductive system of transgenic mice. *The American journal of physiology* 275:C216-226.
31. Srinivas, S., Goldberg, M.R., Watanabe, T., D'Agati, V., al-Awqati, Q., and Costantini, F. 1999. Expression of green fluorescent protein in the ureteric bud of transgenic mice: a new tool for the analysis of ureteric bud morphogenesis. *Developmental genetics* 24:241-251.
32. Shao, X., Somlo, S., and Igarashi, P. 2002. Epithelial-specific Cre/lox recombination in the developing kidney and genitourinary tract. *Journal of the American Society of Nephrology : JASN* 13:1837-1846.
33. Zhu, X., Cheng, J., Gao, J., Lepor, H., Zhang, Z.T., Pak, J., and Wu, X.R. 2002. Isolation of mouse THP gene promoter and demonstration of its kidney-specific activity in transgenic mice. *American journal of physiology. Renal physiology* 282:F608-617.
34. Moeller, M.J., Kovari, I.A., and Holzman, L.B. 2000. Evaluation of a new tool for exploring podocyte biology: mouse Nphs1 5' flanking region drives LacZ expression in podocytes. *Journal of the American Society of Nephrology : JASN* 11:2306-2314.
35. Wong, M.A., Cui, S., and Quaggin, S.E. 2000. Identification and characterization of a glomerular-specific promoter from the human nephrin gene. *American journal of physiology. Renal physiology* 279:F1027-1032.
36. Moeller, M.J., Sanden, S.K., Soofi, A., Wiggins, R.C., and Holzman, L.B. 2002. Two gene fragments that direct podocyte-specific expression in transgenic mice. *Journal of the American Society of Nephrology : JASN* 13:1561-1567.
37. Sequeira Lopez, M.L., Pentz, E.S., Nomasa, T., Smithies, O., and Gomez, R.A. 2004. Renin cells are precursors for multiple cell types that switch to the renin phenotype when homeostasis is threatened. *Developmental cell* 6:719-728.
38. Humphreys, B.D., Lin, S.L., Kobayashi, A., Hudson, T.E., Nowlin, B.T., Bonventre, J.V., Valerius, M.T., McMahon, A.P., and Duffield, J.S. 2010. Fate tracing reveals the pericyte and not epithelial origin of myofibroblasts in kidney fibrosis. *The American journal of pathology* 176:85-97.
39. Kobayashi, A., Valerius, M.T., Mugford, J.W., Carroll, T.J., Self, M., Oliver, G., and McMahon, A.P. 2008. Six2 defines and regulates a multipotent self-renewing nephron progenitor population throughout mammalian kidney development. *Cell stem cell* 3:169-181.
40. He, G., Tavella, S., Hanley, K.P., Self, M., Oliver, G., Grifone, R., Hanley, N., Ward, C., and Bobola, N. 2010. Inactivation of Six2 in mouse identifies a novel genetic mechanism controlling development and growth of the cranial base. *Developmental biology* 344:720-730.
41. Engleka, K.A., Gitler, A.D., Zhang, M., Zhou, D.D., High, F.A., and Epstein, J.A. 2005. Insertion of Cre into the Pax3 locus creates a new allele of Splotch and identifies unexpected Pax3 derivatives. *Developmental biology* 280:396-406.
42. Li, J., Chen, F., and Epstein, J.A. 2000. Neural crest expression of Cre recombinase directed by the proximal Pax3 promoter in transgenic mice. *Genesis* 26:162-164.
43. Ohyama, T., and Groves, A.K. 2004. Generation of Pax2-Cre mice by modification of a Pax2 bacterial artificial chromosome. *Genesis* 38:195-199.

44. Boyle, S., Misfeldt, A., Chandler, K.J., Deal, K.K., Southard-Smith, E.M., Mortlock, D.P., Baldwin, H.S., and de Caestecker, M. 2008. Fate mapping using Cited1-CreERT2 mice demonstrates that the cap mesenchyme contains self-renewing progenitor cells and gives rise exclusively to nephronic epithelia. *Developmental biology* 313:234-245.
45. Ryu, B., Kim, D.S., Deluca, A.M., and Alani, R.M. 2007. Comprehensive expression profiling of tumor cell lines identifies molecular signatures of melanoma progression. *PloS one* 2:e594.
46. Traykova-Brauch, M., Schonig, K., Greiner, O., Miloud, T., Jauch, A., Bode, M., Felsher, D.W., Glick, A.B., Kwiatkowski, D.J., Bujard, H., et al. 2008. An efficient and versatile system for acute and chronic modulation of renal tubular function in transgenic mice. *Nature medicine* 14:979-984.
47. Plachov, D., Chowdhury, K., Walther, C., Simon, D., Guenet, J.L., and Gruss, P. 1990. Pax8, a murine paired box gene expressed in the developing excretory system and thyroid gland. *Development* 110:643-651.
48. Maezawa, Y., Binnie, M., Li, C., Thorner, P., Hui, C.C., Alman, B., Taketo, M.M., and Quaggin, S.E. 2012. A new Cre driver mouse line, Tcf21/Pod1-Cre, targets metanephric mesenchyme. *PloS one* 7:e40547.
49. gossen, M.B., H. 1992. Tight control of gene expressin in mammalian cells by tetracycline-responsive promoters. *Proc Natl Acad Sci U S A* 89:5547-5551.
50. Feil, R., Brocard, J., Mascrez, B., LeMeur, M., Metzger, D., and Chambon, P. 1996. Ligand-activated site-specific recombination in mice. *Proc Natl Acad Sci U S A* 93:10887-10890.
51. Jeansson, M., Gawlik, A., Anderson, G., Li, C., Kerjaschki, D., Henkelman, M., and Quaggin, S.E. 2011. Angiopoietin-1 is essential in mouse vasculature during development and in response to injury. *The Journal of clinical investigation* 121:2278-2289.
52. Appel, D., Kershaw, D.B., Smeets, B., Yuan, G., Fuss, A., Frye, B., Elger, M., Kriz, W., Floege, J., and Moeller, M.J. 2009. Recruitment of podocytes from glomerular parietal epithelial cells. *Journal of the American Society of Nephrology : JASN* 20:333-343.
53. Shifera, A.S., and Hardin, J.A. 2010. Factors modulating expression of Renilla luciferase from control plasmids used in luciferase reporter gene assays. *Analytical biochemistry* 396:167-172.
54. Quaggin, S.E., and Kapus, A. 2011. Scar wars: mapping the fate of epithelial-mesenchymal-myofibroblast transition. *Kidney international* 80:41-50.
55. Hartleben, B., Godel, M., Meyer-Schwesinger, C., Liu, S., Ulrich, T., Kobler, S., Wiech, T., Grahammer, F., Arnold, S.J., Lindenmeyer, M.T., et al. 2010. Autophagy influences glomerular disease susceptibility and maintains podocyte homeostasis in aging mice. *The Journal of clinical investigation* 120:1084-1096.
56. Welsh, G.I., Hale, L.J., Eremina, V., Jeansson, M., Maezawa, Y., Lennon, R., Pons, D.A., Owen, R.J., Satchell, S.C., Miles, M.J., et al. 2010. Insulin signaling to the glomerular podocyte is critical for normal kidney function. *Cell metabolism* 12:329-340.
57. Saburi, S., Hester, I., Fischer, E., Pontoglio, M., Eremina, V., Gessler, M., Quaggin, S.E., Harrison, R., Mount, R., and McNeill, H. 2008. Loss of Fat4

disrupts PCP signaling and oriented cell division and leads to cystic kidney disease. *Nature genetics* 40:1010-1015.
58. Faul, C., Donnelly, M., Merscher-Gomez, S., Chang, Y.H., Franz, S., Delfgaauw, J., Chang, J.M., Choi, H.Y., Campbell, K.N., Kim, K., et al. 2008. The actin cytoskeleton of kidney podocytes is a direct target of the antiproteinuric effect of cyclosporine A. *Nature medicine* 14:931-938.
59. Kim, I., Ding, T., Fu, Y., Li, C., Cui, L., Li, A., Lian, P., Liang, D., Wang, D.W., Guo, C., et al. 2009. Conditional mutation of Pkd2 causes cystogenesis and upregulates beta-catenin. *Journal of the American Society of Nephrology : JASN* 20:2556-2569.
60. Goldberg, S., Adair-Kirk, T.L., Senior, R.M., and Miner, J.H. 2010. Maintenance of glomerular filtration barrier integrity requires laminin alpha5. *Journal of the American Society of Nephrology : JASN* 21:579-586.
61. Kim, J.C., Cook, M.N., Carey, M.R., Shen, C., Regehr, W.G., and Dymecki, S.M. 2009. Linking genetically defined neurons to behavior through a broadly applicable silencing allele. *Neuron* 63:305-315.
62. Wang, H., Yang, H., Shivalila, C.S., Dawlaty, M.M., Cheng, A.W., Zhang, F., and Jaenisch, R. 2013. One-Step Generation of Mice Carrying Mutations in Multiple Genes by CRISPR/Cas-Mediated Genome Engineering. *Cell* 153:910-918.
63. Wiedenheft, B., Sternberg, S.H., and Doudna, J.A. 2012. RNA-guided genetic silencing systems in bacteria and archaea. *Nature* 482:331-338.
64. Ishino, Y., Shinagawa, H., Makino, K., Amemura, M., and Nakata, A. 1987. Nucleotide sequence of the iap gene, responsible for alkaline phosphatase isozyme conversion in Escherichia coli, and identification of the gene product. *Journal of bacteriology* 169:5429-5433.
65. Mojica, F.J., Diez-Villasenor, C., Garcia-Martinez, J., and Soria, E. 2005. Intervening sequences of regularly spaced prokaryotic repeats derive from foreign genetic elements. *Journal of molecular evolution* 60:174-182.
66. Pourcel, C., Salvignol, G., and Vergnaud, G. 2005. CRISPR elements in Yersinia pestis acquire new repeats by preferential uptake of bacteriophage DNA, and provide additional tools for evolutionary studies. *Microbiology* 151:653-663.
67. Makarova, K.S., Grishin, N.V., Shabalina, S.A., Wolf, Y.I., and Koonin, E.V. 2006. A putative RNA-interference-based immune system in prokaryotes: computational analysis of the predicted enzymatic machinery, functional analogies with eukaryotic RNAi, and hypothetical mechanisms of action. *Biology direct* 1:7.
68. Rousseau, C., Gonnet, M., Le Romancer, M., and Nicolas, J. 2009. CRISPI: a CRISPR interactive database. *Bioinformatics* 25:3317-3318.
69. Kunin, V., Sorek, R., and Hugenholtz, P. 2007. Evolutionary conservation of sequence and secondary structures in CRISPR repeats. *Genome biology* 8:R61.
70. Barrangou, R., Fremaux, C., Deveau, H., Richards, M., Boyaval, P., Moineau, S., Romero, D.A., and Horvath, P. 2007. CRISPR provides acquired resistance against viruses in prokaryotes. *Science* 315:1709-1712.
71. Garneau, J.E., Dupuis, M.E., Villion, M., Romero, D.A., Barrangou, R., Boyaval, P., Fremaux, C., Horvath, P., Magadan, A.H., and Moineau, S. 2010. The CRISPR/Cas bacterial immune system cleaves bacteriophage and plasmid DNA. *Nature* 468:67-71.

72. Brouns, S.J., Jore, M.M., Lundgren, M., Westra, E.R., Slijkhuis, R.J., Snijders, A.P., Dickman, M.J., Makarova, K.S., Koonin, E.V., and van der Oost, J. 2008. Small CRISPR RNAs guide antiviral defense in prokaryotes. *Science* 321:960-964.
73. Gasiunas, G., Barrangou, R., Horvath, P., and Siksnys, V. 2012. Cas9-crRNA ribonucleoprotein complex mediates specific DNA cleavage for adaptive immunity in bacteria. *Proceedings of the National Academy of Sciences of the United States of America* 109:E2579-2586.
74. Jinek, M., Chylinski, K., Fonfara, I., Hauer, M., Doudna, J.A., and Charpentier, E. 2012. A programmable dual-RNA-guided DNA endonuclease in adaptive bacterial immunity. *Science* 337:816-821.
75. Deltcheva, E., Chylinski, K., Sharma, C.M., Gonzales, K., Chao, Y., Pirzada, Z.A., Eckert, M.R., Vogel, J., and Charpentier, E. 2011. CRISPR RNA maturation by trans-encoded small RNA and host factor RNase III. *Nature* 471:602-607.
76. Cho, S.W., Kim, S., Kim, J.M., and Kim, J.S. 2013. Targeted genome engineering in human cells with the Cas9 RNA-guided endonuclease. *Nature biotechnology* 31:230-232.
77. Chang, N., Sun, C., Gao, L., Zhu, D., Xu, X., Zhu, X., Xiong, J.W., and Xi, J.J. 2013. Genome editing with RNA-guided Cas9 nuclease in zebrafish embryos. *Cell research* 23:465-472.
78. Shen, B., Zhang, J., Wu, H., Wang, J., Ma, K., Li, Z., Zhang, X., Zhang, P., and Huang, X. 2013. Generation of gene-modified mice via Cas9/RNA-mediated gene targeting. *Cell research* 23:720-723.
79. Draper, J.S., and Nagy, A. 2007. Improved embryonic stem cell technologies. *Handbook of experimental pharmacology*:107-128.
80. Hauser, P.V., Pippin, J.W., Kaiser, C., Krofft, R.D., Brinkkoetter, P.T., Hudkins, K.L., Kerjaschki, D., Reiser, J., Alpers, C.E., and Shankland, S.J. 2010. Novel siRNA delivery system to target podocytes in vivo. *PloS one* 5:e9463.
81. Wan, X., Fan, L., Hu, B., Yang, J., Li, X., Chen, X., and Cao, C. 2011. Small interfering RNA targeting IKKbeta prevents renal ischemia-reperfusion injury in rats. *American journal of physiology. Renal physiology* 300:F857-863.
82. Sproul, A., Steele, S.L., Thai, T.L., Yu, S., Klein, J.D., Sands, J.M., and Bell, P.D. 2011. N-methyl-D-aspartate receptor subunit NR3a expression and function in principal cells of the collecting duct. *American journal of physiology. Renal physiology* 301:F44-54.
83. Henriksen, J.R., Haug, B.H., Buechner, J., Tomte, E., Lokke, C., Flaegstad, T., and Einvik, C. 2011. Conditional expression of retrovirally delivered anti-MYCN shRNA as an in vitro model system to study neuronal differentiation in MYCN-amplified neuroblastoma. *BMC developmental biology* 11:1.
84. Veron, D., Villegas, G., Aggarwal, P.K., Bertuccio, C., Jimenez, J., Velazquez, H., Reidy, K., Abrahamson, D.R., Moeckel, G., Kashgarian, M., et al. 2012. Acute podocyte vascular endothelial growth factor (VEGF-A) knockdown disrupts alphaVbeta3 integrin signaling in the glomerulus. *PloS one* 7:e40589.
85. Okamoto, K., Tokunaga, K., Doi, K., Fujita, T., Suzuki, H., Katoh, T., Watanabe, T., Nishida, N., Mabuchi, A., Takahashi, A., et al. 2011. Common variation in GPC5 is associated with acquired nephrotic syndrome. *Nature genetics* 43:459-463.

86. Premsrirut, P.K., Dow, L.E., Kim, S.Y., Camiolo, M., Malone, C.D., Miething, C., Scuoppo, C., Zuber, J., Dickins, R.A., Kogan, S.C., et al. 2011. A rapid and scalable system for studying gene function in mice using conditional RNA interference. *Cell* 145:145-158.
87. Lindvall, T., Karlsson, J., Holmdahl, R., and Andersson, A. 2009. Dissection of a locus on mouse chromosome 5 reveals arthritis promoting and inhibitory genes. *Arthritis research & therapy* 11:R10.
88. Papeta, N., Chan, K.T., Prakash, S., Martino, J., Kiryluk, K., Ballard, D., Bruggeman, L.A., Frankel, R., Zheng, Z., Klotman, P.E., et al. 2009. Susceptibility loci for murine HIV-associated nephropathy encode trans-regulators of podocyte gene expression. *The Journal of clinical investigation* 119:1178-1188.
89. Jacob, T., Hemavathy, K., Jacob, J., Hingorani, A., Marks, N., and Ascher, E. 2011. A nanotechnology-based delivery system: Nanobots. Novel vehicles for molecular medicine. *The Journal of cardiovascular surgery* 52:159-167.
90. Lehto, T., Simonson, O.E., Mager, I., Ezzat, K., Sork, H., Copolovici, D.M., Viola, J.R., Zaghloul, E.M., Lundin, P., Moreno, P.M., et al. 2011. A peptide-based vector for efficient gene transfer in vitro and in vivo. *Molecular therapy : the journal of the American Society of Gene Therapy* 19:1457-1467.
91. Song, S., Shen, Z., Chen, L., Brayman, A.A., and Miao, C.H. 2011. Explorations of high-intensity therapeutic ultrasound and microbubble-mediated gene delivery in mouse liver. *Gene therapy* 18:1006-1014.
92. Holt, N., Wang, J., Kim, K., Friedman, G., Wang, X., Taupin, V., Crooks, G.M., Kohn, D.B., Gregory, P.D., Holmes, M.C., et al. 2010. Human hematopoietic stem/progenitor cells modified by zinc-finger nucleases targeted to CCR5 control HIV-1 in vivo. *Nature biotechnology* 28:839-847.
93. Lombardo, A., Genovese, P., Beausejour, C.M., Colleoni, S., Lee, Y.L., Kim, K.A., Ando, D., Urnov, F.D., Galli, C., Gregory, P.D., et al. 2007. Gene editing in human stem cells using zinc finger nucleases and integrase-defective lentiviral vector delivery. *Nature biotechnology* 25:1298-1306.
94. Keng, V.W., Ryan, B.J., Wangensteen, K.J., Balciunas, D., Schmedt, C., Ekker, S.C., and Largaespada, D.A. 2009. Efficient transposition of Tol2 in the mouse germline. *Genetics* 183:1565-1573.
95. Mates, L., Chuah, M.K., Belay, E., Jerchow, B., Manoj, N., Acosta-Sanchez, A., Grzela, D.P., Schmitt, A., Becker, K., Matrai, J., et al. 2009. Molecular evolution of a novel hyperactive Sleeping Beauty transposase enables robust stable gene transfer in vertebrates. *Nature genetics* 41:753-761.
96. Nagy, K., Sung, H.K., Zhang, P., Laflamme, S., Vincent, P., Agha-Mohammadi, S., Woltjen, K., Monetti, C., Michael, I.P., Smith, L.C., et al. 2011. Induced pluripotent stem cell lines derived from equine fibroblasts. *Stem cell reviews* 7:693-702.
97. Wang, W., Lin, C., Lu, D., Ning, Z., Cox, T., Melvin, D., Wang, X., Bradley, A., and Liu, P. 2008. Chromosomal transposition of PiggyBac in mouse embryonic stem cells. *Proceedings of the National Academy of Sciences of the United States of America* 105:9290-9295.
98. Woltjen, K., Michael, I.P., Mohseni, P., Desai, R., Mileikovsky, M., Hamalainen, R., Cowling, R., Wang, W., Liu, P., Gertsenstein, M., et al. 2009. piggyBac

transposition reprograms fibroblasts to induced pluripotent stem cells. *Nature* 458:766-770.

Chapter 2 Genetic mapping approaches in mouse

1 Introduction

The mouse is the most widely used model organism to study gene function in development, normal and in disease states. Most of our current knowledge has been derived from reverse genetics where the function of a gene is dissected by altering expression of the gene. As discussed in chapter 1, forward genetics is a complimentary, phenotype-driven approach where the researcher does not have any prior knowledge of the gene of interest nor the molecular pathway involved. Forward genetics generate phenotypic variants. The challenge is to identify causal genetic variation that leads to the observed phenotype. The process requires a separate set of tools to "map" the phenotype onto a genomic region or even a gene. Here we provide a brief review on current technologies used in mapping with a particular focus on the mouse.

2 Linkage maps for quantitative trait loci (QTL)

Assuming each animal within an inbred mouse strain carries a completely identical set of genetic information, by virtue of coding sequences, introns that may affect splicing or regulate gene expression, methylation, and RNA regulation, to name a few, then linkage maps can be created to capture a segment of the genome that is responsible for the phenotypic variants observed in F1 generated by conventional cross between two inbred strains. Genetic linkage refers to the observation that genes that are in close proximity tend to inherit together during meiosis hence they are genetically linked(1). The recombination or crossover events during meiosis between two genes is a by-and-large a function of their physical separation, although this is not always true as some genes tend to be linked more so than others. Therefore, the distance between two genes can be expressed in terms of a centimorgan, rather than the actual physical distance, where 1 centimorgan represents a recombinant frequency of 1%(2). Linkage disequilibrium describes genes or genetic markers that are non-randomly associated and occur more frequently than expected based on random genetic assortment. Linkage disequilibrium can be observed not only among genes or genetic markers in

close physical proximity, but also loci on different chromosome. A linkage map provides a compass of genes or genetic markers relative to each other based on their recombination frequency. Traditionally, linkage maps are essential in the identification of quantitative trait loci that harbor genes involved in complex traits, which are typically expressed in varying degree and in many instances involve interaction with the environment.

2.1 Phenotypic markers

Phenotype-based genetic markers were first introduced by Mendel in the nineteenth century. However, there are a few prerequisites for the purpose of linkage analysis. The phenotype(s) has to be robust, easily assessable, and ideally not affected by environment. In pleiotropic disorders, some phenotypes are easier to identify than others and can be used as phenotypic markers for the disorders such as cataract for Wolfram syndrome(3), tail nonpigmentation in mouse model of ataxia-telangiectasia(4), and looptail in Vangl2 mutation(5). In contrast, molecular markers at the level of the DNA offer more advantages. They are more stable, reproducible, detectable in all tissues, not confounded by environment, pleiotropic and epistatic effects(6). The common molecular markers used in genetic mapping are discussed in the section to follow.

2.2 Molecular markers

2.2.1 Microsatellite

Microsatellites are short repeating sequences of DNA between two to six base pairs and are also known as simple sequence repeats or short tandem repeats(7). They represent greater allelic diversity compared to bi-allelic SNPs. The variability of microsatellites is thought to be generated by mutation through slipped strand mispairing or slippage during DNA replication(8). The use of microsatellites in linkage studies have successfully identified association genes including TCF7L2 and gene loci 8q21 in type 2 diabetes and prostate cancer respectively(9). Minisatellites represent another form of variable number tandem repeat that involves 6 – 500 bp repeat units(10). There are more than 600000 variable number tandem repeats in the human genome,

less than that of SNPs (6-8 million)(10). Specific microsatellite markers are now freely available to researchers online. The Simple repeat annotation in the UCSC human genome browser is an online database for microsatellite. In addition UCSC in conjunction with Tandem Repeat Data Base (TRDB) detected by Tandem Repeat Finders (TRF) in Boston annotated over 20 species. For the laboratory mouse, Mouse Microsatellite Data Base of Japan provides microsatellite data has identified 1223 markers in 22 strains. Furthermore, researchers can search for microsatellites at a particular locus of interest on the genome using online tools such as RepeatMasker that screens DNA sequence for interspersed repeats and low complexity DNA sequences. In addition to representing areas of polymorphism valuable for genetic mapping, microsatellites may act as functional elements binding transcription factors or other promoter or inhibitory proteins, as well as motif elements changing the efficiency of mRNA splicing(10). In the yeasts, many mono- and dinucleotide repeats are found in the 3' untranslated region and intron where they may involve in exon shuffling and gene conversion(11). In contrast, in humans, the effect of these repeats on the function and expression of genes is less clear. However, it is been established that microsatellite instability is not always innocuous as many unstable repeats such as CAG triplet repeats within transcribed region are found to be pathological involving a host of disorders such as neurodegenerative diseases(12, 13).

Microsatellites with repeats equal to or greater than 10 exerts high level of specificity for polymorphism and are ideal as molecular markers(14). Microsatellites are currently analyzed by PCR and can be detected using various methods including size separation by capillary electrophoresis, fluorescently(15) or radio-labeled primers. Genome-wide scan can be produced with a set or microsatellite markers across the entire genome. The main advantage of microsatellite is its high heterozygosity. However, microsatellite instability can lead to mutation within a generation and cause problem with allelic association. Microsatellite experiments also tend to be more costly compared to SNPs. In addition, where available, SNPs markers are more abundant for better genome-wide coverage and can be performed in a high throughput manner.

2.2.2 Single nucleotide polymorphisms

Single nucleotide polymorphism or SNP is a variation in DNA sequence based on a single nucleotide and often found in non-coding and intergenic regions. When found in the coding region, these SNPs can either be synonymous that does not change the amino acid sequence due to redundancy of the genetic code or non-synonymous where an alteration in amino acid sequence ensues. SNPs in the non-coding region may still affect transcription and splicing. The attribution of various SNPs in health and disease process is beyond the scope of the current review. I will now focus the rest of the discussion on its utility in linkage studies.

Several international efforts to curate data on SNPs including the National Center for Biotechnology Information (NCBI), the International SNP Map working group and the International HapMap Project have provided an expansion of data for genetic studies on human and model animals. The genome coordinates for over 80 inbred mouse strains derived from NCBI and can be conveniently retrieved through the Mouse Genome Informatics (MGI) website. SNPs are the most abundant markers in the genome averaging 1 SNP per 1000 bp(16). Millions of SNPs have been identified in the mouse genome(17) and 30 million in cattle. This development has greatly enhanced the design of high throughput SNP arrays by various companies including Affymetrix and Illumina. High throughput genotyping methods include DNA chips, allele-specific PCR and primer extension approaches. The new Affymetrix SNP Array 6.0 for instance features 1.8 million human genetic markers including more than 900000 SNPs and more than 940000 probes for detection of copy number variations. In mouse, the average density of SNPs array varies between 1500 to 5000 SNPs with a mapping resolution as little as 1 cM (averaging 2 Mb), but arrays covering more than 600000 SNPs and 900000 probes for copy number variations are also available. Compared to microsatellite, SNPs offer better resolution due to higher density coverage and coverage for regions such as telomeres that are traditionally underrepresented by microsatellite markers(18), lower genotyping error rates, automation for high throughput, and lower mutation rate compared to microsatellites.

2.2.3 Other: RAPDs, AFLPs

Numerous molecular markers are now available including RAPD, AFLP and STS. Others include restriction fragment length polymorphism, single strand conformation polymorphism, and target region amplification polymorphism, etc. In RAPD, using short random oligonucleotide sequences, genomic DNA is differentially amplified and deduces rearrangements or deletions at or between the universal primer binding sites within the genome(19). Although it is abundant and relatively easy to perform, it lacks specificity, profiling is dependent on the reaction conditions and may not be reproducible, and it does not differentiate between heterozygous and homozygous allele. In contrast, AFLP was developed to improve reproducibility(20). In AFLP, genomic DNA is digested by restriction enzymes followed by ligation with primer-recognition sequences or adaptors, which are subsequent PCR amplified with a limited set of primers.

2.3 Meiotic recombination

Meiotic recombination is the essential process that generates genetic diversity. Meiosis produces daughter cells with distinct assortment of allelic compositions that differ from their parents. During prophase I of meiosis, tetrad consisting of four chromatids are in close proximity with each other which facilitates homologous recombination or crossover between non-sister chromatids, results in shuffling of maternal and paternal genomes(21). Recombination initiates early during prophase I by DNA double strand breaks (DSB). Stable homolog alignment and chromosome synapsis require DNA DSBs generated by SPO11 topoisomerase(22). During recombination, these double strand breaks are repaired by crossover or non-crossover repair pathways(21). Crossover repairs lead to formation of chiasmata, which are crucial for accurate alignment and segregation of the homologous chromosomes during metaphase I(21). In the context of linkage studies where a phenotype is mapped to a certain region flanked by molecular markers, these spontaneous crossover events are invaluable for fine mapping and narrowing the list of candidate genes(23-25).

3 Sequencing technology

DNA sequencing is a critical development in molecular biology where the exact nucleotide arrangements/orders of a DNA fragment is made available. In this section, I will review advances made in sequencing technologies from the gold standard Sanger sequencing to the new high throughput next-generation sequencing technology. The sequencing technology was first developed independently in the 1970's by Sanger and colleagues(26), and Maxam and Gilbert(27). Sanger and Maxam shared the Nobel Prize for chemistry for their contributions concerning the determination of base sequences in nucleic acids in 1980. However, Sanger sequencing is widely adopted due to its practicality.

3.1 Sanger

Sanger sequencing is also referred to as dideoxy sequencing or chain termination. Dideoxynucleotides, unlike naturally occurring nucleotides, contain a hydrogen group on the 3' carbon rather than a hydroxyl group, and when incorporated into a sequence during PCR reaction terminates the extension of the DNA fragment by preventing addition of further nucleotide. This occurs because a hydroxyl group is necessary form a phosphodiester bond between the last nucleotide and the next incoming nucleotide. The process begins with a primer with the 3' end is located next to the DNA sequence of interest, the solution is then divided into 4 tubes with each tube containing regular dNTP's and labeled dideoxynucleotide: G, A, T, and C at a much lower concentration (dideoxynucleotide:dNTP = 1:100). Both radio and fluorescence labeling can be used. These dideoxynucleotides will be randomly integrated into the growing chains by DNA polymerase and terminate the reactions at different stages of extension. When the chain of DNA is being synthesized numerous times, the synthesized chains will terminate at each position of the template DNA and results in bands of all different lengths. Upon completion of amplification, the four reaction tubes are then loaded into a polyacrylamide gel and run on four separate lanes. The products are separated based on the length of the chains and with the knowledge of the specific dideoxynucleotide used, one can then reconstruct the DNA sequence of the original template. This method was automated when all four dideoxynucleotides are

added in a single reaction, where each dideoxynucleotide is labeled with a different color fluorescent dye that can be identified by laser and output in the form of a chromatogram. Newer generation fluorescent dyes minimize dideoxynucleotide incorporation variability and hence produce more even data peaks.

3.2 Maxam-Gilbert

This method radiolabels 5' end of the DNA fragment of interest and uses chemical treatment to generate breaks at the end labeled DNA strand at the following bases: G, A+G, C, and C+T in 4 individual reactions, which are then separated by electrophoresis in a high resolution polyacrylamide gel based on size and detected by autoradiography. Dimethyl sulphate selectively breaks purines whereas hydrazine for pyrimidines at the glycosidic bond between the ribose sugar and the base. Because the procedure orders the fragment based on their sizes, the sequence of the DNA fragment can then be deduced.

3.3 Next generation sequencing

Sequencing large fragments of genomic DNA became a reality with the invention of Sanger sequencing and whole genome shotgun approach where DNA were randomly broken into smaller fragments (100 – 1000 bp) and sequenced by chain termination was attempted as early as late 1970's(28). Over the next few decades, whole genome shotgun became more feasible as Sanger capillary sequencing became higher throughput. Breakthrough in sequencing technologies led to the development of the so-called next-generation technology with substantial improvement in throughput and for the first time enabling more efficient and economic sequencing that led to de novo assemblies of the panda(29) and turkey(30) genomes. The costs of sequencing are now 10000-times less per base compared to conventional Sanger capillary sequencing!

The first next-generation machine was produced in 2005. GS20 by 454 Life Sciences developed a large-scale parallel pyrosequencing system where nebulized and adapter-ligated DNA fragments are fixed to small DNA-capture beads in a water-in-oil

emulsion(31). The technology is based on sequencing by synthesis and the DNA fixed to the beads is amplified by PCR where light produced in luciferase-catalyzed reaction secondary to the release of pyrophosphate upon nucleotide incorporation is detected. The newer GS FLX Titanium XL claims an average read length of 700 bp based on the manufacture specificities. It has a mean error rage of 1.07%, higher in certain areas including presence of homopolymers(32). In contrast, the Genome Analyzer introduced to the market by Illumina in 2007 was characterized by much shorter reads. This technology is based on reversible dye terminators. DNA molecules are attached to primers on a slide and amplified to form local colonies. Four types of fluorescent-labeled reversible terminate bases are added and randomly incorporated into the extending PCR product(33). After each synthesis, laser is used to remove the 3' terminal blocking group, which is then identified through specific fluorescence emission. Read lengths have increased from original 35 bp to 100 bp with 600 Gb throughput with HiSeq 2500. The main advantage of this platform is high sequence yield. Another next-generation sequencing platform employs sequencing by ligation, developed by Life Technologies. The SOLiD™ system, unlike the previous two platforms, does not employ sequencing by synthesis, rather relies on the sensitivity of DNA ligase for base pairing mismatches(34). Targeted DNA is sheared into smaller fragments, and adaptors are ligated to the ends of the fragments producing a library with millions of molecules representing the entire target sequence. Each molecule is then clonally amplified onto beads in an emulsion PCR reaction. The beads are then covalently attached to glass slide allowing the interaction of the beads with universal primers, and fluorescent-labeled di-base probe. Probes with base matching the unknown sequence are preferentially ligated which hybridizes to the template sequences emitting fluorescence for identification. The dye is then cleaved off, leaving a 5' phosphate free end for further reaction. This process is repeated for multiple cycles. This platform is less costly per base, produces shorter read lengths, and slower than the previous two platforms. The third-generation technologies, including single-molecule real-time sequencing and ion semiconductor sequencing, boast even lower costs but may be plagued by higher error rates. To reduce costs, an alternative for re-sequencing is the utility of whole-exome re-sequencing. The genomic regions of

interest are selectively captured through target-enrichment strategies including molecular inversion probes, in-solution capture, and hybrid capture. In hybrid capture, microarrays containing single-stranded oligonucleotides with sequences from the model genome are designed. The sample DNA is then sheared into fragments and then end-repaired to form blunt ends and adaptors with universal priming sequences. They are then hybridized to the oligos on the microarray and then amplified using PCR(35). Many commercially available enrichment kits are available for both humans and mouse such as Agilent SureSelect.

The development of next-generation sequencing makes it possible to sequence the whole-genome in a high throughput manner. This technology has successfully identified many mutations in the mouse including *Ptf1a* for Danforth's short tail(36). However, the technology is not perfect and poses the following challenges to the researchers including: challenges in assembly and alignment such as read errors, genomic regions that are under-represented, detection of copy number variation, requirement for larger coverage (usually 30X) due to shorter reads (compared to 3X for Sanger reads). For the purpose of re-sequencing to identify candidate genetic variants for a specific phenotype of interest, each SNP or Indel called has to be confirmed by traditional Sanger sequencing. This step can be labor intensive especially when the genomic region of interest is large. Finally, the ultimate challenge is to ascribe causality between genetic variant and observed phenotypic variant.

4 Mouse GWAS

Until recently, genetic cross is the main strategy to identify sequence variants that contribute to phenotypic variation in mice. However, one of the main disadvantages of this strategy is the yielding of large QTL regions containing tens of megabases and hundreds of genes. This significantly impedes on the ease and time required to identify the causal genetic variant and therefore making the exercise labor intensive and very costly. However, one prudent advantage of using the mouse as a model animal is that in a genetic cross only a few hundred animals are required to identify loci that together explain 50% or more of the phenotypic variance for a

particular trait(37). This contrast experiences with human GWAS, where tens of thousands of subjects are required to identify loci that are involved in traits, which only explain a small fraction of phenotypic variance(38). Newer strategies are being developed to compliment the traditional cross approach. This includes large scale breeding strategies, advances in microarray(39, 40) and sequencing(41) technologies. The Sanger Institute has recently completed sequencing 17 mouse genomes and discovered 71 million SNPs(42). The Jackson Laboratory together with the University of North Carolina developed the Mouse Diversity Array for high-density genotyping based on over 600000 SNPs present in the laboratory mouse(43).

4.1 Large-scale breeding strategies

In an effort to generate inbred strains for genetic studies, four strategies have been employed and will be briefly discussed in the following paragraphs.

F2 generation cross: In this approach, two parental inbred strains are crossed to generate F1 strains. The F1 strains are subsequently either mated with each other, also known as intercross, or mated with one of the parental strains, also known as backcross, to generate F2 offspring.

Recombinant inbred strains: To further the traditional F2 generation cross as discussed above, sibling mating F2 intercross for at least 20 generations produces fully new inbred strain containing genetic materials from both the two original strains. This recombinant inbred strain is characterized by identical genetic make up in each offspring and hence abrogating the need to genotype them as their genotypes are available in publically accessible domains.

The Collaborative Cross project(44): This project involves the generation of recombinant inbred strains based on eight parental strains. The resultant inbred strains are characterized by about equal ancestry from each of the eight parental strain. Again because these mice are bred until they are fully inbred, their complete genotype is freely available.

Heterogeneous stock: They represent outbred offspring of eight parental strains and contain unique genetic make up making it necessary to genotype each animal.

4.2 Mapping strategies for GWAS

In general, there are five general strategies including the classical inbred strain association, the Hybrid Mouse Diversity Panel (HMDP), the Collaborative Cross, and outbred stocks.

In the classical inbred strain association, commonly used laboratory mouse strains with known SNPs are used. For example, in an effort to identify the genetic loci for high-density lipoprotein, of HDL, genotypes from forty-eight inbred mouse strains were used and successfully identified eleven distinct loci(45). The inbred strains association provides a higher mapping resolution than genetic cross owing to their genetic distance from their founders, which allows more recombination events and increases the resolution by reducing the critical region to as little as 2 Mb(45). Further, this strategy also offers the following advantages. It does require breeding, unlike the classical cross and greatly reduced the time required to generate data. Since, a larger number of inbred strains are used compared to two, and this translates into a much greater variation particularly valuable for assessment of complex disease loci. The data generated is reproducible because each laboratory mouse used within each inbred strain has identical genetic make up. Each mouse is homozygous at each locus, which increases the power of association for recessive loci. The availability of certain phenotypic characterization of inbred mouse strains through the Mouse Phenome Project developed by the Jackson Laboratory provides additional invaluable research tools(46, 47). One major problem with the use of the inbred strains association is that the quality of the association is dependent on the population structure based on the inbred strains used. With the current commercially available inbred strains, the degree of their relatedness are unfortunately not far enough to identify association to the level of the gene(48) and more often than not problematically provides false positives due to

spurious associations(49-52) after correcting for population structure using efficient mixed-model association (EMMA).

To address the lack of power for GWAS that plagued the classical inbred strain association, addition of seventy recombinant inbred strains in the mapping panel by the HMDP approach provides a much greater statistical power(49). Typically 30 inbred mouse strains are used in combination with 70 recombinant inbred strains. This gives an 80% power to detect loci that account for approximately 5% of the variance of the trait. Successes with this approach include the mapping of apolipoprotein A2 in HDL(49) and the identification of a gene network specific to the osteoblast-lineage(53).

The Collaborative Cross (CC) as described earlier in the section of “large-scale breeding strategies” consists of generating new inbred strains based on eight founder strains where five of the founders are classical inbred strains and the remaining three are wild-derived strains. The use of wild-derived strains greatly enhances variance and corrects for population structure. The CC consists of hundreds of independently bred octo-parental recombinant inbred lines. Although the final CC strains are not yet available, researchers have used pre-CC (incompletely inbred) to map hematological phenotypes(54), and to identify a novel allele in the myxovirus resistance 1(Mx1) gene that increases susceptibility to influenza infection(55).

Outbred stocks provide the genetic diversity and minimize the effect of population structure. However, the main disadvantage is that each animal used is genetically distinct and requires genotyping. Heterogeneous stock specifically refers to the animals descended from eight classical inbred founder strains including A/J, AKR/J, BALB/cJ, C3H/MeJ, C57BL/6J, CBA/J, DBA/2J, and LP/J(56). Diversity Outbred mice consist of animals generated from the eight CC founder strains including AJ, C57BL/6, 129S/1, NOD, NZO, PWK, CAST, and WSB(57). Alternatively, there exists commercially available outbred stocks that have been used in validation studies with peak associations within 500 kb of the causal variant(58).

4.3 Confirming causality

There are a few ways to prove confirm a gene variant in contributing to a complex trait and they include reciprocal hemizygosity that involves the generation of F1 strains with the allelic variant and deletion of the gene on the homologous chromosome mainly in the yeast literature(59); quantitative complementation that involves a pair of strains carrying different alleles at the locus and breeding with a knockout strain for the gene and the background strain used in the knockout(60); resequencing candidate genes and look for enrichment of rare variants relative to controls(61, 62); generation of congenic strains(63-66) where recombinant between two inbred strains are backcrossed to produce a strain that carries a single genomic segment from one strain on the genetic background of the other. They are usually generated in the process of fine mapping the critical region. When combined with gene expression assays, one might narrow down the number of potential genes(67, 68).

5 Summary

The identification of a genetic locus for a phenotypic variant generated by forward genetics can be a challenging task. Fortunately, with technological advancements, such a genome-wide SNPs, linkage maps with workable critical regions can be more easily identified; next-generation re-sequencing enables a quick in-depth examination at the sequence level. The main challenge, in my opinion, is to confirm causality between a genetic variant and the observed phenotypic variant. This is particularly challenging if the variant is in a non-coding region given our limited understanding in the genetics beyond the exons. Once causality is made, the researchers now face another challenging task of working out the molecular mechanisms that produce a certain phenotype of interest.

5 References:

1. Murray, J.C., Buetow, K.H., Weber, J.L., Ludwigsen, S., Scherpbier-Heddema, T., Manion, F., Quillen, J., Sheffield, V.C., Sunden, S., Duyk, G.M., et al. 1994. A comprehensive human linkage map with centimorgan density. Cooperative Human Linkage Center (CHLC). *Science* 265:2049-2054.
2. Jackson, J.A., and Fink, G.R. 1985. Meiotic recombination between duplicated genetic elements in Saccharomyces cerevisiae. *Genetics* 109:303-332.
3. Titah, S.M., Meunier, I., Blanchet, C., Lopez, S., Rondouin, G., Lenaers, G., Amati-Bonneau, P., Reynier, P., Paquis-Flucklinger, V., and Hamel, C.P. 2012. Cataract as a phenotypic marker for a mutation in WFS1, the Wolfram syndrome gene. *European journal of ophthalmology* 22:254-258.
4. Hibma, J.C., Neufeld, D.A., Halaby, M.J., and Yang, D.Q. 2007. A novel phenotypic marker for ATM-deficient 129S6/SvEvTac-ATMtm1Awb/J mice. *Anatomical record* 290:243-250.
5. Torban, E., Patenaude, A.M., Leclerc, S., Rakowiecki, S., Gauthier, S., Andelfinger, G., Epstein, D.J., and Gros, P. 2008. Genetic interaction between members of the Vangl family causes neural tube defects in mice. *Proceedings of the National Academy of Sciences of the United States of America* 105:3449-3454.
6. Agarwal, M., Shrivastava, N., and Padh, H. 2008. Advances in molecular marker techniques and their applications in plant sciences. *Plant cell reports* 27:617-631.
7. Tautz, D., and Renz, M. 1984. Simple sequences are ubiquitous repetitive components of eukaryotic genomes. *Nucleic acids research* 12:4127-4138.
8. Schlotterer, C., and Tautz, D. 1992. Slippage synthesis of simple sequence DNA. *Nucleic acids research* 20:211-215.
9. Gulcher, J. 2012. Microsatellite markers for linkage and association studies. *Cold Spring Harbor protocols* 2012:425-432.
10. Breen, G. 2010. Practical informatics approaches to microsatellite and variable number tandem repeat analysis. *Methods in molecular biology* 628:181-194.
11. Gendrel, C.G., Boulet, A., and Dutreix, M. 2000. (CA/GT)(n) microsatellites affect homologous recombination during yeast meiosis. *Genes & development* 14:1261-1268.
12. Nelson, D.L., Orr, H.T., and Warren, S.T. 2013. The unstable repeats--three evolving faces of neurological disease. *Neuron* 77:825-843.
13. Bowater, R.P., and Wells, R.D. 2001. The intrinsically unstable life of DNA triplet repeats associated with human hereditary disorders. *Progress in nucleic acid research and molecular biology* 66:159-202.
14. Queller, D.C., Strassmann, J.E., and Hughes, C.R. 1993. Microsatellites and kinship. *Trends in ecology & evolution* 8:285-288.
15. Wenz, H., Robertson, J.M., Menchen, S., Oaks, F., Demorest, D.M., Scheibler, D., Rosenblum, B.B., Wike, C., Gilbert, D.A., and Efcavitch, J.W. 1998. High-precision genotyping by denaturing capillary electrophoresis. *Genome research* 8:69-80.
16. Sachidanandam, R., Weissman, D., Schmidt, S.C., Kakol, J.M., Stein, L.D., Marth, G., Sherry, S., Mullikin, J.C., Mortimore, B.J., Willey, D.L., et al. 2001. A

map of human genome sequence variation containing 1.42 million single nucleotide polymorphisms. *Nature* 409:928-933.
17. Frazer, K.A., Eskin, E., Kang, H.M., Bogue, M.A., Hinds, D.A., Beilharz, E.J., Gupta, R.V., Montgomery, J., Morenzoni, M.M., Nilsen, G.B., et al. 2007. A sequence-based variation map of 8.27 million SNPs in inbred mouse strains. *Nature* 448:1050-1053.
18. Kulathinal, R.J., Stevison, L.S., and Noor, M.A. 2009. The genomics of speciation in Drosophila: diversity, divergence, and introgression estimated using low-coverage genome sequencing. *PLoS genetics* 5:e1000550.
19. Williams, J.G., Kubelik, A.R., Livak, K.J., Rafalski, J.A., and Tingey, S.V. 1990. DNA polymorphisms amplified by arbitrary primers are useful as genetic markers. *Nucleic acids research* 18:6531-6535.
20. Vos, P., Hogers, R., Bleeker, M., Reijans, M., van de Lee, T., Hornes, M., Frijters, A., Pot, J., Peleman, J., Kuiper, M., et al. 1995. AFLP: a new technique for DNA fingerprinting. *Nucleic acids research* 23:4407-4414.
21. Bolcun-Filas, E., and Schimenti, J.C. 2012. Genetics of meiosis and recombination in mice. *International review of cell and molecular biology* 298:179-227.
22. Keeney, S., Giroux, C.N., and Kleckner, N. 1997. Meiosis-specific DNA double-strand breaks are catalyzed by Spo11, a member of a widely conserved protein family. *Cell* 88:375-384.
23. Super, H.J., Hasenkrug, K.J., Simmons, S., Brooks, D.M., Konzek, R., Sarge, K.D., Morimoto, R.I., Jenkins, N.A., Gilbert, D.J., Copeland, N.G., et al. 1999. Fine mapping of the friend retrovirus resistance gene, Rfv3, on mouse chromosome 15. *Journal of virology* 73:7848-7852.
24. Moen, C.J., Groot, P.C., Hart, A.A., Snoek, M., and Demant, P. 1996. Fine mapping of colon tumor susceptibility (Scc) genes in the mouse, different from the genes known to be somatically mutated in colon cancer. *Proceedings of the National Academy of Sciences of the United States of America* 93:1082-1086.
25. Snoek, M., Groot, P.C., Spies, T., Campbell, R.D., and Demant, P. 1991. Fine mapping of the crossover-sites in the C4-H-2D region of H-2 recombinant mouse strains. *Immunogenetics* 34:409-412.
26. Sanger, F., and Coulson, A.R. 1975. A rapid method for determining sequences in DNA by primed synthesis with DNA polymerase. *Journal of molecular biology* 94:441-448.
27. Maxam, A.M., and Gilbert, W. 1977. A new method for sequencing DNA. *Proceedings of the National Academy of Sciences of the United States of America* 74:560-564.
28. Staden, R. 1979. A strategy of DNA sequencing employing computer programs. *Nucleic acids research* 6:2601-2610.
29. Li, R., Fan, W., Tian, G., Zhu, H., He, L., Cai, J., Huang, Q., Cai, Q., Li, B., Bai, Y., et al. 2010. The sequence and de novo assembly of the giant panda genome. *Nature* 463:311-317.
30. Dalloul, R.A., Long, J.A., Zimin, A.V., Aslam, L., Beal, K., Blomberg Le, A., Bouffard, P., Burt, D.W., Crasta, O., Crooijmans, R.P., et al. 2010. Multi-platform next-generation sequencing of the domestic turkey (Meleagris gallopavo): genome assembly and analysis. *PLoS biology* 8.

31. Binladen, J., Gilbert, M.T., Bollback, J.P., Panitz, F., Bendixen, C., Nielsen, R., and Willerslev, E. 2007. The use of coded PCR primers enables high-throughput sequencing of multiple homolog amplification products by 454 parallel sequencing. *PloS one* 2:e197.
32. Gilles, A., Meglecz, E., Pech, N., Ferreira, S., Malausa, T., and Martin, J.F. 2011. Accuracy and quality assessment of 454 GS-FLX Titanium pyrosequencing. *BMC genomics* 12:245.
33. Liu, L., Li, Y., Li, S., Hu, N., He, Y., Pong, R., Lin, D., Lu, L., and Law, M. 2012. Comparison of next-generation sequencing systems. *Journal of biomedicine & biotechnology* 2012:251364.
34. Koboldt, D.C., Larson, D.E., Chen, K., Ding, L., and Wilson, R.K. 2012. Massively parallel sequencing approaches for characterization of structural variation. *Methods in molecular biology* 838:369-384.
35. Turner, E.H., Ng, S.B., Nickerson, D.A., and Shendure, J. 2009. Methods for genomic partitioning. *Annual review of genomics and human genetics* 10:263-284.
36. Vlangos, C.N., Siuniak, A.N., Robinson, D., Chinnaiyan, A.M., Lyons, R.H., Jr., Cavalcoli, J.D., and Keegan, C.E. 2013. Next-generation sequencing identifies the Danforth's short tail mouse mutation as a retrotransposon insertion affecting Ptf1a expression. *PLoS genetics* 9:e1003205.
37. Burke, D.T., Kozloff, K.M., Chen, S., West, J.L., Wilkowski, J.M., Goldstein, S.A., Miller, R.A., and Galecki, A.T. 2012. Dissection of complex adult traits in a mouse synthetic population. *Genome research* 22:1549-1557.
38. Manolio, T.A., Collins, F.S., Cox, N.J., Goldstein, D.B., Hindorff, L.A., Hunter, D.J., McCarthy, M.I., Ramos, E.M., Cardon, L.R., Chakravarti, A., et al. 2009. Finding the missing heritability of complex diseases. *Nature* 461:747-753.
39. Gunderson, K.L., Steemers, F.J., Lee, G., Mendoza, L.G., and Chee, M.S. 2005. A genome-wide scalable SNP genotyping assay using microarray technology. *Nature genetics* 37:549-554.
40. Matsuzaki, H., Dong, S., Loi, H., Di, X., Liu, G., Hubbell, E., Law, J., Berntsen, T., Chadha, M., Hui, H., et al. 2004. Genotyping over 100,000 SNPs on a pair of oligonucleotide arrays. *Nature methods* 1:109-111.
41. Bentley, D.R., Balasubramanian, S., Swerdlow, H.P., Smith, G.P., Milton, J., Brown, C.G., Hall, K.P., Evers, D.J., Barnes, C.L., Bignell, H.R., et al. 2008. Accurate whole human genome sequencing using reversible terminator chemistry. *Nature* 456:53-59.
42. Keane, T.M., Goodstadt, L., Danecek, P., White, M.A., Wong, K., Yalcin, B., Heger, A., Agam, A., Slater, G., Goodson, M., et al. 2011. Mouse genomic variation and its effect on phenotypes and gene regulation. *Nature* 477:289-294.
43. Yang, H., Ding, Y., Hutchins, L.N., Szatkiewicz, J., Bell, T.A., Paigen, B.J., Graber, J.H., de Villena, F.P., and Churchill, G.A. 2009. A customized and versatile high-density genotyping array for the mouse. *Nature methods* 6:663-666.
44. Churchill, G.A., Airey, D.C., Allayee, H., Angel, J.M., Attie, A.D., Beatty, J., Beavis, W.D., Belknap, J.K., Bennett, B., Berrettini, W., et al. 2004. The Collaborative Cross, a community resource for the genetic analysis of complex traits. *Nature genetics* 36:1133-1137.

45. Pletcher, M.T., McClurg, P., Batalov, S., Su, A.I., Barnes, S.W., Lagler, E., Korstanje, R., Wang, X., Nusskern, D., Bogue, M.A., et al. 2004. Use of a dense single nucleotide polymorphism map for in silico mapping in the mouse. *PLoS biology* 2:e393.
46. Hancock, J.M., Adams, N.C., Aidinis, V., Blake, A., Bogue, M., Brown, S.D., Chesler, E.J., Davidson, D., Duran, C., Eppig, J.T., et al. 2007. Mouse Phenotype Database Integration Consortium: integration [corrected] of mouse phenome data resources. *Mammalian genome : official journal of the International Mammalian Genome Society* 18:157-163.
47. Bogue, M.A., Grubb, S.C., Maddatu, T.P., and Bult, C.J. 2007. Mouse Phenome Database (MPD). *Nucleic acids research* 35:D643-649.
48. Kirby, A., Kang, H.M., Wade, C.M., Cotsapas, C., Kostem, E., Han, B., Furlotte, N., Kang, E.Y., Rivas, M., Bogue, M.A., et al. 2010. Fine mapping in 94 inbred mouse strains using a high-density haplotype resource. *Genetics* 185:1081-1095.
49. Bennett, B.J., Farber, C.R., Orozco, L., Kang, H.M., Ghazalpour, A., Siemers, N., Neubauer, M., Neuhaus, I., Yordanova, R., Guan, B., et al. 2010. A high-resolution association mapping panel for the dissection of complex traits in mice. *Genome research* 20:281-290.
50. Kang, H.M., Zaitlen, N.A., Wade, C.M., Kirby, A., Heckerman, D., Daly, M.J., and Eskin, E. 2008. Efficient control of population structure in model organism association mapping. *Genetics* 178:1709-1723.
51. Manenti, G., Galvan, A., Pettinicchio, A., Trincucci, G., Spada, E., Zolin, A., Milani, S., Gonzalez-Neira, A., and Dragani, T.A. 2009. Mouse genome-wide association mapping needs linkage analysis to avoid false-positive Loci. *PLoS genetics* 5:e1000331.
52. Payseur, B.A., and Place, M. 2007. Prospects for association mapping in classical inbred mouse strains. *Genetics* 175:1999-2008.
53. Calabrese, G., Bennett, B.J., Orozco, L., Kang, H.M., Eskin, E., Dombret, C., De Backer, O., Lusis, A.J., and Farber, C.R. 2012. Systems genetic analysis of osteoblast-lineage cells. *PLoS genetics* 8:e1003150.
54. Kelada, S.N., Aylor, D.L., Peck, B.C., Ryan, J.F., Tavarez, U., Buus, R.J., Miller, D.R., Chesler, E.J., Threadgill, D.W., Churchill, G.A., et al. 2012. Genetic analysis of hematological parameters in incipient lines of the collaborative cross. *G3* 2:157-165.
55. Ferris, M.T., Aylor, D.L., Bottomly, D., Whitmore, A.C., Aicher, L.D., Bell, T.A., Bradel-Tretheway, B., Bryan, J.T., Buus, R.J., Gralinski, L.E., et al. 2013. Modeling host genetic regulation of influenza pathogenesis in the collaborative cross. *PLoS pathogens* 9:e1003196.
56. Valdar, W., Solberg, L.C., Gauguier, D., Burnett, S., Klenerman, P., Cookson, W.O., Taylor, M.S., Rawlins, J.N., Mott, R., and Flint, J. 2006. Genome-wide genetic association of complex traits in heterogeneous stock mice. *Nature genetics* 38:879-887.
57. Svenson, K.L., Gatti, D.M., Valdar, W., Welsh, C.E., Cheng, R., Chesler, E.J., Palmer, A.A., McMillan, L., and Churchill, G.A. 2012. High-resolution genetic mapping using the Mouse Diversity outbred population. *Genetics* 190:437-447.

58. Zhang, W., Korstanje, R., Thaisz, J., Staedtler, F., Harttman, N., Xu, L., Feng, M., Yanas, L., Yang, H., Valdar, W., et al. 2012. Genome-wide association mapping of quantitative traits in outbred mice. *G3* 2:167-174.
59. Steinmetz, L.M., Sinha, H., Richards, D.R., Spiegelman, J.I., Oefner, P.J., McCusker, J.H., and Davis, R.W. 2002. Dissecting the architecture of a quantitative trait locus in yeast. *Nature* 416:326-330.
60. Long, A.D., Mullaney, S.L., Mackay, T.F., and Langley, C.H. 1996. Genetic interactions between naturally occurring alleles at quantitative trait loci and mutant alleles at candidate loci affecting bristle number in Drosophila melanogaster. *Genetics* 144:1497-1510.
61. Nejentsev, S., Walker, N., Riches, D., Egholm, M., and Todd, J.A. 2009. Rare variants of IFIH1, a gene implicated in antiviral responses, protect against type 1 diabetes. *Science* 324:387-389.
62. Rivas, M.A., Beaudoin, M., Gardet, A., Stevens, C., Sharma, Y., Zhang, C.K., Boucher, G., Ripke, S., Ellinghaus, D., Burtt, N., et al. 2011. Deep resequencing of GWAS loci identifies independent rare variants associated with inflammatory bowel disease. *Nature genetics* 43:1066-1073.
63. Wakeland, E., Morel, L., Achey, K., Yui, M., and Longmate, J. 1997. Speed congenics: a classic technique in the fast lane (relatively speaking). *Immunology today* 18:472-477.
64. Markel, P., Shu, P., Ebeling, C., Carlson, G.A., Nagle, D.L., Smutko, J.S., and Moore, K.J. 1997. Theoretical and empirical issues for marker-assisted breeding of congenic mouse strains. *Nature genetics* 17:280-284.
65. Shao, H., Sinasac, D.S., Burrage, L.C., Hodges, C.A., Supelak, P.J., Palmert, M.R., Moreno, C., Cowley, A.W., Jr., Jacob, H.J., and Nadeau, J.H. 2010. Analyzing complex traits with congenic strains. *Mammalian genome : official journal of the International Mammalian Genome Society* 21:276-286.
66. Davis, R.C., Jin, A., Rosales, M., Yu, S., Xia, X., Ranola, K., Schadt, E.E., and Lusis, A.J. 2007. A genome-wide set of congenic mouse strains derived from CAST/Ei on a C57BL/6 background. *Genomics* 90:306-313.
67. Cooper, G.M., and Shendure, J. 2011. Needles in stacks of needles: finding disease-causal variants in a wealth of genomic data. *Nature reviews. Genetics* 12:628-640.
68. Verdugo, R.A., Farber, C.R., Warden, C.H., and Medrano, J.F. 2010. Serious limitations of the QTL/microarray approach for QTL gene discovery. *BMC biology* 8:96.

Chapter 3 Sweet Pee, a novel mouse model for Sglt2 mutation

1 Abstract

Inhibition of renal glucose transport represents a novel target for the treatment of diabetes. A new class of therapeutic agents that selectively block the renal tubular sodium-glucose co-transporter 2 (SGLT2) is under active clinical investigation. SGLT2 transporters play a crucial role in the reabsorption of 90% of filtered glucose load. Patients with mutations in the solute carrier family 5, member 2 (*SLC5A2*) that encodes SGLT2, exhibit a varying degree of glucosuria. Due to a lack of animal models with sglt2 dysfunction, the efficacy and safety of SGLT2 inhibitors have remained unclear. Here, we describe *Sweet Pee (SP),* a novel mouse model generated by *N*-ethyl-*N*-nitrosourea (ENU) mutagenesis that carries a nonsense mutation in the *Slc5a2* gene resulting in loss of sglt2 protein function. The phenotype of SP mutants is remarkably similar to patients with mutations in the *Scl5a2* gene. The SP mutants have improved glucose tolerance, but higher urinary excretion of calcium, and magnesium. They also exhibit growth retardation. Renal physiologic studies demonstrate a prominent distal osmotic diuresis without enhanced natriuresis. KIM-1 and NGAL, markers of acute tubular injury, are not increased in SP mutants at baseline. SP mice with induced diabetes exhibit better overall glycemic control, but have a higher risk of infection and exaggerated mortality rate (70% in homozygous mutants versus 10% in wild-type controls at 20 weeks of diabetes). Taken together, the *Sweet Pee* model represents a powerful new tool to examine the long-term benefits and risks associated with inhibition of SGLT2 for the management of diabetes.

2 Introduction

2.1 Background and Rationale

Over 170 million people worldwide were suffering from diabetes in the year of 2000 and the prevalence is projected to increase to an alarming figure of 366 million by 2030, according to the World Health Organization (WHO). In the United States, more than 10% of the population aged 20 and over are diabetic (The National Institute of Diabetes and Digestive and Kidney Diseases, NIDDK, NIH). According to the Canadian Diabetes Association, more than 9 million Canadians are living with diabetes or pre-diabetes and the forecast is that by 2020, this number will reach 3.7 million. Diabetes is a contributing factor in the deaths of approximately 41500 Canadians each year. Diabetes is a systemic disease and the common cause of health complications including macrovascular (myocardial infarction, peripheral vascular disease, and cerebral vascular disease) and microvascular (nephropathy, neuropathy and retinopathy), as well as enhanced risk for infections and death. In the face of this impending pandemic, however, the management of diabetes remains to be a major clinical challenge. Three recent landmark multicenter randomized clinical trials studying patients with Type 2 diabetes including the Veterans Administration Diabetes Trial (VADT)(1), the Action in Diabetes and Vascular Disease (ADVANCE) trial(2), and the Action to Control Cardiovascular Risk in Diabetes (ACCORD) trial(3) underscore the potential benefits of tight glycemic control in improving microvascular outcomes, yet, these studies also highlighted an increased incidence of hypoglycemia and complications associated with aggressive management. Hypoglycemia has been associated with increased risk of motor vehicle accident(4), major macrovascular

events, major microvascular events, death from both cardiovascular cause and all cause mortality(5). It is therefore necessary to develop new therapies with high efficacy of lowering blood glucose yet a low propensity for side effects.

2.1.1 Maintenance of glucose homeostasis

Blood glucose is tightly regulated under normal physiology. This is at least in part due to the fact that the central nervous system relies almost exclusively on glucose as the source of energy for survival. The brain is particularly vulnerable to hypoglycemia because it lacks the capacity to synthesize or store glucose. Hyperglycemia, however, as in the case of diabetes, results in multitudes of systemic complications. Hence blood glucose is exquisitely controlled as we go between fasting and fed state several times a day.

Many hormones are involved in glucose metabolism, insulin and two counter-regulatory hormones glucagon and epinephrine are three critical hormones that work in concert and are crucial in glucose homeostasis. Other hormones include incretins, growth hormone, and cortisol. As plasma glucose levels rise, insulin is released from pancreatic beta cells. Insulin then exerts its functions on glucose metabolism and maintenance of euglycemia through:

- Inhibition of glycogenolysis and gluconeogenesis;
- Increased glucose transport into fat and muscle cells via translocation of Glut-4 to the cell membrane;
- Increased glycolysis in fat and muscle cells;

- Stimulation of glycogen synthesis;
- Inhibition of glucagon production and secretion by direct downregulation of transcription in the glucagon gene within the pancreatic alpha cells.

Apart from the pancreas, the three major organs contribute to the maintenance of glucose homeostasis are the kidneys, the intestine and the liver. The intestinal mucosa secrets two main incretin peptides, the glucose-dependent insulinotropic polypeptide (GIP) and the glucagon-like peptide-1 (GLP-1), to exert further glucose regulation (see review by Baggio and Drucker(6)). Pharmacological agents specifically targeting this pathway, namely the GLP-1-receptor agonists and the dipeptidyl peptidase-4 inhibitors, have been developed. The intestine is crucial for regulating glucose metabolism, however, the discussion is beyond the scope of this review.

It is increasingly recognized that the kidneys also contribute to glucose homeostasis and they play two critical roles. Firstly, up to 40% of all gluconeogenesis is of renal origin, which occurs along the proximal tubule(7). Secondly, the kidneys are responsible for the filtering and reabsorption of glucose. Over 99% of filtered plasma glucose is reabsorbed in the proximal tubules of the kidney(8) resulting in less than 0.5 g of urinary excretion on a daily basis(9-11). This represents an average of 180 g of glucose (640 Kcal) reabsorption from the glomerular filtrate each day on a typical North American diet(12). In diabetes, glucosuria ensues when the serum glucose exceeds the maximum renal tubular capacity (260-350 mg/min/1.73 m^2)(13), and this in general represents a serum glucose concentration greater than 10 mmo/L(14).

2.1.2 Sodium-glucose linked transporter (SGLT)

Tubular glucose reabsorption relies on two classes of transport proteins: the facilitative glucose transporters (GLUTS) that allow transport of glucose from the basolateral aspect of renal tubular epithelium into the systemic circulation driven by a concentration gradient; and the sodium-dependent glucose co-transporters (SGLTs), which are sodium glucose symporters located in the apical brush border membrane of the proximal tubules. The reabsorption of glucose by SGLTs is therefore coupled with sodium reabsorption, which expends energy through the maintenance of a sodium gradient by the basolateral Na^+/K^+-ATPase. SGLTs are encoded by *SLC5* (solute carrier family 5) family of genes. Twelve members of the *SLC5* have been described in human(15, 16). Two major SGLT transporters exist in the kidneys, SGLT1 and SGLT2, which differ in their affinity, substrate specificity, and tissue expression. Whereas SGLT1 is more widely expressed and is found in the small intestine, the distal (S2, S3) segments of the renal proximal tubule, in the brain and in cardiomyocytes(17-22), SGLT2 is primary expressed in the apical brush border of the S1 and S2 portion of the proximal renal tubule(19-23). SGLT1 is a high affinity ($K_{0.5}$ = 0. 4 mM) low capacity transporter and accounts for a small amount (10%) of filtered glucose in normal states(17, 24, 25) and it does not discriminate between glucose or galactose(21). Stoichiometrically, each transporter carries two molecules of sodium for each molecule of glucose or galactose(12). SGLT2 is a low affinity ($K_{0.5}$ = 2 mM) high capacity transporter and is responsible for the majority (over 90%) of glucose reabsorbed from the filtrate. It is exclusively selective for glucose and not other monosaccharides(25, 26). SGLT2 spans over 7.8 kilobases in chromosome 16. The protein product consists of 672 amino acids, approximately 72.9 KDa in size, and shares around 60% homology

with SGLT1(27). Both SGLT1 and SGLT2 contain 14 transmembrane helices and extracellular hydrophobic C- and N-terminus(11). Unlike SGLT1, SGLT2 has a sodium to glucose coupling ratio of 1:1. Apart from SGLT1 and SGLT2, there may be other transporters that play a very minor role in glucose reabsorption, such as *SLC16A12* that encodes MCT12(9, 28). Individuals with mutation in *SLC16A12* exhibit very mild degree of renal glucosuria(9, 28). The role of SGLT4, SGLT6, and SMIT1, which are also expressed in the kidneys, are yet to be defined(11). SGLT6, for instance, has been shown to glucose transporter in rabbit(8), its role in humans remains elusive. In addition to transporting solutes, some SGLTs have other functions including enhancing GLUT2 insertion into the enterocytes by SGLT1(29) and acting as a glucose sensor in neuronal cells as in the case of SGLT3(30).

2.1.3 Regulation of SGLT2 expression in disease

In rodent models of diabetes, expression of GLUT2 in the proximal tubules is enhanced(31, 32), without changes in SGLT1 expression(31). Similar to GLUT2, the transcription of SGLT2, the principle glucose transporter in the kidneys, seems to be upregulated in diabetic animal models(33-36). And this effect is reversible upon treatment with insulin(33) and SGLT inhibitors(37). In addition, the observation that the proximal tubular cells recovered from the urine of diabetic patients exhibit a higher SLGT2 mRNA level compared to healthy individuals provides further evidence that transcription of SGLT2 is modulated in diabetes(24). Although it is unclear whether the "sensor" is at the level of plasma glucose, renal glucose load or via other mechanisms, there is indirect evidence that this regulation is at least in part mediated by HNF1α. Firstly, HNF1α expression is also increased in rodent models of diabetes(33). The

decrease in expression of SGLT2 when diabetic rats are treated with insulin is also associated with a decrease in HNF1α expression(33). Secondly, mutation in *TCF1*, which encodes HNF1α, leads to a syndrome known as maturity-onset diabetes of the young type 3 and has been associated with renal glucose wasting(38, 39). HNF1α is a transcription factor and its binding site has been identified in the promoter region of mouse *Slc5a2*(39). Interesting HNF1α knockout animals exhibit deficiency in insulin secretion independent of insulin transcription(40). Unlike SGLT2, diabetic state does not affect SGLT1 expression(31).

In addition to glucose, hypertension may have an effect on sglt2 expression, at least in rodent models of hypertension. The effect of blood pressure on sglt2 expression was first shown by Bautista et al., who described an increase in sglt2 mRNA and protein expressions in kidneys from rats with renovascular hypertension induced by aortic coarctation(41). Further, this upregulation in sglt2 expression could be ameliorated with either ramipril (an angiotensin converting enzyme inhibitor) or losartan (angiotensin II receptor blocker) treatment(42). Interesting, hypertension alone does not necessarily correlate with a higher expression of sglt2 as demonstrated by Osorio et al, where control rats treated with high salt diet developed hypertension without alterations in sglt2 expressions(37). Furthermore, rats treated with angiotensin II infusion developed hypertension and elevated slgt2 expressions(41). Administration of nifedipine to these hypertensive rats reversed the blood pressure effect of angiotensin II infusion but not sglt2 expressions(41). Taken together, the effect of blood pressure on expression of sglt2 seems to be mediated by angiotensin II.

2.1.4 Familial renal glucosuria

Mutations in critical genes involved in glucose transport have led to various well characterized disorders including glucose-galactose malabsorption syndrome in *SLC5A1* (SGLT1), Faconi-Bickel syndrome in *SLC2A2* (GLUT2), and Familial renal glucosuria in *SLC5A2* (SGLT2) mutations. Familial renal glucosuria describes patients with a rare mutation in the solute carrier family 5, member 2 (*SLC5A2*) gene that encodes for a 75kDa sodium-glucose co-transporter 2 (SGLT2). Renal glucosuria is distinctively not a result from hyperglycemia or global proximal tubule dysfunction as in the case of Fanconi-de Toni-Debré syndrome. Affected individuals typically have normal oral glucose tolerance test, plasma insulin, free fatty acids, and glycated haemoglobin levels(43). Urinary glucose excretion is usually stable except during pregnancy when the amount excreted is typically increased as a result of an increase in the glomerular filtration rate or GFR(43). Familial renal glucosuria was further characterized into types A, B and O. Patients with type A are characterized by a low renal threshold for glucose and a low maximum tubular glucose reabsorption, whereas type B patients also have a low threshold but normal maximum tubular glucose reabsorption(44). Type O, in contrast, exhibits a complete absence of renal glucose reabsorption(45). From pedigree analyses, persistent heavy glucosuria is the distinguishing phenotype in putative homozygous individuals, whereas heterozygotes have mild or no glucosuria(46). Since the successful cloning of *SLC5A2*, the principle transporter for glucose reabsorption in the kidneys, in 1992(27) mutations that affect the function of this gene is now known to cause familial renal glucosuria. Santer et al. reported the first confirmed mutation (in 16p11.2) on an abstract in 2000(47). Since then, there have been more case reports of private mutations, and to date there are

over forty mutations described in the literature(48). As mentioned above, patients with this disorder manifest a variable degree of glucosuria, without generalized proximal tubular dysfunction, depending on the type of mutation and the number of alleles affected; massive glucosuria of 169 g/1.73 m^2/day has been reported (49), yet most of them remain euglycemic and have no other major clinical sequela (50). Although in severe cases, renin-angiotensin-aldosterone system (RAAS) can be affected as evidenced by an increase in plasma renin and plasma aldosterone levels(9, 48, 51). Other reported ill effects include dehydration and ketosis during pregnancy and starvation(45), hypercalciuria(52), aminoaciduria(53-55), predilection to genitourinary tract infections(48, 51), and mild growth and pubertal maturation delays(56). In general, patients with mild glucosuria (<10 g/1.73 m^2/day) are usually heterozygous for mutations in *SLC5A2*(9). Severe renal glucosuria (>10 g/1.73 m^2/day) are described in patients with homozygous inheritance or compound heterozygosity(48, 57). Mutations that result in haploinsufficency will cause a decreased number of transporters in the renal tubules and clinically type A glucosuria(9). Certain mutations, however, may cause a change in affinity for glucose and lead to type B glucosuria(9, 57). Given the apparent benign nature of loss of function of SGLT2, particularly partial loss, and its restricted renal expression, it follows that SGLT inhibition might be a valuable treatment for diabetes to enhance renal glucose excretion and thereby improve glycemic control. Indeed, preliminary clinical trials have shown SGLT2 inhibitors to be effective in lowering HgbA1c with little propensity to induce hypoglycaemia(58) in addition to achieving an average weight loss of 1.8 kg, of which fat loss is the predominant feature(59).

2.1.5 Rationale

Numerous SGLT inhibitors have been developed and are currently under investigation in the treatment of diabetic patients; they include *Dapagliflozin, Canagliflozin, YM543, GSK189075, SAR7226, and ISIS 388626*(26, 60, 61)(also see summary of current pharmaceutical agents on clinical trials (62)). Importantly, this class of agents will soon be made available for the management of type 2 diabetes. Because of the paucity of systematic follow up and characterization of patients carrying *SLC5A2* mutations, and a lack of animal models that target sglt2, the efficacy and safety of long-term inhibition of SGLT2 is yet to be established.

3 Overview of experimental approach

Here we report the generation, mapping, and characterization of a novel mouse mutant named *Sweet Pee* (SP) that carries a nonsense mutation in the *Slc5a2* gene. To understand the impact of sglt2 inhibition on renal physiology, we determined urine flow, renal hemodynamics, and electrolyte excretion in homozygous, heterozygous and control littermates. We show that at baseline, sglt2 mutants manifest a distal osmotic diuresis with no change in proximal tubular water reabsorption. Mutants also exhibit slower growth with calcium, and magnesium wasting. At baseline, mutants have superior glucose tolerance but no difference in insulin sensitivity. Finally, we generated a diabetic cohort to determine the effect of impaired sglt2 function in a streptozotocin (STZ)-induced model of diabetes. Although diabetic sglt2 mutants exhibit improved glycemic control, they have markedly higher overall mortality and occasional development of overwhelming urosepsis, suggesting that these therapies may be associated with significant adverse effects.

4 Hypotheses

We propose the following hypotheses:

1. *Sweet Pee* model will demonstrate an altered renal flow and glomerular filtration rate.
2. *Sweet Pee* will exhibit a better tolerance to glucose.
3. *Sweet Pee* will be at a higher risk for hypoglycemia due to altered insulin tolerance.
4. *Sweet Pee* will achieve a lower growth curve.
5. *Sweet Pee* will demonstrate a greater urinary loss of fluids, glucose, and calcium.
6. Urinary Calcium loss will contribute to a decreased bone mineral density in *Sweet Pee* mutants.
7. *Sweet Pee* is predisposed to acute kidney injury.
8. Diabetic *Sweet Pee* will demonstrate a better glucose profile but will not result in significant amelioration in nephropathy.
9. Diabetic *Sweet Pee* is more prone to infection.

5 Methods

5.1 Generation of Sweet Pee mutant

Inbred mouse strains C57BL/6J (B6) and C3H/HeJ (C3H) were obtained from the Jackson laboratory (Bar Harbor, ME). Mutant *Sweet Pee* was generated on a genetic background of mutagenized B6 and wild-type C3H, as part of an ENU project in the Center for Modeling Human Disease (CMHD) for genome-wide mutagenesis, Toronto, Canada. ENU mutagenesis was performed as described previously (63).

Mutant SP was identified on a dominant screen at week 6. A mutant breeding line was established by backcrossing this founder to wild-type C3H. The heritability of glucosuria was confirmed. Subsequent backcross that involved breeding between the newly identified SP mutant and the wild-type C3H/HeJ mice, as well as intercross between SP mutants were set up for mapping and further phenotypic characterization. The use of the mice in this study was approved by the Mount Sinai Hospital Animal Care Committee, in accordance to the Ontario's Animals for Research Act, and the federal Canadian Council on Animal Care. All mice used in this study were male and maintained on standard rodent chow.

5.2 Mutation mapping

A rough map was generated with Illumina® genome-wide single nucleotide polymorphism (SNP)-based chip analysis, consisting of 1449 SNP markers, and was performed at the Center for Applied Genomics (TCAG), the Hospital for Sick Children, Toronto, Canada. A total of 10 G2 mice exhibiting intermittent glucosuria from backcross breeding, 3 intercross mice with persistent high-grade (>55 mmol/L) glucosuria, and 3 mice G2 mice with no glucosuria were used. Fine mapping was provided fee-for-service by the TCAG.

5.3 Sequencing

Direct genomic sequencing using tail DNA was carried out to cover all the exons and splice regions. Genomic DNA was isolated from mouse tails as described previously (64). The insertion mutation identified in exon 4 was amplified with Platinum® DNA polymerase (Invitrogen) and the following PCR primers, which were

designed based on sequence information from the Mulan ECR browser: (Sense 5'–AAC CCA GGA AGG AGT GCT CTT GAC-3', antisense 5'-ACC CAC AGC TTG GAG ACT TGC T-3'). The above primers produced a 2164 bp PCR product, which was then confirmed with agarose gel electrophoresis. The correct band was excised and purified with GeneClean® kit (MP Biomedicals). The product was then sent to TCAG sequencing facility using traditional Sanger chain termination method. The following nested primers were used to identify our mutation (a total of 6 homozygous mutants and 3 wild-type were used for sequencing): (Sense 5'-AGG CAC TTC CGC TGT GTC TTC T-3', antisense (for confirmation): 5'-CCA CAG CTT GGA GAC TTG CT-3').

5.4 Genotyping

Genomic DNA was isolated from mouse tails (64) and PCR was used to identify *Sweet Pee* mutants with the following primers to produce a 470 bp PCR product: (Sense 5'-TGT GAG GCT GTC CCA AGA ATG T-3', antisense 5'-TCA GAG TCC CAG CAT TTG GTC T-3'). The PCR product was then digested with restriction enzyme TaqI (T↓CGA) Fast Digest (Fermentas) for 5 minutes at 65 ^{o}C (wild-type: 2 bands at 225 bp, 245 bp; Heterozygous mutant: 3 bands at 225 bp, 245 bp, 470 bp; homozygous mutant: 1 band at 470 bp).

5.5 Immunofluorescence assay

Freshly dissected kidneys were fixed in 4% PFA overnight at 4^{o}C, treated with 30% sucrose at 4^{o}C overnight, then embedded with OCT for cryopreservation. The kidneys were then sectioned at 6 μm with a Cryostat. They were allowed to dry

overnight. Non-specific staining was minimized by incubating sections in 10% BSA blocking PBS buffer before the application of the primary antibody. The primary antibody was applied overnight at 4^{o}C. The sections were then rinsed with PBS before incubating with a secondary antibody at room temperature for 1 hour in the dark. VECTASHIELD® mounting medium with DAPI for nuclear stain was added before applying cover slips and sealing with nail polish. The following primary antibodies and dilutions were used: K-17 and C-19 goat polyclonal IgG anti-mouse sglt2 at 1:100 and 1:50 respectively (Santa Cruz Biotechnology, Inc). Fluorescein (FITC)-conjugated AffiniPure donkey anti-goat IgG at 1:100 (Jackson Laboratories Inc).

5.6 Real-time PCR

Total RNA was extracted from the renal cortex using Trizol reagent (Invitrogen) and reverse transcribed into cDNA using M-MLV reverse transcriptase (Ferments) and random hexamer primers (Fermentas) according to the manufacturer's protocol. cDNA samples and standards were amplified in qPCR MasterMix Plus for SYBR Green I (BioRad). Samples were analyzed in triplicate. Relative quantification of target gene expression was evaluated using comparative C_T method (65). The Δ C_T value was determined by subtracting the Hprt C_T value of each sample from its respective target C_T. Fold changes in gene expression of the target gene were equivalent to $2^{-\Delta\Delta CT}$. The following primers were used in the study: glut1 sense 5'- TCC GGT ATC GTC AAC ACG GCC T-3', antisense 5'- AGC ACA GCA CAG CCT GCC AT-3'; glut2 sense 5'- CGG CTG TCT CTG TGC TGC TT-3'; antisense 5'- GCA GCA CAA GTC CCA CCG ACA T-3'; sglt1 sense 5'- GGA AGC ATA TGA CCT GTT CTG-3', antisense 5'- GAC

AGA GTG TCA GAC AAC AC-3'; sglt2 sense 5'- ATG CGC TCT TCG TGG TGC TG-3', antisense 5'- ACC AAA GCG CTT GCG GAG GT-3').

5.7 24-hour urine study

Three mice of the same genotype were used for each 24-hour study. Two Nalgene metabolic cages were used simultaneously as paired experiments (matched for age and weights). Amount of water consumed was obtained based on the difference between pre- and post-study water bottle weights. Similarly, urine output was estimated with the same strategy. The urine was centrifuged at 4^{o}C for 10 minutes at 10000 rpm. The urine samples were then flash frozen with liquid nitrogen before sending to the hospital biochemistry laboratory (Mount Sinai Hospital, Toronto, Canada). Roche Diagnostics: automated Roche Modular was the platform used for analysis.

5.8 Metabolic tests

Intraperitoneal glucose tolerance test: Mice were maintained at a normal light/dark cycle and fasted for 14 h with free access to water. Each conscious mouse then received an IP injection of D-dextrose (1 mg/g body weight). Blood samples were collected from the tail at time 0, 5, 15, 30, 60, 120 minutes, and were analyzed with the Bayer Contour® blood glucose monitoring system.

Intraperitoneal insulin tolerance test: Mice were fasted for 6 hours with free access to water. Conscious mice then received an IP injection of insulin (Linco Research, St. Charles) (1.2 u/kg body weight). Blood samples were collected at 0, 20

40, 60, 90, 120, 150, 210, and 230 minutes when their blood glucose returned to baseline.

Streptozotocin (STZ) treatment: For diabetes induction, mice were aged to 3 – 4 weeks and received intraperitoneal injections of streptozotocin (Sigma Life Science, Sigma-Aldrich) at a low dose protocol of 50 mg/kg after a 4-hour fast for 5 consecutive days. The dosage was adjusted daily based on their daily weights. STZ was dissolved in 10 mmol/L citrate buffer pH 4.5 and was injected within 5 min of dissolution. Hemoglobin A1C (Hgb A1C): Diabetic mice were aged for at least 16 weeks before blood samples were collected with EDTA-Vaccu tubes. The tubes were immediately put on ice and Hgb A1C assay performed with Siemens DCA™ System and read by Bayer DCA 2000-1 (Model 5031C).

5.9 Micropuncture study, invasive mean arterial blood pressure measurement, and bladder urine collection for analysis

The micropuncture methodologies were validated as described previously (66). To determine kidney GFR and nephron filtration and reabsorption rates, mice were infused with ^{125}I iothalamate (Glofil, Questcor Pharmaceuticals, Hayward, CA) at about 40 μCi/h. End proximal segments were identified by injecting a bolus of artificial tubular fluid stained with FD&C green from a 3- to 4 μm tip pipette. All proximal collections were done in the last surface segment. Fluid volume was determined from column length in a constant-bore capillary. Radioactivity in tubular fluid as well as in duplicate samples of plasma and urine was determined in a gamma counter.

5.10 GFR by FITC inulin

GFR in conscious mice was measured according to the protocol described previously (67). Briefly, FITC-inulin (3.7 ml/g BW) was injected into the retroorbital plexus during brief isoflurane anesthesia from which the animals recovered within about 20 sec. At 3,7,10,15,35,55 and 75 min after the injection mice were placed in a restrainer, and 2 ml blood was drawn from the tail vein. Samples were centrifuged and 500 nl plasma was transferred into a microcapillary and diluted 1:10 in 500 mmol HEPES (pH 7.4). Fluorescence was determined in 1.7 ml of each sample in a Nanodrop-ND-3300 fluorescence spectrometer (Nanodrop Technologies Inc, Wilmington, USA). GFR was calculated using a two-compartment model of two-phase exponential decay (68).

5.11 Acute kidney injury biomarkers

Urine samples were freshly collected and put on ice and centrifuged within 30 min to remove insoluble elements. Urinary aliquots were stored at -80°C and sent to Dr. Joseph Bonventre Laboratory for blinded analysis.

Real-time PCR primers for NGAL: sense 5'-CTC AGA ACT TGA TCC CTG CC-3', antisense 5'-TCC TTG AGG CCC AGA GAC TT-3'.

5.12 Histological analysis

Freshly dissected kidneys were fixed in 10% formalin/PBS, embedded in paraffin, sectioned at 4 μm, and stained with hematoxylin and eosin, periodic acid-Schiff. Sections were examined and photographed with a DC200 Leica camera and Leica DMLB microscope (Leica Microsystems Inc).

5.13 Statistical analysis

Data are presented as the mean ± SEM. One-way ANOVA with Bonferroni's post-test for parametric data and two-tailed Chi-Square for categorical data, with multiple comparisons was performed using Graph Pad Prism version 4.00 for Windows, Graph Pad Software (San Diego, CA, USA). For subgroup analyses between 2 groups, a two-tailed Student's t test assuming homoscedasticity was used. The null hypothesis was rejected when $P < 0.05$.

6 Results

6.1 Generation and Identification of the Sweet Pee (SP) mutants

In collaboration with the Centre for Modeling Human Disease (CMHD) in Toronto, we performed an autosomal dominant *N*-ethyl-*N*-nitrosourea (ENU) screen to identify mutations in genes responsible for renal phenotypes. ENU is a well-validated chemical mutagen that is often used in high throughput mutagenesis programs. It induces point mutations in the genomic DNA of germ cells at a frequency of 1×10^{-3} per locus, which represents over a 100-fold increase in frequency compared to baseline spontaneous mutation rate(69). Numerous ENU consortiums have been established internationally to generate novel mouse models for a variety of human diseases (refer

to previous chapter and recent review by Soewarto(70)). In this study, the high throughput renal screen consisted of urinalysis of G1 offspring. ENU mutagenesis was performed on the C57BL/6J background. 150 G1 mice were screened and we identified a single phenotypic variant, *Sweet Pee* that exhibited isolated renal glucosuria with normoglycemia. Backcrossing this founder mutant with wild-type C3H strain generated litters to confirm heritability of the phenotype. Intermittent glucosuria was robust and heritable as a dominant trait, as it represented close to 100% penetrance in 50% of the G2's.

6.2 Genetic Mapping Studies

Rough mapping with genome-wide single nucleotide polymorphism (SNP) markers identified mouse chromosome 7 syntenic to human chromosome 16 as the region of interest (Table 1 only includes partial data for illustration). The corresponding logarithm of odds (LOD) score was greater than 4 (Figure 1B), which strongly supports the presence of a quantitative trait locus (QTL). Further recombination from back crossing mapped the critical region between 127-146 Mb (Figure 1A). Analysis of genes found within this interval pointed towards the Solute Carrier Family 5 member 2, *Slc5a2*, as the candidate gene. Interestingly, the phenotype of the *Sweet Pee* mutants closely resembles the human genetic disorder of familial renal glucosuria due to mutations in *SLC5A2*.

Phenotype			No Glucosuria			Intermittent Glucosuria				High grade Glucosuria (> 55 mmol/L)		
SNPs	Chr	Position	7189-3-24	7189-3-4	7189-2-3	7189-3-23	C77189j-2-22	7189-1-21	7189-2-22	6008-1-21	6008-2-2	6015-2-21
rs13479139	7	17147281	Het	Het	Het	Het	WT	WT	WT	MT	MT	MT
rs6361142	7	18234664	Het	Het	Het	Het	WT	WT	WT	MT	MT	MT
rs13479153	7	25722935	Het	WT	Het	Het	WT	WT	WT	MT	MT	MT
rs4226499	7	29617230	Het	WT	Het	Het	Het	WT	WT	MT	MT	MT
rs3719256	7	51794017	Het	WT	Het	Het	Het	WT	WT	Het	Het	Het
rs8255275	7	53422380	Het	WT	Het	Het	Het	WT	WT	WT	Het	WT
rs8260975	7	53682778	Het	WT	Het	Het	Het	WT	WT	WT	Het	WT
rs13479251	7	59660323	Het	WT	Het	Het	Het	WT	WT	WT	Het	WT
rs3718641	7	60962267	Het	WT	Het	Het	Het	WT	WT	WT	Het	WT
rs3663313	7	63388111	Het	WT	Het	Het	Het	WT	WT	WT	Het	WT
mCV23423763	7	54746471	Het	WT	Het	Het	Het	WT	WT	WT	Het	WT
rs3679779	7	71545170	Het	WT	Het	Het	Het	WT	WT	WT	Het	WT
rs3714908	7	71657721	Het	WT	Het	Het	Het	WT	WT	WT	Het	WT
rs6160140	7	73426174	Het	WT	Het	Het	Het	WT	WT	WT	Het	WT
rs3705155	7	75667606	Het	WT	WT	Het	Het	WT	WT	WT	Het	WT
rs13479319	7	76941382	Het	WT	WT	Het	Het	WT	WT	WT	Het	WT
rs13479324	7	77988828	Het	WT	WT	Het	Het	Het	Het	WT	Het	WT
rs3676254	7	79831151	Het	WT	WT	Het	Het	Het	Het	WT	Het	WT
rs13479338	7	81203872	Het	WT	WT	Het	Het	Het	Het	WT	Het	WT
rs13479347	7	83432559	Het	WT	WT	Het	Het	Het	Het	WT	Het	WT
rs13479363	7	88283068	Het	WT	WT	Het	Het	Het	Het	WT	Het	WT
rs13479375	7	91417513	Het	WT	WT	Het	Het	Het	Het	WT	Het	WT
rs4226783	7	100081465	Het	WT	WT	Het	Het	Het	Het	WT	Het	WT
rs13479414	7	102651419	Het	WT	WT	Het	Het	Het	Het	WT	Het	WT
rs3699086	7	103251220	Het	WT	WT	Het	Het	Het	Het	WT	Het	WT
rs3713052	7	108918190	Het	WT	WT	Het	Het	Het	Het	WT	Het	WT
rs6357312	7	109389815	Het	WT	WT	Het	Het	Het	Het	WT	Het	WT
rs3673653	7	114219950	Het	WT	WT	Het	Het	Het	Het	WT	Het	WT
rs6386601	7	114746367	Het	WT	WT	Het	Het	Het	Het	WT	Het	WT
rs13479461	7	119092066	WT	WT	WT	Het	Het	Het	Het	WT	Het	WT
rs6194926	7	121509575	WT	WT	WT	Het	Het	Het	Het	WT	Het	WT
rs13479477	7	124381995	WT	WT	WT	Het	Het	Het	Het	WT	Het	WT
rs3023159	7	126426677	#N/A	WT	WT	Het	Het	Het	Het	WT	Het	WT
rs3709679	7	127271546	WT	WT	WT	Het	Het	Het	Het	WT	Het	WT
rs13479522	7	136179208	WT	WT	WT	Het	Het	Het	Het	MT	MT	MT
rs3716088	7	140189839	WT	WT	WT	Het	Het	Het	Het	MT	MT	MT
rs3663988	7	146505067	WT	HET	WT	Het	Het	Het	Het	Het	Het	MT

Table 1 Genome-wide SNP maps the critical region to mouse chromosome 7. An 1449 Illumina® SNP array platform was used. Genomic DNA samples from a total of 16 mice (10 G2 mice exhibiting intermittent glucosuria from backcross breeding, 3 intercross mice with persistent high-grade (>55 mmol/L) glucosuria, and 3 G2 mice with no glucosuria) were obtained. Only partial data was presented due to space restriction. WT, wild-type allele; Het, heterozygous; MT, homozygous mutant allele at the specific SNP.

A

Phenotype			No Glucosuria			High grade Glucosuria (> 55 mmol/L)					
SNPs	Chr	Position	6134-1-2	6134-3-1	6134-3-2	I2b-1-21	I3a-1-1	I3b-5-1	C10a-1-1	C10d-1-1	C11b-1-22
rs13479139	7	17147281				WT					
rs13479145	7	19988355					MT	MT	WT	WT	WT
rs13479153	7	25722935	WT	WT	WT		MT	MT	WT	WT	WT
rs4226499	7	29617230	WT	WT	WT	Het	MT	WT			
rs3709679	7	127271546				MT	WT				
rs13479522	7	136179208	WT	WT	WT	MT	MT	MT	MT	MT	MT
rs3716088	7	140189839	MT	MT	MT	MT	MT	MT	MT	MT	MT
rs3663988	7	146505067				WT	Het				

B

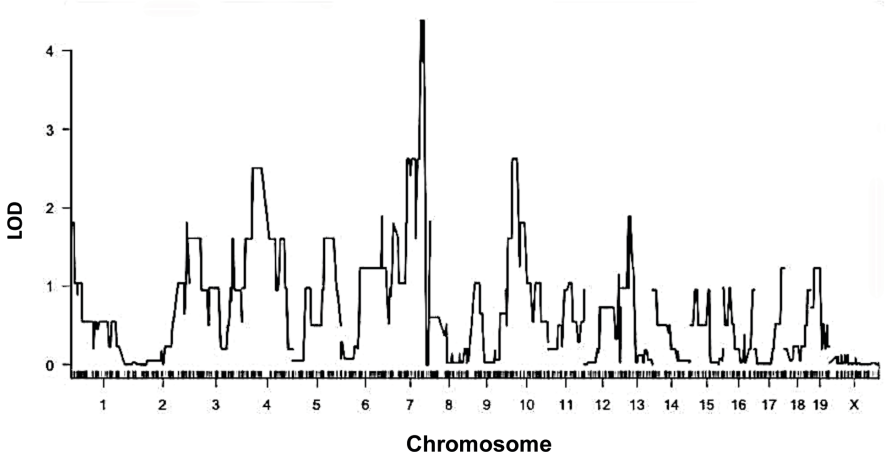

Figure 1 Mapping of renal glucosuria to mouse chromosome 7. A) Recombination further narrows the critical region between SNPs rs3709679 and rs3716088. WT represents wild-type allele, Het represents heterozygous, and MT represents homozygous mutant allele at the specific SNP. B) Chromosome 7 contains the critical region for the *Sweet Pee* mutation. The logarithm of odds scores were performed under the condition of a single quantitative trait locus genome scan, normal model assumption, binary phenotype, and inclusion of covariates by expectation-maximization algorithm(71-73).

6.3 Establishing SLC5a2 to be the mutated gene for Sweet Pee mutants

Slc5a2 is found in mouse chromosome 7 between 135 409 171 and 135 415 944. It consists of 14 exons spanning over 6.7 kilobases. The transcript and translation lengths are 2277 bp and 674 residues, respectively. To confirm that this gene harbors the mutation that is underlying the phenotype in our SP mutants, we performed immunofluorescence assays with two separate sglt2 antibodies against both the N- and the C-terminus and observed no specific signal in the renal tubules of the homozygous mutants (Figure 2A, and data not shown) compared to normal signal in the wild-type (WT).

Genomic DNA isolated from the tails of 6 homozygous mutants and 3 WT mice were used for sequencing (refer to *Materials and Methods* for details). We discovered a mutation with an insertion of a single thymine at position 433 in exon 4. This 433insT frameshift mutation leads to the generation of a theoretical unique 73 amino acid neo-peptide and a premature stop signal (Figure 2B). The mutation occurs in the fourth transmembrane helix, which is necessary for glucose translocation(57). Furthermore, such a mutation has been previously reported to result in a nonfunctional transporter in humans due to the deletion of the critical domains 10 to 13, which are crucial for substrate binding (57). Of note, in humans, homozygosity for premature stop codon [347X] in exon 9 results in almost complete renal glucose wasting, however, a truncating mutation in exon 11 [W440X] leads to renal excretion of only half of the filtered glucose load(9).

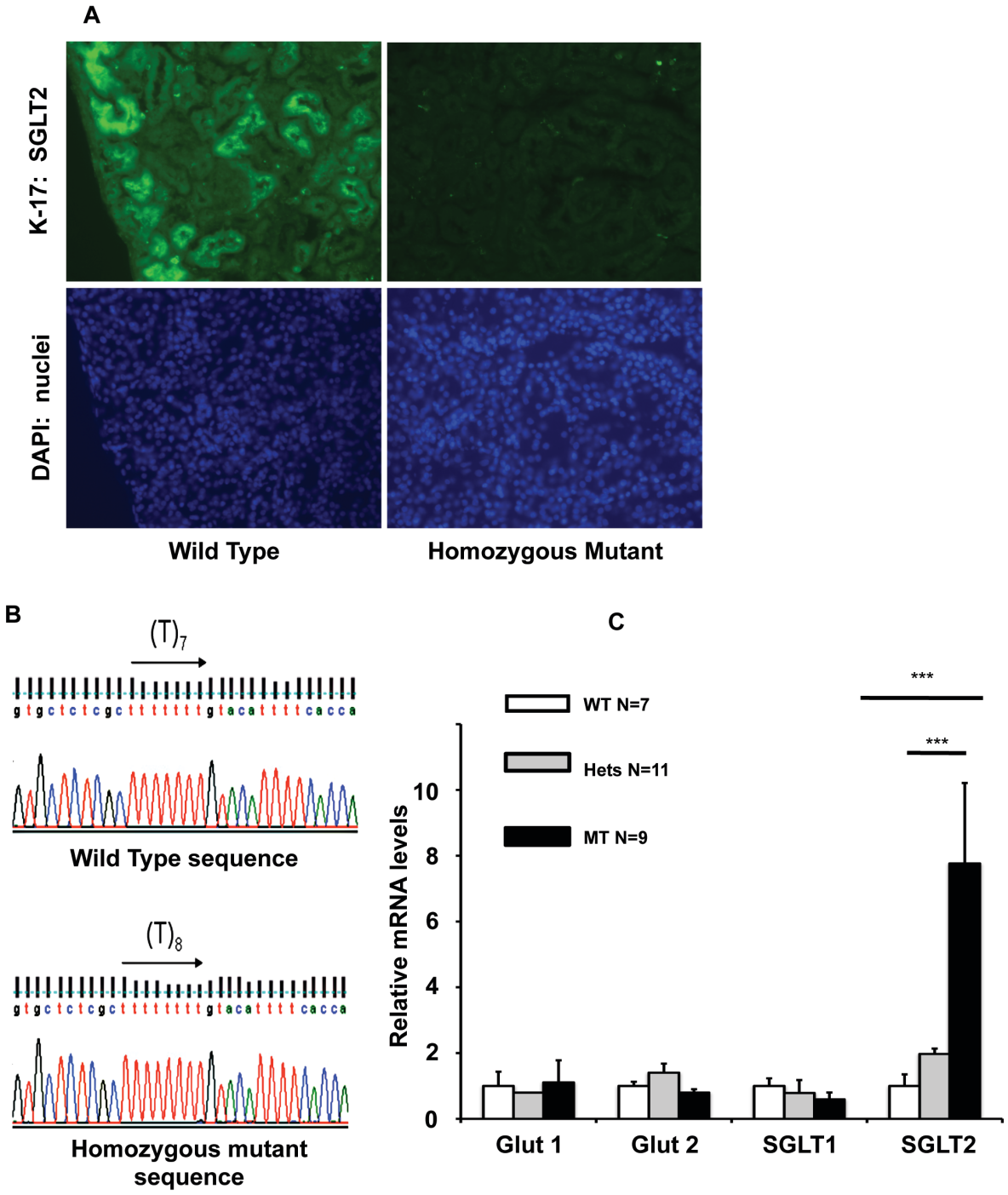

Figure 2 Expression of sglt2 is altered in *Sweet Pee* mutants. A) Homozygous mutants demonstrated no sglt2 protein expression in the kidney: Immunofluorescence with goat polyclonal IgG antibody against the N-terminus (K17) of mouse sglt2 at 20X magnification. B) Sequencing revealed an insertion of a single Thymine in exon 4 at position 433. This mutation causes a frameshift and premature stop codon. C) The

Sweet Pee mutants showed a significant elevation of sglt2 mRNA expression in the renal cortex (***p<0.001). No significant difference in glut1, glut2, and sglt1 between mutants and WT were detected. Data normalized to WT control. Housekeeping gene Hprt used as internal control. WT: Wild-type; Hets: Heterozygous mutants; MT: Homozygous mutants.

6.4 Characterization of Sweet Pee mutants

6.4.1 mRNA expression of glucose transporters in the renal cortex

Similar to patients with benign familial glucosuria, the SP mutants waste glucose in their urine due to inefficient reabsorption of the filtered glucose load. Interestingly however, they are able to maintain a euglycemic state as confirmed with multiple random blood glucose sampling and identical hemoglobin A1C (HgbA1c) levels between mutant and WT mice. In addition to the expected changes in gluconeogenesis and cellular uptake of glucose, we speculate, in part, there might be a compensatory increase in glucose uptake through the distal sglt1 high affinity low capacity Na^+ glucose co-transporter. This process might involve an increased number of sglt1 transporters that would depend upon an accelerated transcription of the *Slc5a1* gene. However, mRNA measurement by quantitative PCR in the renal cortex of 7 WT, 11 heterozygous, and 9 homozygous mutant mice, with hypoxanthine phosphoribisyltransferase 1, Hprt, as the housekeeping gene, which is not regulated by changes in glucose (C_T values for Hprt similar between WT and mutants), showed that mRNA levels for sglt1 were similar between genotypes (Figure 2C). As expected, no difference in the levels of glut 1 and glut 2 mRNA expression was found between the mutants and the WT mice. This is similar to observations made in knockout mouse model of sglt1 where no changes were detected in sglt2, glut1 and glut2 at both the

transcript and protein levels(74). Surprisingly, the sglt2 mRNA levels were significantly upregulated especially in the homozygous mutants, which showed an approximately 8-fold increase compared to their WT littermates. Of note, the region amplified was proximal to the identified mutation. The sglt2 mRNA levels of the heterozygous mutants were approximately double over their WT littermates. The above observation suggests that the expression of sglt2 is regulated, likely by the elevated glucose levels in the tubular filtrate.

6.4.2 Excretory and hemodynamic function in Sweet Pee mutants exhibit calcium and magnesium wasting

Given the degree of glucosuria in SP mutants, we wondered if there would also be a defect in proximal renal tubular reabsorption of fluid and electrolytes. To address these questions, we collected 24-hour urine samples from 18 WT, 12 heterozygous mutants, and 30 homozygous mutants. In addition, we carried out free flow micropuncture studies to directly measure proximal tubular reabsorption. As depicted in Figure 3A, homozygous mutants consumed more water and produced an approximately 4-fold greater urine volume ($p<0.001$). The amount of water intake was much greater than urine output, which is consistent with insensible loss as shown by others in mice(75). Even more dramatic is the 24-hour urinary glucose wasting. The average glucose excretion normalized to 25 g body weight was 0.34 and 0.85 in the WT and heterozygotes respectively, compared to 445.3 mg/day in the homozygotes ($p<0.001$) (Figure 3B). Homozygous mutants also had enhanced excretion of urea and creatinine ($p<0.05$) (Figure 3C).

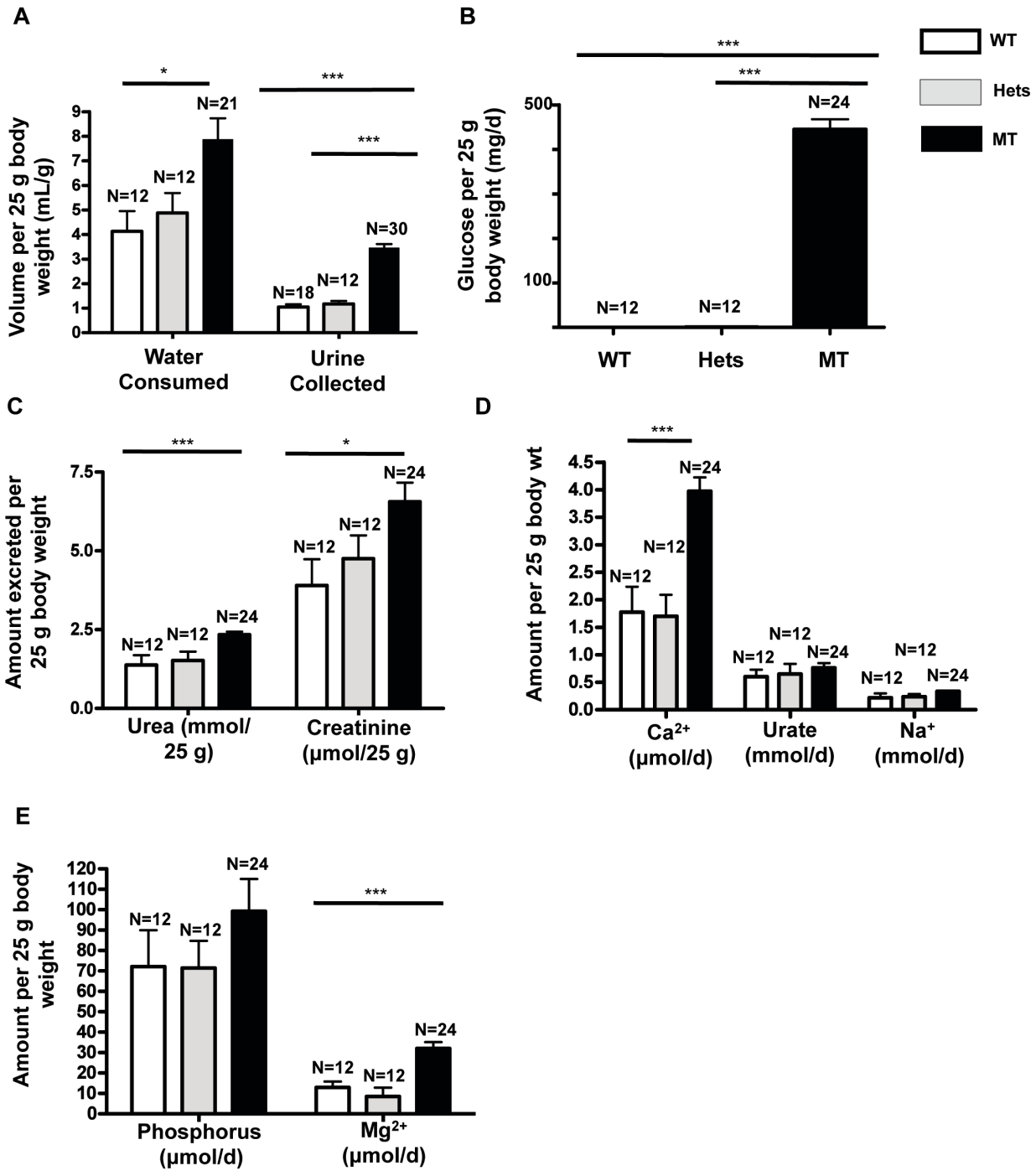

Figure 3 Twenty-four-hour urinary excretion of fluid and electrolytes varies in homozygous *Sweet Pee* mutants. Data normalized to 25 g body weight. A) MT consumed more water and produced a significantly higher volume of urine output. B) MT lost massive amount (>400 mg) of glucose on a daily basis. In contrast, WT and Hets excreted only 0.3 and 0.8 mg/d. C) MT had a significantly higher urinary urea and

creatinine excretion each day compared to their heterozygous mutants and WT littermates. D) MT excreted more calcium. No significant difference in urinary urate and sodium excretion. E) MT lost significantly more magnesium. There was also a trend towards higher urinary phosphorous excretion in the MT. WT, wild-type; Hets, heterozygous mutants; MT, homozygous mutants. (*p<0.05; ***p<0.001).

As described previously, patients with benign familial glucosuria are able to maintain normal serum electrolytes(56) but may present with loss of other micronutrients(49). Hypercalciuria was identified in five of seven male children in one case series(52), and an elevated spot urine calcium creatinine ratio was reported in a long-term 20-year follow up of the original patient identified with type O glucosuria and *SLC5A2* mutation(56). Nephrolithiasis has also been observed but due to the rarity of this disorder, the risk has never been systematically studied(52). Similar to human data, homozygous mutants have comparable serum levels of sodium, potassium, chloride, bicarbonate, urea and creatinine relative to their WT littermates. We then quantified urinary calcium, phosphorous, magnesium, and urate excretion (Figure 3D, E). Urinary excretion of calcium and magnesium were both significantly increased in homozygous mutants compared with that of WT mice (p<0.05). There was also a trend towards an increased phosphate excretion but not statistically significant. However, maximal tubular phosphate reabsorption was shown to be normal in a single report in human(56). Mutants also exhibited greater potassium output (24-hour excretion per 25 g body weight in mmol/d: 0.52 (WT), 0.57 (heterozygotes), 0.76 (homozygotes); p<0.05). Although there is a trend towards higher urinary urate excretion in the mutants, the difference was not statistically significant. Finally, none of the mice had

significant proteinuria. Unaltered urinary Na^+ excretion is consistent with direct measurements of proximal tubular reabsorption that revealed comparable single nephron GFRs (SNGFRs) and there were no major differences in absolute or fractional fluid reabsorption between WT and the homozygous mutants (percent absorption 46.4% and 43.9% respectively; *p*=0.7) (Table 2). Furthermore, there were no significant differences in whole kidney glomerular filtration rate determined by fluorescein isothiocyanate (FITC)-inulin (GFR) in conscious mice as depicted in Table 2. The average GFR for WT and homozygous SP mutants was 522.8 and 460 μl/min (*p*=NS). Because SP mutants tend to have smaller kidneys, when corrected for kidney weight, the GFR for WT and homozygotes was identical (0.96 versus 0.97 $\mu l.min^{-1}mg^{-1}$ respectively; *p*=NS). In addition, mean arterial pressures were also not different between WT and SP mutants (89 and 85 mmHg respectively). In conjunction with comparable urine osmolarity, plasma renin activity (1047 vs 1274 ng Ang1/ml hr; *p*=0.4), and serum hematocrit (Table 2) between the WT control and the mutants, our data suggest that under normal conditions, loss of function in sglt2 does not have any significant impact on volume status as long as fluid consumption can be maintained (Figure 3A).

	Wild Type	SEM	N	MT Mutant	SEM	N	*p*
Weight (g)	28.7	0.3	6	28.1	1.0	9	0.66
Kidney wgt (mg)	563	14.8	4	481	14.1	7	<0.005
MAP	89	3	4	85	2	5	0.5
Uosmol (mosmol/L)	2013	175	4	1596	44	6	0.02
HCT (%)	46.9	0.5	6	46.5	0.6	9	0.63
GFR (µL/min)	522.8	32.2	6	460	21.1	9	0.11
SNGFR	13.6	0.9	4	15.6	1.4	5	0.1
Prox. Absorb.	46.4	1.8	4	43.9	3.2	5	0.68

Table 2 *Sweet Pee* mutants do not show signs of extravascular volume contraction under normal conditions. No difference in weight, mean arterial blood pressure (MAP), Hematocrit (HCT) and renin. However, urine osmolarity (Uosmol) was significantly lower. Glomerular Filtration rate (GFR) as well as single nephron GFR (SNGFR) were similar between the mutants and the wild-type. No difference in the percent of proximal absorption (Prox. Absorb.) was observed.

6.4.3 Growth is restricted in Sweet Pee mutants

As noted above, homozygous mutants, exhibit greater urinary loss of glucose and some essential micronutrients. Accordingly, we followed the weight gain in 10 WT, 8 heterozygotes, and 15 homozygotes from 3-14 weeks of age. At each time point, body weights were significantly lower in the homozygous mutants. Weights were also reduced in the heterozygotes compared to WT (p=0.001). Thus, it appears that the

severity of growth restriction correlates with the number of alleles affected (Figure 4). Of note, growth delay was reported in humans with familial renal glucosuria(56).

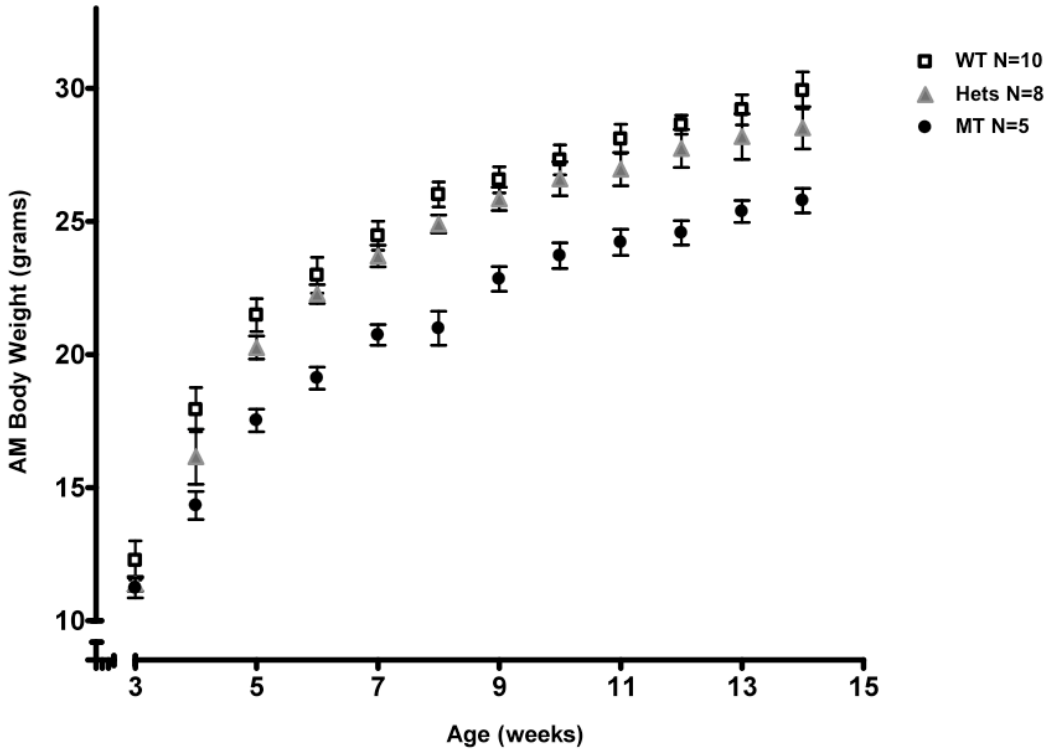

Figure 4 A decreased expression of sglt2 is associated with growth retardation and the effect is dose dependent. Homozygous mutants weighed significantly less at each time point compared to their heterozygous and WT littermates (****p<0.0001). Heterozygotes also demonstrated less weight gained compared to WT (***p=0.001). WT, wild-type; Hets, heterozygous mutants; MT, homozygous mutants.

6.4.4 Sweet Pee Mutants exhibit improved glucose tolerance but no change in insulin sensitivity

Because the SP mutants exhibit dramatic glucosuria, we investigated whether inhibition of sglt2 affects glucose metabolism. A total of 8 WT, 8 heterozygous mutants, and 9 homozygous mutants were studied. As shown in Figure 5A, serum glucose levels peaked at 15 minutes, which is consistent with other studies reported in the literature(76). After administration of glucose, the average peak glucose value achieved was significantly lower in the homozygous mutants. Moreover, their blood glucose returned to baseline earlier than the heterozygous and the WT littermates.

To further evaluate the mechanism(s) of the improved glucose tolerance in the SP mutants, we performed a standard insulin challenge test. Although one homozygous mutant and two WT mice developed significant hypoglycemia during the study, there was no difference in the response to insulin challenge between the mutants and the WT control (Figure 5B). Thus, inhibition of sglt2 function does not affect tissue sensitivity to insulin, and the observed superior glucose tolerance is likely due to enhanced glucosuria alone. Furthermore, mutants were not more susceptible to hypoglycemia compared to their WT littermates.

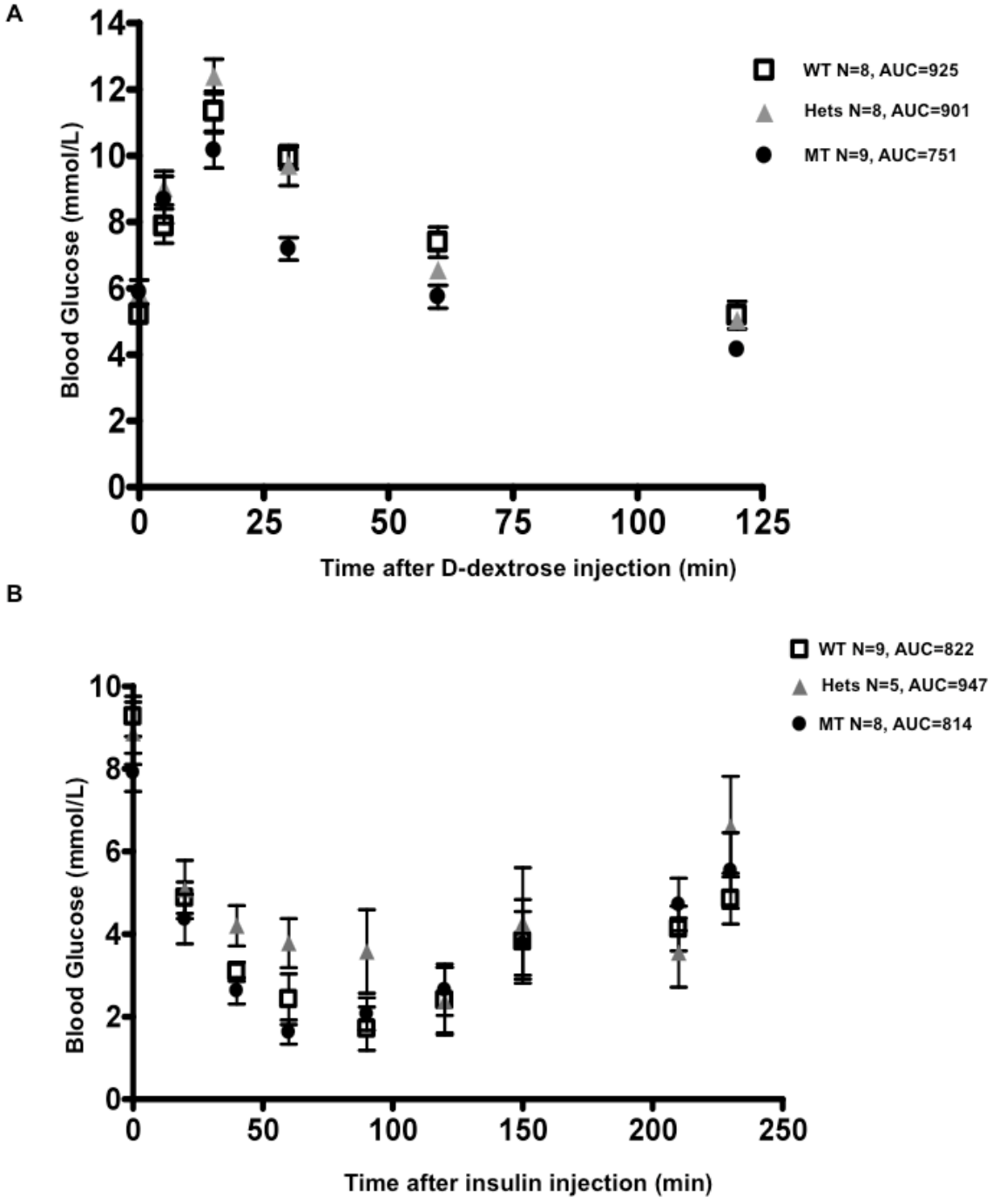

Figure 5 Sglt2 dysfunction results in better glucose tolerance without hypoglycemia. A) Standard intraperitoneal D-dextrose challenge test: 1 mg/g body weight after a 14-hour fast. MT exhibited significantly lower glucose levels at the peak

and the recovery phase (*p<0.05). B) Standard insulin tolerance test: insulin 2 units per kg body weight after a 6-hour fast. No difference in insulin sensitivity between the *Sweet Pee* mutants and WT mice. WT, wild-type; Hets, heterozygous mutants; MT, homozygous mutants; AUC, area under the curve.

6.4.5 Sweet Pee mutants do not show tubular injury at baseline

The Kidney injury molecule-1 (KIM-1) and the neutrophil gelatinase-associated lipocalin (NGAL) are two well-validated biomarkers that are upregulated in the acute phase of kidney injuries in both humans and rodents. Given the persistent exposure to high luminal glucose concentrations and persistent osmotic diuresis, we wondered if the SP mutants, particularly the homozygotes, might exhibit tubular injury at baseline. As shown in Figure 6, mRNA levels for NGAL in SP mutants were not elevated compared to the WT controls. Furthermore, random urine samples obtained from 8 adult WT, 4 adult heterozygous mutants, and 10 adult homozygous mutants for urinary KIM-1 analysis showed no increase in KIM-1 excretion amongst the mutant mice (Figure 7).

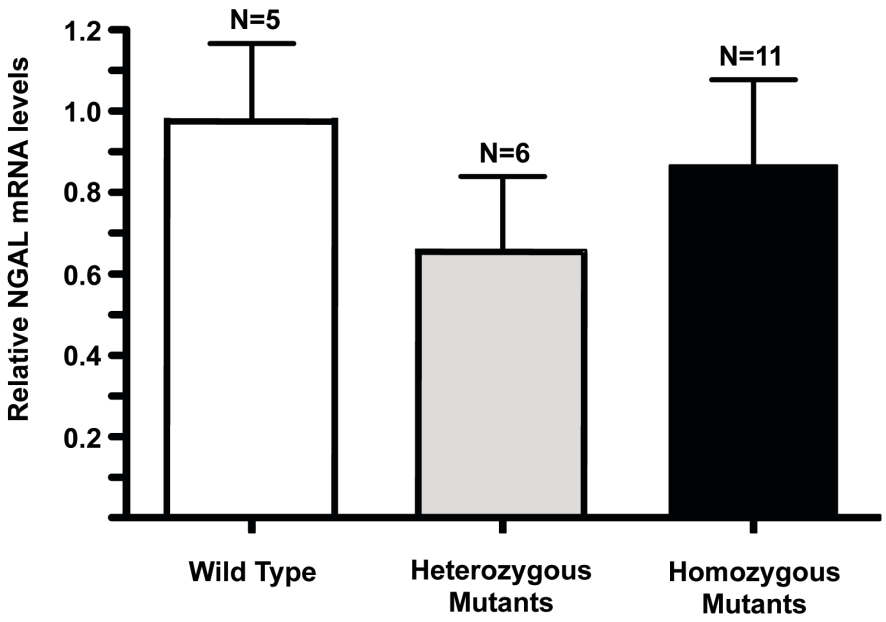

Figure 6 ***Sweet Pee*** **mutants do not demonstrate any upregulation in the mRNA expression of NGAL.** Quantitative PCR for NGAL mRNA expression reported relative to wild-type. Hprt used as internal control.

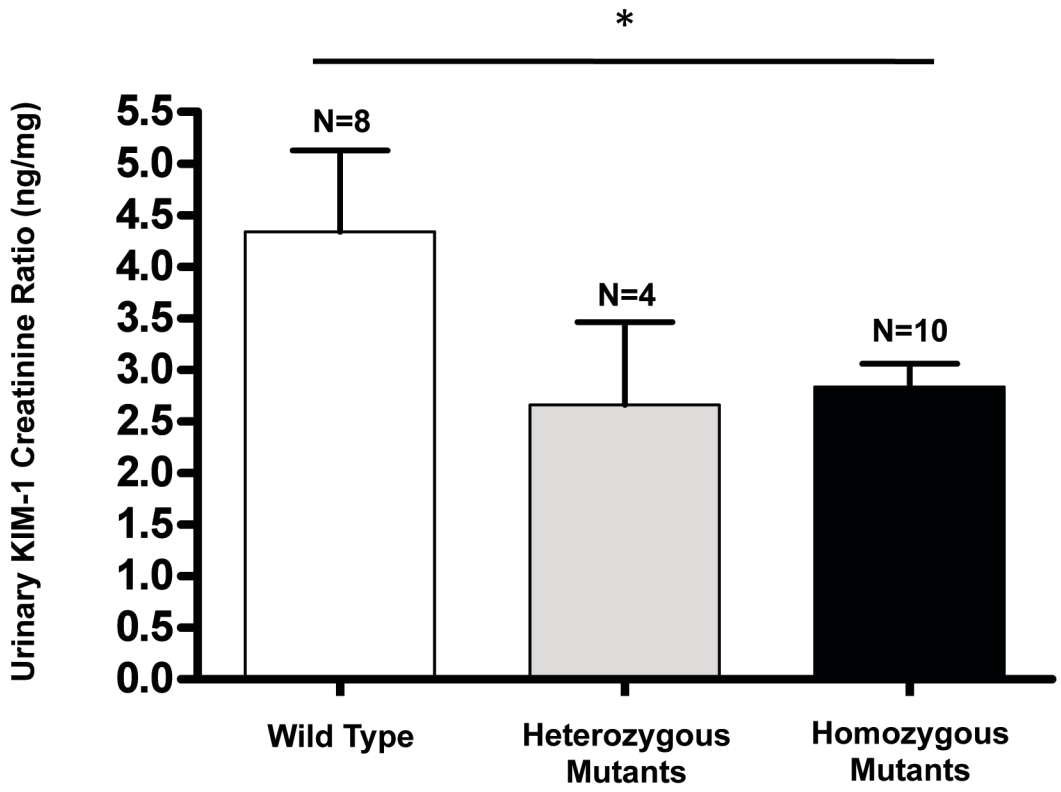

Figure 7 ***Sweet Pee*** **mutants do not demonstrate any upregulation in KIM-1 protein.** Random urine KIM-1 to creatinine ratio was determined for each group. Unexpectedly, the homozygous mutants had significantly lower ration than wild-type (*p<0.05).

6.4.6 Diabetic Sweet Pee had better glucose profile but higher mortality

Given the superior glucose tolerance at baseline, we speculated that the SP mutants might be protected from the development of diabetic complications. Therefore, we induced diabetes in SP male mutants and WT male controls with the low-dose streptozotocin (STZ) protocol. Only mice with persistent blood sugars greater than 20 mmol/l were included in the analysis (7 diabetic WT, 12 diabetic heterozygotes, and 23 diabetic homozygotes). Notably, upon the first round of STZ injection, 86% of the WT, 93% of heterozygotes, and 52% of homozygous SP mutants became diabetic ($p<0.01$) as defined by a random blood glucose level of equal to or greater than 20 mmol/l. Non-responding mice were reinjected according to a 5-day low-dose STZ protocol (one WT, one heterozygote, and nine MT). Of the 16 MT nonresponders, 9 were reinjected. *Sweet Pee* mutants had significantly attenuated levels of glycosylated hemoglobin (HgbA1C) measured at 16 weeks or over, from the time of STZ induction. As shown in Figure 8A, both mutants and WT mice had similar baseline HgbA1C of approximately 3%. This level is comparable to that reported in the literature for C3H/HeJ inbred mouse strain (77). However, no significant proteinuria was detected. The protein-to-creatinine ratios ± SEM at 21 weeks were 4.79 ± 1.4, 4.02 ± 1.08, and 4.18 ± 1.0 mg/mg for WT, heterozygotes, and MT respectively (p= NS).

Diabetic STZ-induced mutants had similar plasma levels of sodium, potassium, chloride, and bicarbonate compared to diabetic WT. However, diabetic mutants exhibited a significantly higher 24-hour urinary excretion of sodium (0.7 versus 0.3 mmol/25 g; $p<0.01$), potassium (1.7 versus 0.8 mmol/25 g; $p<0.01$), magnesium (68.1 versus 25.6 mmol/25 g; $p<0.01$), phosphorus (141.7 versus 62.8 µmol/25 g; $p<0.05$),

urate (0.46 versus 0.13 mmol/25 g; $p<0.05$), creatinine (9.1 versus 5.2 µmol/25 g; $p<0.01$), and urea (5.4 versus 2.4 mmol/25 g; $p<0.01$) compared to diabetic WT. However, 24-hour urinary calcium excretion did not differ between diabetic SP mutants and diabetic WT (4.8 versus 4.7 µmol/25 g; $p<0.8$).

Despite the improvement in glycemic control, diabetic STZ induced mutants with random serum glucose values greater than 20 mmol/l exhibit a markedly higher mortality rate compared with diabetic WT mice. As illustrated in Figure 8B, <30% of the homozygous mutants survived to week 20 from the day of STZ induction, compared to 50% and 90% of the heterozygotes and the WT, respectively. Although the cause of death could not be determined for all the mice, urinary tract infections were observed in a number of cases manifested as cloudy urine and detection of bacteria on gram stain amongst the diabetic homozygous and heterozygous cohorts (15% and 20% respectively versus none in WT: $p=$ NS). Moreover, kidneys of these mice when harvested at a pre-terminal stage, showed massive infiltration by polymorphonuclear white blood cells, together with parenchymal necrosis (Figure 8D). Furthermore, diabetic homozygous SP mutants excreted substantially higher amount of glucose averaging 1197 mg each day, a 2.7 fold higher compared to non-diabetic homozygous mutants (444 mg) and 1.8 fold higher compared to diabetic WT littermates (662 mg). Diabetic homozygous SP mutants excreted massive volumes of urine. As depicted in Figures 8C and 9, an average 25 g mouse produced 29 ± 2.3 ml of urine per day, which is greater than its entire body weight. The degree of polyuria in the diabetic WT was significantly less, they excreted an average of 12.5 ml of urine per 24 hours ($p<0.0001$).

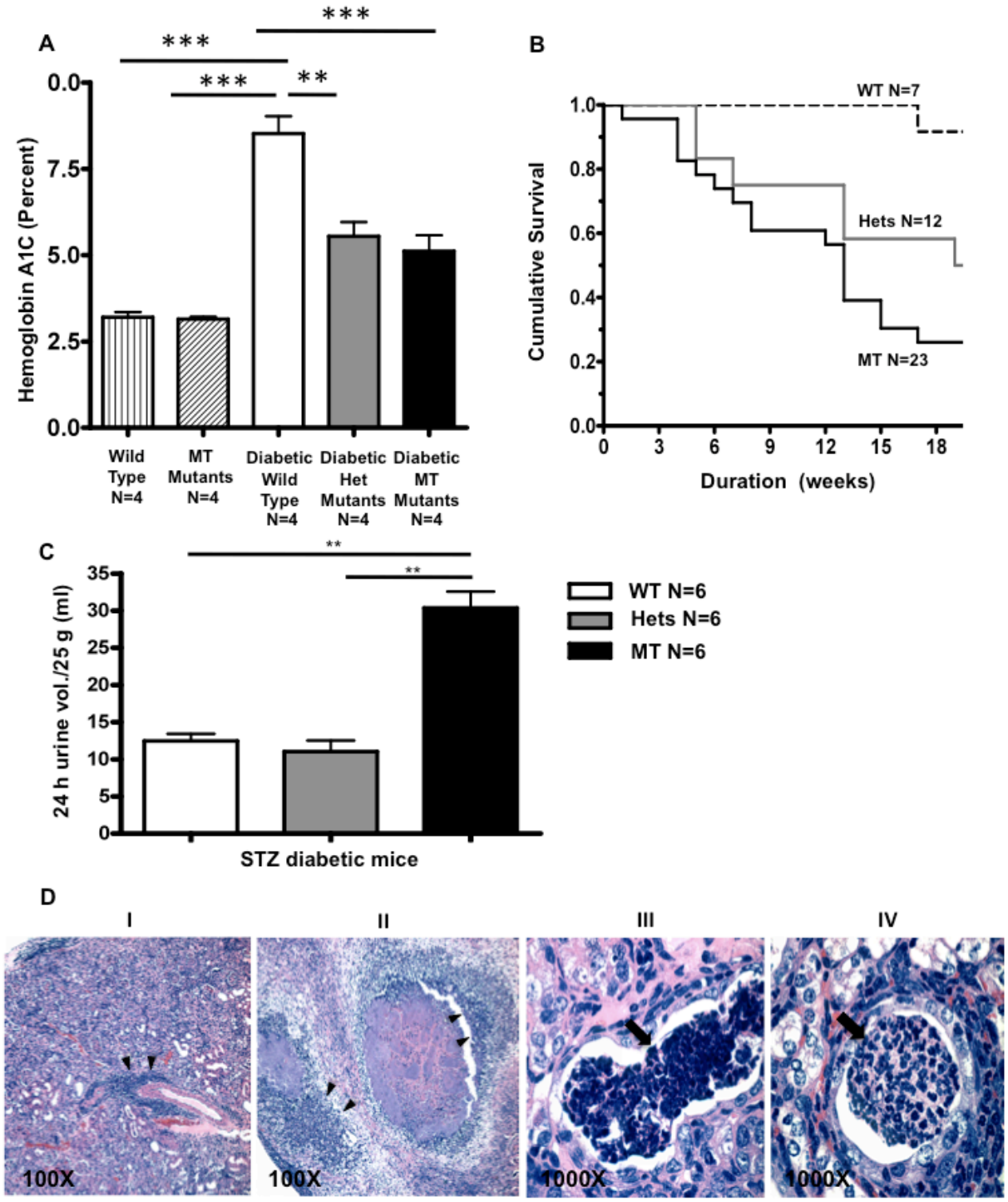

Figure 8 Diabetic *Sweet Pee* demonstrates a superior glycemic control but a higher mortality. A) The diabetic *Sweet Pee* mutants (both Hets and MT) had better glycemic control, they had significantly lower HgbA1C compared to diabetic WT mice.

No difference in HgbA1C between nondiabetic homozygous mutants and WT. As expected, diabetics had significantly higher average HgbA1C compared with the nondiabetics ($p<0.05$). Blood samples were obtained from studied animals after >16 weeks from STZ injection. Diabetes was confirmed with random blood glucose > 20 mmol/L. (One way ANOVA: ** $p<0.01$; ***$p<0.001$). B) The diabetic *Sweet Pee* mutants exhibited significantly higher mortality compared to the diabetic WT mice ($p<0.05$: Log rank Test – χ^2). Mice were followed from the date of low-dose STZ injection. C) Diabetic homozygous *Sweet Pee* Mutants exhibited dramatic 24-hour urine output (t-test:***$p < 0.005$). D) Severe pyelonephritis and sepsis in a diabetic *Sweet Pee* mutant. (I and II) At lower magnification, there was a significant leukocytic infiltration (double arrowhead), (II) showed dramatic necrotic kidney parenchyma; (III and IV) higher magnifications delineate tubular white blood cell casts (blocked arrow). Infections were not observed in diabetic WT mice or nondiabetic WT and mutants.

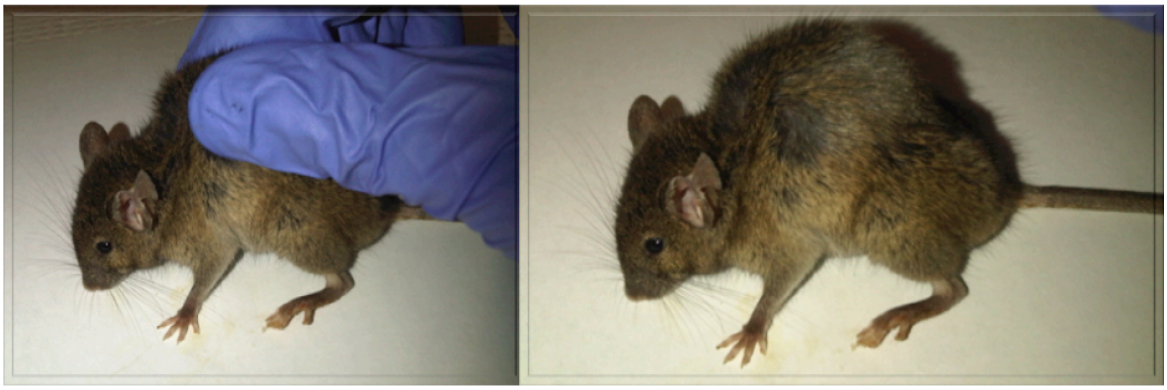

Figure 9 Diabetic *Sweet Pee* mutant exhibited significant dehydration. We demonstrated tenting of the skin fold in this pre-morbid mouse.

7 Discussions

Promoting urinary excretion of glucose is an emerging strategy for the management of Type 2 diabetics. To this end, SGLT inhibitors are under investigation in 13 current clinical trials around the world. In the past, the utility of SGLT inhibitors such as *phlorizin* were limited because of their lack of selectivity for SGLT2(78). Because SGLT1 cotransporters are predominantly expressed in the brush border surface of the small intestine, non-selective SGLT inhibition leads to osmotic diarrhea and other intolerable gastrointestinal side effects in addition to glucose and galactose malabsorption. The compounds currently in clinical trials have >1400-fold selectivity for SGLT2 relative to other SGLTs(79). In this study, we generated a mouse lacking sglt2 using ENU mutagenesis, which provides an excellent model system to study the effect of sglt2 inhibition in diabetic and non-diabetic states.

First, we showed that the genetic mutation that underlies the *Sweet Pee* phenotype is due to a single thymine insertion in exon 4 of the *Slc5a2* gene. This mutation is predicted to result in a frameshift and a premature stop codon. Although ENU mutagenesis usually generates point mutations resulting in single base changes, insertion mutations have been reported previously(80, 81). In fact, one- or two-base insertion mutation occurred up to 37% in one series(82). Both Western blotting (not shown) and immunofluorescence provided evidence that the sglt2 protein is not expressed in proximal tubules of *Sweet Pee* mutants. Moreover, our mutants behave similarly to patients with familial renal glucosuria, which arises as the result of loss of function *SLC5A2* mutations. In contrast, at the mRNA level, we observed an

upregulation of sglt2 expression in isolated renal cortex of the *Sweet Pee* mutants, suggesting that expression of sglt2 may be regulated, perhaps by the elevated tubular glucose levels. It has been documented that glucose sensors in the intestine such as taste receptor, type 1, members 2 and 3 (T1R2, T1R3) affect expressions of intestinal sglt expressions. Interestingly, T1R2 is expressed in HEK-293 cell line (Model Organism Protein Expression Database (MOPED)) as well as kidneys based on high-density oligonucleotide array (BIOGPS: biogps.org). Similarly, T1R3 RNA is detected in the kidneys (Human BodyMap 2.0 data from Illumina – Ensembl). Furthermore, it has been well established that renal sglt2 expressions are increased in diabetic state(33, 35) where both plasma and urine glucose concentrations are elevated. Thus, it is possible that the regulation of renal SGLT2 expressions occurs at the renal tubules. Our real-time primers were designed to amplify a region proximal to the nonsense mutation, which was likely protected from endogenous nonsense-mediated mRNA decay(83-87). The expression of sglt1 transcripts was not different. However, this does not preclude changes at the protein level. It has been shown recently that infusion of D-glucose in the intestine, specifically the duodenum and proximal jejunum of Sprague-Dawley rats, led to a 2.9-fold upregulation in total sglt1 proteins (inside intestinal cells as well as on the luminal brush border) compared to water or D-mannitol infusions(88). The increase in sglt2 was not due to activation in gene transcription(88), rather, it seems to be at least in part mediated by Hsp70 at the post-translational level(89).

Similar to patients with mutations in both *SLC5A2* alleles, homozygous *Sweet Pee* mutants exhibit dramatic glucosuria of >400 mg each day. Despite their

remarkable glucosuria, like patients with type O glucosuria, homozygous SP are euglycemic and have similar HgbA1c as their WT littermates. The heterozygous mutants have a phenotype intermediate between WT and the homozygotes. We did not detect any overt urinary sodium wasting, consistent with an analysis of proximal tubular reabsorption and renal hemodynamics that revealed only mild differences between mutants and WT mice, perhaps mediated by the epithelium sodium channel activated by a higher flow state. Importantly, proximal tubular fluid reabsorption was not affected by lack of sglt2 function. Finally, there was no evidence that persistent massive glucosuria results in acute tubular injury or stress as KIM-1 and NGAL levels were not elevated in homozygous mutants. The apparent benign nature of persistent glucosuria and the isolated distal osmotic diuresis that promotes free water loss without sodium wasting, raises the intriguing possibility that SGLT2 inhibitors might be a therapeutic option to treat conditions of water overload, such as the syndrome of inappropriate anti-diuretic hormone (SIADH). Despite the absence of major differences in electrolyte excretion, the massive glucosuria was associated with an increased urinary excretion of calcium, magnesium, potassium, creatinine and urea. According to a review on nutrients for laboratory mice, the daily recommended dietary intake for sodium, chloride, potassium, calcium, phosphorus, and magnesium are 4 g, 4 g, 9 g, 5 g, 3 g, and 0.5 g per kg of diet respectively(90). Assuming an average diet of 5 g each day, the corresponding daily intake amounts to 20 mg (870 µmol), 20 mg (564 µmol), 45 mg (1152 µmol), 25 mg (624 µmol), 15 mg (484 µmol), and 2.5 mg (103 µmol) respectively. Although the daily urinary excretion of calcium and phosphorous are significantly higher amongst the mutants, 4 and 31.1 µmol/25 g body weight, this may not be physiologically significant as their minimal dietary intake is 256 and 484 µmol

respectively. Of note, gastrointestinal absorption of calcium and magnesium as well as their respective serum levels were not investigated in the current study. In humans, hypercalciuria without hypocalcemia was previously reported(52, 56). The higher amount of calcium and magnesium loss in the urine may reflect an impaired voltage mediated absorption in the distal nephron secondary to a high flow state (91, 92). This is consistent with a distal nephron flow-mediated mechanism for the observed accentuated urinary potassium excretion of 760 µmol /25 g body weight/day amongst the homozygous SP mutants. This daily urinary excretion of potassium represents a significant amount compared to the average daily potassium intake of 1152 µmol. However, these mice were consuming a greater amount of food and were able to maintain a normal serum potassium level.

Diabetic SP mutants have significantly higher urinary excretion of almost all of the electrolytes analyzed in this study compared to both diabetic WT and non-diabetic SP mutants, except for calcium. Interesting, 24-hour urate excretion was significantly higher amongst the diabetic SP mutants compared to diabetic WT controls consistent with clinical data on patients treated with SGLT inhibitors(93). In the renal tubules, urate reabsorption is dependent on a number of transporters: GLUT9, URAT1, OAK4, OAK10(94). GLUT9b is an apical uniporter whose urate uptake could be inhibited by SGLT inhibitors such as phlorizin(95), which may explain the observations of a lower serum acid levels in patients treated with SGLT inhibitors but not for our mouse model. Interestingly, diabetes has been associated with low serum uric acid levels(96, 97), which has been correlated with urine glucose excretion(98) and may explain the observed enhanced uric acid excretion in our diabetic SP mutants.

Given the significant reduction in growth of mutants compared to WT, the safety of SGLT2 inhibition in diabetic children and the long term effects on bone mineral metabolism in adults should be scrutinized. Delayed growth and pubertal maturation in patients affected by familial renal glucosuria was previously reported(56). Due to the rarity of this condition and the various severity of glucosuria, patients are not systematically followed. The observed significantly larger creatinine and urea output in the mutants while their GFR was comparable to the WT, together with a trend towards increased urinary phosphate excretion and a retardation to weight gain, suggest that these mice may well be in a catabolic state(99). We speculate that the heterozygous mutants may also be in a relative catabolic state to explain the observed lower weight gain. In the management of Type 2 diabetes, induction of weight loss may be desirable. However, this effect on the nutritional status in special populations including those with end-stage renal failure will require further investigation.

The potential benefit of SGLT2 inhibition to lower blood glucose in diabetes is supported by our study. *Sweet Pee* mutants demonstrated better glucose tolerance, presumably related to renal glucose wasting since insulin sensitivity is unaffected. Furthermore, at baseline, sglt2 inhibition does not predispose to hypoglycemia or acute kidney injury. In turn, with diabetes, the mutants have improved glucose control including lower HgbA1c levels. This mirrors an average 6% reduction in HgbA1c in patients treated with SGLT2 inhibitors(100) and the effect seems to maintain when patients are evaluated at the 52-week mark(59). Despite an improvement in metabolic control, this did not translate into a better overall clinical outcome amongst the *Sweet*

Pee mutants. There was no observed difference in protein/creatinine ratios, although the C3H strain is relatively resistant to diabetic nephropathy. Moreover, mortality rate was significantly higher in diabetic *Sweet Pee* mutants that can be explained, at least in part, by increased risk of urosepsis. Future study with antibiotic administration will elucidate the impact of urosepsis on mortality. Interestingly, a pilot study of SGLT inhibitors in patients with type 2 diabetes also showed a predilection to genitourinary tract infections(58, 101). More importantly, diabetic SP mutants, particularly the homozygotes, generate extremely large daily urine volumes that are comparable to their body weights. Failure to maintain adequate fluid intake to replace the urinary loss will result in severe intravascular volume contraction.

It is interesting that homozygotes appear more resistant to STZ-induced diabetes. Nine of 26 homozygotes required a second STZ induction compared to 1 in each of the other groups. Although the cumulative STZ dose was higher in those injected twice, statistical analysis of mortality differences in diabetic mice injected only once with STZ was similar to whole group analysis. None of the mice died within the first two weeks following re-injection. Taken together, the data suggests that mortality is not due to direct STZ toxicity, but the mechanism of STZ resistance requires further investigation.

In summary, we report here the generation of a novel sglt2 mouse mutant. This mutant represents a useful model for the study of SGLT2 inhibition in the treatment of diabetes. The short-term efficacy in better glucose control has been demonstrated in our diabetic mutants. Since SGLT inhibitors may lower blood pressure, the effect on

blood pressure in STZ-induced diabetic mutants remains to be examined. Finally, our data point to the potential risks of using SGLT2 inhibitors for glycemic control in diabetes with respect to infection, malnutrition and volume contraction and suggests that these areas should be carefully evaluated in patients receiving SGLT2 inhibitors.

8 Future directions

Based on the data from the current study, we have proposed some interesting areas to pursue for future endeavors.

8.1 Long-term effect on bone metabolism

A potential concern of SGLT2 inhibition is its effect on calcium, phosphorus and bone metabolism. Although we demonstrated in this study homozygous SP mutants exhibit hypercalciuria and a trend towards increased urinary phosphorus excretion, serum levels of calcium, phosphorus, and parathyroid hormone were not measured. We propose ageing homozygous SP mutants (males and females) and their WT littermates (males and females) to 1 year of age and obtain blood levels of calcium, phosphorus, and parathyroid hormone. Both males and females are used due to potential differences in bone metabolism secondary to sex(102). Homozygous SP mutants and WT littermates are generated by setting up breeding between heterozygous males and females. This is to avoid the potential effect of plausible differences in maternal milk production and contents, as well as feeding between homozygous and heterozygous parents, on bone formation in the offspring. In addition, kidneys will be harvested for evaluation of presence of tissue calcifications with

hemotoxylin and eosin, and von Kossa stain. Bone mineralization can be assessed by measuring whole body bone mineral density (g/cm^2), bone mineral content (g), and bone area (cm^2) following euthanasia using peripheral dual-energy X-ray absorptiometry (pDXA)(103). In addition, trabecular and cortical bone morphology can be measured using high-resolution μCT(84). The experiment will be repeated for diabetic animals. Due to the observed high mortality in the diabetic homozygous SP cohort, only serum levels of calcium, phosphorus, and parathyroid hormone will be measured and compared to diabetic WT controls at 3 weeks after confirmation of induction with STZ (3 weeks is chosen because diabetic homozygotes started to die at around 5 weeks). Bone density and morphology will not be assessed due to the short duration of diabetic state.

8.2 Effect of GFR on serum electrolytes and glucose

Pregnancy is a normal physiological state that results in an increase in GFR(104). To evaluate if an increase GFR will affect total daily glucose and electrolyte excretion and serum electrolyte profile, near term pregnant homozygous SP mutants and their pregnant WT littermates will be used in the experiment. Serum levels of glucose, sodium, potassium, calcium, phosphorus, magnesium, uric acid, and HgbA1C will be collected. A 24-hour urine collection and measurement of urine volume, urine excretion of sodium, potassium, calcium, phosphorus, magnesium, and uric acid will also be performed.

To induce a lower GFR state, both 6- to 8-week old homozygous SP mutants and WT littermates are treated with 6-day reversible right-sided unilateral ureteral

obstruction, followed by permanent left-sided ureteral obstruction 1 week after relief of right-sided obstruction(105). At 3 weeks after the procedure for left-sided ureteral obstruction, serum levels of creatinine, urea, glucose, sodium, potassium, calcium, phosphorus, magnesium, uric acid, and HgbA1C will be collected. A 24-hour urine collection and measurement of urine volume, urine excretion of sodium, potassium, calcium, phosphorus, magnesium, and uric acid will also be performed.

9 Acknowledgements

We thank Jasmine Bahrami and the Drucker Lab for assistance and advice regarding metabolic tests and Dr. Kamel Kamel for critical appraisal and discussion. We gratefully acknowledge the measurement of plasma renin by Yuning Huang and Diane Mizel. This work was funded by CIHR grants MOP 77756, 62931, TF grant 016002 and KFOC grant to SEQ, MRC grant GSP 36653 to CMHD. SEQ holds the Gabor-Zellerman Chair in Renal Research, UHN, University of Toronto and is the recipient of a CRC Canada Research Chair Tier II. JL is supported by KRESCENT program, Kidney Foundation of Canada and CIHR. SLA holds the Anne and Max Tanenbaum Chair, MSH.

10 References

1. Duckworth, W, Abraira, C, Moritz, T, Reda, D, Emanuele, N, Reaven, PD, Zieve, FJ, Marks, J, Davis, SN, Hayward, R, Warren, SR, Goldman, S, McCarren, M, Vitek, ME, Henderson, WG & Huang, GD: Glucose control and vascular complications in veterans with type 2 diabetes. *The New England journal of medicine,* 360**:** 129-39, 2009.
2. Patel, A, MacMahon, S, Chalmers, J, Neal, B, Billot, L, Woodward, M, Marre, M, Cooper, M, Glasziou, P, Grobbee, D, Hamet, P, Harrap, S, Heller, S, Liu, L, Mancia, G, Mogensen, CE, Pan, C, Poulter, N, Rodgers, A, Williams, B, Bompoint, S, de Galan, BE, Joshi, R & Travert, F: Intensive blood glucose control and vascular outcomes in patients with type 2 diabetes. *The New England journal of medicine,* 358**:** 2560-72, 2008.
3. Gerstein, HC, Riddle, MC, Kendall, DM, Cohen, RM, Goland, R, Feinglos, MN, Kirk, JK, Hamilton, BP, Ismail-Beigi, F & Feeney, P: Glycemia treatment strategies in the Action to Control Cardiovascular Risk in Diabetes (ACCORD) trial. *The American journal of cardiology,* 99**:** 34i-43i, 2007.
4. Redelmeier, DA, Kenshole, AB & Ray, JG: Motor vehicle crashes in diabetic patients with tight glycemic control: a population-based case control analysis. *PLoS medicine,* 6**:** e1000192, 2009.
5. Zoungas, S, Patel, A, Chalmers, J, de Galan, BE, Li, Q, Billot, L, Woodward, M, Ninomiya, T, Neal, B, MacMahon, S, Grobbee, DE, Kengne, AP, Marre, M & Heller, S: Severe hypoglycemia and risks of vascular events and death. *The New England journal of medicine,* 363**:** 1410-8, 2010.
6. Baggio, LL & Drucker, DJ: Biology of incretins: GLP-1 and GIP. *Gastroenterology,* 132**:** 2131-57, 2007.
7. Marsenic, O: Glucose control by the kidney: an emerging target in diabetes. *Am J Kidney Dis,* 53**:** 875-83, 2009.
8. Wright, EM & Turk, E: The sodium/glucose cotransport family SLC5. *Pflugers Arch,* 447**:** 510-8, 2004.
9. Santer, R & Calado, J: Familial renal glucosuria and SGLT2: from a mendelian trait to a therapeutic target. *Clinical journal of the American Society of Nephrology : CJASN,* 5**:** 133-41, 2010.
10. Brown, GK: Glucose transporters: structure, function and consequences of deficiency. *Journal of inherited metabolic disease,* 23**:** 237-46, 2000.
11. Wright, EM, Hirayama, BA & Loo, DF: Active sugar transport in health and disease. *Journal of internal medicine,* 261**:** 32-43, 2007.
12. Wright, EM: Renal Na(+)-glucose cotransporters. *Am J Physiol Renal Physiol,* 280**:** F10-8, 2001.
13. Hardman, TC & Dubrey, SW: Development and potential role of type-2 sodium-glucose transporter inhibitors for management of type 2 diabetes. *Diabetes therapy : research, treatment and education of diabetes and related disorders,* 2**:** 133-45, 2011.
14. Dye, L, Mansfield, M, Lasikiewicz, N, Mahawish, L, Schnell, R, Talbot, D, Chauhan, H, Croden, F & Lawton, C: Correspondence of continuous interstitial glucose measurement against arterialised and capillary glucose following an oral glucose tolerance test in healthy volunteers. *The British journal of nutrition,* 103**:** 134-40, 2010.

15. Ganapathy, V, Thangaraju, M, Gopal, E, Martin, PM, Itagaki, S, Miyauchi, S & Prasad, PD: Sodium-coupled monocarboxylate transporters in normal tissues and in cancer. *The AAPS journal,* 10**:** 193-9, 2008.
16. Wright, EM & Turk, E: The sodium/glucose cotransport family SLC5. *Pflugers Archiv : European journal of physiology,* 447**:** 510-8, 2004.
17. Hediger, MA & Rhoads, DB: Molecular physiology of sodium-glucose cotransporters. *Physiol Rev,* 74**:** 993-1026, 1994.
18. Zhou, L, Cryan, EV, D'Andrea, MR, Belkowski, S, Conway, BR & Demarest, KT: Human cardiomyocytes express high level of Na+/glucose cotransporter 1 (SGLT1). *J Cell Biochem,* 90**:** 339-46, 2003.
19. Quamme, GA & Freeman, HJ: Evidence for a high-affinity sodium-dependent D-glucose transport system in the kidney. *The American journal of physiology,* 253**:** F151-7, 1987.
20. Turner, RJ & Moran, A: Further studies of proximal tubular brush border membrane D-glucose transport heterogeneity. *The Journal of membrane biology,* 70**:** 37-45, 1982.
21. Turner, RJ & Moran, A: Heterogeneity of sodium-dependent D-glucose transport sites along the proximal tubule: evidence from vesicle studies. *The American journal of physiology,* 242**:** F406-14, 1982.
22. Turner, RJ & Moran, A: Stoichiometric studies of the renal outer cortical brush border membrane D-glucose transporter. *The Journal of membrane biology,* 67**:** 73-80, 1982.
23. Kanai, Y, Lee, WS, You, G, Brown, D & Hediger, MA: The human kidney low affinity Na+/glucose cotransporter SGLT2. Delineation of the major renal reabsorptive mechanism for D-glucose. *The Journal of clinical investigation,* 93**:** 397-404, 1994.
24. Rahmoune, H, Thompson, PW, Ward, JM, Smith, CD, Hong, G & Brown, J: Glucose transporters in human renal proximal tubular cells isolated from the urine of patients with non-insulin-dependent diabetes. *Diabetes,* 54**:** 3427-34, 2005.
25. Lee, YJ & Han, HJ: Regulatory mechanisms of Na(+)/glucose cotransporters in renal proximal tubule cells. *Kidney Int Suppl***:** S27-35, 2007.
26. Gerich, JE: Role of the kidney in normal glucose homeostasis and in the hyperglycaemia of diabetes mellitus: therapeutic implications. *Diabet Med,* 27**:** 136-42.
27. Wells, RG, Pajor, AM, Kanai, Y, Turk, E, Wright, EM & Hediger, MA: Cloning of a human kidney cDNA with similarity to the sodium-glucose cotransporter. *Am J Physiol,* 263**:** F459-65, 1992.
28. Kloeckener-Gruissem, B, Vandekerckhove, K, Nurnberg, G, Neidhardt, J, Zeitz, C, Nurnberg, P, Schipper, I & Berger, W: Mutation of solute carrier SLC16A12 associates with a syndrome combining juvenile cataract with microcornea and renal glucosuria. *American journal of human genetics,* 82**:** 772-9, 2008.
29. Kellett, GL & Brot-Laroche, E: Apical GLUT2: a major pathway of intestinal sugar absorption. *Diabetes,* 54**:** 3056-62, 2005.
30. Diez-Sampedro, A, Hirayama, BA, Osswald, C, Gorboulev, V, Baumgarten, K, Volk, C, Wright, EM & Koepsell, H: A glucose sensor hiding in a family of transporters. *Proceedings of the National Academy of Sciences of the United States of America,* 100**:** 11753-8, 2003.
31. Kamran, M, Peterson, RG & Dominguez, JH: Overexpression of GLUT2 gene in renal proximal tubules of diabetic Zucker rats. *Journal of the American Society of Nephrology : JASN,* 8**:** 943-8, 1997.
32. Chin, E, Zamah, AM, Landau, D, Gronbcek, H, Flyvbjerg, A, LeRoith, D & Bondy, CA: Changes in facilitative glucose transporter messenger ribonucleic acid levels in the diabetic rat kidney. *Endocrinology,* 138**:** 1267-75, 1997.

33. Freitas, HS, Anhe, GF, Melo, KF, Okamoto, MM, Oliveira-Souza, M, Bordin, S & Machado, UF: Na(+) -glucose transporter-2 messenger ribonucleic acid expression in kidney of diabetic rats correlates with glycemic levels: involvement of hepatocyte nuclear factor-1alpha expression and activity. *Endocrinology,* 149**:** 717-24, 2008.
34. Abdul-Ghani, MA, Norton, L & Defronzo, RA: Role of sodium-glucose cotransporter 2 (SGLT 2) inhibitors in the treatment of type 2 diabetes. *Endocrine reviews,* 32**:** 515-31, 2011.
35. Tabatabai, NM, Sharma, M, Blumenthal, SS & Petering, DH: Enhanced expressions of sodium-glucose cotransporters in the kidneys of diabetic Zucker rats. *Diabetes research and clinical practice,* 83**:** e27-30, 2009.
36. Vestri, S, Okamoto, MM, de Freitas, HS, Aparecida Dos Santos, R, Nunes, MT, Morimatsu, M, Heimann, JC & Machado, UF: Changes in sodium or glucose filtration rate modulate expression of glucose transporters in renal proximal tubular cells of rat. *The Journal of membrane biology,* 182**:** 105-12, 2001.
37. Osorio, H, Bautista, R, Rios, A, Franco, M, Arellano, A, Vargas-Robles, H, Romo, E & Escalante, B: Effect of phlorizin on sglt2 expression in the kidney of diabetic rats. *J Nephrol*.
38. Menzel, R, Kaisaki, PJ, Rjasanowski, I, Heinke, P, Kerner, W & Menzel, S: A low renal threshold for glucose in diabetic patients with a mutation in the hepatocyte nuclear factor-1alpha (HNF-1alpha) gene. *Diabetic medicine : a journal of the British Diabetic Association,* 15**:** 816-20, 1998.
39. Pontoglio, M, Prie, D, Cheret, C, Doyen, A, Leroy, C, Froguel, P, Velho, G, Yaniv, M & Friedlander, G: HNF1alpha controls renal glucose reabsorption in mouse and man. *EMBO reports,* 1**:** 359-65, 2000.
40. Pontoglio, M, Sreenan, S, Roe, M, Pugh, W, Ostrega, D, Doyen, A, Pick, AJ, Baldwin, A, Velho, G, Froguel, P, Levisetti, M, Bonner-Weir, S, Bell, GI, Yaniv, M & Polonsky, KS: Defective insulin secretion in hepatocyte nuclear factor 1alpha-deficient mice. *The Journal of clinical investigation,* 101**:** 2215-22, 1998.
41. Bautista, R, Manning, R, Martinez, F, Avila-Casado Mdel, C, Soto, V, Medina, A & Escalante, B: Angiotensin II-dependent increased expression of Na+-glucose cotransporter in hypertension. *American journal of physiology. Renal physiology,* 286**:** F127-33, 2004.
42. Bautista, R, Manning, R, Martinez, F, Avila-Casado Mdel, C, Soto, V, Medina, A & Escalante, B: Angiotensin II-dependent increased expression of Na+-glucose cotransporter in hypertension. *Am J Physiol Renal Physiol,* 286**:** F127-33, 2004.
43. Camerini-Davalos, RA & Marble, A: Incidence and causes of secondary failure in treatment with tolbutamide. Experience with 2,500 patients treated up to five years. *JAMA : the journal of the American Medical Association,* 181**:** 1-4, 1962.
44. Reubi, F: *Glucose titration in renal glucosuria,* London, JA Churchill Limited 1954.
45. Oemar, BS, Byrd, DJ & Brodehl, J: Complete absence of tubular glucose reabsorption: a new type of renal glucosuria (type 0). *Clinical nephrology,* 27**:** 156-60, 1987.
46. Khachadurian, AK & Khachadurian, LA: The Inheritance of Renal Glycosuria. *American journal of human genetics,* 16**:** 189-94, 1964.
47. Santer, R, Kinner,M., Schneppenheim,R., Hillebrand,G., Kemper,M., Ehrich,J., Swift,P., Skovby,F., Schaub,j.: The molecular basis of renal glucosuria: Mutations in the gene for a renal glucose transporter (SGLT2). *Journal of inherited metabolic disease,* 23**:** 178, 2000.
48. Calado, J, Sznajer, Y, Metzger, D, Rita, A, Hogan, MC, Kattamis, A, Scharf, M, Tasic, V, Greil, J, Brinkert, F, Kemper, MJ & Santer, R: Twenty-one additional cases of familial

renal glucosuria: absence of genetic heterogeneity, high prevalence of private mutations and further evidence of volume depletion. *Nephrology, dialysis, transplantation : official publication of the European Dialysis and Transplant Association - European Renal Association,* 23**:** 3874-9, 2008.
49. Magen, D, Sprecher, E, Zelikovic, I & Skorecki, K: A novel missense mutation in SLC5A2 encoding SGLT2 underlies autosomal-recessive renal glucosuria and aminoaciduria. *Kidney Int,* 67**:** 34-41, 2005.
50. Bakris, GL, Fonseca, VA, Sharma, K & Wright, EM: Renal sodium-glucose transport: role in diabetes mellitus and potential clinical implications. *Kidney Int,* 75**:** 1272-7, 2009.
51. Calado, J, Loeffler, J, Sakallioglu, O, Gok, F, Lhotta, K, Barata, J & Rueff, J: Familial renal glucosuria: SLC5A2 mutation analysis and evidence of salt-wasting. *Kidney international,* 69**:** 852-5, 2006.
52. Schneider, D, Gauthier, B & Trachtman, H: Hypercalciuria in children with renal glycosuria: evidence of dual renal tubular reabsorptive defects. *The Journal of pediatrics,* 121**:** 715-9, 1992.
53. Magen, D, Sprecher, E, Zelikovic, I & Skorecki, K: A novel missense mutation in SLC5A2 encoding SGLT2 underlies autosomal-recessive renal glucosuria and aminoaciduria. *Kidney international,* 67**:** 34-41, 2005.
54. Gotzsche, O: Renal glucosuria and aminoaciduria. *Acta medica Scandinavica,* 202**:** 65-7, 1977.
55. Sankarasubbaiyan, S, Cooper, C & Heilig, CW: Identification of a novel form of renal glucosuria with overexcretion of arginine, carnosine, and taurine. *American journal of kidney diseases : the official journal of the National Kidney Foundation,* 37**:** 1039-43, 2001.
56. Scholl-Burgi, S, Santer, R & Ehrich, JH: Long-term outcome of renal glucosuria type 0: the original patient and his natural history. *Nephrology, dialysis, transplantation : official publication of the European Dialysis and Transplant Association - European Renal Association,* 19**:** 2394-6, 2004.
57. Santer, R, Kinner, M, Lassen, CL, Schneppenheim, R, Eggert, P, Bald, M, Brodehl, J, Daschner, M, Ehrich, JH, Kemper, M, Li Volti, S, Neuhaus, T, Skovby, F, Swift, PG, Schaub, J & Klaerke, D: Molecular analysis of the SGLT2 gene in patients with renal glucosuria. *J Am Soc Nephrol,* 14**:** 2873-82, 2003.
58. Bailey, CJ, Gross, JL, Pieters, A, Bastien, A & List, JF: Effect of dapagliflozin in patients with type 2 diabetes who have inadequate glycaemic control with metformin: a randomised, double-blind, placebo-controlled trial. *Lancet,* 375**:** 2223-33, 2010.
59. Nauck, M: Dapagliflozin vs glipizide in patients with type 2 diabetes mellitus inadequately controlled on metformin: 52-week results of a double-blind, randomised, controlled trial. . *Diabetologia,* 53**:** S107, 2010.
60. Patel, AK & Fonseca, V: Turning glucosuria into a therapy: Efficacy and safety with SGLT2 inhibitors. *Curr Diab Rep,* 10**:** 101-7.
61. Bailey, CJ, Gross, JL, Pieters, A, Bastien, A & List, JF: Effect of dapagliflozin in patients with type 2 diabetes who have inadequate glycaemic control with metformin: a randomised, double-blind, placebo-controlled trial. *Lancet,* 375**:** 2223-33.
62. Jones, D: Diabetes field cautiously upbeat despite possible setback for leading SGLT2 inhibitor. *Nature reviews. Drug discovery,* 10**:** 645-6, 2011.
63. Jun, JE, Wilson, LE, Vinuesa, CG, Lesage, S, Blery, M, Miosge, LA, Cook, MC, Kucharska, EM, Hara, H, Penninger, JM, Domashenz, H, Hong, NA, Glynne, RJ, Nelms, KA & Goodnow, CC: Identifying the MAGUK protein Carma-1 as a central

regulator of humoral immune responses and atopy by genome-wide mouse mutagenesis. *Immunity,* 18**:** 751-62, 2003.
64. Eremina, V, Wong, MA, Cui, S, Schwartz, L & Quaggin, SE: Glomerular-specific gene excision in vivo. *J Am Soc Nephrol,* 13**:** 788-93, 2002.
65. Schmittgen, TD & Livak, KJ: Analyzing real-time PCR data by the comparative C(T) method. *Nat Protoc,* 3**:** 1101-8, 2008.
66. Hashimoto, S, Adams, JW, Bernstein, KE & Schnermann, J: Micropuncture determination of nephron function in mice without tissue angiotensin-converting enzyme. *Am J Physiol Renal Physiol,* 288**:** F445-52, 2005.
67. Chen, L, Kim, SM, Oppermann, M, Faulhaber-Walter, R, Huang, Y, Mizel, D, Chen, M, Lopez, ML, Weinstein, LS, Gomez, RA, Briggs, JP & Schnermann, J: Regulation of renin in mice with Cre recombinase-mediated deletion of G protein Gsalpha in juxtaglomerular cells. *Am J Physiol Renal Physiol,* 292**:** F27-37, 2007.
68. Qi, Z, Whitt, I, Mehta, A, Jin, J, Zhao, M, Harris, RC, Fogo, AB & Breyer, MD: Serial determination of glomerular filtration rate in conscious mice using FITC-inulin clearance. *Am J Physiol Renal Physiol,* 286**:** F590-6, 2004.
69. Justice, MJ, Noveroske, JK, Weber, JS, Zheng, B & Bradley, A: Mouse ENU mutagenesis. *Hum Mol Genet,* 8**:** 1955-63, 1999.
70. Soewarto, D, Klaften, M & Rubio-Aliaga, I: Features and strategies of ENU mouse mutagenesis. *Curr Pharm Biotechnol,* 10**:** 198-213, 2009.
71. Broman, KW: Review of statistical methods for QTL mapping in experimental crosses. *Lab Anim (NY),* 30**:** 44-52, 2001.
72. Broman, KW, Wu, H, Sen, S & Churchill, GA: R/qtl: QTL mapping in experimental crosses. *Bioinformatics,* 19**:** 889-90, 2003.
73. Lander, ES & Botstein, D: Mapping mendelian factors underlying quantitative traits using RFLP linkage maps. *Genetics,* 121**:** 185-99, 1989.
74. Gorboulev, V, Schurmann, A, Vallon, V, Kipp, H, Jaschke, A, Klessen, D, Friedrich, A, Scherneck, S, Rieg, T, Cunard, R, Veyhl-Wichmann, M, Srinivasan, A, Balen, D, Breljak, D, Rexhepaj, R, Parker, HE, Gribble, FM, Reimann, F, Lang, F, Wiese, S, Sabolic, I, Sendtner, M & Koepsell, H: Na(+)-D-glucose cotransporter SGLT1 is pivotal for intestinal glucose absorption and glucose-dependent incretin secretion. *Diabetes,* 61**:** 187-96, 2012.
75. Fox, JG: *The Mouse in biomedical research,* Amsterdam ; New York, Academic Press 2007.
76. Andrikopoulos, S, Blair, AR, Deluca, N, Fam, BC & Proietto, J: Evaluating the glucose tolerance test in mice. *Am J Physiol Endocrinol Metab,* 295**:** E1323-32, 2008.
77. Kaku, K, Fiedorek, FT, Jr., Province, M & Permutt, MA: Genetic analysis of glucose tolerance in inbred mouse strains. Evidence for polygenic control. *Diabetes,* 37**:** 707-13, 1988.
78. Ehrenkranz, JR, Lewis, NG, Kahn, CR & Roth, J: Phlorizin: a review. *Diabetes Metab Res Rev,* 21**:** 31-8, 2005.
79. Whaley, JM, Tirmenstein, M, Reilly, TP, Poucher, SM, Saye, J, Parikh, S & List, JF: Targeting the kidney and glucose excretion with dapagliflozin: preclinical and clinical evidence for SGLT2 inhibition as a new option for treatment of type 2 diabetes mellitus. *Diabetes, metabolic syndrome and obesity : targets and therapy,* 5**:** 135-48, 2012.
80. Harbach, PR, Mattano, SS, Zimmer, DM, Filipunas, AL, Wang, Y & Aaron, CS: DNA sequence analysis of hprt mutants persisting in peripheral blood of cynomolgus monkeys more than two years after ENU treatment. *Environ Mol Mutagen,* 33**:** 42-8, 1999.

81. Wang, H, Feng, J, Qi, C & Morse, HC, 3rd: An ENU-induced mutation in the lymphotoxin alpha gene impairs organogenesis of lymphoid tissues in C57BL/6 mice. *Biochem Biophys Res Commun,* 370**:** 461-7, 2008.
82. Cao, J, Yin, M, Chen, J & Xu, S: [Studies on gene mutation and micronucleus formation induced by ethylnitrosourea (ENU) in transgenic mice in vivo]. *Zhonghua Yu Fang Yi Xue Za Zhi,* 34**:** 28-30, 2000.
83. Buhler, M, Paillusson, A & Muhlemann, O: Efficient downregulation of immunoglobulin mu mRNA with premature translation-termination codons requires the 5'-half of the VDJ exon. *Nucleic Acids Res,* 32**:** 3304-15, 2004.
84. DeMambro, VE, Kawai, M, Clemens, TL, Fulzele, K, Maynard, JA, Marin de Evsikova, C, Johnson, KR, Canalis, E, Beamer, WG, Rosen, CJ & Donahue, LR: A novel spontaneous mutation of Irs1 in mice results in hyperinsulinemia, reduced growth, low bone mass and impaired adipogenesis. *J Endocrinol,* 204**:** 241-53.
85. Makarov, R, Steiner, B, Gucev, Z, Tasic, V, Wieacker, P & Wieland, I: The impact of CFNS-causing EFNB1 mutations on ephrin-B1 function. *BMC Med Genet,* 11**:** 98.
86. Silva, AL, Pereira, FJ, Morgado, A, Kong, J, Martins, R, Faustino, P, Liebhaber, SA & Romao, L: The canonical UPF1-dependent nonsense-mediated mRNA decay is inhibited in transcripts carrying a short open reading frame independent of sequence context. *RNA,* 12**:** 2160-70, 2006.
87. You, KT, Li, LS, Kim, NG, Kang, HJ, Koh, KH, Chwae, YJ, Kim, KM, Kim, YK, Park, SM, Jang, SK & Kim, H: Selective translational repression of truncated proteins from frameshift mutation-derived mRNAs in tumors. *PLoS Biol,* 5**:** e109, 2007.
88. Stearns, AT, Balakrishnan, A, Rhoads, DB & Tavakkolizadeh, A: Rapid upregulation of sodium-glucose transporter SGLT1 in response to intestinal sweet taste stimulation. *Annals of surgery,* 251**:** 865-71, 2010.
89. Ikari, A, Nakano, M, Kawano, K & Suketa, Y: Up-regulation of sodium-dependent glucose transporter by interaction with heat shock protein 70. *The Journal of biological chemistry,* 277**:** 33338-43, 2002.
90. Subcommittee on Laboratory Animal Nutrition, CoAN, Board on Agriculture, National Research Council *nutrient requirements of the mouse*, The national academies Press 1995.
91. Kamel, KS, Oh, MS & Halperin, ML: Bartter's, Gitelman's, and Gordon's syndromes. From physiology to molecular biology and back, yet still some unanswered questions. *Nephron,* 92 Suppl 1**:** 18-27, 2002.
92. Ellison, DH: Divalent cation transport by the distal nephron: insights from Bartter's and Gitelman's syndromes. *Am J Physiol Renal Physiol,* 279**:** F616-25, 2000.
93. Katsiki, N, Papanas, N & Mikhailidis, DP: Dapagliflozin: more than just another oral glucose-lowering agent? *Expert opinion on investigational drugs,* 19**:** 1581-9, 2010.
94. So, A & Thorens, B: Uric acid transport and disease. *The Journal of clinical investigation,* 120**:** 1791-9, 2010.
95. Bibert, S, Hess, SK, Firsov, D, Thorens, B, Geering, K, Horisberger, JD & Bonny, O: Mouse GLUT9: evidences for a urate uniporter. *American journal of physiology. Renal physiology,* 297**:** F612-9, 2009.
96. Golik, A, Weissgarten, J, Cotariu, D, Cohen, N, Zaidenstein, R, Ramot, Y, Averbukh, Z & Modai, D: Renal uric acid handling in non-insulin-dependent diabetic patients with elevated glomerular filtration rates. *Clinical science,* 85**:** 713-6, 1993.
97. Bandaru, P & Shankar, A: Association between Serum Uric Acid Levels and Diabetes Mellitus. *International journal of endocrinology,* 2011**:** 604715, 2011.

98. Gotoh, M, Li, C, Yatoh, M, Iguchi, A & Hirooka, Y: Serum uric acid concentrations in type 2 diabetes: its significant relationship to serum 1,5-anhydroglucitol concentrations. *Endocrine regulations,* 39**:** 119-25, 2005.
99. Carlotti, AP, Bohn, D, Matsuno, AK, Pasti, DM, Gowrishankar, M & Halperin, ML: Indicators of lean body mass catabolism: emphasis on the creatinine excretion rate. *QJM,* 101**:** 197-205, 2008.
100. Musso, G, Gambino, R, Cassader, M & Pagano, G: A novel approach to control hyperglycemia in type 2 diabetes: sodium glucose co-transport (SGLT) inhibitors: systematic review and meta-analysis of randomized trials. *Annals of medicine,* 44**:** 375-93, 2012.
101. Wilding, JP, Norwood, P, T'Joen, C, Bastien, A, List, JF & Fiedorek, FT: A study of dapagliflozin in patients with type 2 diabetes receiving high doses of insulin plus insulin sensitizers: applicability of a novel insulin-independent treatment. *Diabetes Care,* 32**:** 1656-62, 2009.
102. Grasemann, C, Devlin, MJ, Rzeczkowska, PA, Herrmann, R, Horsthemke, B, Hauffa, BP, Grynpas, M, Alm, C, Bouxsein, ML & Palmert, MR: Parental diabetes: the Akita mouse as a model of the effects of maternal and paternal hyperglycemia in wildtype offspring. *PloS one,* 7**:** e50210, 2012.
103. Bouxsein, ML, Pierroz, DD, Glatt, V, Goddard, DS, Cavat, F, Rizzoli, R & Ferrari, SL: beta-Arrestin2 regulates the differential response of cortical and trabecular bone to intermittent PTH in female mice. *Journal of bone and mineral research : the official journal of the American Society for Bone and Mineral Research,* 20**:** 635-43, 2005.
104. Davison, JM & Dunlop, W: Renal hemodynamics and tubular function normal human pregnancy. *Kidney international,* 18**:** 152-61, 1980.
105. Puri, TS, Shakaib, MI, Chang, A, Mathew, L, Olayinka, O, Minto, AW, Sarav, M, Hack, BK & Quigg, RJ: Chronic kidney disease induced in mice by reversible unilateral ureteral obstruction is dependent on genetic background. *American journal of physiology. Renal physiology,* 298**:** F1024-32, 2010.

Chapter 4 A new cystic kidney phenotype identified by ENU mutagenesis

1 Abstract

Cystic kidney diseases represent the primary genetic cause of end-stage renal disease in North America, contributing up to 5% of incident cases. Glomerulocystic kidney disease (GCKD), a subtype of renal cystic disorder that embodies a heterogeneous group of disorders characterized by dilatation of the Bowman's space. Recently, mice with mutations in the Bardet-Biedl syndrome genes and *fat4* demonstrate perturbed planar cell polarity (PCP) at the molecular level. Here, we report a new mouse model of GCKD with possible PCP involvement. **Method:** To generate the GCKD mouse mutant, we took the forward genetic approach with *N-ethyl-N-nitrosourea* (ENU) mutagenesis. Mutagenized C57BL/6J male mice were bred with wild-type C3H/HeJ female mice. GCKD mutant was found on a dominant screen and further characterized. **Results:** We identified a point mutation in *Samd9l* that causes a single amino acid substitution from serine to threonine (S169T). GCKD mutants demonstrate variable degree of Bowman's capsule dilation and tubular cystic disease. Homozygous mutants do not survive beyond P0. Glomerulocysts are present in most P0 homozygous mutants. GCKD mutants manifest "kinked" tail and disoriented inner ear hair cells, phenotypes suggestive of PCP defects. Immunoprecipitation from HEK293T cells transiently transfected with vector expressing wild-type Samd9l cDNA and further mass spectrometry reveals potential protein partners involved in the ubiquitin proteasome pathway, specifically Stub1, whose substrate is P53. Surprisingly, we found lower protein levels of P53 and P21 in whole kidney lysate from homozygous mutants compared to their wild-type littermates. **Summary:** Taken together, we generated a mouse novel model of cystic kidneys using forward genetics. The mutation seems to manifest some PCP phenotypes and affect cell cycle regulation. The connection between PCP and cell cycle regulation, if exists, is yet to be determined.

2 Introduction

2.1 Background and Rationale

2.1.1 Cystic kidney diseases

Cystic kidney disease is the most common genetic cause of end-stage renal disease (ESRD)(1), and it is responsible for approximately 5% of incident cases in North America(2), and 8-10% in Europe and Australia(3). Notwithstanding the astounding financial burden of ESRD, which accounted for almost 15% of the total annual Medicare spending in the United States(4), its impact on the level of the individual patient is enormous. Dialysis patients have an average 5-year survival of only 37% and an all-cause hospitalization of 2 per patient year(4).

Over the past 2 decades, great strides have been made in our understanding of cystic kidney disease. Positional cloning in humans and mice led to the discovery of some key critical genes responsible for cyst formation and disease. These range from monogenic mutations in genes responsible for autosomal dominant polycystic kidney disease (ADPKD)/(*PKD1*, *PKD2*) and autosomal recessive polycystic kidney disease (ARPKD)/(*PKHD1*), to complex pleiotropic disorders including nephronopthisis, medullary cystic kidney disease (MCKD) type 2 (*UMOD*/*THP*)(5, 6), and Hepatocyte Nuclear Factor 1β (*HNF1β*) in MODY type 5(7). Hepatocyte Nuclear Factor 1β is a transcription factor and appears to regulate the expression of a number of these cystic genes including *PKHD1*, *PKD2*, *UMOD* and *IFT88*(7). Interestingly, one of the most penetrant phenotypes is the presence of an unusual form of cystic kidney disease involving the glomeruli. Kidney cysts are observed in a transgenic mouse model expressing dominant-negative HNF1β(8). Furthermore, two novel mutations in *Hnf1β* characterized by glomerulocystic kidneys, pancreas hypoplasia, and abnormal development of genital tracts, also showed an increased expression of polycystin-1, polycystin-2, fibrocystin, and uromodulin in the cysts(9). The following sections are

devoted to a general summary of both cystic kidney diseases and glomerulocystic kidney diseases.

The most common form of adult monogenic cystic kidney disease is ADPKD, which occurs in approximately 1 in 400(10) to 1 in1000(11) live births. Mutations in *PKD1* (16p13.3) or *PKD2* (4q21)(12) have been established as the cause of ADPKD. About 50-75% of the patients with ADPKD progress to ESRD(13, 14). The annual incidence of ESRD due to ADPKD in men and women were 8.7 and 6.9 per million in the United States (1998-2001)(11, 15), 7.8 and 6.0 per million in Europe (1998-1999)(16), and 5.6 and 4.0 per million in Japan (1999-2000)(17). *PKD1* consists of 46 exons and encodes a large receptor-like protein comprising 4303 amino acids known as polycystin-1 (PC1). Polycystin-1 contains 11 transmembrane domains, a large extracellular amino-terminus of over 3000 amino acids with 12 PKD domains, and a short intracellular 200 amino acid carboxyl-terminal tail(18-20). Polycystin-1 is involved in a number of cellular processes including cell-cell and cell-matrix adhesion, cell signaling cascades and renal tubulogenesis(21). Polycystin-2 (PC2), the protein product of *PKD2*, consists of 15 exons, and plays a role in cell calcium signaling(22-24) through the transport of calcium into the plasma membrane and the endoplasmic reticulum(25). The two polycystins interact via their cytoplasmic domains to form a dimeric complex(23). Interestingly, both PC1 and PC2 are found in the cilium/basal body complex (CBC) ((26, 27) where many other cystic genes are localized. Mutations in *PKD1* are generally associated with more aggressive progression, and an earlier age of ESRD at 54.3 years compared to 74 years in patients with mutations in *PKD2*(28, 29). This observation is most likely attributable to an earlier age of onset in *PKD1*(30). *PKD1* mutations accounts for about 85% of ADPKD(31). Candidate mutations are identified in about 90% of the ADPKD cases(28). A larger proportion of truncating compared to missense mutations have been identified, however, the position of the mutations rather than the type predicts the severity of the phenotype(32). Autosomal recessive PKD (ARPKD) is another monogenic disorder caused by mutations in *PKHD1*, which encodes fibrocystin. It presents much earlier in life during neonatal or early childhood(33), and affects about 1 in 10,000 live births(34).

Fibrocystin is also localized to the CBC and it interacts with PC2. The main phenotype in both ADPKD and ARPKD is the development of kidney cysts. They share a common feature of having a variable degree of phenotypic expression even for affected individuals within the same family(15). In ADPKD, cysts in other organs including the liver, pancreas, seminal vesicles, and arachnoid have been reported. In addition, intracranial aneurysm is about 5 times more common than that in the general population(11). Cardiac defects, predominantly valvular abnormalities, have also been reported(1).

Although ADPKD is inherited in an autosomal dominant fashion, at the cellular level, a two-hit hypothesis has been widely accepted, based on the observation that focal cyst development is associated with loss of heterozygosity or other somatic mutations(35, 36). Mice homozygous for *Pkd1* or *Pkd2* mutations die embryonically between E12.5 to E16.5 with cystic kidneys(37). Heterozygous mutants have fewer tubular cysts; glomerular and hepatic cysts have been observed and they do not die prematurely(38). In some cysts, the second hit does not lead to inactivation of both alleles of a single PKD locus, but rather inactivation of a single allele at each PKD locus suggesting that trans-heterozygosity of the two genes is sufficient for cystogenesis(39). The observation that a hypomorphic mouse model expressing about 20% Pkd1 are viable and develop kidney cysts, hepatic cysts and aortic aneurysm(40), leads to the threshold model of cystogenesis whereby cysts ensue when the combined expression of PC1 and PC2 has fallen below a critical threshold(41).

Apart from the prototypic monogenic cystic kidney diseases, there exists a separate rare group of pleiotropic disorders where kidney cysts and in many cases, glomerular cysts, and cystic dysplasia are part of the constellation of phenotypes. These disorders are characterized by marked genetic heterogeneity and are reviewed in the following sections.

2.1.2 Glomerulocystic kidney diseases

Glomerulocystic kidneys were identified at least as early as 1941 in an infant suffered from renal failure and cystic changes in the glomeruli(42). Since then, there were case reports of this disease mainly appearing in the pediatric literature(43-45). Glomerular cysts have been identified in 3 clinical settings 1) isolated non-syndromic glomerulocystic disease (GCKD) that are heritable or due to sporadic mutations 2) glomerulocystic disease associated with heritable malformation syndromes and 3) glomerulocystic disease in connection with dysplastic kidneys (46-48). Most recently, due to the complexity of GCKD, a new classification has been proposed(49). In addition to the original GCKD associated with heritable malformation syndromes (such as tuberous sclerosis complex or TSC(50), Jeune syndrome(48), Meckel-Gruber syndrome(51), orofaciodigital syndrome(52), brachymesomelia renal syndrome(53), short rib-polydactyly syndrome(54), Zellweger syndrome(55), nephronophthisis(56), medullary cystic kidney disease type 2(57), Bardet-Biedl syndrome(58), and maturity-onset diabetes of the young (MODY5)(59) etc), a new category of non-mendelian syndromic GCKD including trisomy 9, 13, and 18 has been added; acquired GCKD (as in hemolytic uremic syndrome) is combined with dysplastic kidneys; sporadic GCKD is separated from familial non-syndromic which mainly comprises of autosomal dominant polycystic kidney diseases. It is worth noting that most of these diseases are also associated with tubular cysts, although to a lesser extent. In the next few paragraphs, I will highlight some of these interesting disorders.

Mutation in TSC have resulted in variable degree of glomerulocystic changes which can sometimes be undetectable or even found in unilateral kidneys(50). The protein products, tuberin and hamartin, are believed to be tumor suppressors and function to regulate cell growth and proliferation. Interestingly, these proteins are critical in suppressing the activity of the mammalian target of rapamycin complex 1 (mTORC1) and therefore loss of function results in constitutively active mTORC1 pathway(60).

GCKD have been described in patients with medullary cystic kidney disease type 2 (MCKD2), also known as familial juvenile hyperuricemic nephropathy in the pediatric literature(61, 62). The *UMOD* encodes the protein uromodulin/Tamm-Horsfall protein, which is exclusively secreted in the thick ascending limb of the loop of Henle(63). A majority of the mutations found in human results in abnormal assembly of uromodulin and subsequent accumulation within the endoplasmic reticulum(64-66). Immature tubular developments in addition to glomerular cystic changes have also been reported(57). Although MCKD2 is inherited in an autosomal dominant pattern, patients with both alleles affected have a more aggressive course of the disease(67).

Nephronophthisis (NPHP) is a group of autosomal recessive disorder characterized by cysts formation in the renal medullar and at the corticomedullary junction(68) in addition to tubular basement membrane abnormalities and interstitial fibrosis(69). It leads to kidney impairment much earlier in life. The majority of the cases of NPHP have ben associated with mutations in the *NPHP1* gene, which encodes the protein nephrocystin-1(68). However, only *NPHP3* has been specifically linked to GCKD. Mutations in *NPHP3* lead to early embryonic patterning defects with a multisystem involvement including and not limited to GCKD, structural heart defects, situs inversus, and polydactyly(51). A double heterozygous hypomorphic *Nphp3*$^{pcy/ko}$ mouse model recapitulates kidney cysts affecting both the Bowman's capsule and the renal tubules(70). Interestingly, nephrocystin-3, the protein product of *NPHP3*, coprecipitates with inversin (*NPHP2* gene product), which plays a critical role in inhibiting the canonical Wnt signaling pathway(51). In addition, nephrocystin-3 inhibits disheveled-1 mediated canonical Wnt signaling independent of inversin and involves the planar cell polarity (PCP) pathway, a non-canonical Wnt pathway. Knockdown of *NPHP3* results in abnormal convergent extension in *Xenopus*, asserting its role in PCP signaling. Nephrocystin-3, similar to other NPHP proteins, is expressed in the primary cilium/basal body complex(51). In addition to *NPHP*, other rare pleiotropic disorders of cystic kidneys where the respective protein products are localized within the primary cilia/basal bodies/centrosomes include mutations in *IFT88*, *OFD1*, and *BBS*. The Oak Ridge polycystic kidney disease (orpk) mouse represents a hypomorphic model of

Ift88, which encodes polaris, and results in polycystic kidney phenotype involving both glomeruli and tubules, laterality defects, and biliary hyperplasia and dysplasia inherited in an autosomal recessive pattern(71). Polaris functions specifically for intraflagellar transport within the primary cilia. *Ofd1* (oral-facial-digital syndrome 1) targeted knockout mouse also manifests renal cysts (tubular and glomerular) and laterality defect apart from neural tube defect(72). Ofd1 is a component within the centriole and important for the biogenesis of cilia and specification of left-right axis(72). Bardet-Biedl syndrome (BBS) is characterized by obesity, mental retardation, retinal degeneration, and kidney cysts. *Bbs1*, *Bbs4*, and *Bbs6* KO mice display neural tube defects and cochlear stereociliary bundle disruption suggestive of abnormal PCP signaling(73). Furthermore, their phenotypes are enhanced by *Vangl2* mutation, a core PCP gene. The protein products of *BBS* are involved in dynein-driven microtubular transport(74). *BBS8*, whose protein also localize to the cilia, have been shown to cause randomization of left-right body axis symmetry(75).

Analysis of genes involved in cystic kidney diseases in model systems has given crucial insights into the possible molecular mechanisms of cystogenesis. In addition to those transgenic mouse models mentioned above, at least 3 other existing mouse mutants exhibit glomerular cysts in addition to cysts throughout the nephron: jcpk, bpk and nm1633(47, 76, 77). Recently, disruption of the murine homolog for the Drosophila gene bicaudal in chromosome 10 was discovered to underlie the defect in both the jcpk and allelic bpk mice.

Having reviewed the genetics of cystic kidney diseases and GCKD, the next section focuses on the molecular mechanisms that have been implicated in these disorders.

2.1.3 Pathways associated with cystic kidney diseases

2.1.3a Cilium/basal body complex (CBC)

A rich literature exists linking ciliary defects to cystic kidney diseases. As alluded in previous section, many of the cystic proteins are localized to the primary cilium/basal body complex(78-84). These include the proteins identified in monogenic polycystic kidney diseases (polycystin-1, polycystin-2 and fibrocystin) as well as those in complex pleiotropic disorders including BBS and NPHP. In fact BBS and OFD1 are known clinical examples of ciliopathy. Since cilia function is also involved in photoreception, defects in photoreceptors are observed in orpk mice, BBS(85) and NPHP(69). The serendipitous discoveries of cystic kidney phenotypes in animals with *Ift88*(86) and *kif3a*(87, 88) mutations, both of which are crucial for intraflagellar transport and cilia assembly, led to an emergence of evidence that ciliary dysfunction underlies the pathogenesis of multiple forms of renal cystic diseases. To date, a handful of mouse models of GCKD associated with defects in cilia exist and these include *pcy* (*Nphp3*)(51), *Wwtr1*(89), *Glis3*(90), *jcpk* (*Bicc1*)(76) and *Pkd* overexpression(91).

The primary cilium is a non-motile hair-like organelle that is found virtually in almost all mammalian cells. It consists of 9+0 microtubule doublets(92), and unlike most motile cilium, it lacks the central pair(93). The cilium originates from one of the two centrioles that form the centrosome (mother and daughter centrioles), which is a microtubule-organizing center in most cells(93). In renal tubular epithelial cells, the mother centriole migrates to the apical membrane of polarized cells(94), transforms into the basal body, and nucleates the microtubular skeleton of the cilium. The external part of the cilium is made up of the axonome that is covered by ciliary membrane which is distinct from the cell membrane(93). The basal body and the transition fibers at the base regulate protein content of the cilia membrane(93). Proteins are transported in and out of the axonome by anterograde and retrograde intraflagellar transport, a microtubule motor-based transport system(95). The anterograde movement from the

base to the tip of the cilium is mediated by kinesin-II, which is a heterotrimeric protein composed of two motor subunits, KIF3A and KIF3B, and one non-motor subunit (KAP3)(95). Retrograde transports protein from the tip to the base and is mediated by dynein 1b(96).

Solitary cilium is expressed in most mammalian cells. In the kidneys, primary cilium is found in the tubular epithelium, it is also expressed in the parietal epithelial cells of the Bowman's space (our data). In fact, only certain intercalated cells in the kidneys lack these interesting structures(26, 97, 98). The traditional role of these non-motile cilia is thought to be sensors of the extracellular environment in the capacity of mechanosensation, chemosensation, and receptor-mediated signal transduction(99). Urinary flow has been suggested to promote nephron development, tubular elongation, and differentiation(100). Renal tubular diameter is tightly regulated(101) and the primary cilium governs the tubular diameter by its mechanosensor function(26, 102). In tubular epithelial cells, these cilia protrude into the apical lumen and respond to flow mediated mechanical deflection(102) by stimulating an increase in cytosolic calcium(103). Polycystin-2, a cation channel, is involved in this calcium flux. Interestingly, in the absence of the polycystin-1 and -2, and fibrocystin, mechanical stimulation of cilia failed to induce calcium signaling(102). Intriguingly, the effect of ciliary defect on cyst development is time dependent. In mice, cilia dysfunction induced prior to postnatal day 12 results in severe and rapidly progressive cystic phenotype(104, 105). In contrast, induction after day 14 leads to mild and delayed phenotype(104, 105) suggesting a critical window within which cystogenesis initiates. In addition to growth and proliferation during tubulogenesis, ciliary responses also modulate cell polarity and mitotic spindle orientation during cell division(106, 107). Because cilium also establishes left-right asymmetry through the embryonic node, some animal models of cystic kidney diseases also manifest randomization of left-right axis(108).

Ciliary signaling has intimate interactions with other critical pathways involved in cystic kidney diseases including planar cell polarity (PCP), canonical Wnt, and sonic

hedgehog (SHH). All of these pathways have also been implicated in cystic kidney diseases, and will be discussed in the following paragraphs.

2.1.3b Planar cell polarity (PCP)

Wnt signaling is an evolutionary conserved pathway critical for development and proliferation particularly in embryogenesis and tumor growth. Non-canonical Wnt consists of planar cell polarity (PCP) and the Wnt calcium pathways. In organogenesis, PCP is crucial to organize tissue in the plane of organ extension and it tightly governs the orientation of cell division(109, 110). In vertebrates, PCP effects convergent extension which has been implicated in polycystic kidney disease, mitotic spindle orientation, formation of cilia, and inner ear development(111). The PCP literature emerges initially from studies in *Drosophila* eye and wing patterning. This pathway involves 3 classes of proteins: upstream Fat/Dachsous (Ds) proteins, core PCP proteins, and downstream PCP effectors (see review in (112, 113)). In *Drosophila* wing, Fz, Dsh, and Dgo are found in the distal aspect of the cell; Pk, Vangl in the proximal area; and Fmi in both. PCP effectors include Inturned (In), Fuzzy (Fy), and RhoA, which coordinately regulate cell morphogenesis; c-Jun N-terminal kinase (JNK)(114, 115) mediates gene expressions in controlling wing hair and mitotic spindle orientation. More specifically, inhibition of the Fz-Dsh complex by Vangl and Pk preserves the asymmetrical distribution of Fz-Dsh-Dgo complex which in turn activates 2 separate pathways: the Caam1/Rho/ROK pathway mediates cytoskeletal changes; whereas the Cdc42/Rac/c-Jun N-terminal kinase pathway induces transcription and effects wing hair orientation and mitotic spindle orientation(116). In vertebrates, additional genes previously not found to have PCP effect in *Drosophila,* demonstrate PCP defects when mutated such as neural tube(117) and inner ear kinocilia polarity defects(118) in *Scribble* mutants.

With respect to cilia, it is unclear if PCP plays a role in establishing cellular apical-basal polarity, a process necessary for the proper docking of the mother

centriole before forming the basal body. In this process, cadherin-mediated cell-cell contact is crucial in reorganizing the actin cytoskeleton. Microtubules are organized in either longitudinal arrays along the apical-basal axis having their plus ends toward the apical membrane or network parallels to the apical membrane(119). The adheren junctions facilitate recruitment of the PAR complex, which in turn establishes the apical and basolateral membrane domains(120), a critical process to direct mother centriole migration. The complex consists of Par6, a Ras-related Rho-GTPases that control microtubule interaction with the cortex and coordinate the growth of cortical microtubules(121, 122); Par3, a PDZ containing scaffold protein that interacts with the anterograde intraflagellar transport motor protein KIF3A(123); and atypical protein kinase C (aPKC). The PAR complex recruits the Crumbs (Crb) complex to the tight junction in the apical membrane where it forms a complex with the scaffold protein Pals1 and Par6(124). The basolateral membrane contains a complex of Scribble, Disc Large (Dlg), and Lethal Giant Larvae (Lgl). The two complexes are mutually exclusive to maintain the apical/basolateral polarity(125, 126). PAR complex has been postulated to be involved in establishing an apical membrane for the mother centriole to find its correct location to form the basal body. Mutations in *VHL* lead to defective ciliogenesis and kidney cysts through interaction with Par6(127). The PCP protein Dsh in conjunction with tumor suppressor product of Lgl are required to regulate the PAR complex for specification of the apical-basal polarity in *Xenopus* ectoderm(128). Interestingly, loss of Dsh leads to absence of cilia formation in bronchial epithelium(129). In addition to the docking of the mother centrioles, other lines of evidence substantiating the link between PCP and cilia include the observations that loss of PCP effectors In and Fy disrupts cytoskeleton and cilia assembly(130); Dgo affects the normal tilting of the cilia on the ventral node of mouse embryo(131); Vangl2 and Fat4 are expressed at the base of the cilia(112, 132). Finally, human ciliopathies including BBS and OFD also exhibit PCP phenotypes such as neural tube defects and loss of polarized inner ear hair cells(133, 134).

The discovery of kidney cysts in NPHP2 due to mutations in *inversin* was the first suggestion linking PCP to cystic kidney diseases. Further, many cystic diseases

including NPHP also manifest PCP phenotype. Inversin acts as a switch between canonical Wnt and PCP signaling by negatively regulating canonical Wnt(135). During kidney development, the tubular epithelial cells proliferate and contribute to the elongation process. The dividing cells align along the anterior-posterior axis of the growing nephron(106). In order to achieve oriented extension, mitotic spindle axis is tightly controlled within 34° in the majority of dividing tubular cells(106). Loss of PCP genes has been shown to result in disruption in mitotic axis in other species as well including the fish and the flies(110, 136). A random axis of cell division is commonly seen in mammalian models of polycystic kidneys(106, 137). For example, loss of the PCP gene *Fat4* in mice leads to randomization of spindle orientation and cystic kidneys together with classic PCP phenotypes including neural tube defects and disoriented inner ear hair cells(132). The exact mechanism by which PCP regulates mitotic axis remains unclear. Disruption of normal apical-basolateral polarity in the cysts is another common PCP phenotype in both human polycystic kidney disease(138, 139) and animal models of cystic kidney diseases including cpk(140), orpk(34), bpk(141, 142), Pkd1(38), Kif3a(88).

2.1.3c Canonical Wnt/β-Catenin

The Wnt pathway is composed of a large family of glycoproteins that work in concert to regulate a multitude of critical cellular processes from organ patterning to cell cycle regulation, cell fate determination, cell proliferation, transformation and apoptosis (refer to reviews (116, 143, 144)). Upon canonical Wnt activation, Frizzled (Fz) (G-protein coupled receptor) together with low-density lipoprotein receptor-related protein (LRP) co-receptors(145, 146) are recruited. The interaction between Fz and LRP results in phosphorylation of LRP by glycogen synthase kinase-3β (GSK3β) and casein kinase 1 (CK1)(147). This process leads to recruitment of Axin to LRP and Dishevelled (Dsh) to Fz. Phosphorylation of Dsh inhibits β-catenin degradation complex(116, 143). The complex comprises 3 critical proteins including adenomatous polyposis coli (APC), Axin, and GSK3β. Coordinately, GSK3β phosphorylates β-

catenin, which in turn leads to proteasomal degradation by the ubiquitin-ligase transductin repeat-containing protein (β-TrCP)(148). When β-catenin degradation is inhibited, cytosolic β-catenin accumulates and translocates into the nucleus to activate Lymphoid-enhancer factor/T-cell factor (LEF/TCF)-sensitive transcription of genes(149, 150). Although, activation of the canonical Wnt has been attributed mainly to post-translational modification of β-catenin, there is emerging evidence that tight regulation also exists at the mRNA level. β-catenin mRNA translation is regulated as in the case of astrocyte migration during development and following neuronal trauma by CPE-binding protein (CPEB1)(151). Increased in β-catenin mRNA levels have been reported in many cancer literature including intestinal cancers and desmoid tumors(152-154). Genetic mutations in both β-catenin and APC have been reported. It is unclear whether these observations represent an increase in transcription or decreased degradation of the transcripts. Recently, the promotion of β-catenin transcript degradation, by the mRNA decay-promoting factor KSRP, an AU-rich element (ARE)-binding protein, which recruits the exoribonucleolytic complex exosome (an RNA decay machinery) at the 3' UTR of the transcript, has been shown to be modulated by AKT. AKT phosphorylates KSRP at a unique serine residue (Ser193) and promotes its binding to multifunctional protein 14-3-3 and prolongs half-lives of β-catenin transcripts(155).

In the kidneys, Wnt signaling is crucial for renal morphogenesis. Wnt-1 is important for the induction of the developing metanephric mesenchyme to differentiate and form the glomerular and tubular epithelium(156). Further, Wnt-4 expression in the mesenchymal cells is obligatory for tubulogenesis as KO mice do not form pretubular cell aggregates(157) and Wnt-11 is localized to the tip of the ureteric bud through contact with the metenephric mesenchyme(158). Interestingly, the C-terminus of PC1 increases cytosolic β-catenin level in HEK 293T cells by inhibiting the degradation complex, specifically GSK3β activity(159). Further, injection of expression vector for the C-terminus of PC1 into zebrafish embryos at 1-2 cell stage results in dorsalizing effect and defects in posterior trunk and tail development, phenotypes of β-catenin overexpression(159). Animal models of both over and under expression of canonical

Wnt lead to renal cysts formation highlighting that normal tubular development is exquisitely sensitive to dosage and perhaps temporal activation of this complicated pathway. β-catenin(160) overexpression and APC inactivation(161) lead to canonical Wnt activation and cystic kidney phenotype; canonical Wnt loss-of-function mutants also develop cysts(162). This mirrors the observations that KO, hypomorphic and overexpression models of *Pkd1* and *2* result in cysts development(40, 163, 164). Further, a reduction in canonical Wnt, cystic kidneys, and ciliopathy were observed in a mouse KO for *Ahi1*, a gene responsible for Joubert syndrome(165).

2.1.3d Mammalian target of rapamycin (mTor)

The evidence linking excessive mTOR activity to cystogenesis in PKD is quite extensive(166). MTOR is a serine/threonine kinase that provides the catalytic activity for two distinct multiprotein complexes known as mTOR complex 1 (mTORC1) and 2 (mTORC2). Activation of mTORC1 promotes cell growth and cell proliferation. Its activity is tightly regulated by the availability of amino acids, growth factors, and energy stores. The effects of mTORC2 are different from those of mTORC1 and include modulation of cell survival, cell polarity, cytoskeletal organization, and activity of aldosterone-sensitive sodium channel(167). Loss of function of TSC complex 1 and 2, an upstream negative regulator of mTOR, has been associated with kidney cysts development in both human and rodent models(168, 169). In humans, renal cysts have been reported in patients with tuberous sclerosis, a rare hereditary pleomorphic disorder characterized by the development of benign hamartomas in multiple organs due to inactivation of either *TSC1* or *TSC2* gene(170). Furthermore, patients with large deletions on chromosome 16 encompassing both *PKD1* and the adjacent *TSC2* develop an unusually severe form of PKD reaching ESRD during second decade of life, suggesting synergy between these intersecting pathways(171, 172). In vitro studies seem to suggest the interaction between cytoplasmic tail of polycystin-1 with tuberin(173). This interaction increases the activity of TSC2, which in turn results in inhibition of mTOR(174). PC1 prevents ERK1/2-mediated phosphorylation and

inhibition of TSC2(175, 176); and protects TSC2 from inhibition by AKT(174). MTOR has been shown to be activated in PKD. Activation in mTORC1 as evidenced by increased phosphorylation of its downstream S6 kinase 1 and 2 (S6K1/2) as well as 4E-BPs have been demonstrated in human with ADPKD(173, 174, 177), mouse model of *Pkd1*(173, 178), and Han:SPRD rat model(179-181). In jck mouse model of *Nphp9*, loss of ganglioside Gm3 synthase reduces cyst progression with associated decreased Akt-mTOR signaling(182). Administration of rapamycin mediates reduction in cysts growth and preservation of renal function in mice with inactivating mutations of *Pkd1*(173, 178) and *Pkd2*(183), *Nphp3* (pcy)(184, 185) as well as Han:SPRD rat model(179, 181) but not in PCK rats(186). In addition, analysis of transplanted ADPKD patients who received mTOR inhibitors showed a reduction in size of the native kidney and liver compared to other immunosuppressive regimens(173, 187). The effect of mTOR inhibition and cysts regression in prospective study is less clear with mixed results(188-190).

Interestingly the protein products of both TSC1(191) and TSC2(168) localize to the basal body of primary cilia. Flow induced bending of the primary cilia inhibits mTORC1 activity and reduces cell size through activation of the kinase LKB1, which in turn activates AMPK, an upstream positive regulator of TSC(192). In addition, mutation of *INPP5E* , causes MORM syndrome, a condition related to Bardet-Biedl syndrome characterized by mental retardation, obesity, congenital retinal dystrophy and micropenis in males(193, 194). INPP5E hydrolyzes ins(1,4,5)P3, which mobilizes intracellular calcium and acts as a second messenger for downstream cellular responses. The action of INPP5E has been linked to suppression of the PDGF-AA-PDGFRα-PI3K signaling and premature cell cycle entry and TOR signaling(194). Mutant mice developed cystic kidneys (along the entire nephrons), glomerulocystic changes, skeletal defects including bifid sternum, and occasional anencephaly and exencephaly(193). The action of Inpp5e has been linked to suppression of the PDGF-AA-PDGFRα-PI3K signaling and premature cell cycle entry and TOR signaling(194).

2.1.3e Sonic hedgehog signaling (Shh)

Studies of defective ciliogenesis revealed that cilia are critical for vertebrate Shh signaling, a pathway that is crucial for embryonic patterning, organogenesis, and tumour formation(195). The Shh pathway consists of diffusible morphogens, receptors, co-receptors and transduction factors(196). Vertebrates have three hedgehog orthologs (namely Sonic, Indian and Desert), two Patched receptors, and three intracellular effector Gli family of proteins including Gli1, Gli2, and Gli3(197). Gli transcription factors are vertebrate homologues of Drosophila zinc-finger-containing *Cubitus interruptus* (*Ci*). The proteins Gli1 and Gli2 act as activator; Gli3 is an activator of transcription, however, can become a repressor by the process that requires primary cilia(198). Loss of function of *GLIS2* results in cystic kidney disease and causes nephronophthisis type 7 in humans and mice(199, 200). *GLIS2* is a negative regulator of Shh signaling and is critical to maintain tubular cells in a differentiated state by suppressing *Snai1* (transcription factor acts as an inducer of epithelial-to-mesenchymal transition) and *Wnt4*(201). Joubert syndrome is a rare inherited developmental disorder characterized by CNS malformation, retinal degeneration, renal cysts and liver fibrosis(202). In fact, more than 10 genes have been implicated in Joubert including aforementioned *NPHP1* and *OFD1*, and all of which are involved in primary cilia/basal body/centrosome(203). Cystic kidneys are not uncommonly observed, *Arl13b*, another Joubert gene, has been shown to be associated with defective Shh, ciliopathy, and cystic kidneys(204). OFD1 is an x-linked dominant condition characterized by malformation of the oral cavity, face, digits and cystic kidney disease(205). Its protein is located in the centrosome and its inactivation is associated with defective Shh and canonical Wnt signaling pathways(205). *KIF7*, the latest addition to the list of genes causative of Joubert, is a cilia motor protein and known regulator of Shh signaling when disrupted leads to a decrease in cilia and fragmentation of golgi network secondary to a lack of microtubule dynamics(202). Interestingly, KIF7 specifically co-precipitates with nephrocystin-1 (NPHP1). Finally, deletion of In or Fy causes defects in ciliogenesis in *Xenopus* embryos in combination with PCP and Shh signaling abnormalities linking both pathways to ciliogenesis(130).

2.1.3f Summary

In summary, the molecular mechanisms of renal cystic disease are extremely complex and seem to involve multiple pathways and cross-talks among these pathways. It is interesting that many “cystic proteins” localize to the primary cilium and whether it represents a common unifying pathway for cystogenesis is yet to be proven.

2.1.4 Rationale

With the understanding of the pathomechanisms of cysts growth in autosomal dominant and recessive polycystic kidney diseases, specific therapies are being designed and tested in clinical trials. Numerous genes have since been identified to cause cystic kidneys. The knowledge from studying the perspective gene(s) functions is critical for our understanding of the complex mechanisms involved in cysts formation, better termed as cystogenesis. Despite advancements made in the discoveries of genes involved in cystic kidney diseases, to date, many patients whose underlying mutations are still not known and treatment options remain restricted. In order to further identify new therapeutic targets, we aim to discover and characterize new genes and the molecular pathways that underlie renal cystic diseases.

3 Overview of experimental approach

Over the past three decades, great strides have been made to further our understanding of polycystic kidney diseases. Human genetic studies, positional cloning, and gene targeting in animals have provided tremendous insights into the function of a number of genes which are important for renal cyst formation. However, gene targeting is a labor-intensive approach, which requires the design of a separate targeting vector for each gene in question. Furthermore, mutations introduced often cause major gene disruptions such as total knockout and are not commonly seen in

human diseases. For these reasons, we utilized forward genetics and a complementary phenotype-driven approach to discover new genes involved in cystic kidneys.

In collaboration with the Centre for Modeling Human Disease (CMHD) in Toronto, we performed an autosomal dominant *N*-ethyl-*N*-nitrosourea (ENU) screen to identify mutations in genes responsible for renal phenotypes. ENU is a well validated chemical mutagen that induces point mutations in the genomic DNA at a frequency of 1 X 10^{-3} per locus, which represents over a 100-fold greater than the estimated spontaneous mutation rate(206). Numerous ENU consortiums have been established internationally to generate novel mouse models for a variety of human diseases (refer to recent review by Soewarto(207)). ENU mutagenesis was performed on males of C57BL/6 background, which were then bred to wild-type females from inbred mouse strain C3H/HeJ. Over 150 G1 mice were screened. With this approach, we successfully identified an autosomal dominant heritable renal mutant that exhibits cystic kidney disease and glucosuria. This mutation maps to a region of the mouse genome that is syntenic to a region in the human genome that has not previously been identified in patients with this disease or other cystic renal diseases.

4 Hypothesis

Based on these exciting results, we hypothesize that:

The molecular and phenotypic characterization of the ENU mutant will provide us with a novel gene and/or pathway that underlie human renal cystic disease.

5 Methods

5.1 Generation of cystic kidney mutant

Inbred mouse strains C57BL/6J (B6) and C3H/HeJ (C3H) were obtained from the Jackson laboratory (Bar Harbor, ME). Mutant was generated on a genetic background of mutagenized B6 male and wild-type C3H females, as part of an ENU project in the Center for Modeling Human Disease (CMHD) for genome-wide mutagenesis, Toronto, Canada. ENU mutagenesis was performed as described previously(208). Mutant with glucosuria was identified on a dominant screen at week 6. A mutant breeding line was established by backcrossing this founder to wild-type C3H. Subsequent backcrosses that involved breeding between the newly identified mutant and the wild-type C3H/HeJ mice were set up for mapping and further phenotypic characterization. The use of the mice in this study was approved by the Mount Sinai Hospital Animal Care Committee and Toronto Center of Phenogenomics (TCP) Animal Care Committee, in accordance to the Ontario's Animals for Research Act, and the federal Canadian Council on Animal Care. All mice used in this study were maintained on standard rodent chow.

5.2 Mutation mapping

A rough map was generated with 98 microsatellite markers using 11 affected (4 F1, 3 F2, and 4 F3) and 11 unaffected animals (2 F1, 6 F2, and 3 F3). Mapping was repeated using Illumina® genome-wide single nucleotide polymorphism (SNP)-based chip analysis, consisting of 1449 SNP markers, therefore better resolution than

previous microsatellite analysis. The SNP analysis was performed at the Center for Applied Genomics (TCAG), the Hospital for Sick Children, Toronto, Canada. A total of 21 mutant mice (5 G2, 3 G3, 5 G4, 6 G5, 1 G6, and 1 G7) with cystic kidneys and 3 wild-type animals (2 G7, and 1 G9) were analyzed. Further fine mapping was provided fee-for-service at the TCAG.

5.3 Whole-exome next-generation re-sequencing

DNA from a homozygous mutant was isolated and purified. Genomic library preparation was performed in accordance with Agilent's SureSelect Target Enrichment System protocol (adapted from the SOLiD Fragment Library Construction Kit (Life Technologies) and compatible with SOLiD multiplexed paired end sequencing (Agilent Technologies; Version 1.3, January 2011). All Steps were performed in 0.5 or 1.5 ml DNA LoBind tubes (Eppendorf: P/N 022431005 and 022431021). Three microgram of genomic DNA with an OD260/280 ratio between 1.8 and 2.0 was diluted in 120 ul of nuclease free water, loaded in a Covaris microtube and fragmented to 200 bp using the Covaris-S2 instrument and at the following conditions: bath temperature = 4°C; bath temperature limit = 8°C; mode frequency = sweeping; duty cycle 10%, intensity 5, cycles per burst 100; time = 60 seconds. Fragmented DNA is end-repaired using end polishing reagents and PureLink PCR Purification columns provided in the SOLiD Fragment Library Construction Kit and SizeSelect Gels (Life Technologies, P/N 4443471). Truncated versions of the SOLiD P1 and IA Adapters provided in the Agilent Mouse All Exon Kit are ligated to the purified fragments at RT for 15 minutes following Agilent's SureSelect protocol. After ligation, fragments are purified with PureLink columns, and size-selected when the 200-bp band from the TrackIt 50-bp DNA ladder (Life Technologies; P/N 10488043) are in the center of the collection well of an E-gel SizeSelect 2%. Size-selected fragments are purified using PureLink, and amplified in 400 ul distributed in four 0.2 ml tubes on a GeneAmp PCR System 9700 (Applied Biosystems) using Platinum PCR Amplification Mix (provided in the SOLiD

Fragment Library Construction Kit) and SureSelect Pre-Capture Primers (provided in the Agilent Human All Exon 50 Mb Kit). The amplification is performed as follows: nick translation at 72°C for 20 minutes; denaturation at 95°C for 5 minutes, 12 cycles of denaturation at 95°C for 1 minute (increased from 15 seconds in the original protocol), annealing at 54°C for 45 seconds, extension at 70°C for 1 minute, and final extension at 70°C for 5 minutes, and hold infinitely at 4°C. After amplification, PCR products (pre-capture library) are purified using PureLink. The pre-capture library is quantified with the Agilent 2100 Bioanalyzer DNA 1000 or DNA High Sensitivity assay. A successful pre-capture library shows a peak size at around 250-270 bp.

5.3.1 Exome capture

An aliquot of 500 ng of the pre-capture library is completely lyophilized on low heat in a Centrifugal Concentrator CC-105 (Tomy Tech) and re-suspended to a final concentration of 147 ng/ul and used in the capture experiment. The exome is captured using the reagents provided in the Agilent Human All Exon 50 Mb Kit. Hybridization buffers and blockers are processed according to the Agilent SureSelect protocol. Hybridization is performed at 65°C for 24 hours in a GeneAmp PCR System 9700 (Applied Biosystems) using a MicroAmp Optical 96-well reaction plate (Life Technologies P/N 4306737) double-sealed with MicroAmp Optical Adhesive Film (Life Technologies P/N 4311971). A CM-FLAT silicone compression mat (Axygen; P/N 521-01-601) is placed on top of the sealed plate to avoid evaporation. Wells in the two outermost columns or rows of the 96-well plate are avoided. Dynal MyOne Streptavidin T1 beads (Life Technologies; P/N 65602) are prepared following the instructions in the Agilent SureSelect protocol, and re-suspended in a final volume of 200 ml of the SureSelect Binding Buffer. The hybridization mixture is transferred to the Dynal MyOne beads, incubated and washed, and the captured library is purified using AMPure XP beads (Agencourt, P/N A63881) following the Agilent SureSelect protocol. The captured library is amplified once more in a GeneAmp PCR System 9700 (Applied Biosystems) to add the barcodes for multiplex sequencing. The post-capture amplification is performed with Herculase II Fusion DNA Polymerase (Agilent; P/N

600679) using the following conditions: denaturation at 95°C for 5 minutes, 9 cycles of denaturation at 95°C for 1 minute (increased from 15 seconds in the original protocol), annealing at 54°C for 45 seconds, extension at 70°C for 1 minute, and final extension at 70°C for 5 minutes, and hold infinitely at 4°C. The amplified captured library is purified with AMPure XP beads (Agencourt) following the Agilent SureSelect protocol, and checked on an Agilent 2100 Bioanalyzer DNA High Sensitivity assay for quantification and fragment size determination.

5.3.2 High throughput sequencing on a SOLiD 4 System

Prior to emulsion PCR (ePCR) an equimolar pool of six samples is prepared and diluted to a final concentration of 0.5 pM to be used in the ePCR. Emulsification, amplification and bead enrichment are performed on the EZ Bead system following the manufacturer's instruction (Life technologies; P/N 4448417). Oil and aqueous phase are prepared separately using the EZ Bead Emulsifier E80 Reagents and Accessories Kits (P/N 4452722, 4453070 and 4457185), and mixed together in the EZ Bead Emulsifier (P/N 4448419). The emulsion are carefully transferred to a bag (P/N 4453072) to avoid breaking the emulsified droplets, and immediately placed in the EZ Bead Amplifier (P/N 4448418) following the conditions appropriate for the scale of the reactions (ePCR conditions are proprietary and not publicly released by Life Technologies). The ePCR is transferred to a bottle and enriched for positive beads (i.e., beads containing amplified captured library) using the reagents provided in the EZ Bead Enricher E80 Reagent and Accessories Kits (P/N 4452725 and 4453073), and following the specifications in the manual for the EZ Bead Enricher (P/N 4448420). Enriched beads have their 3'- end modified to add a dUTP by a terminal transferase reaction following the EZ Bead Enrichment manual. This 3'- end modification will covalently link the beads to the glass surface of the sequencing slide. Approximately 778 million beads are loaded onto the slide, and paired-end sequencing is performed with the SOLiD ToP Paired End Sequencing Kit – BC Fragment Library MM50/35/5 (P/N 4459181) following Applied Biosystems SOLiD 4 System Instrument Operation Guide (Applied BioSystems; P/N 4448379 Rev. B, April 2010).

5.3.3 Primary data analysis and read mapping

The image data collected by SOLiD 4 is analyzed using Applied Biosystems corona pipeline to produce sequence data in colour space (in which each colour represents two consecutive DNA bases on the DNA sequence) and quality metrics using a normalization procedure. The paired end reads generated by ABI SOLiD 4 platform are then mapped to the reference mouse genome and BFAST implemented BWA version 0.6.5a. The 35-bp ends are aligned using BFAST's implementation of BWA and the 50-bp reads are aligned using BFAST. The suggested default parameters for mapping to the human genome are used in most cases except for the post-processing step where the known insert library size is provided to reduce the computational time required for paired end rescuing. MarkDuplicates (Picard tools version 1.35; http://picard.sourceforge.net) is used to remove any duplicate paired end reads (that is, reads for which the start and end positions of any given paired read in hg19 are the same as those of other pairs). Next, the duplicated-free alignments are refined using local realignment in colourspace implemented in SRMA version 0.1.15. To remove reference bias introduced by the aligners due to colourspace conversions, GATK version 1.05506 base quality score recalibration is used with the default parameters optimized for SOLiD dataset except that all no-call reads are removed from the analysis and if a reference base was inserted the base quality will be set to zero and the inserted reference nucleotide was set to “N”.

5.3.4 Variant calling: Indels

GATK version 1.0.5506 Unified Genotyper with the parameter DINDEL is used for the initial indel calling. The following restrictions are put into place in ensure the quality of the indels called:

Greater than or equal to 3 consensus indels is required for genotyping.

• The maximum number of mismatches must be less than or equal to 5 within a 40-bp window around the suspected variant for the read to be used for calling.

• The minimum base quality score must be greater than or equal to 20 for that base to

be used to call variants.

• The minimum mapping quality score must be greater than or equal to 20 for the read to be used to call variants

• The hard-to-validate indels are defined as MQ0 >= 4 && ((MQ0 / (1.0 * DP)) > 0.1), where MQ0 stands for total mapping quality zero reads, and DP represents total depth. Any variants that do not meet this requirement are filtered.

• The quality score of the variant should be greater than or equal to 30.

• The quality by depth of the variant should be greater than or equal to 1.

The indels called are used as a filter in GATK UnifiedGenotyper's SNP calling.

5.3.5 Variant calling: SNP

The default parameters used for SNP calling are set with the following thresholds:

• The maximum number of mismatches must be less than or equal to 5 within a 40-bp window around the suspected variant for the read to be used for calling.

• The maximum deleted fraction of a read to be used for variant calling should be less than or equal to 0.05.

• The minimum base quality score must be greater than or equal to 20 for that base to be used to call variants.

• The minimum mapping quality score must be greater than or equal to 20 for the read to be used to call variants.

• Any SNPs that are called in the same location as an indel are filtered.

• If more than 3 SNPs are called within a 10bps window, those SNPs are filtered.

• The hard-to-validate SNPs are defined as MQ0 >= 4 && ((MQ0 / (1.0 * DP)) > 0.1), where MQ0 stands for total mapping quality zero reads, and DP represents total depth. Any variants that do not meet this requirement are filtered.

• The quality score of the variant should be greater than or equal to 10.

After GATK's variant recalibration using default parameters with the level of false discovery rate filter specified at 1.0, external data to refine the genotypes called.

5.3.6 Annotation

SIFT 4.0.3 is used to annotate the variant calls and predict whether the variant is damaging to the protein. GATK's readbackedphasing module is used to determine phrasing information for SNPs. Then custom PERL scripts and BEDTools version 2.10.1 are used to annotate information. If array data is available for the same exome sample, concordance to the array genotypes is added using custom scripts.

5.4 Sanger sequencing

Direct genomic sequencing using tail DNA was carried out to cover all the exons and splice regions. Genomic DNA was isolated from mouse tails as described previously(209). The point mutation identified in Samd9l was amplified with Platinum® DNA polymerase (Invitrogen) and the following PCR primers, which were designed based on sequence information from the Mulan ECR browser: (Sense 5'–ACCTTCACCTGCCCAGTCACT-3', antisense 5'-CTCCTGTGGCTCCTCCTCTG-3'). The above primers produced a 520 bp PCR product, which was then confirmed with agarose gel electrophoresis. The correct band was excised and purified with GeneClean® kit (MP Biomedicals). The product was then sent to TCAG sequencing facility using traditional Sanger chain termination method. The following nested primers were used to identify our mutation (a total of 6 homozygous mutants and 3 wild-type were used for sequencing): (Sense 5'-AGGGAAGGTTTTGGTGGTGTTCCT -3', antisense (for confirmation): 5'-TGCCCTCCTGTGGCTCCTCC-3').

5.5 Genotyping

Genomic DNA was isolated from mouse tails(209) and PCR was used to identify Sweet Pee mutants with the following primers to produce a 470 bp PCR product: (Sense 5'- GTGGTGTTCCTCTTACTTTCTCCC -3', antisense 5'-ATTCCACCAGGATACTCTGCCT -3').

Reaction:

Hotlid 105 , 0:30

1	94	3:00
2	94	0:30
3	59	0:30
4	72	0:45
5	Go to 2, 35X	
6	72	10:00
7	10	forever

The PCR product was then digested with restriction enzyme TaaI Fast Digest (Fermentas FD1364) for 5 minutes at 65^{o}C (wild-type: 1 bands at 459; Heterozygous mutant: 3 bands at 459 bp, 245 bp, 214 bp; homozygous mutant: 2 bands at 245, 214 bp).

TaaI:

5’ ACN↓GT 3’

3’ TG↑NCA 5’

Primers set used for amplifying a 2216 bp CDNA fragment for splice variant detection:

Sense 5’- AGAAATGGGCTTGCCACGGG -3’

Antisense 5’- AGCTCCATGTTCCTTGCGTTGT -3’

5.6 Immunofluorescence and immunohistochemistry assays

For immunofluorescence assay freshly dissected kidneys and livers were fixed in 4% PFA overnight at 4^{o}C, treated with 30% sucrose at 4^{o}C overnight, then embedded with OCT for cryopreservation. The kidneys were then sectioned at 6 μm

with a Cryostat. They were allowed to dry overnight. Non-specific staining was minimized by incubating sections in 10% BSA blocking PBS buffer before the application of the primary antibody. Alternatively, paraffin embedded kidney and liver sections were treated with standard deparaffinization protocol involving immersion in xylene followed by ethanol from 100% to 70% to 50% before rinsing with PBS and followed by microwave double boiling antigen retrieval protocol with 0.01 M citrate buffer. The primary antibody was applied overnight at 4^{o}C. The sections were then rinsed with PBS before incubating with a secondary antibody at room temperature for 1 hour in the dark. VECTASHIELD® mounting medium with DAPI for nuclear stain was added before applying cover slips and sealing with nail polish. The following primary antibodies and dilutions were used:

Lotus tetragonolobus lectin (FL-1321, Vector Laboratories), Tomato-lectin (TL-1176, Vector Laboratories), E-cadherin (Mouse, 610181, BD Transduction Laboratories), THP H-135 (Rabbit, sc-20631, Santa Cruz), Peanut Agglutinin PNA (FL-1071, Vector Laboratories), Phospho-Histone H3 (Rabbit, Ser 10 #3377, Cell Signaling), Gamma-Tubulin (Mouse, ab11316, Abcam), Beta-Catenin (Mouse, 610153, Transduction Lab), KI67 (Rabbit, RM-9106, Fischer Scientific), Caspase-3 (Rabbit, AB3623, Millipore), Sodium Potassium ATPase (Rabbit, ab76020, Abcam), Flag (Mouse, F3165, Sigma-Aldrich), Alexa 488-Phalloidin (12379, Invitrogen) at 1:100 to 1:400. Fluorescein (FITC)-conjugated AffiniPure donkey anti-goat IgG at 1:100 (Jackson Laboratories Inc). Alexa secondary antibodies (488, 536, 647, Invitrogen).

Similarly, standard immunohistochemistry protocol was followed. Following microwave double boiling antigen retrieval step, slides were immersed into a 3% hydrogen peroxide diluted in PBS for 30 minutes at RT for endogenous peroxidase quenching to minimize non-specific background staining when HRP conjugated

antibodies were used. POD reaction was performed with Vector Peroxidase Substrate Kit DAB SK-4100 as per manufacture's manual. This step was followed by hematoxylin counterstaining and mounting. Blocking soloution containing 10% goat serum, 3% BSA, 0.1% trinton in PBS.

5.7 Real-time PCR

Total RNA was extracted from the renal cortex using Trizol reagent (Invitrogen) and reverse transcribed into cDNA using M-MLV reverse transcriptase (Ferments) and random hexamer primers (Fermentas) according to the manufacturer's protocol. cDNA samples and standards were amplified in qPCR MasterMix Plus for SYBR Green I (BioRad). Samples were analyzed in triplicate. Relative quantification of target gene expression was evaluated using comparative C_T method (210). The ΔC_T value was determined by subtracting the Hprt C_T value of each sample from its respective target C_T. Fold changes in gene expression of the target gene were equivalent to $2^{-\Delta\Delta CT}$. The following primers were used in the study:

Samd9l:

sense 5'- ATGGTCTCAGGGAGACAGGGCA -3',

antisense 5'- TGGCGTGCAAGACATCTGTTCTGG -3'

P53:

sense 5'- GGAAGACTCCAGTGGGAACC -3',

antisense 5'- GCGGAAATTTTCTTCTTCTGTACG -3'

P21:

sense 5’- GTCTGAGCGGCCTGAAGAT -3’,

antisense 5’- TCTGCGCTTGGAGTGATAGA -3’

NGAL:

sense 5’- CTCAGAACTTGATCCCTGCC -3’,

antisense 5’- TCCTTGAGGCCCAGAGACTT -3’

CD14:

sense 5’- TTTCAATTGTTTGGGGGCGGCA -3’,

antisense 5’- ACCGTAAGCCGCTTTAAGGACAGA -3’

E-Cadherin:

sense 5’- TTTTCTACAGCATCACCGGCCAAG -3’,

antisense 5’- AGGATGTACTTGGCAATGGCTTCTC -3’

Smad3:

sense 5’- ACTTACAAGGCGACACATTGGGAG -3’,

antisense 5’- TTGCAGTTGGGAGACTGGACGAAA -3’

TGFβ:

sense 5’- AAAATGCCATCCCGCCCACTTT -3’,

antisense 5’- TTGGGGTTTTGCAAGCGGAAGA -3’

Vementin:

sense 5’- TGCTTCTCTGGCACGTCTTG -3’,

antisense 5'- GGACATGCTGTTCCTGAATCTG -3'

5.8 24-hour urine study

Four mice of the same genotype were used for each 24-hour study. Four Nalgene metabolic cages were used simultaneously as paired experiments (matched for age and weights). Amount of water consumed was obtained based on the difference between pre- and post-study water bottle weights. Similarly, urine output was estimated with the same strategy. The urine was centrifuged at 4^{o}C for 10 minutes at 10000 rpm. The urine samples were then flash frozen with liquid nitrogen before sending to the hospital biochemistry laboratory (Mount Sinai Hospital, Toronto, Canada, and TCP core). Roche Diagnostics: automated Roche Modular was the platform used for analysis.

5.9 MRI imaging

MRI imaging was performed at the Mouse Imaging Center at the Toronto Center for Phenogenomics using a 7-T a Magnex Scientific magnet powered by a Varian Inc. Unity INOVA console.

Body composition was performed using Ecko MRI-100 analyzer.

5.10 Histological analysis

Freshly dissected kidneys were fixed in 10% formalin/PBS, embedded in paraffin, sectioned at 4 μm, and stained with hematoxylin and eosin, periodic acid-

Schiff. Sections were examined and photographed with a DC200 Leica camera and Leica DMLB microscope (Leica Microsystems Inc).

5.11 Statistical analysis

Data are presented as the mean ± SEM. One-way ANOVA with Bonferroni's post-test for parametric data and two-tailed Chi-Square for categorical data, with multiple comparisons was performed using Graph Pad Prism version 4.00 for Windows, Graph Pad Software (San Diego, CA, USA). For subgroup analyses between 2 groups, a two-tailed Student's t test assuming heterscedasticity was used. The null hypothesis was rejected when $P < 0.05$.

6 Results

6.1 Identification of the cystic kidney mutant

The cystic kidney mutant was identified through routine urinalysis in the ENU dominant G1 screen from breeding between 2 inbred mouse strains; a wild-type C3H/HeJ female and a mutagenized C57BL/6J male. Our working definition of glomerulocystic disease is defined by Berstein to include the presence of Bowman's capsule dilation 2 times normal and the occurrence of glomerular tufts within at least 5% of otherwise identical cysts(211). Glucosuria was observed on urine dipstick at the 6 weeks of age in a G1 female, 198-6-23, which had normal serum glucose at this time. No other urinary abnormalities were seen, specifically, urinary protein was not identified by urine dipstick or SDS-PAGE gel. Interestingly, the expression of HNF1ß was not altered, mutation of which causes glomerulocystic kidney disease and glucosuria(212, 213). This mutant, 198-6-23, was bred to wild-type C3H/HeJ to assess for penetrance of the trait. Glucosuria was a heritable trait with close to 100% penetrance in 50% of the F2 offspring, consistent with an autosomal dominant pattern of inheritance. Histologic analysis of both male and female heterozygous F2 mutants demonstrated dramatic cystic kidneys, particularly featuring massive dilation of the Bowman's capsule, and collapse of glomerular tufts (n = 20) (**Figure 1**). Multiple backcross breeding between heterozygotes and wild-type C3H/HeJ were set up, and at G8 the two key phenotypes of glucosuria and cystic kidneys segregated.

Figure 1 Adult heterozygous mutants exhibit glomerulocystic dilation of the Bowman's capsule (G) and renal tubules (T); H&E staining at 100X magnification. **A** – adult WT at age 76 weeks with H&E staining at 100X magnification; **B** – adult heterozygous littermate at age 76 weeks.

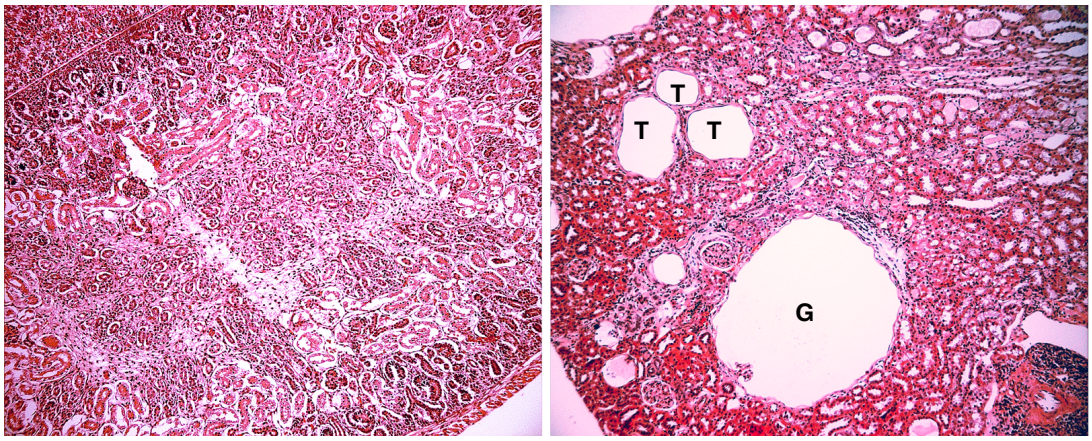

A Adult wild-type 100X **B** Adult heterozygote 100X

6.2 Map position

The glomerulocystic kidney disease (GCKD) mutation was mapped to mouse chromosome 6. Taking advantage of the unique microsatellites/simple sequence length polymorphisms between the two parental strains, C3H/HeJ and C57BL/6J, a rough map consisting of 98 microsatellite markers using 11 affected (4 F1, 3 F2, and 4 F3) and 11 unaffected animals (2 F1, 6 F2, and 3 F3) was generated (**Supplementary Table 1**, p167). A region between the centromere and distal marker D6MIT119 (50.8 Mb) in chromosome 6 was identified. Additional backcross breeding cages were set up between the heterozygous mutants and wild-type C3H/HeJ for the purpose of narrowing down the critical region with chromosomal crossover. Chromosomal crossovers are independent recombination events that occur during prophase I of meiosis when the four chromatids are in tight formation facilitating homologous recombination between two chromatids from each parent (a bivalent). Further microsatellite study of mouse 80-1-2 limits the map location to a distance of 23 Mb between the centromere and not exceeding the distal marker D6MIT204 (**Supplementary Table 2**).

Fine mapping was performed with single nucleotide polymorphisms (SNPs) around 1 Mb apart. As depicted in **Supplementary Table 3**, the critical region was further reduced by the latest crossover event in mouse mutant c77189j-3-2, bordered proximally by the centromere and distally by SNP rs13478611 at 6.29 Mb. This represents an approximate size of 3 Mb since the first gene in chromosome 6 starts at 3.2 Mb.

Not all mutants exhibit glucosuria. Thirteen percent (54 mice) of the 424 mice tested, with weekly urinalysis for 7 consecutive weeks, did not have glucosuria. This was initially thought to be due to incomplete penetrance or variable degree of phenotypic expression. However, we noticed further discrepancies between genotype and the phenotype of glucosuria (**Supplementary Table 4**). Nineteen mutants (4.5%) genotyped as wild-type in the critical region exhibited glucosuria. We saturated the critical region with 7 SNP markers at about 1 Mb apart for better resolution (SS5106741 at 3.1 Mb, rs3695631 at 3.35 Mb, SS16376485 at 3.5 Mb, SS5045907 at 4 Mb, D6MIT138 at 4.45 Mb, rs30856904 at 4.49 Mb, and rs13478611 at 6.29 Mb). Since one centimorgan represents a recombination frequency between 2 loci of 1% in a single generation and corresponds to an estimated distance of 2 Mb in mice(214), it is highly unlikely for a double recombination event to produce the observed genotype. Moreover, the evidence that the phenotypic glucosuria was a result from a different mutation began to surface when two heterozygous mutants, C67189g-11-1 and C67189i-11-21, were intercrossed to produce two mutants with high-grade glucosuria, I17189b-2-2 and I17189b-1-21, both were wild-type for the SNP markers in the critical region. When these two mice were intercrossed, they produced 4 litters with 100% of the pups demonstrating consistent high-grade glycosuria (4+ glucose; 55 mmol/L). Interesting, their genotypes were all wild-type within the critical region (**Supplementary Table 5**, p171) although their phenotypes would suggest otherwise. This prompted us to re-analyze our data with mouse whole-genome SNPs genotyping based on a medium density linkage panel of 1449 SNPs on an Illumina platform. This technology was recently made available at the Centre for Applied Genomics in Toronto. A total of 21 mutant mice (5 G2, 3 G3, 5 G4, 6 G5, 1 G6, and 1 G7) with cystic kidneys and 3

wild-type animals (2 G7, and 1 G9) were analyzed, and the results are depicted in **Supplementary Table 6**. We identified a critical region in chromosome 6 between the centromere and the distal marker rs13478656 at 22 Mb with a "logarithm of odds" score of 2.2 (**Supplementary Figure 4)**. The latest crossover in c77189j-2-22 shortened the distal boundary to SNP rs6172481 at 5 Mb, further shrinking the critical region into a 1.8 Mb distance. There are 13 genes and 2 known microRNAs in this region *Samd9l*, *Hepacam2*, *Bet1*, *Calcr*, *Casd1*, *Ccdc132*, *Col1a2*, *Gng11*, *Gngt1*, *Peg10*, *Sgce*, *Tfpi2*, and *Ppp1r9a*. None of these genes have been described to cause cystic kidney diseases. Among these genes in the region, four has no known function, including *Samd9l*, *Hepacam2*, *Ccdc132*, and *Casd1*.

Next, we performed whole exome next generation re-sequencing on a homozygous mutant, E32, based on the SOLiD^{TM} 4 system. The data were then analyzed with three separate bioinformatics pipelines for depth coverage, quality score recalibrator, SNP/indel (indel:insertion/deletion) caller, and realigner. The pipelines used were Genome Analysis Toolkit/GATK developed by the Broad Institute, SAMtools mpileup, and Marth Lab's FreeBayes. The data were filtered simultaneously with a quality by depth at > 10 and strand bias < -0.01. The mean sequencing coverage was 21.0 reads. Approximately 76.5% of the exons were sequenced at 10X depth or more, about 2.5% were deficient of any coverage. Within the critical region, the mean sequencing coverage was 21 reads (**Supplementary Figure 3)**. Of the 264 exons within the region in chromosome 6, 2 (<0.8%) had no coverage, and more than 80% of the exons were sequenced at 10X depth or more. Since the average coverage depth for 50% false positive error rate degradation in SOLiD has been estimated to be 39-fold, the present experiment is expected to result in high false positive error rates. Furthermore, detection of indels still represents a technological challenge in next generation sequencing platforms(215).

Primers were designed for regions with <10X depth of coverage for Sanger sequencing to capture inadequately covered regions. After exclusion of all variants located in non-exonic regions (except splice sites) and known polymorphic variants,

three variants were identified in the critical region: a transversion mutation in exon 2 of the gene *Samd9l* at position 3,325,411 from T to A; a transversion mutation in exon 45 at position 4,486,219 of the gene *Col1a2* from G to T; and another transversion mutation in exon 45 of the gene *Col1a2* at position 4,486,237 from C to G. The next SNP identified was a known SNP at position 22,922,890, more than 17.9 Mb beyond the distal margin of our critical region. Only the SNP called in *Samd9l* was a true positive as confirmed by Sanger sequencing (**Figure 2A**). The mutation results in a change in amino acid from serine to threonine. The first Indel identified in chromosome 6 was at position 47,895,511, outside of the boundaries of the critical region. Areas along the genome within the critical region with deficient coverage were identified and sequenced with Sanger sequencing. No further SNPs or Indel were found. Thus, we have reasonable evidence to suggest that the SNP in *Samd9l* may be responsible for the observed cystic phenotype. Comparative genomic analysis shows that serine residue at the position of the mutation is relatively conserved across various species (**Figure 2B**). The point mutation, S619T, identified in *Samd9l* at nucleotide 1849 is an area that is evolutionary conserved in x-tropicalis, chicken, opossum, rat and human, but not in dog or tetraodon (C rather than T).

It is not uncommon that missense mutations lead to splice variations. To determine if the point mutation cause splice changes, we amplified a 2074 cDNA region. Embedded within this region at position 804 is the mutation of interest. As depicted in **Figure 2C** both the homozygous mutant and wild-type exhibit a single band at around 2 kb on gel making it unlikely for any splice changes.

Figure 2 **A** Transversion mutation from thymine to adenine at position 3325411 of the gene *Samd9l*. **B** Comparative genomics of a variety of species shows relative conservation of serine at the position of the point mutation. **C** Mutation did not cause splicing variation. PCR of CDNA from a wild-type and a homozygous mutant amplifies a single band around the mutation.

A

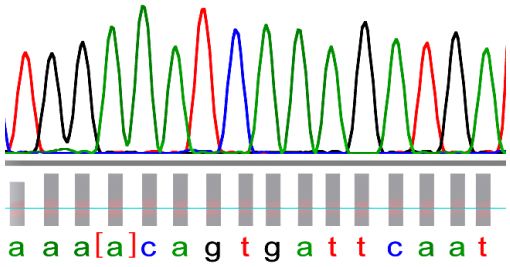

Reverse strand

B

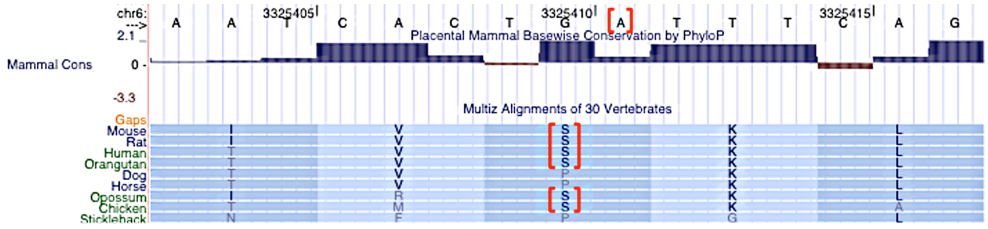

C

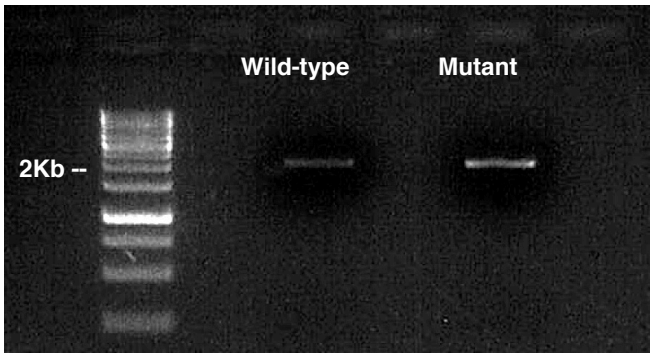

6.3 Phenotypic Characterization

Heterozygous mutants live a normal lifespan. Both male and female heterozygotes are fertile. Similar to human cystic kidney diseases, heterozygotes exhibit variable severity of cystic changes as depicted in **Figure 3**. Body composition analyzed at 9 months of age did not show differences in percent lean body mass, fat body mass and water between heterozygous males and their wild-type male littermates, which were 83% versus 80%, 9.6% versus 12.6%, and 7.3 % versus 7% respectively (p=ns). Although there was a trend towards lower body weights among the heterozygotes compared to wild-type, 26 g and 31.9 g but the difference was not statistically significant (p=0.2). There was also no discernible difference in serum concentrations of sodium, potassium, creatinine, glucose, calcium, magnesium, and albumin; 24-hour urine volume and excretion of protein, protein-to-creatinine ratio, urine sodium excretion, urine potassium excretion, urine calcium excretion and urine magnesium excretion; as well as hemoglobin, hematocrit, white blood cell count and platelet count. In contrast, homozygous mutants die perinatally. None of them survived beyond first few hours after birth. They developed tachypnea and respiratory distress in their pre-morbid stage. Seizure activities were not observed. Live homozygous P0 mutants and their wild-type littermates were fixed in 10% formalin for 36 hours and total body CT and MRI images were obtained. As depicted in **Figure 4A-B** highlighted by white arrow, the mutants developed internal hemorrhages notably in the thoracic cavity. Blood was detected in the lungs and the pericardium. We then fixed embryos at the age of 18.5 days for whole body MRI, hemorrhages in the lungs were observed in one out of four mutants. Complete blood count obtained immediately postpartum did not reveal any significant differences in hematocrit and platelet counts between the homozygotes and the wild-type. However, homozygous mutants had a significant higher average white blood cell counts of 10.8 X 10^9/L compared to their wild-type littermates, 3.4 X 10^9/L; p<0.01. The differentials failed to point to the expansion of any particular subpopulation of white blood cells and elevations in both lymphoid and myeloid lineages were equally observed.

Figure 3 A variable degree in expression of the cystic phenotype. Arrows point towards the glomeruli. H&E staining of kidney sections at 100X magnification. **A** wild-type; **B-D** heterozygous mutant littermates. **B** Two times normal Bowman's size; **C** Three times normal Bowman's size; **D** Greater than or equal to four times normal Bowman's size.

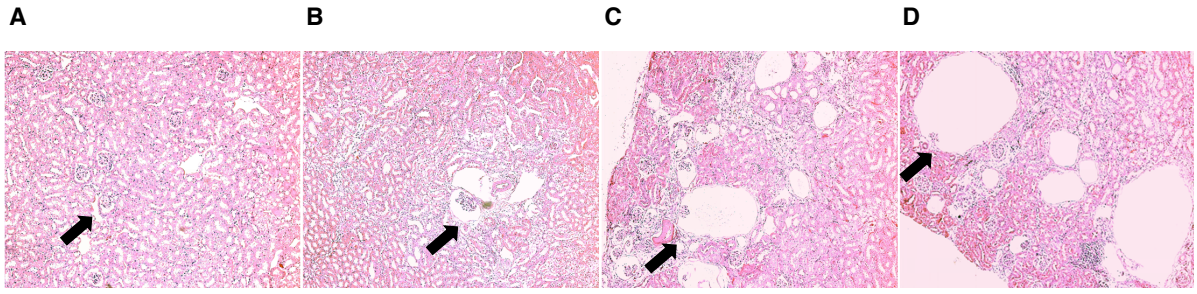

Wild-type 100X Heterozygotes 100X

Figure 4 MRI and histology of homozygous mutants at P0. **A-C** MRI images of a pre-morbid P0 homozygous mutant (white arrow points towards area of hemorrhage; yellow arrow points towards abnormal liver). **A** Sagittal view of whole mouse; **B** transverse view of the thorax; **C** transverse view of the upper abdomen at the level of the liver. **D-F** Histology with H&E staining of liver sections; CV – central vein. In normal liver, hepatocytes are arranged in single file manner radiating from the CV as depicted in wild-type at P0 in panel **D**. In contrast, most homozygous mutants at P0 exhibited increased cellularity and lost of the normal liver architecture as depicted in panel **E**. Some sinusoids become obliterated. **F** depicts a grossly abnormal liver with "moth-eaten" morphology and dilated structures. Some of these structures turn out to be vasculatures as highlighted in red using Tomato Lectin (TI) stain for immunofluorescence (**G**).

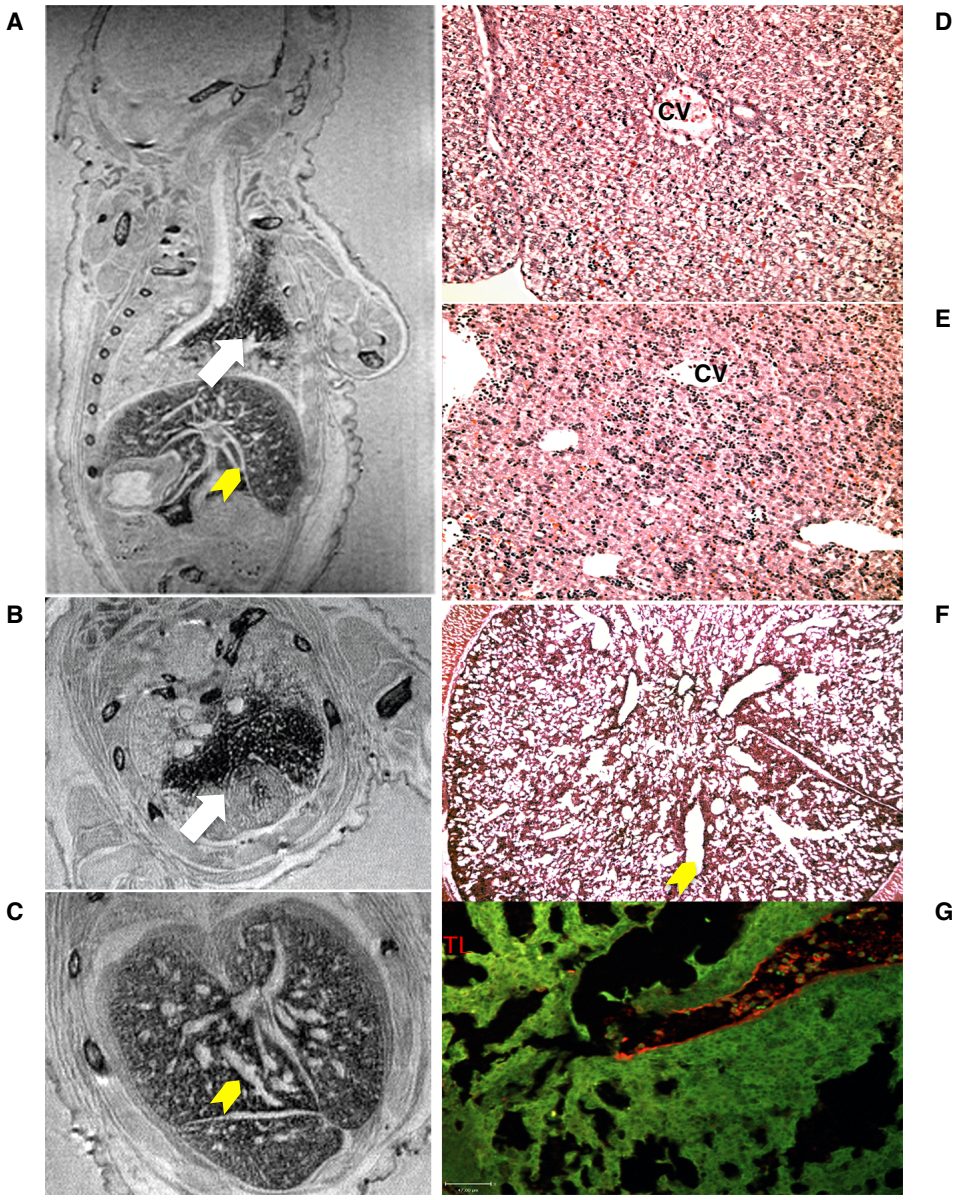

Figure 5 Mutants are significantly smaller at birth. The average weight of the homozygous mutants (MT 6) is much lower than their heterozygous littermates (Het 6), which in turn is smaller than the wild-type littermates (WT 6); $p<0.05$. N denotes number of animals.

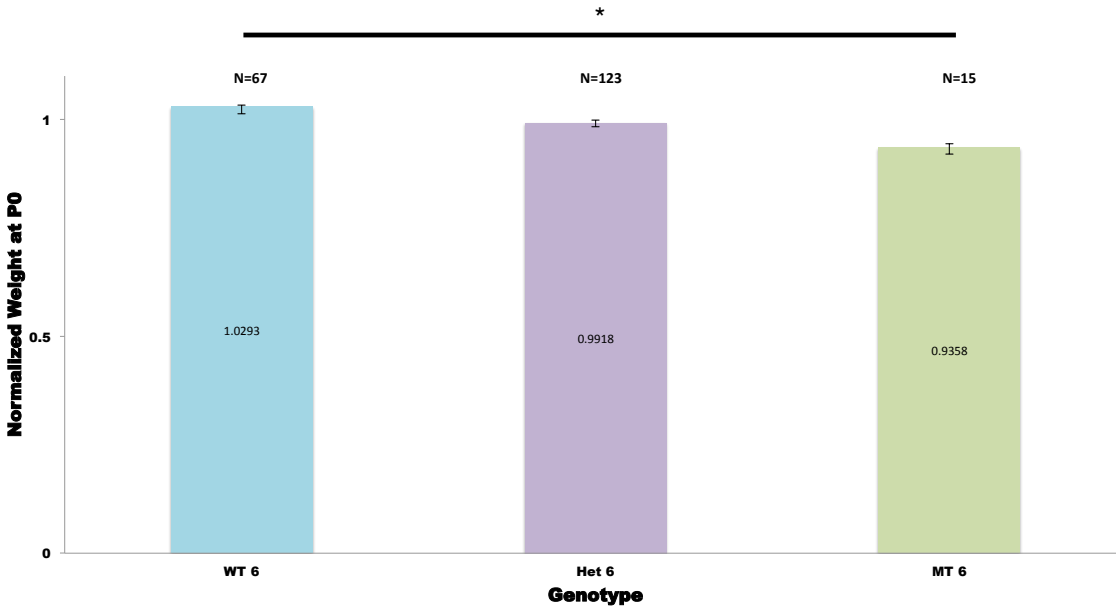

Figure 6 Most homozygous mutants (MT 6) exhibit kidney cysts at birth. 74% of the homozygous mutants are cystic at birth compared to only 15% amongst their heterozygous (Het 6) littermates; $p<0.01$. N denotes the number of animals.

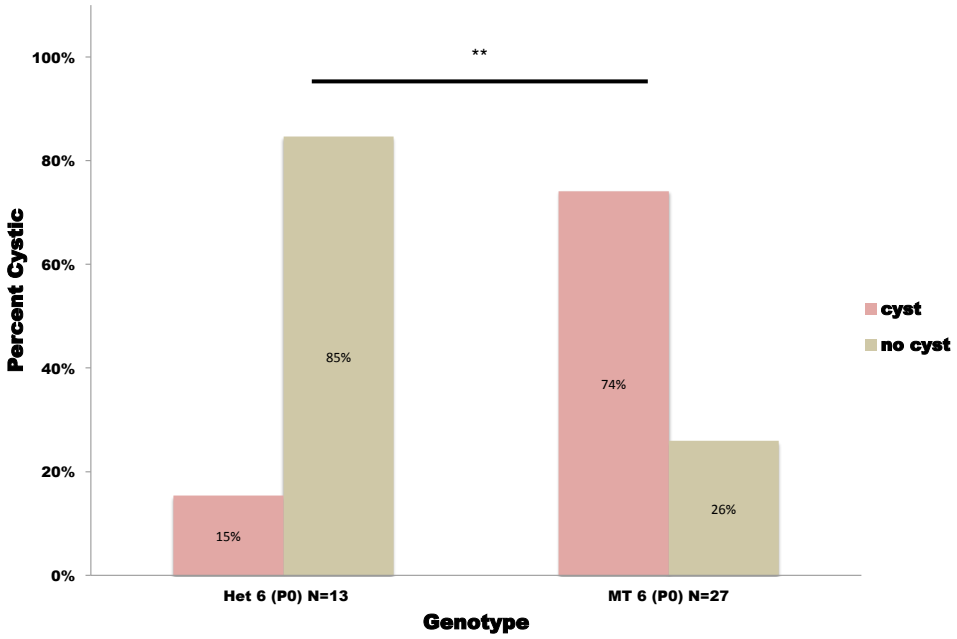

Mutants were significantly smaller at birth ($p < 0.05$; two-way ANOVA). Although the length of the homozygous mutants appeared to be shorter, unfortunately, we did not formally measure the lengths of the P0 pups. However, a total of 205 animals were weighed at birth and the average weight (normalized weight to average weight of each individual litter) of wild-type, heterozygotes, and homozygotes were 1.3178, 1.2692, 1.1600 g respectively (1.0293, 0.9918, 0.9358)(**Figure 5**). More mutants exhibited cystic changes at birth among the homozygotes. Seventy-four percent of the homozygotes (n=27), as depicted in **Figure 6**, compared to only 15% (N=13) of the heterozygotes were found to be cystic at birth ($p < 0.01$; two-tailed Fisher's exact). Wild-type littermates do not develop cysts in the kidneys. Cysts were occasionally found in the peritoneal cavity and within the uterus of the heterozygous female mutants (**Supplementary Figure 2**). Although we did not observe any cystic changes in the liver, histologic sections of the homozygotes revealed gross abnormalities ranging from disorganized hepatocytes arrangement (**Figure 4E**) to "moth-eaten" pattern significance yet to be determined (**Figure 4C, F** yellow arrow). Using tomato lectin to delineate the endothelial compartment, the vasculatures were also found to be ectatic. Interestingly, homozygous mutants were found to have very subtle "kinked" in their tails, which were not always immediately apparent (**Figure 7**).

The kidneys of mutants demonstrated a variable degree of cystic changes. Homozygous mutants had more severe cystic phenotype. Cysts were found in majority of homozygous P0 kidneys as mentioned earlier. In fact, cysts were detected as early as embryonic day 17.5. In addition, none of the heterozygous P0 kidneys had cystic involvement in more than 30% of the glomeruli. The primary structures involved were the glomeruli. As depicted in **Figure 8A**, we observed dramatic dilation of the Bowman's capsule with relatively preserved glomerular structures. There were no significant differences in the number of glomeruli between the mutants and the wild-type littermates. Cystic dilations were also observed in the renal tubules (**Figure 8A**). Notably on Periodic acid-Schiff (PAS) staining, the proximal tubules also lost its thick brush borders (**Figure 8B** wild-type**; Figure 8C** mutant). To further identify the tubular segments involved in cystic dilatation, immunofluorescent assays were carried out with

antibodies specific for the proximal tubules (LTL; Lotus Tetragonolobus Lectin), thick ascending limb of the Loop of Henle (Tamm-Horsfall protein) and the distal segments (PNA; Peanut Agglutinin Lectin). Cystic dilatations were found in all segments of the renal tubules (**Figure 9**).

Figure 7 Mutants demonstrate "kinked tails". **A** Homozygous mutant (MT 6) exhibits a slight kink in the tail compared to their heterozygous (Het 6) and wild-type (WT 6) littermates. Notice that the homozygous mutant is cyanotic at its premorbid state. **B** Another homozygous mutant exhibiting a more obvious abnormal tail morphology.

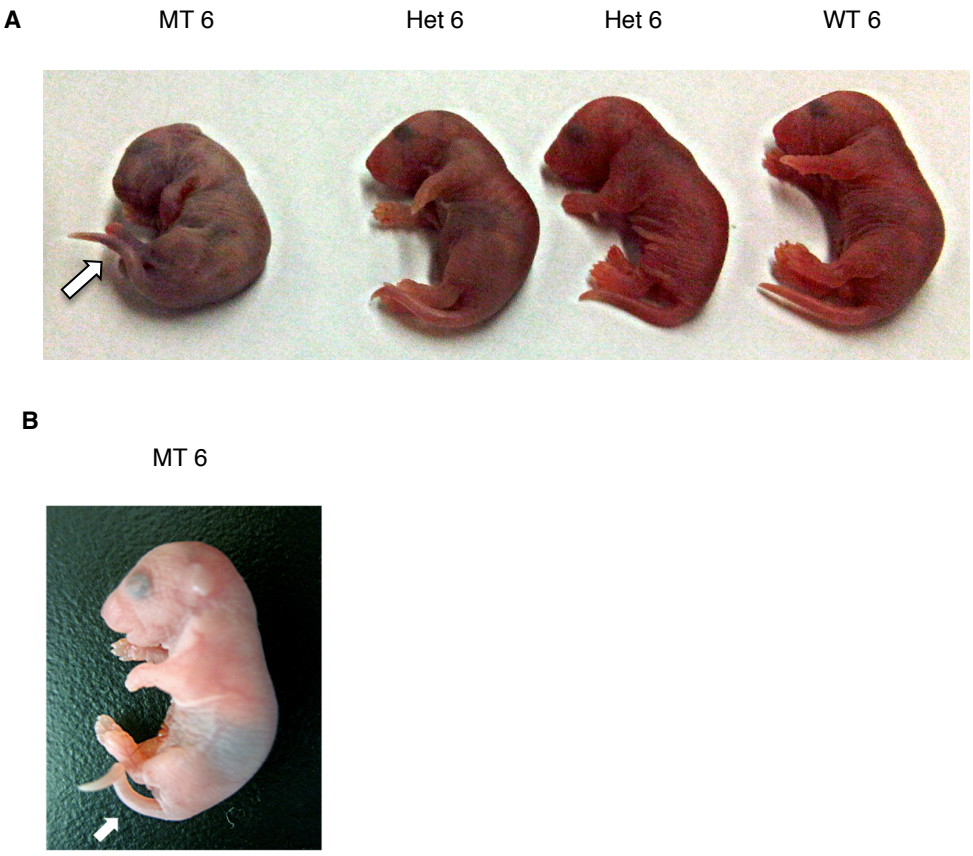

Figure 8 Mutants lost the thick brush border in the lumen of the proximal convoluted tubules (PCT). **A** H&E staining of the whole homozygous mutant kidney histology at P0. **B-C** PAS staining of wild-type (**B**) and homozygous mutant (**C**) kidneys at P0. Yellow arrow points towards luminal brush border in the proximal tubules.

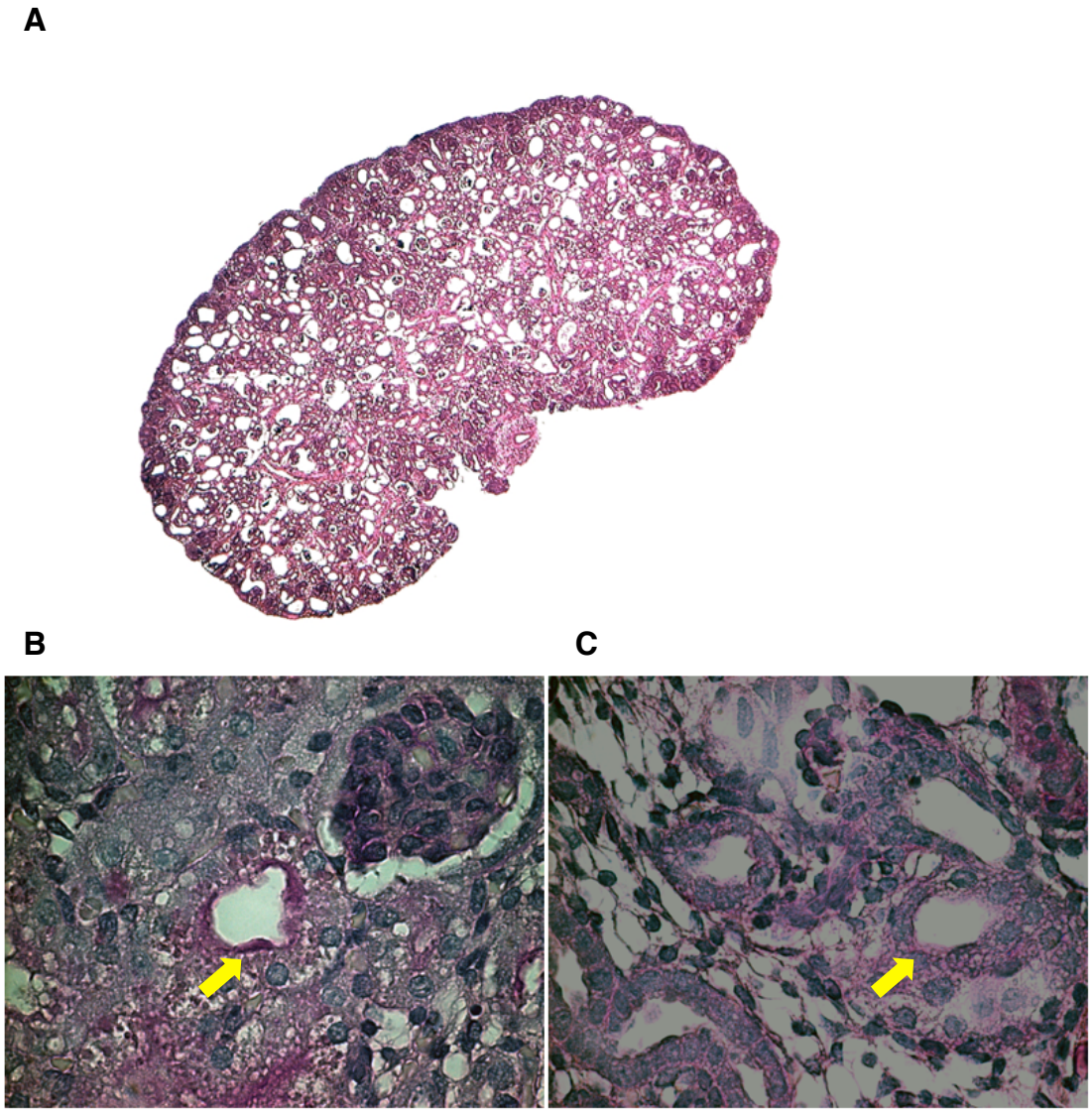

Figure 9 Cystic dilatation involves the entire nephron. Immunofluorescent assays of wild-type (WT 6) and homozygous mutants (MT 6) kidney sections at P0 demonstrating cystic dilatation in all segments of the tubules (white arrows) and loss of apical-basolateral polarity (yellow arrow).

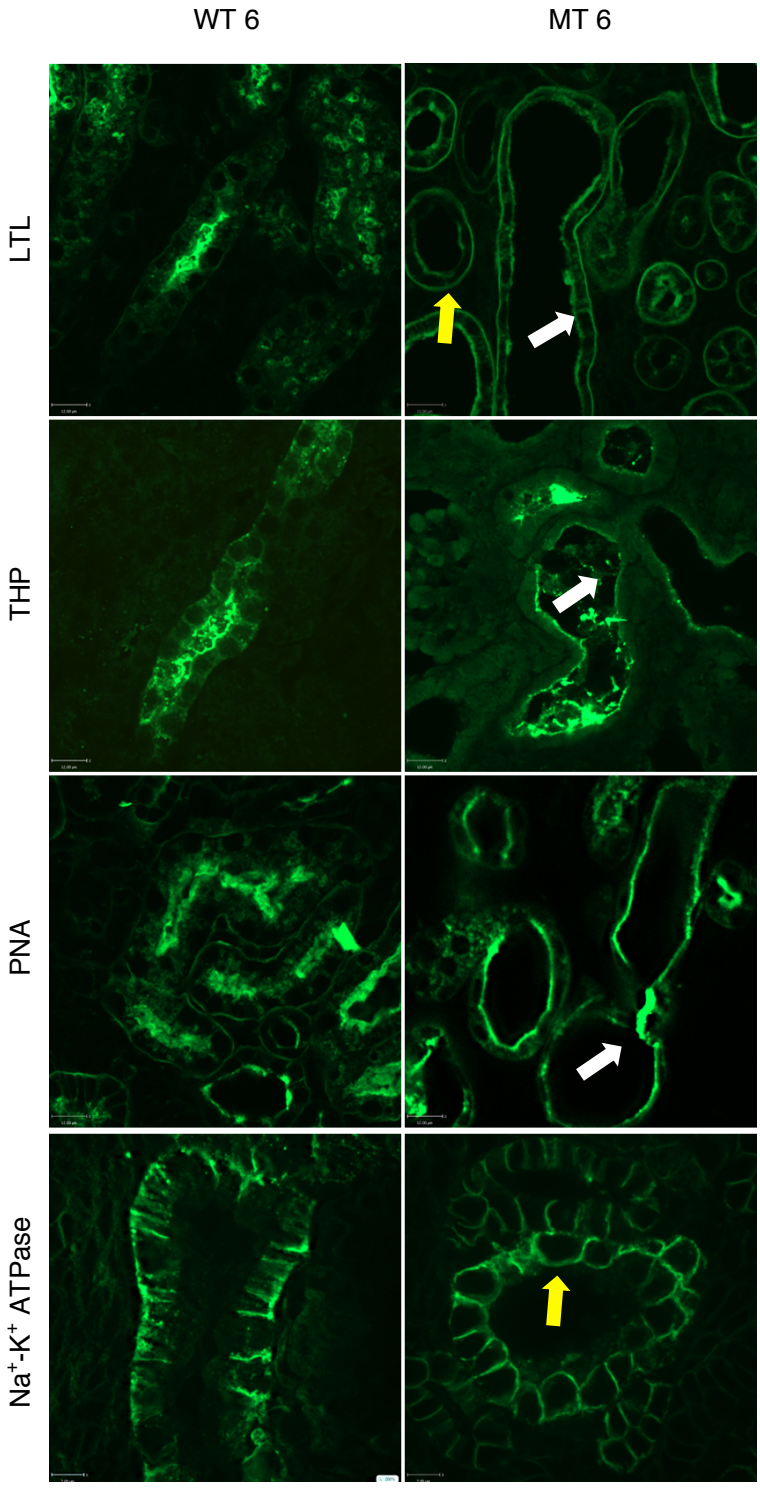

6.4 Cystic tubules loss the epithelial apical/basaolateral polarity

Polarity established by renal tubular cells is critical for their roles in governing fluid and electrolytes reabsorption among many other functions. It is clear that our cystic model demonstrates loss of apical/basolateral polarity. In normal proximal tubules, fluorescein labeled LTL only binds to specific alpha-linked L-fucose containing oligosaccharides in the luminal brush borders, and gives a specific signal delineating the luminal border. However, both luminal and basolateral signals were detected in the proximal tubules of the mutants (double contouring). We further examined the renal tubules with antibodies specific for the alpha subunit of the Na^+/K^+ ATPase (rabbit polyclonal antibody) and discovered that, as depicted in **Figure 9**, the mutant tubules lost the polarized distribution of the pumps. Luminal or apical signal for Na^+/K^+ ATPase was detected, which was not observed in the normal wild-type. This observation has been reported in other mouse models of cystic kidney diseases(216). Similar to humans with cystic kidney diseases, we did not observe any significant difference in electrolytes (sodium, potassium, calcium and magnesium) at 4 weeks or 9 months of age between heterozygotes and wild-type littermates. This might be due to a less severe cystic phenotype and fewer tubules involved in cystic changes amongst the heterozygous mutants.

6.5 Mutants exhibit phenotypes suggestive of abnormal planar cell polarity (PCP)

Abnormal mouse-tail morphology is a phenotypic readout characteristic of genetic mutations resulting in disrupted PCP pathway. This includes loop tail in *Vangl2* mutants carrying a S464N mutation; circletail from a nonsense mutation due to a single base insertion at codon 947 in *Scrib*; and curly tails in null *Fat4* mutants. Our mutants demonstrate subtle kink in their tails. To further evaluate if the PCP pathway was affected in our genetic model, we dissected the Organ of Corti in the newborn inner ear and performed immunostaining of the inverted “V” shaped apical microvilli derived stereocilia (with phalloidin stain in green) and primary cilia/kinocilia (acetylated tubulin

stain in red). Normally, the vertex of the hair cells points towards the periphery of the cochlea. Usually, there is a tight distribution of the vertices. However, our mutants showed markedly disrupted planar organization across all four layers of hair cells (**Figure 10**). By quantitating the orientation of these polarized structures, and comparing the orientations of 391 hair cells from 3 mutants and 427 hair cells from 3 wild-type, we discovered an abnormally wide distribution in the mutants as depicted in the histograms. The range of axis for the wild-type and mutants were between -32^{o} to +18^{o} and -58^{o} to +38^{o} respectively (p<0.001; Mann Whitney Rank Sum Statistics).

Kidney development, particular tubular morphogenesis, is highly dependent on coordinated proliferation and mitotic orientation(106). Cell divisions along the longitudinal axis of tubules will result in growth in length, whereas radial division causes widening of the lumen(106, 217). It has been previously shown that mammalian tubular elongation is regulated by tightly controlled oriented cell division, and has been shown in one study to be within 11^{o} to the plane of tubules(106). Recently, under- or overexpression of *ErbB4* in mouse was shown to result in cystic kidneys associated with abnormal polarization of epithelial cells and a markedly increased radial division in renal tubular cells(218). To investigate the orientation of mitotic axis, P0 kidneys from mutants and wild-type littermates were immunoblotted with antibodies specific for phosphorylated Ser10-histone H3 (Ser10), which is derived from a tightly conserved event during chromosome condensation in mitosis(219). E-Cadherin was used to delineate cell borders (**Figure 11A**). Six P0 kidneys from the wild-type and six P0 from homozygous mutants were used for the purpose of scoring. The sessions were cut at 12 micrometer in thickness. Over 50 tubular cells in meiosis were scored in each arm in an un-blinded fashion. An analysis of the number of longitudinal versus radial cell divisions along the plane of axis of the tubules revealed a significantly higher proportion of radial cell divisions in the mutants, 15% in the wild-type versus 45% in mutants (p<0.05; two-tailed Fisher's exact), as depicted in **Figure 11B**. The proportion of tubular non-axial division in the wild-type controls is comparable to that reported in the literature(218). A more precise quantitation involves direct measurement of mitotic angle and scoring in a blinded fashion is currently underway.

Although homozygous mutants did not develop any overt cardiac phenotypes, such as septal defects or outflow tract abnormalities, subtle differences were observed. At E17.5, the mutants had a significantly thinner myocardium compared to the wild-type controls (0.32 mm and 0.71 mm respectively; $p < 0.05$). Septal wall thickness was not different (0.53 mm and 0.6 mm). Interestingly, this is reminiscent of some of the cardiac phenotypes including stunted trabeculation, reduction in myocardial wall thickness, and cardiomyopathy reported in *Scrib* mutants, which is known to involve abnormal planar cell polarity(220).

Figure 10 Mutants have abnormal inner ear hair cells orientation. **A** Immunofluorescence of the Organ of Corti at P0. Wild-type (WT 6) exhibits organized polarized hair cells with a narrow distribution of vertices. In contrast, homozygous mutant (MT 6) hair cells are disorganized (phalloidin staining "^" shaped stereocilia in green; acetylated tubulin staining kinocilia in red). **B** Pictorial representation of the immunofluorescence images delineating orientation of the hair cells. **C** Histograms on distribution of hair cells orientation. Y-axis represents the number of hair cells and x-axis the angulation in degrees. ($p<0.001$; Mann Whitney Rank Sum Statistics)

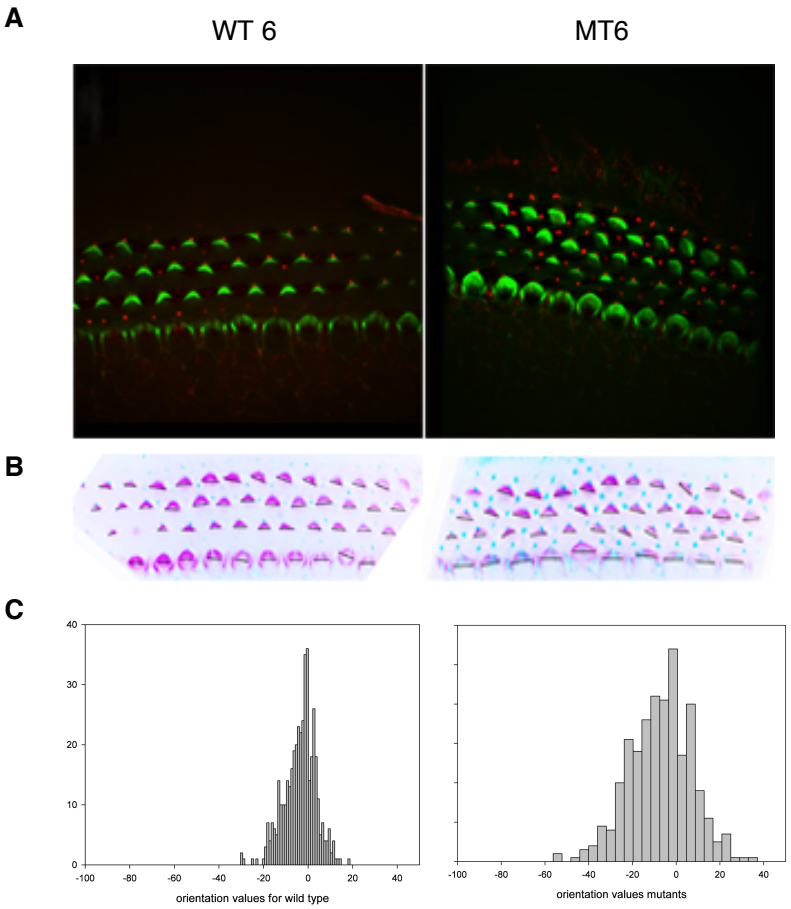

Figure 11 A higher proportion of the P0 mutants exhibit radial cell division. **A** Top panels are sections from P0 wild-type (WT 6) where white arrows represent longitudinal cell divisions; bottom panels are sections from homozygous mutants where yellow arrows represent radial division. **B** Percent radial division is much higher in the homozygous mutants. (p<0.05; two-tailed Fisher's exact; 6 kidneys in each group with > 50 meiosis scored in each group.)

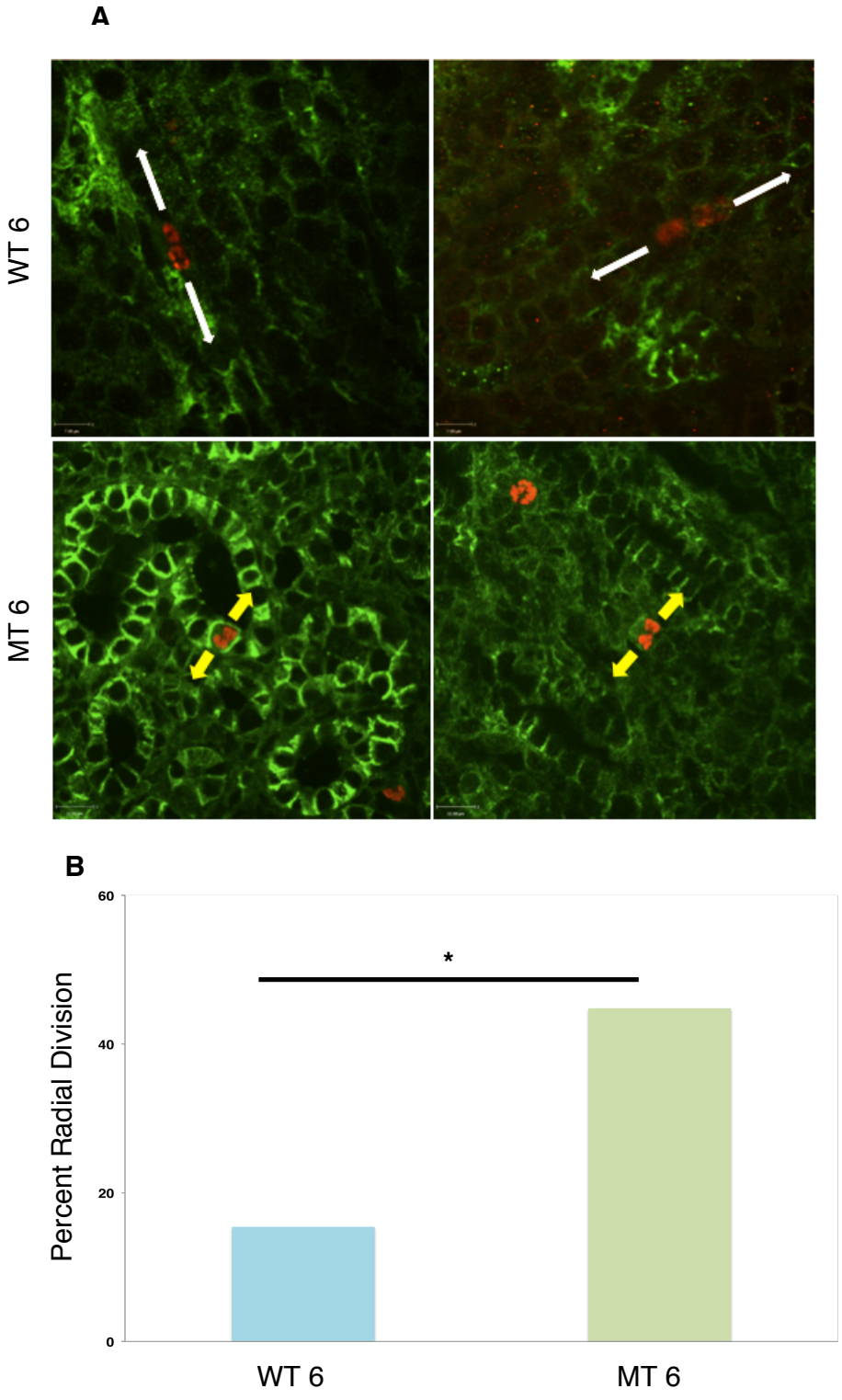

Figure 12 Mutants are smaller in size at birth (WT 6 - wild-type critical region, wild-type *Vangl*; WT 6/$V^{LP/+}$ - wild-type critical region, heterozygous *Vangl LP*; Het 6 – heterozygous critical region, wild-type *Vangl*; Het 6 6/$V^{LP/+}$ - heterozygous critical region, heterozygous *Vangl LP*; MT 6 – homozygous mutant critical region, wild-type *Vangl*; MT 6 6/$V^{LP/+}$ - homozygous critical reigon, heterozygous *Vangl LP); p*<0.0001, one-way ANOVA for difference in weights amongst WT6, Het 6 and MT6 with WT *Vangl*; *p*<0.0002, one-way ANOVA for difference in weights amongst WT6, Het 6 and MT6 with *Vangl*$^{Lp/+.}$

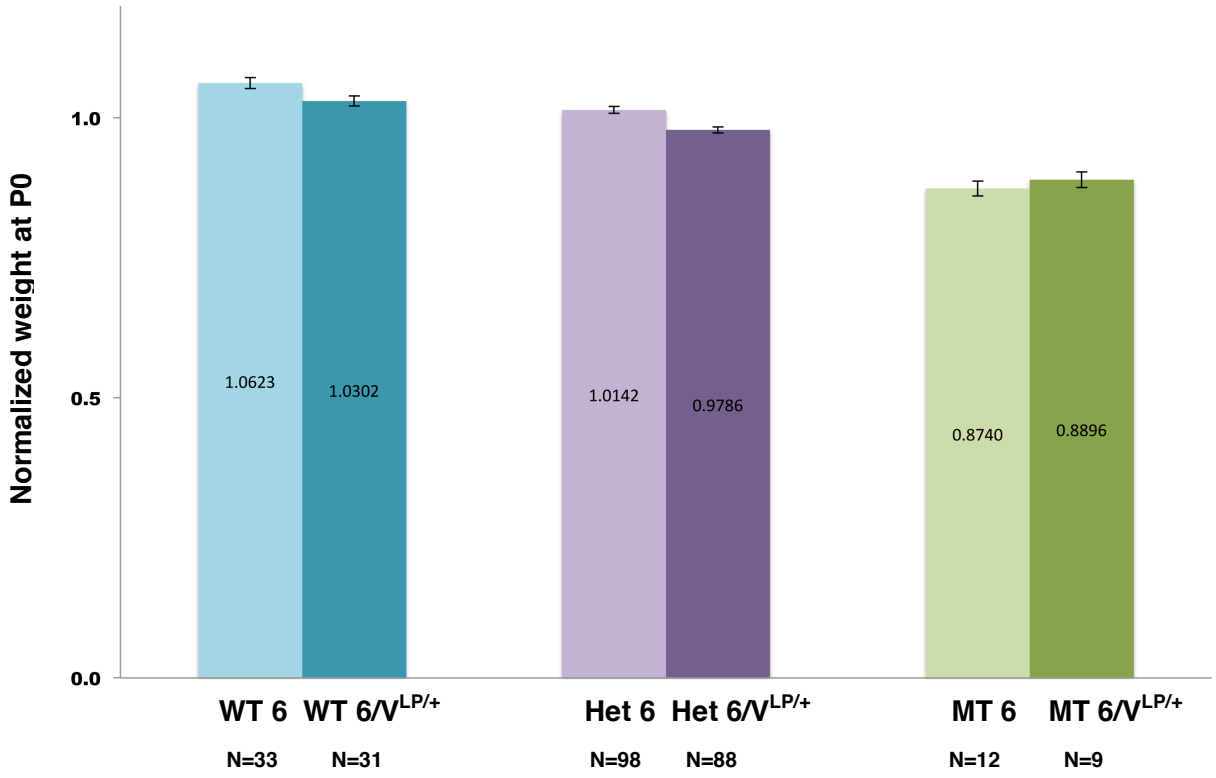

Figure 13 Mutants do not demonstrate changes in ß-Catenin expression.
A Immunohistochemistry assay on kidney tissues at P0 for β-Catenin (WT 6 – wild-type; MT 6 – homozygous mutant) demonstrating no difference between 3 wild-type and 3 mutants. **B** Real-time PCR quantifying transcript levels of genes involved in canonical Wnt signaling pathway did not show difference between 3 wild-type and 6 homozygous mutants whole kidney lysate at P0.

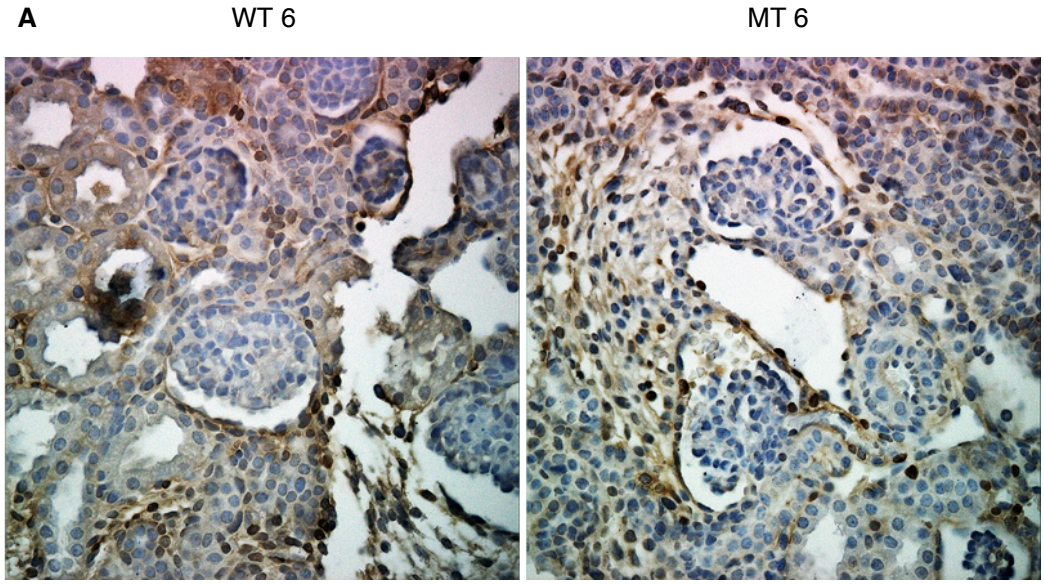

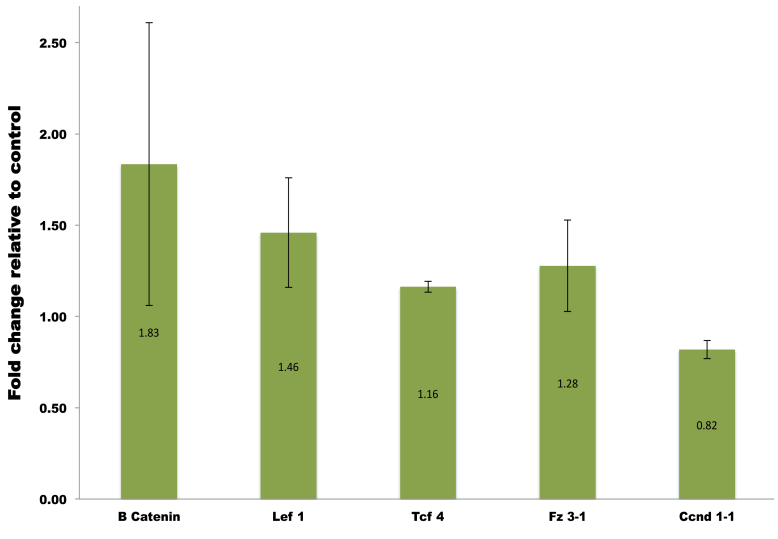

6.6 The underlying genetic mutation does not seem to have an overt interaction with Vangl2$^{LP/+}$

Previously, Saburi et al has shown a genetic interaction of *Fat4* with *Vangl2* (core PCP gene), where loss of one copy of *Vangl2* enhances cyst formation in *Fat4*$^{-/-}$ mutants(221). To test whether our model mutation interacts with core PCP genes, we bred our heterozygous mutants to *Vangl2*$^{LP/+}$. As reported previously, mice that were homozygous for *Vangl2*$^{LP/LP}$ (LP) died around the time of birth whereas heterozygotes had characteristic loop-tails and enlarged brain ventricles(222). Mice homozygous for LP occasionally developed dilated tubules(223). Heterozygotes were viable and fertile; the only reported renal phenotype was a modest reduction in glomerular numbers(222, 223). We observed a trend towards smaller birth weights in *Vangl2*$^{LP/+}$ compared to *Vangl2*$^{+/+}$ (p=0.22; two-tailed t-test heteroscedastic) (see **Figure 12**). Heterozygosity in both our critical region and *Vangl2* was associated with a significantly smaller birth weight compared to animals heterozygous for the critical region but wild-type for *Vangl2* (p<0.05; two-tailed t-test heteroscedastic). However, no difference was observed between the homozygous mutant within the critical region with either wild-type *Vangl2* or heterozygous *Vangl2* (p=0.67). Homozygous mutants, as mentioned previously, were significantly smaller and the phenomenon was dose dependent (p<0.01; one-way ANOVA). Sixty-two percent of the homozygous mutants exhibited cysts at P0 irrespective to *Vangl2* genotype (*Vangl2*$^{+/+}$ N=13; *Vangl2*$^{LP/+}$ N=8). Thus, we did not observe any accentuation in the cystic phenotype with a loss of one copy of *Vangl2*.

6.7 Beta-catenin pathway does not seem to be affected

Changes in canonical Wnt signaling have been associated with cystic kidney diseases(165). We performed immuno-staining on kidney sections of 3 homozygous mutants and 3 wild-type controls at P0 and scored the number of cells with specific ß-catenin nuclear staining. Overall, there was no difference in ß-catenin signal between

the homozygous mutants and the wild-type controls (**Figure 13A**). Specifically, for the epithelial cells lining the Bowman's capsule, nuclear staining was observed in 7.7% and 6.2% in homozygous mutants and wild-type control respectively (*p*=ns). To determine the gene expression of various components of the Canonical Wnt pathway at the transcript level, we isolated homogenized whole kidney RNAs from 6 homozygous mutants and 3 wild-type controls at P0. Comparisons made in transcript levels did not show any significant difference between mutants and wild-type in frizzled (*Fz 3*), a G-coupled receptor protein that is activated with Wnt ligand; beta-catenin, which is upregulated when the canonical pathway is active; T-cell factor (*Tcf 4*) and lymphoid enhancing binding factor (*Lef1*), both of which are transcription factors that interact with activated beta-catenin and; cyclin D1 (*Ccnd1*), which expression is increased upon activation of canonical Wnt (**Figure 13B**). Finally, our data showed no significant difference in proliferation and apoptosis in the kidneys from 3 homozygous mutants and 3 wild-type littermates at P0 (immunohistochemistry KI67, Caspase 3) (**Figure 14**). We have not looked at proliferation and apoptosis at earlier time points.

6.8 Transient transfection of vector expressing WT Samd9l

To further characterize our candidate gene, *Samd9l*, we attempted to use a commercially available antibody against the C-terminus of Samd9l (Abgent BP5166b) for Western blotting on proteins isolated from whole P0 kidneys. Unfortunately, it failed to produce any specific bands in both wild-type and mutant kidneys. Therefore, we cloned the wild-type *Samd9l* cDNA into the p3XFLAG-CMV-7.1 expression vector that is tagged with triple flag for detection. As illustrated in **Figure 15B**, HEK 293T cells transiently transfected with the construct demonstrated pancytosolic expression. A lower level of nuclear expression was also observed. No significant membranous signal was detected. To validate the expression vector, we performed Western blotting on proteins isolated from transfected cells using anti-flag antibody and demonstrated a clear single band in close proximity to the molecular marker for 170 KDa (predicted size of Samd9l is 185 KDa) (**Figure 15A**).

Figure 14 There is no significant difference in apoptosis and proliferation in the kidneys between wild-type (WT 6; N=3) and homozygous mutants (MT 6; N=3) at P0. **A** Immunohistochemistry assay on kidney tissues using Caspase 3 (marker for apoptosis). **B** Immunohistochemistry assay on kidney tissues using KI 67 (marker for proliferation).

A Caspase 3

WT 6 MT 6

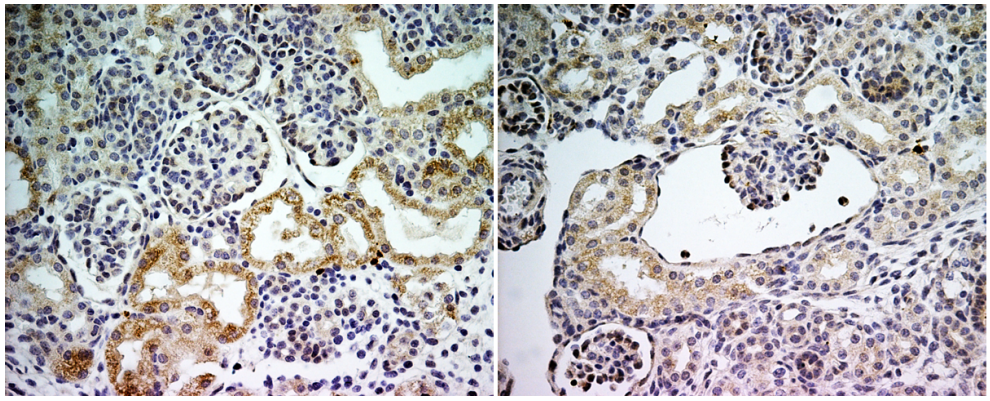

B KI 67

WT 6 MT 6

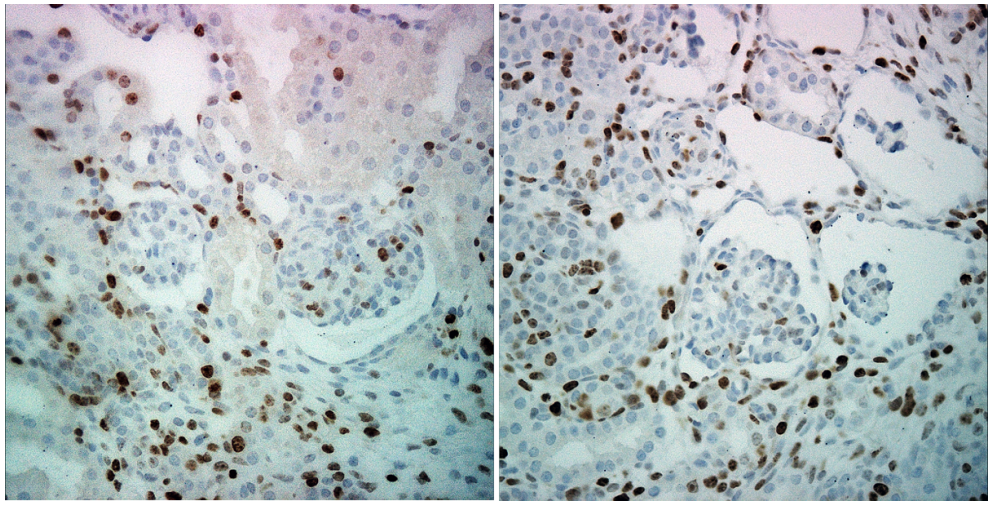

Figure 15 Western blot and immunofluorescence of HEK293T cells transiently transfected with expression vector for *Samd9l*. **A** Western blotting showing a distinct single band at 170 kDa representing Samd9l protein. The bottom bands represent β Actin loading control ("Ctrl" – HEK 293T cells transfected with control vector; "Samd9l" – HEK 293T cells transfected with Samd9l expression vector. **B** Immunofluorescence assay on HEK 293T cells transfected with Samd9l expression vector (red - Samd9l; green – phalloidin delineating cell border; blue – DAPI staining for nuclei).

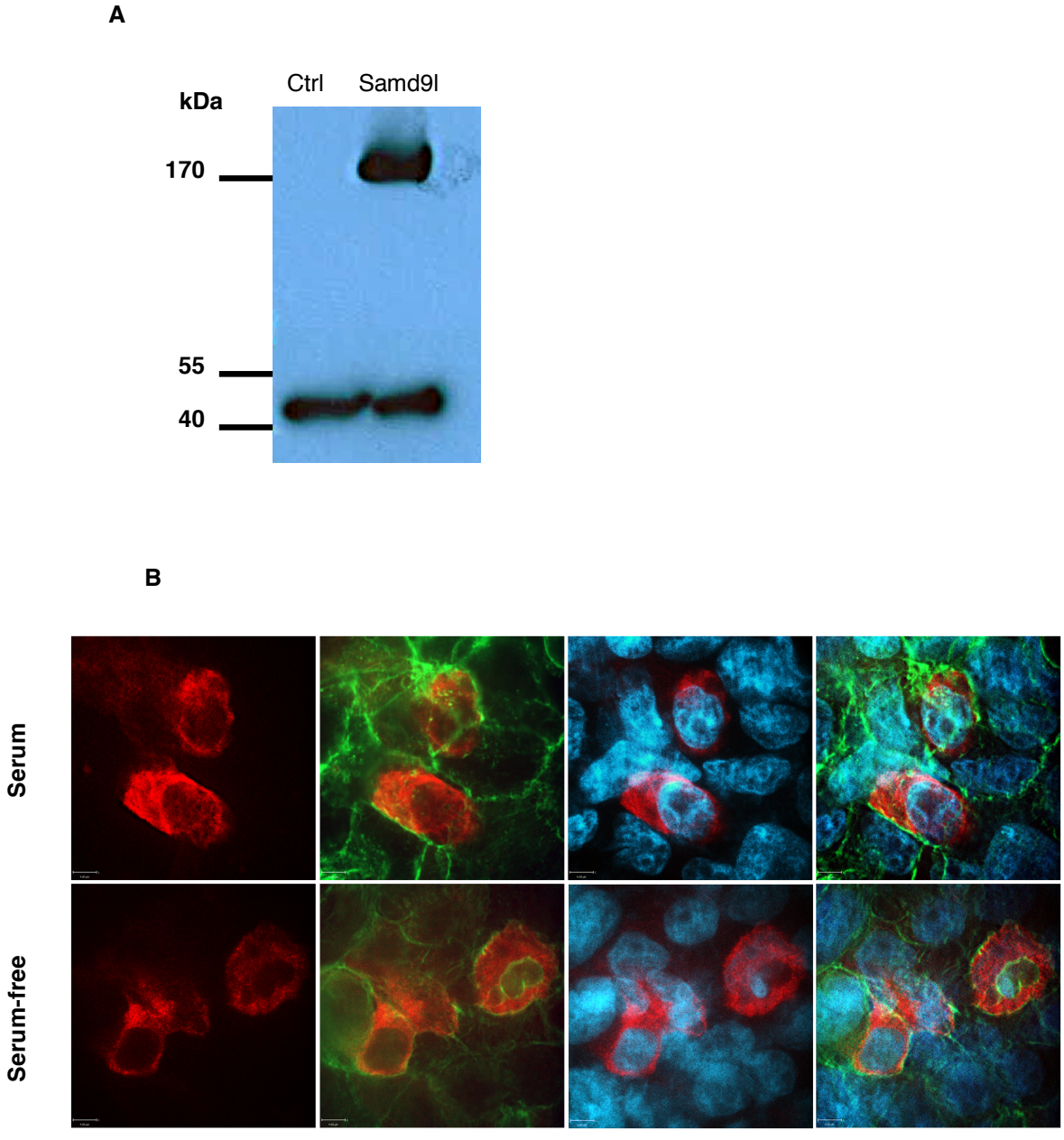

6.9 Mutants have lower expressions of p53 and p21 proteins

SAM domains are known to form homo and heterodimers(224), to further elucidate potential interacting protein partners with Samd9l, we performed immunoprecipitation using HEK293T cells that were transiently transfected with the expression vector. Mass spectrometry identified proteins involved in the ubiquitin pathway, including Stub1 (STIP1 homology and U-box containing protein E3 ubiquitin ligase) whose substrate is p53. This data leads us to study the expression of p53 and its downstream effector, p21, in the kidneys of 3 wild-type and 6 mutants at P0. Interesting, the expression of p53 was not different between wild-type and mutants at the transcript level, however, the level of p21 transcripts was significantly decreased in mutants (**Figure 16A**; $p<0.05$ two-tailed t-test). Immunostaining using p53 antibodies detected a much lower protein expressions (brown stained cells) in mutant kidneys compared to wild-type kidneys (**Figure 16B**). This observation was confirmed with Western blotting showing a significant reduction in p53 protein expressions at P0. Furthermore, the expression of p21 proteins, were also markedly decreased in mutant kidneys at P0 (**Figure 16C**).

Figure 16 Differential expressions of P53 and P21 between wild-type and mutants. **A** Real-time PCR showing that whole kidney lysate from 6 P0 homozygous mutants demonstrate a significantly lower P21 transcript level (p<0.05, two tailed t-test) but similar P53 transcript level compared to 3 wild-type littermates.

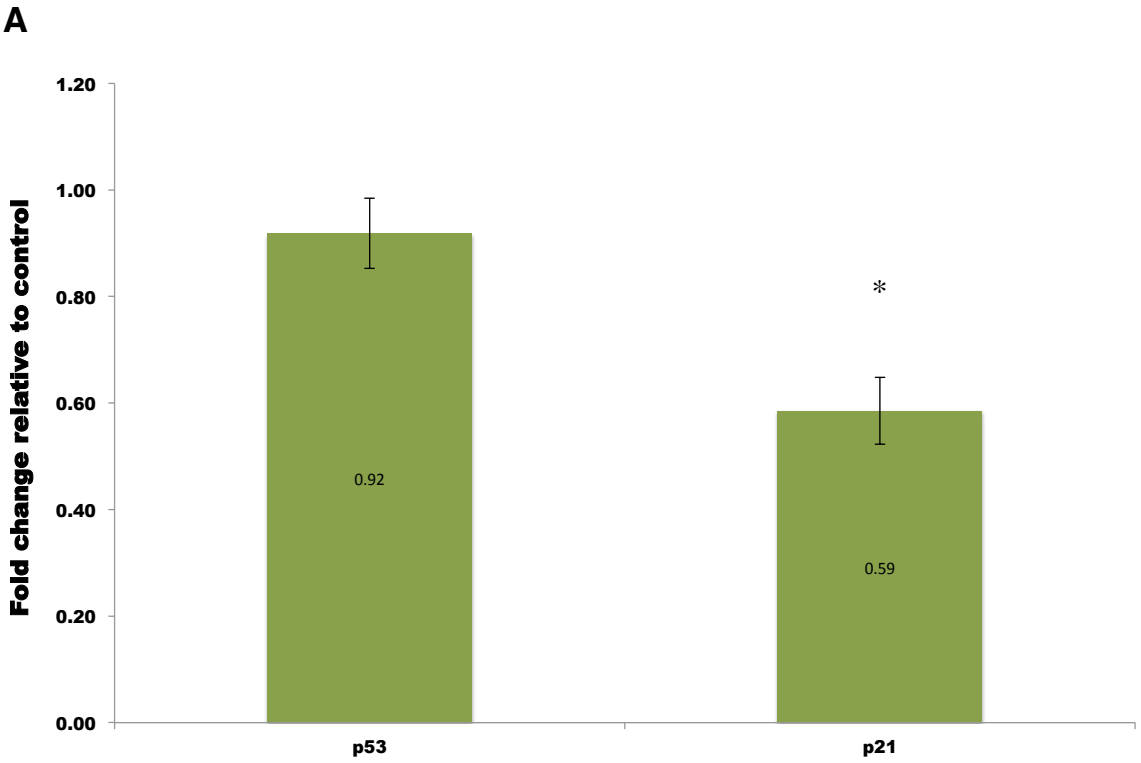

Figure 16 B P53 immunohistochemistry. Wild-type (WT) exhibits many positively stained nuclei (brown); homozygous mutant (MT) only has a few. **C** Western blotting showing diminishing levels of P53 and P21 proteins in the mutants. Despite higher loading of proteins with larger β Actin bands amongst the mutants (MT), P21 bands are much smaller compared to wild-type (WT) littermate controls.

B

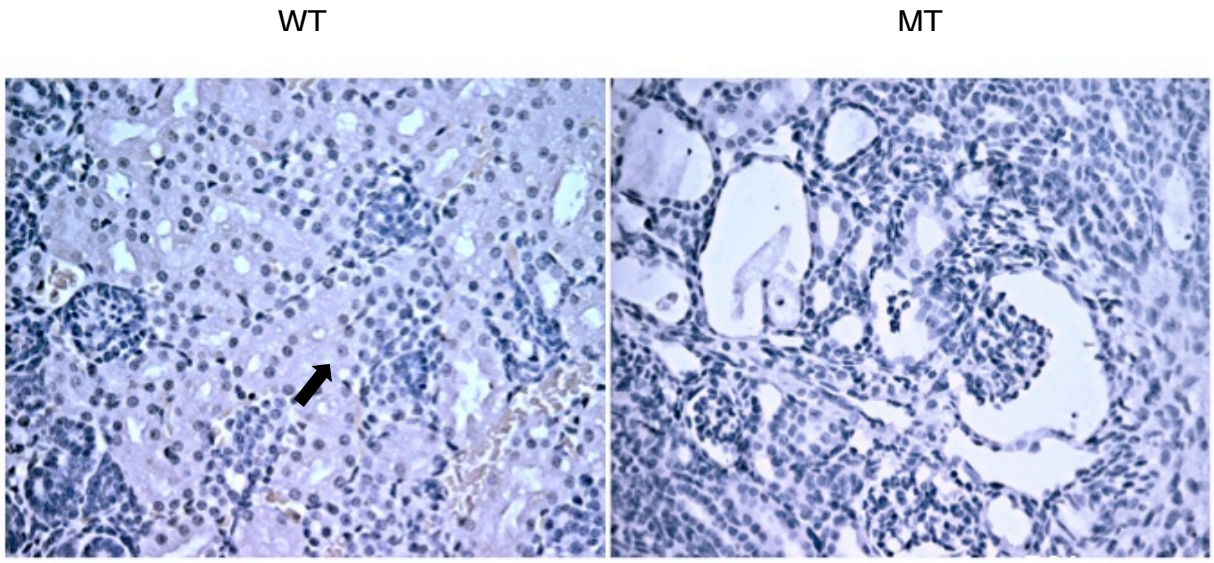

C

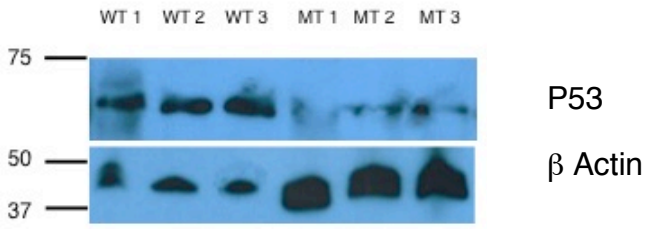

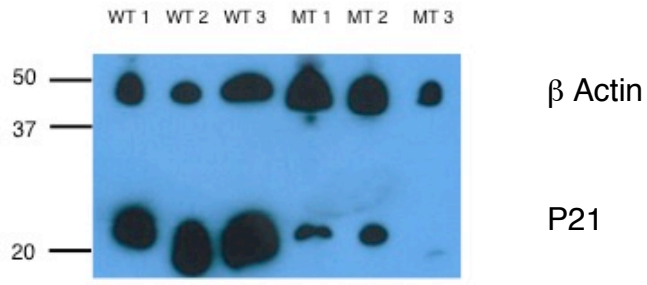

7 Discussions

In this study, we report a point mutation in the candidate novel gene *Samd9l* and associated cystic kidney phenotype. This gene has two isoforms due to a canonical and a non-canonical alternate splicing, which results in peptides of 1579 and 103 residues in size respectively (annotated by Havana). Although they vary greatly in size, both of the transcripts consist of two exons and translation begins in exon 2. Both peptides contain the SAM domain found in the amino-terminal that spans 66 amino acids in length. Human *SAMD9L*, located on chromosome 7q21.2 between 92,759,368 - 92,777,682, shares 76.1% similarity with mouse at the protein level (UniGene), and encodes a peptide of 1584 amino acids. It too has a non-canonical isoform of 406 residues in length. In humans, its paralogue gene, *SAMD9,* is located 3' downstream in a head-to-tail orientation, however, the gene *Samd9* is thought to be lost in the mouse lineage due to a unique genomic rearrangement(225). *SAMD9L* and *SAMD9* share about 78% sequence homology at the DNA level(225) and 58% at the protein level(226). Using human adult and fetal multiple tissue cDNA panel, SAMD9L has been shown to express ubiquitously in human tissues (225) as well as in the mouse with the highest level in the kidney(226). In mouse embryos, no *Sam9l* transcripts were detected at E8.5 and 9.5; however, low levels were detectable at E12.5 and 19(226). SAM domains are found in diverse eukaryotic organisms(227). They are able to mediate homotypic and heterotypic interactions to form multiple self-association architectures and also to bind to various non-SAM domain-containing proteins(224) and RNA(228). Structural analyses show that the SAM domain is arranged in a small five-helix bundle with two large interfaces(224) and as in the case of EphB2, each interphase can form dimers and hence an extended elaborate polymeric structure(229, 230). Examples of proteins containing the SAM domain include p73, ΔNp63α, EphB2, Samd6 (SamCystin in Han:Sprd-Cy cystic rat model and NPHP(231)), and Bicc1 (Bpk mouse model of cystic kidney disease).

There is a paucity of literature around this novel gene *SAMD9L* and its function(s) remains elusive. *SAMD9L* was first identified in conjunction with its

paralogue gene, *SAMD9,* which expression was shown to be decreased in the mesenchymal neoplasm aggressive fibromatosis, through subtractive hybridization assays(225). Due to their structural similarities and physical proximity, *SAMD9L* is speculated to share similar function(s) as *SAMD9*. There exist several lines of evidence suggesting *SAMD9*'s anti-proliferative function: a lower level of expression in neoplasms associated with β-catenin stabilization including aggressive fibromatosis, breast, and colon cancers(225); and the identification of a common microdeletion on 7q21.3 spanning the *SAMD9*, *SAMD9L*, and *LOC253012* (*Miki*) genes in patients with myeloid leukemia, juvenile myelomonocytic leukemia, and myelodysplastic syndrome(232). Interestingly, our P0 homozygous mutants have a significantly higher total white blood cell count (10.84 X 10^9/L) compared to their wild-type (3.38 X 10^9/L) littermates ($p < 0.01$). This expansion in white blood cell colonies involves neutrophils, lymphocytes, monocytes and eosinophils. Deficiency in SAMD9 has also been linked to a rare hereditary form of dystrophic calcification known as normophosphatemic familial tumoral calcinosis in individuals carrying biallelic loss-of-function mutation at K1496E(233). Transcription of *SAMD9* may be regulated by inflammatory cytokines including TNF-α and INF-γ mediated through p38 and NF-κB, and interferon-regulatory-factor 1 (IRF-1) transcription factor respectively(230, 234). Further, analysis of the promoter region of *SAMD9* reveals an IRF-1 transcription factor response element(234). IRF-1 is a member of a large family of proteins that function as transcription activators of genes induced by IFN-α, β, and γ(235). The associations between IRF-1 deficiency and various cancers including gastric, esophageal squamous cell, malignant transformation of hepatitis C infection and leukemia further tie the pathways of neoplasm and inflammation with *SAMD9*(236-239). Although the expression of *SAMD9L* was not different in aggressive fibromatosis, levels were lower in breast cancers compared to normal breast epithelial tissues(225). Mice deficient in Samd9l have a higher risk to develop myelogenous leukemia at older ages(226). However, *Samd9l* knockout mice did not develop ectopic calcification and hence unlikely to represent a functional paralogue to human *SAMD9*(240). Most recently, the expression of *SAMD9L* has been shown to be repressed by ΔNp63α(241), which also contains a SAM domain. ΔNp63α is a member of the p53 family of transcription

factors(242). Opposite to p53, ΔNp63α acts as a critical proliferative factor(243). Whilst it is essential for normal development as evidenced by profound developmental anomalies in *TP63* knockout mice (244), overexpression has been associated with various squamous cell carcinomas (SCC) of the head and neck, lung, and esophagus(245, 246) and hence it is suggested to be a potent oncogene. Using H226 cell line from lung SCC, shRNA mediated knockdown of ΔNp63α results in proliferation arrest with little change in apoptosis. ΔNp63α has been shown to repress canonical p53 target genes such as *p21*, *SFN*, *GADD45A*, *PUMA*, and *NOXA*(246, 247). However, the observed proliferation arrest with ΔNp63α shRNA cannot be rescued by simultaneous p53 knockdown(241). Interestingly, in H226 cells, ΔNp63α represses *SAMD9L* and this may be mediated through the deposition of histone variant H2A.Z(241) which has previously been identified as a transcriptional regulator(248, 249). H226 cells stop to proliferate when ΔNp63α is knocked down, which in turn, can be rescued by concurrent knockdown of *SAMD9L*(241). Furthermore, *SAMD9L* has been found to be downregulated not only in lung squamous cell carcinoma, but also in large and small cell lung carcinomas asserting its anti-proliferative action(241). The molecular mechanism by which this occurs remains elusive.

Aligning with the evidence from current literature suggestive of an anti-proliferative role in Samd9l, we observed a significantly lower mRNA expression of p21 in the kidneys of our homozygous mutants, although the transcript levels of p53 were similar (**Figure 16**). P21 or cyclin-dependent kinase inhibitor 1 binds to and inhibits the activity of cyclin-CDK1 or CDK2 complexes and regulates cell cycle progression at G1 by promoting G1 arrest. Interestingly, from our immunoprecipitation experiments using HEK293T cells temporarily transfected with the vector expressing WT *Samd9l* cDNA aiming to identify potential interacting proteins, we discovered various proteins involved in the ubiquitin proteasome pathway. One of which is Stub1 (STIP1 homology and U-box containing protein E3 ubiquitin ligase) whose human ortholog is CHIP. CHIP is a highly conserved protein containing a tetratricopeptide repeat domain at its amino terminus and a U-box domain at its carboxy terminus(250). It interacts with the molecular chaperones Hsc70-Hsp 70 and Hsp90 through its tetratricopeptide repeat

domain whilst the U-box domain confers its E3 ubiquitin ligase activities. The combination of chaperone binding and ubiquitin ligase activity suggests a multifaceted role for CHIP in mediating the switch from chaperone-dependent folding and maturation to proteasome induced degradation by ubiquitination (250-252). Recently, inhibition of Hsp90 with STA-2842 in a conditional KO mouse model of *Pkd1* results in a reduction in cysts growth(253). However, the exact mechanism is yet to be determined. CHIP also promotes aggresome formation when the proteasome system is overwhelmed for delayed protein degradation(254). CHIP substrates include p53(255-257), MKKS(258), and Runx1(259). P53 is upstream of and regulates p21. In addition, CHIP interacts and ubiquitinates death domain-associated protein (Daxx) in a stress-dependent manner, which blocks the subsequent phosphorylation of serine 46 in p53 and inhibits p53-dependent apoptotic program(260). McKusick-Kaufman syndrome (MKKS) is a recessively inherited human genetic disease that causes various developmental anomalies and Bardet-Biedl syndrome(258). Disease causing mutant MKKS protein has been shown to be rapidly degraded via CHIP(258). Runx1 is a member of the Runt-related transcription factor that encodes the DNA-binding α-chain partner of the heterodimeric core binding factor complex(261). Mutations and elevated expression of Runx1 are associated with different forms of leukemia(262, 263). Furthermore, antibodies against CHIP are found in patients with chronic lymphocytic leukemia (CLL) and in colorectal cancer. Regulation of ubiquitin has recently been affirmed in genes that are involved in cystic kidneys. Polycystin-1 is involved in regulation of ubiquitination of transcription factor Jade-1, which is a tumour suppressor(264). Jade-1 is a growth suppressive ubiquitin ligase for β-catenin. Jade-1 also has transcriptional activities, a key target of PC1, the cyclin-dependent kinase inhibitor p21, is upregulated by Jade-1. Jade-1 ubiquitination is mediated by Siah-1, an E3 ligase that binds polycystin-1 thus its expression is regulated by polycystin-1.

Downregulation of p21 expression in the whole embryos of *Pkd1*$^{-/-}$ mice have previously been reported and speculated to be involved in the proliferation of cyst(265). In addition attenuated expression of p53 has been reported in several cystic models: kidneys from mouse model of PKD1(266); in vitro human embryonic kidney 293 cells

with loss of polycystin-1 activity(267); and kidneys from humans with ADPKD(268). P53 inhibits cell cycle by induction of P21 and causes G1/S arrest(269). Polycystin-1 may regulate growth of renal tubular epithelial cells through induction of P53 and activation of JAK2 and hence upregulation of P21(265). Using a chimeric *Pkd*$^{-/Lz+}$ mouse model, Nishio et al. proposed the following model of cystogenesis(266): when tubular epithelial cells receive stimulation, both normal and abnormal cells proliferate to expand the tubular size. The abnormal cells lack negative signals for proliferation by polycystin-1 and continue to proliferate where the surrounding normal tubular epithelial cells also proliferate to retain both the round shape and diameter of the tubule, normal epithelial cells are gradually lost by JNK-mediated apoptosis at the intermediate stage. Some abnormal cells change shape from cuboidal to flat (dedifferentiation), and the flat epithelial cells grow in an immortalized fashion to form large cysts. Polycystin-1 plays a role in prevention of immortalized proliferation of renal tubular epithelial cells via JNK activation and p53 induction.

Cystogenesis is accompanied by characteristic changes in tubular epithelial cells, including increased proliferation, apoptosis, acquisition of a secretory phenotype, dysregulation of the cell cycle, intracellular calcium and cAMP signaling and activation of several molecular pathways, including the PCP, Wnt, sonic hedgehog, and Akt/mTOR (23, 173, 265, 270-277). It is interesting that ubiquitination of P53 and the consequent decrease in P21 level may be the potential molecular mechanism underlying the cystic kidney phenotype in this model. What more intriguing is the observation that the planar cell polarity signaling pathway may also play a role in the observed phenotype. Interestingly, we did not observe any overt changes in the canonical Wnt signaling pathway. Furthermore, Patch 1 and Gli 1 in situ (data not shown) on kidney sections at P0 were not different between wild-type and the mutants. Together with a lack of polydactyly, and exencephaly, sonic hedgehog is likely not affected in our cystic model. Finally, to test if mTOR interacts with our model, we crossed our mutants with haploinsufficient mTOR mice and observed no significant difference in proportion of P0 homozygous mutant with cysts, cysts severity, and survival (all homozygous *Samd9l* mutant still dies at P0). Taken together, we are

submitting a novel gene mutation that results in lowering level of cell cycle regulator P21 and cystic kidney disease. We propose that wild-type Samd9l negatively regulates Stub1-mediated ubiquitination of p53. Our current mutation in *Samd9l* alters the protein structure and its interaction with Stub1 and results in polyubiquitination of p53 for downstream degradation (**Supplementary Figure 5**).

8 Future Directions

To confirm causality between *Samd9l* mutation and the cystic phenotypes:

A more definitive approach to study if the point mutation/genetic polymorphism identified in *Samd9l* is responsible for the interesting phenotypes observed in our mouse model: kidney cysts, liver abnormality, leukocytosis, planar cell polarity, and perinatal lethality, we will create a knockin mutant with the exact genetic alteration using R1-129 in ICR host embryo donor. Chimeras with the point mutation will be identified and crossed with WT C3H/HeJ and homozygous mutants will be phenotyped.

To investigate the function of wild-type and mutant *Samd9l* in *in vitro* assays:

We have already cloned wild-type and mutant *Samd9l* CDNA into the p3XFLAG-CMV expression vectors. Expressions have been validated with Western blotting. These vectors will be transfected into both human HEK293T cells and mouse embryonic fibroblasts. Cells transfected with the expression vectors will be harvested and proteins isolated for Western blot to study the expressions of p53 and p21. In parallel, we will obtain mouse embryonic fibroblasts from homozygous embryos and wild-type embryos and look for differential expression of p53 and p21 proteins. Further, since Stub1 has been identified as a potential interacting partner with Samd9l, we plan to use siRNA to knockdown *Stub1* expression and study p53 and p21 expressions. Further, we will knockdown *Samd9l* using siRNA and compare its effect on p53 and p21 protein expressions with Western blotting.

To further validate the involvement of P21, we plan to perform cell cycle and proliferation assays with flow cytometry using cytosolic stain and Propidium Iodide.

To continue to search for candidate mutations within the critical region:

Our analysis of the quality of our present whole-exome next-generation re-sequencing data showed areas of deficient coverage. In addition to the inherent lower sensitivity in detecting indels, we aim to continue to search for mutation within the critical region. We will first perform Northern blotting on all the genes within the region to look for differences between wild-type and homozygous mutants. We are also planning on collaborating the findings with commercially available whole genome sequencing with Complete Genomics.

Supplementary Table 1 Rough mapping using 96-microsatellite markers. C – WT C3H/HeJ; H – Heterozygous (Pos = position; Chromo = chromosome). Critical region is highlighted in gray color.

Pos. (cM)	Chromo	Primer	Size		Affected											Unaffected										
			C3H/HeJ	C57BL/6J	3-23	3-5	3-2	3-25	2-22	2-1	1-25	1-21	1-26	2-21	1-22	3-1	3-4	3-24	2-6	1-23	1-24	2-2	2-3	2-5	2-7	2-4
4.4	1	D1MIT429	92	104	H	H	H	H	H	H	C	C	C	C	C	H	H	H	H	C	C	H	H	C	H	H
17.5	1	D1MIT278	239	223	H	H	H	H	H	H	C	C	C	C	C	H	H	H	C	C	H	H	H	C	C	H
43.7	1	D1MIT132	163	145	H	H	H	H	H	C	C	C	C	C	C	H	H	H	C	C	H	H	H	C	C	H
60.1	1	D1MIT136	107	101	H	H	H	H	H	C	C	C	C	C	C	H	H	H	C	C	H	C	H	C	C	H
82	1	D1MIT424	131	123	H	C	C	C	H	H	C	C	H	H	C	H	C	C	C	C	H	C	C	C	H	H
94	1	D1MIT206	115	125	H	C	C	C	H	H	C	C	H	H	C	C	C	C	C	C	H	C	C	C	H	H
103.7	1	D1MIT407	123	118	C	C	C	C	H	H	C	C	H	H	C	C	C	C	C	C	H	C	C	C	H	H
2.2	2	D2MIT1	120	125	H	H	H	C	H	H	C	H	C	H	C	C	H	C	H	C	C	H	C	H	H	C
27.3	2	D2MIT372	116	120	H	H	H	C	H	H	C	H	H	H	C	C	H	H	C	C	H	H	C	C	C	C
42.6	2	D2MIT92	205	148	H	H	H	C	C	H	C	H	H	C	C	C	H	H	C	C	H	H	C	C	C	C
61.2	2	D2MIT525	124	118	H	C	C	H	C	H	C	H	H	C	C	H	C	H	H	H	H	H	C	C	C	C
72.1	2	D2MIT285	148	138	H	C	C	H	C	H	C	H	H	H	C	C	C	H	H	H	H	H	H	C	C	H
84.2	2	D2MIT145	137	147	H	C	C	H	C	H	C	H	H	H	C	C	C	H	H	H	H	H	C	C	C	H
2.4	3	D3MIT164	116	132	C	H	H	H	C	H	H	H	H	C	H	H	H	C	H	H	C	H	H	C	C	H
11.2	3	D3MIT203	145	159	C	H	H	H	C	H	H	H	H	C	C	H	H	C	H	H	C	C	H	C	C	H
25	3	D3MIT119	148	143	C	C	H	H	C	H	H	H	H	C	C	H	-	-	-	H	C	H	H	C	C	H
35.2	3	D3MIT137	158	181	C	C	H	C	C	H	H	H	C	C	C	C	C	C	H	H	H	H	H	H	H	C
41	3	D3MIT175	133	139	C	H	C	C	H	H	H	C	C	C	C	C	C	C	H	H	H	H	H	H	C	C
70.3	3	D3MIT258	190	216	H	C	H	C	H	C	H	C	H	H	C	C	C	H	H	C	H	C	H	H	H	H
79.4	3	D3MIT147	139	131	H	C	H	H	H	C	H	C	H	C	C	C	C	H	H	C	H	C	H	H	H	H
87.6	3	D3MIT19	166	156	H	C	H	H	H	C	H	H	H	C	C	C	C	H	H	C	H	C	H	H	H	H
10.9	4	D4MIT106	126	132	C	H	C	C	C	H	H	C	C	H	C	H	H	H	H	C	H	C	C	H	H	H
12	4	D4MIT193	120	137	C	H	C	C	C	H	H	C	C	H	C	H	H	H	H	C	H	C	C	H	H	H
23	4	D4MIT162	146	138	H	H	C	H	C	H	H	C	C	H	C	H	H	H	H	C	C	H	C	C	H	H
54.6	4	D4MIT308	112	84	C	C	C	H	C	C	C	H	H	H	H	C	C	H	H	C	C	H	C	C	H	H
60.1	4	D4MIT203	122	106	C	C	C	H	C	C	C	H	H	H	H	H	C	H	H	C	C	H	C	C	H	H
15.3	5	D5MIT352	118	110	H	C	C	H	C	H	C	H	C	C	H	C	C	C	H	C	H	C	C	H	C	H
19.7	5	D5MIT233	177	144	H	C	C	H	C	C	C	C	C	C	H	C	H	C	H	H	H	C	C	H	C	H
59	5	D5MIT426	108	118	H	H	C	C	H	C	C	C	C	H	C	H	H	C	H	H	H	C	H	H	H	H
73.2	5	D5MIT247	166	160	H	H	C	C	H	C	C	C	H	H	C	H	H	C	H	C	H	C	H	C	H	H
82	5	D5MIT287	143	149	H	H	C	C	C	H	C	C	C	H	H	H	C	C	H	C	H	C	H	C	H	H
2.2	6	D6MIT138	134	112	H	H	H	C	H	H	H	H	H	H	H	C	C	H	H	C	C	H	C	H	C	C
4.4	6	D6MIT204	128	151	H	H	H	H	H	H	H	H	H	H	H	C	C	H	H	C	C	H	C	H	H	C
7	6	D6MIT159	139	112	H	H	H	C	H	H	H	H	H	H	H	H	C	H	H	C	C	H	C	H	H	C
12	6	D6MIT119	112	108	H	C	C	C	H	C	H	H	H	H	C	H	C	H	H	C	C	H	C	H	H	C
27.3	6	D6MIT9	120	136	C	C	C	H	C	C	H	C	H	C	C	C	C	C	C	C	C	H	C	H	H	C
47	6	D6MIT366	139	123	C	C	C	H	C	C	H	C	H	H	H	H	C	C	H	C	H	H	C	H	H	C
0	7	D7MIT178	188	204	H	C	C	C	C	H	C	H	C	C	C	H	H	H	C	C	H	C	H	H	C	C
63.4	7	D6MIT14	150	160	C	H	C	C	C	H	H	C	H	H	H	H	C	H	H	C	C	H	C	C	C	H
3.3	7	D7MIT191	194	154	H	C	C	C	C	H	C	H	C	C	C	H	H	H	H	C	C	H	C	H	H	C
15.3	7	D7MIT270	119	149	H	C	C	C	C	H	C	H	C	C	C	H	H	H	H	C	C	H	C	H	H	C
36.1	7	D7MIT321	130	114	H	H	H	H	H	H	C	H	C	C	C	H	C	H	C	C	H	C	C	H	C	C
43.7	7	D7MIT66	149	166	H	H	H	H	H	H	C	H	C	C	C	H	C	C	C	C	H	C	C	H	C	C
67.8	7	D7MIT259	152	148	H	C	H	H	H	H	C	H	C	H	C	C	H	C	H	C	C	C	C	C	C	C
8.7	8	D8MIT281	118	123	H	C	H	H	H	H	H	C	C	C	C	H	C	C	C	C	C	C	C	H	C	C
21.9	8	D8MIT190	100	136	H	C	H	H	H	H	H	C	C	C	C	H	C	C	C	C	C	C	C	H	C	C
39.3	8	D8MIT106	115	146	H	C	H	C	C	H	H	C	C	C	C	C	C	C	C	C	C	C	C	H	H	C
47	8	D8MIT242	198	168	H	C	H	C	C	H	H	C	C	C	C	H	C	C	C	C	C	C	C	H	H	C
59	8	D8MIT35	249	243	H	H	H	C	C	H	C	C	C	C	C	H	C	C	C	C	C	C	C	H	H	C
75.4	8	D8MIT156	154	138	H	H	H	C	C	H	H	C	H	C	H	H	C	C	H	C	H	C	C	H	H	H
13	9	D9MIT67	134	120	H	H	C	H	C	H	H	H	C	C	C	H	H	H	H	H	C	H	C	H	C	C
33.9	9	D9MIT336	103	117	H	H	C	H	H	H	H	H	C	C	C	H	H	H	H	C	C	H	C	H	H	C
47	9	D9MIT35	109	122	H	H	C	H	H	H	H	H	C	C	C	H	H	H	H	C	C	H	H	H	H	C
61	9	D8MIT46	200	229	H	H	C	H	H	H	H	H	C	C	C	H	H	H	H	C	C	H	H	H	H	C
69.9	9	D9MIT151	112	116	H	H	C	H	H	H	H	H	C	C	C	H	H	H	H	C	C	H	C	H	H	C
16.4	10	D10MIT3	220	243	C	H	H	C	H	H	C	C	C	C	C	H	H	H	H	H	C	C	H	C	H	H
20.8	10	D10MIT194	93	81	C	H	H	C	H	H	C	H	C	H	C	H	H	H	C	C	H	C	C	H	H	H
30.2	10	D13MIT67	143	159	C	H	H	C	H	H	H	H	H	H	C	H	H	H	C	H	C	H	H	H	H	C
41.5	10	D10MIT42	196	182	C	H	H	C	H	H	C	H	C	H	C	H	H	H	C	H	C	C	H	C	H	H
50.3	10	D10MIT95	178	198	C	H	H	C	H	H	H	H	C	H	C	H	H	H	C	H	C	H	H	H	H	C
63.4	10	D10MIT233	106	126	C	C	H	C	H	H	H	H	H	H	H	H	H	C	C	H	C	H	H	H	H	C
4.3	11	D11MIT2	117	103	H	H	C	C	C	C	C	H	H	H	H	H	C	C	H	C	H	C	H	H	C	H
25.1	11	D11MIT131	142	154	C	H	C	C	C	H	C	H	H	C	H	H	H	H	H	C	H	C	C	H	H	H
36.1	11	D11MIT4	247	255	H	H	C	C	C	H	C	H	H	C	H	H	H	H	H	C	H	H	C	H	H	H
49.5	11	D11MIT285	130	118	H	H	C	C	C	H	C	H	H	C	H	H	H	H	H	C	H	H	C	H	H	H
60	11	D11MIT67	122	130	H	H	C	C	H	H	C	H	H	C	H	H	H	H	H	C	H	H	C	H	C	H
77.6	11	D11MIT214	133	149	H	C	C	H	H	C	C	C	H	H	H	H	H	H	H	C	C	H	C	H	C	C
13.1	12	D12MIT221	87	107	H	C	C	C	H	C	C	C	C	H	H	C	C	C	C	C	C	H	H	H	C	C
32.8	12	D12MIT158	136	154	C	C	C	C	C	C	C	C	C	H	C	C	C	C	C	C	H	H	H	C	C	C
47	12	D12MIT167	144	150	C	C	C	C	C	C	C	C	C	H	C	C	C	C	C	C	H	C	H	C	C	C
56.8	12	D12MIT263	125	111	C	C	C	C	C	C	C	C	C	H	C	H	H	C	C	C	H	C	C	H	C	C
13.1	13	D13MIT88	180	168	C	H	C	C	C	C	H	H	C	C	H	H	H	C	H	C	C	C	C	H	H	H
35	13	D13MIT107	141	153	H	H	C	C	C	H	H	C	H	H	H	H	H	C	C	C	C	C	C	H	H	C
43.6	13	D13MIT53	154	146	H	H	H	H	C	H	H	C	H	H	H	H	H	C	C	C	C	C	C	H	H	C
59	13	D13MIT35	181	195	H	H	H	H	C	H	H	C	H	H	H	H	H	C	C	C	H	C	C	H	H	C
3.3	14	D14MIT98	147	155	C	C	H	H	H	C	C	C	C	C	C	H	C	H	H	H	H	H	H	H	C	C
24	14	D14MIT60	111	133	H	H	H	H	H	C	H	C	H	C	H	H	C	C	H	C	H	C	C	H	H	C
35	14	D14MIT157	146	150	C	C	H	H	H	C	C	C	H	C	H	C	C	C	H	C	H	C	C	H	H	H
47	14	D14MIT160	162	140	H	H	H	H	C	C	H	C	H	C	H	C	C	C	H	C	C	C	C	H	H	C
9.8	15	D15MIT130	197	183	H	H	C	H	C	C	C	H	H	C	C	C	C	H	C	H	C	C	C	H	H	H
17.5	15	D15MIT154	140	154	H	H	H	H	C	C	C	H	H	C	C	C	C	H	H	H	C	C	C	H	H	C
27.3	15	D15MIT270	179	199	H	H	H	H	C	C	H	H	H	C	C	C	H	H	H	H	C	C	C	H	H	C
41.5	15	D15MIT107	146	154	H	H	H	H	H	C	H	H	H	C	C	C	H	H	H	H	H	C	C	C	H	C
52.5	15	D15MIT171	133	125	H	H	H	H	H	C	H	H	H	C	C	C	H	H	C	H	H	C	C	C	H	C
17.5	16	D16MIT101	146	150	C	C	C	H	C	H	C	C	H	H	C	H	C	C	H	C	H	C	H	H	H	H
33.9	16	D16MIT105	108	112	H	C	C	H	C	H	H	C	C	H	C	H	C	C	H	C	C	H	H	C	H	C	C
45.9	16	D16MIT153	273	269	H	H	C	H	-	H	H	-	C	-	C	H	H	C	H	C	C	H	C	H	C	C
3.3	17	D17MIT100	133	121	C	H	C	H	H	C	H	C	C	H	H	H	C	C	C	C	C	C	C	H	H	C	C
14.2	17	D17MIT51	139	157	C	H	C	H	H	C	H	C	C	H	H	H	C	C	C	C	C	H	C	H	C	C	C
29.5	17	D17MIT20	165	177	C	H	C	H	H	C	H	C	C	H	H	H	C	C	C	C	C	C	C	H	C	C	C
50.3	17	D17MIT123	151	129	C	H	C	H	C	C	H	C	H	H	H	H	C	C	C	H	C	C	H	H	H	C	C
4.4	18	D18MIT197	133	125	H	C	C	C	H	C	H	C	H	C	C	C	C	C	H	H	C	H	C	H	C	C	C
15.3	18	D18MIT58	207	183	H	C	C	H	H	H	H	C	H	C	C	H	C	C	H	H	H	C	H	C	C	C	C
25.1	18	D18MIT40	125	137	H	C	C	H	H	H	H	C	C	C	C	C	H	C	C	H	H	H	H	C	C	C	C
35	18	D18MIT48	158	166	H	C	C	H	C	H	H	C	C	C	C	C	H	C	C	H	H	H	H	C	C	C	C
9.7	19	D19MIT28	154	146	C	C	H	C	C	C	C	C	H	C	H	C	C	C	H	C	C	C	C	H	C	H	H
24	19	D19MIT63	148	154	C	C	H	C	C	H	C	C	H	C	H	H	H	C	H	C	C	C	C	H	C	C	C
40.4	19	D19MIT103	129	123	C	C	H	C	H	H	C	C	H	C	H	H	H	C	C	C	C	H	C	H	H	C	C

Supplementary Table 2 Further crossover in the mutant “80-1-2” narrowed the distal microsatellite marker to D6MIT204. C – wild-type C3H/HeJ; H – Heterozygous; Pos - position; Chromo – chromosome.

Pos. (cM)	Chromo	Primer	Size		Affected								
			C3H/HeJ	C57BL/6J	80-1-2	80-2-21	80-2-22	80-2-23	80-2-24	77-5-6	77-5-21	77-5-22	89a-1-1
2.2	6	**D6MIT138**	134	112	H	H	H	C	H	H	H	H	H
4.4	6	**D6MIT204**	128	151	C	H	H	H	H	H	H	H	H
7	6	**D6MIT159**	139	112	C	H	C	H	C	H	H	H	H

Supplementary Table 3 Fine mapping narrows the critical region to about 3 Mb in size. The latest crossover in the mouse mutant, c77189j-3-2, narrows the critical region to distal marker rs13478611. C-wild-type C3H/HeJ; H-Heterozygous.

Ensembl(Mb)	Markers	C47189e-4-23	8077-5-21	C57189c-15-22	C67189c-7-1	8080-1-2	C57189b-2-24	C57189b-2-26	C57189b-4-23	C57189b-8-22	C57189b-9-21	C47189e-4-2	C67189d-3-22	c77189j-3-2
3.35	rs3695631	H	H	H	H	H	H	H	H	H	H	H	H	H
3.5	SS-16376485	H	H			H	H	H	H	H	H	H		
3.99	rs30558274													H
4.0	SS-5045907	H	H			H	H	H	H	H	H	H		
4.45	D6MIT138	H	H			H	H	H	H	H	H	H		
4.49	rs30856904													
6.29	rs13478611			H	H								H	C
7.4	SS5045921	H	H			H	H	H	H	H	H	H		
9.05	rs33347375													
9.16	rs33348282													
12.37	rs33391668													
13.1	SS5055070	H	H			H	H	H	H	H	H	H		
13.8	rs3716714													C
16.01	rs13478641			H	H								H	C
17.16	rs29980924												H	C
17.5	M-02094-1	H	H			H	H	H	H	H	H	H		
17.67	MHAa74g5			H	H								C	
18.1	rs3161298													C
20.9	SS5074905	H	H			H	H	H	H	H	H	C		
21.01	rs3698725													C
23.08	D6Mit204	H	H			C	C	C	C	C	C	C		C
23.1	SS-5060329	H	H			C						C		
25.7	SS-5047202	H	H			C						C		
25.80	rs13478669			C	C									
28.30	M-02116-2	H	H			C						C		
29.70	D6Mit159		H			C								
44.50	D6Mit207		C			C								
50.30	rs6320585	C		C	C							C		

Supplementary Table 4 Genotype-phenotype discrepancy. Mice were wild-type based on genotype within the critical region using SNPs but exhibited glucosuria. Week – age in weeks; values under "Mutants" were level of glucosuria based on urine dipstick; C – wild-type C3H/HeJ.

Week		Mutants		
3	Urine Glucose	0.0	5.5	0.0
4	Urine Glucose	14.0	14.0	5.5
5	Urine Glucose	5.5	2.8	5.5
6	Urine Glucose	5.5	0.0	14.0
7	Urine Glucose	14.0	0.0	0.0
8	Urine Glucose	5.5	5.5	0.0
9	Urine Glucose	5.5	2.8	14.0
10	Urine Glucose	0.0	14.0	2.8
Ensembl (Mb)	Markers	C47189a-1-25	C47189e-4-22	C77189c-3-22
3.10	SS-5106741	C	C	
3.35	rs3695631			C
3.50	SS-16376485	C	C	
4.00	SS-5045907	C	C	
4.45	D6MIT138	C	C	
4.49	rs30856904			C
6.29	rs13478611	C	C	C
7.40	SS5045921	C	C	
9.05	rs33347375			
9.16	rs33348282			C
12.37	rs33391668			C
13.10	SS5055070	C	C	
16.01	rs13478641	C	C	C
17.16	rs29980924			C
17.50	M-02094-1	C	C	
17.67	MHAa74g5			
20.90	SS5074905	C	C	
23.08	D6Mit204	C	C	
23.10	SS-5060329	C	C	
25.70	SS-5047202	C	C	
25.80	rs13478669			
28.30	M-02116-2	C	C	
29.70	D6Mit159	C		
44.50	D6Mit207	C		
50.30	rs6320585		C	

Supplementary Table 5 Wild-type mice by genotype exhibited high-grade glucosuria. Intercross between two heterozygous G7 mutants generated G8. Two of the "wild-type" G8 with persistent high-grade glucosuria were intercrossed to produce 4 litters of G9, all of which exhibited high-grade glucosuria. Week – age in weeks; values under "Mutants" were levels of glucosuria based on urine dipstick; C – wild-type C3H/HeJ.

Week		G7		G8		G9 Litter 1								G9 Litter 2		G9 Litter 3						G9 Litter 4	
3	Urine Glucose	5.5	0	0	55	55	55	55	55	55	55	55		55	55	55	55	55	55	55	55	55	55
4	Urine Glucose	0	0	55	55	55	55	55	55	55	55	Died		55	55	55	55	55	55	55	55	55	55
5	Urine Glucose	0	55	55	55	55	55	55	55	55	55			55	55	55	55	55	55	Died	55	55	55
6	Urine Glucose	0	0	55	55	55	55	55	55	55	55			55	55	55	55	55	55		55	55	55
7	Urine Glucose	5.5	2.8	55	55	55	55	55	55	55	55			55	55	55	55	55	55		55	55	55
8	Urine Glucose	5.5	0	55	55	55	55	55	55	55	55			55	55	55	55	55	55		55	55	55
9	Urine Glucose	0	0	55	55	55	55	55	55	55	55			55	55	55	55	55	55		55	55	55
10	Urine Glucose	5.5	5.5	55	55	55	55	55	55	55	55			55	55	55	55	55	55		55	55	55
Ensembl (Mb)	Markers	c57189g-11-1	c77189i-11-21	i117189b-1-21	i117189b-2-2	i27189a-1-1	i27189a-1-2	i27189a-1-3	i27189a-1-4	i27189a-1-5	i27189a-1-21	i27189a-1-22		i27189a-2-1	i27189a-2-21	i27189a-3-1	i27189a-3-2	i27189a-3-3	i27189a-3-4	i27189a-3-5	i27189a-3-21	i27189a-4-1	i27189a-4-21
3.35	rs3695631	H	H	C	C	C	C	C	C	C	C	C		C	C	C	C	C	C	C	C	C	C
3.50	SS-16376485																						
4.00	SS-5045907																						
4.45	D6MIT138																						
4.49	rs30856904																						
6.29	rs13478611	H	H	C	C	C	C	C	C	C	C	C		C	C	C	C	C	C	C	C	C	C
7.40	SS5045921																						
9.05	rs33347375																						
9.16	rs33348282																						
12.37	rs33391668																						
13.10	SS5055070																						
13.80	rs3716714	H	H													C	C	C	C	C	C	C	C
15.02	rs38471300																						
16.01	rs13478641	H	H	C	C	C	C	C	C	C	C	C		C	C	C	C	C	C	C	C	C	C
17.16	rs29980924																						
17.50	M-02094-1																						
17.67	MHAa74g5																						
20.9	SS5074905																						
21.01	rs3698725	H	H																				
23.08	D6Mit204	H	H	C	C																		

Supplementary Table 6 Reanalysis of the whole-genome SNPs genotyping based on a medium density linkage panel of 1449 SNPs on an Illumina platform. Renal cysts rather than glucosuria was used as the differentiating phenotype. C – wild-type C3H/HeJ; H – Heterozygous.

		7189-2-1	7189-1-25	7189-1-26	7189-2-21	7189-3-23	8077-5-21	8080-2-23	C47189a-1-1	C47189e-3-23	C47189e-4-2	C57189b-2-24	C57189b-2-26	C57189b-4-23	C57189b-8-22	C57189b-9-21	C57189c-12-32	C67189b-2-1	8080-1-2	C47189e-3-24	C47189e-4-23	c77189j-2-22	6008-1-21	6008-2-2	6015-2-21
Animal #		1	2	3	4	5	6	7	8	9	10	11	12	13	14	15	16	17	18	19	20	21	22	23	24
Markers	**Chromosome**	Cystic	Cystic	Cystic	Cystic	Cystic	Cystic	Cystic	Cystic	Cystic	Cystic	Cystic	Cystic	Cystic	Cystic	Cystic	Cystic	Cystic	Cystic	Cystic	Cystic	Cystic	Wild-type	Wild-type	Wild-type
rs3661828	6	H	H	H	H	H	H	H	H	H	H	H	H	H	H	H	H	H	H	H	H	H	C	C	C
rs13478602	6	H	H	H	H	H	H	H	H	H	H	H	H	H	H	H	H	H	H	H	H	H	C	C	C
rs6172481	6	H	H	H	H	H	H	H	H	H	H	H	H	H	H	H	H	H	H	H	H	C	C	C	C
rs3699833	6	H	H	H	H	H	H	H	H	H	H	H	H	H	H	H	H	H	H	H	H	C	C	C	C
rs3678711	6	H	H	H	H	H	H	H	H	H	H	H	H	H	H	H	H	H	H	H	H	C	C	C	C
rs13478641	6	H	H	H	H	H	H	H	H	H	H	H	H	H	H	H	H	H	H	H	H	C	C	C	C
rs3655269	6	H	H	H	H	H	H	H	H	H	H	H	H	H	H	H	H	H	H	H	H	C	C	C	C
rs13478656	6	H	H	H	H	H	H	H	H	H	C	C	C	C	C	C	H	H	C	H	H	C	C	C	C
rs3671709	6	H	H	H	H	H	H	H	H	H	C	C	C	C	C	C	C	C	C	H	H	C	C	C	C
rs13478677	6	H	H	H	H	H	H	H	H	H	C	C	C	C	C	C	C	C	C	H	H	C	C	C	C
gnf06.026.418	6	H	H	H	H	H	H	H	H	H	C	C	C	C	C	C	C	C	C	H	H	C	C	C	C
rs13478697	6	H	H	H	H	H	H	H	H	H	C	C	C	C	C	C	C	C	C	H	H	C	C	C	C
rs13478705	6	H	H	H	H	H	H	H	H	H	C	C	C	C	C	C	C	C	C	H	H	C	C	C	C
rs13478719	6	H	H	H	H	H	H	H	H	H	C	C	C	C	C	C	C	C	C	H	H	C	C	C	C
gnf06.037.785	6	H	H	H	H	H	H	H	H	H	C	C	C	C	C	C	C	C	C	H	H	C	C	C	C
rs13478727	6	C	H	H	H	H	C	H	H	C	C	C	C	C	C	C	C	C	C	C	C	C	C	C	C
rs13478745	6	C	H	H	H	H	C	H	H	C	C	C	C	C	C	C	C	C	C	C	C	C	C	C	C
rs13478761	6	C	H	H	H	H	C	H	H	C	C	C	C	C	C	C	C	C	C	C	C	C	C	C	C
CEL-6_57082524	6	C	H	H	H	H	C	C	H	C	C	C	C	C	C	C	C	C	C	C	C	C	C	C	C
rs13478780	6	C	H	H	H	C	C	C	C	C	C	C	C	C	C	C	C	C	C	C	C	C	C	C	C
rs13478783	6	C	H	H	H	C	C	C	C	C	C	C	C	C	C	C	C	C	C	C	C	C	C	C	C
rs6378343	6	C	H	H	H	C	C	C	C	C	C	C	C	C	C	C	C	C	C	C	C	C	C	C	C
rs13478801	6	C	H	H	H	C	C	C	C	C	C	C	C	C	C	C	C	C	C	C	C	C	C	C	C
mHcCD8b4	6	C	H	H	H	C	C	C	C	C	C	C	C	C	C	C	C	C	C	C	C	C	C	C	C
rs3672029	6	C	H	H	H	C	C	C	C	C	C	C	C	C	C	C	C	C	C	C	C	C	C	C	C
rs3699367	6	C	H	H	H	C	C	C	C	C	C	C	C	C	C	C	C	C	C	C	C	C	C	C	C
CEL-6_86289708	6	C	H	H	H	C	C	C	C	C	C	C	C	C	C	C	C	C	C	C	C	C	C	C	C
rs13478882	6	C	H	H	H	C	C	C	C	C	C	C	C	C	C	C	C	C	C	C	C	C	C	C	C
rs6285738	6	C	H	H	H	C	C	C	C	C	C	C	C	C	C	C	C	C	C	C	C	C	C	C	C
rs4138572	6	C	H	H	H	C	C	C	C	C	C	C	C	C	C	C	C	C	C	C	C	C	C	C	C
rs3718735	6	C	H	H	H	C	C	C	C	C	C	C	C	C	C	C	C	C	C	C	C	C	C	C	C
rs6208251	6	C	H	H	H	C	C	C	C	C	C	C	C	C	C	C	C	C	C	C	C	C	C	C	C
rs13478952	6	C	H	H	H	C	C	C	C	C	C	C	C	C	C	C	C	C	C	C	C	C	C	C	C
rs3670475	6	C	H	H	H	C	C	C	C	C	C	C	C	C	C	C	C	C	C	C	C	C	C	C	C
rs13478971	6	C	H	H	H	C	C	C	C	C	C	C	C	C	C	C	C	C	C	C	C	C	C	C	C
rs6401637	6	C	H	H	H	C	C	C	C	C	C	C	C	C	C	C	C	C	C	C	C	C	C	C	C
mCV23042866	6	C	H	H	H	C	C	C	C	C	C	C	C	C	C	C	C	C	C	C	C	C	C	C	C
rs3695724	6	C	H	H	H	C	C	C	C	C	C	C	C	C	C	C	C	C	C	C	C	C	C	C	C
rs13479006	6	C	H	H	H	C	C	C	C	C	C	C	C	C	C	C	C	C	C	C	C	C	C	C	C
gnf06.122.747	6	C	H	H	H	C	C	C	C	C	C	C	C	C	C	C	C	C	C	C	C	C	C	C	C
rs13479014	6	C	H	H	H	C	C	C	C	C	C	C	C	C	C	C	C	C	C	C	C	C	C	C	C
rs6389420	6	C	H	H	H	C	C	C	C	C	C	C	C	C	C	C	C	C	C	C	C	C	C	C	C
rs3681620	6	C	H	H	H	C	C	C	C	C	C	C	C	C	C	C	C	C	C	C	C	C	C	C	C
CEL-6_130920075	6	C	H	H	H	C	C	C	C	C	C	C	C	C	C	C	C	C	C	C	C	C	C	C	C
rs6339546	6	C	H	H	H	C	C	C	C	C	C	C	C	C	C	C	C	C	C	C	C	C	C	C	C
rs13479053	6	C	H	H	H	C	C	C	C	C	C	C	C	C	C	C	C	C	C	C	C	C	C	C	C
rs3023102	6	C	H	H	H	C	C	C	C	C	C	C	C	C	C	C	C	C	C	C	C	C	C	C	C
rs13479063	6	C	H	H	H	C	C	C	C	C	C	C	C	C	C	C	C	C	C	C	C	C	C	C	C
gnf06.149.306	6	H	C	C	C	H	C	C	C	C	C	C	C	C	C	C	C	C	C	C	C	C	C	C	C

Supplementary Figure 1 Real-time PCR for transcript levels of genes involved in EMT using whole kidney lysate from 6 homozygous mutants compared to 3 wild-type littermates at P0.

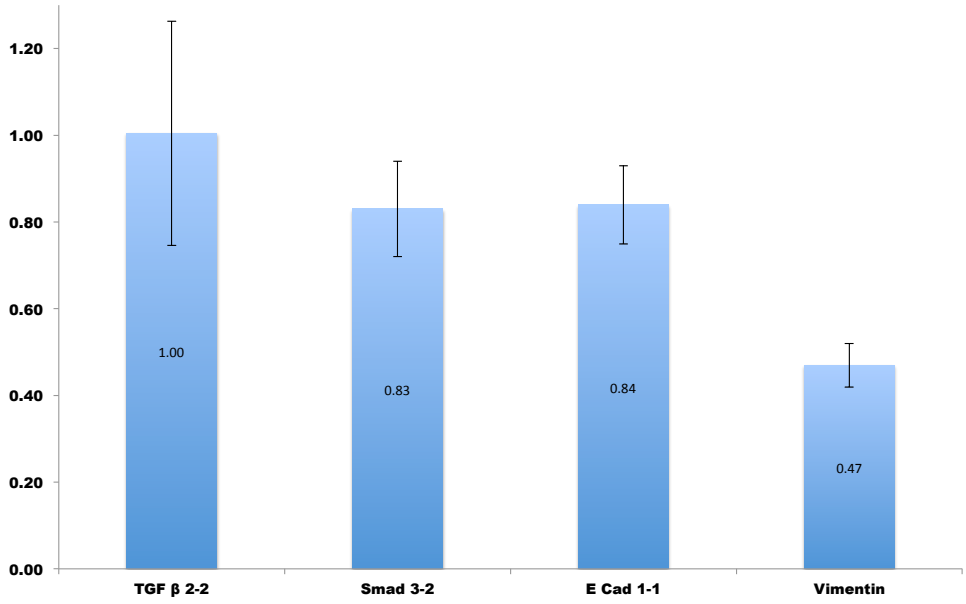

Supplementary Figure 2 Cysts are occasionally observed in the uterus of the heterozygous mutants. The black arrow points towards a cyst.

Supplementary Figure 3 Sequencing coverage within the critical region.

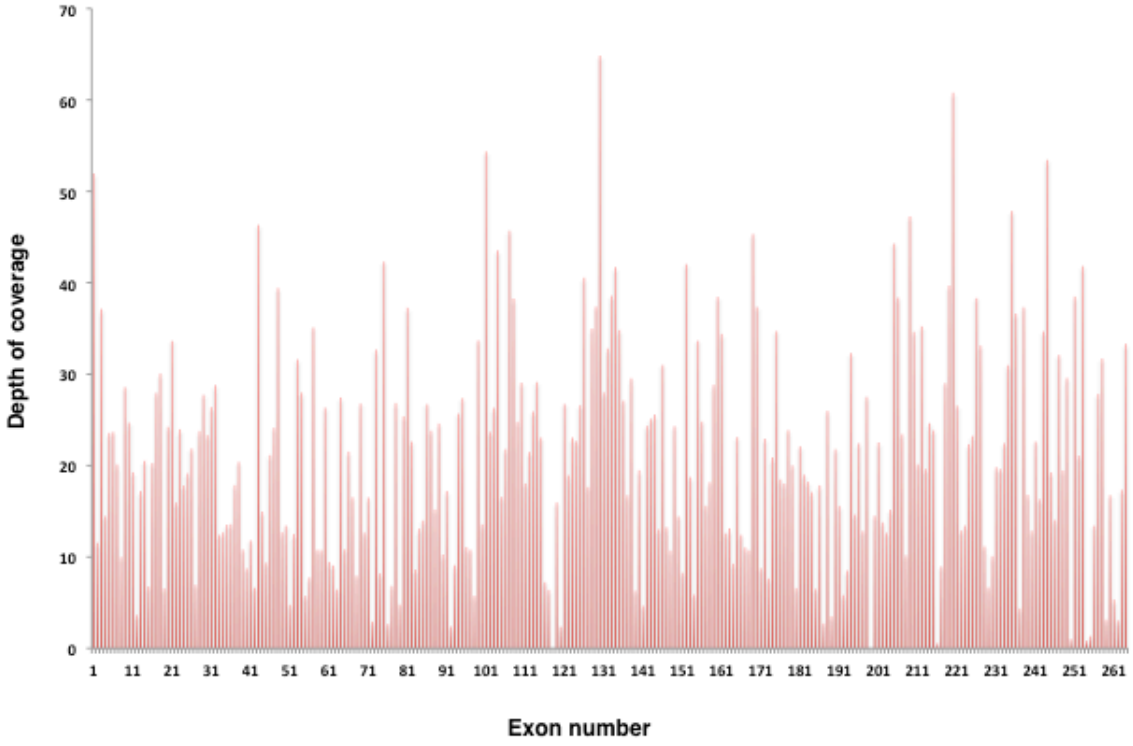

Supplementary Figure 4 Chromosome 6 has the highest LOD score in our linkage analysis. An 1449 Illumina SNP array platform was used for 21 mutant and 3 wild-type animals. Chromosome 6 contains the critical region for the cystic mutation. The logarithm of odds scores was performed under the condition of a single quantitative trait locus genome scan, normal model assumption, binary phenotype, and inclusion of covariates by expectation-maximization algorithm.

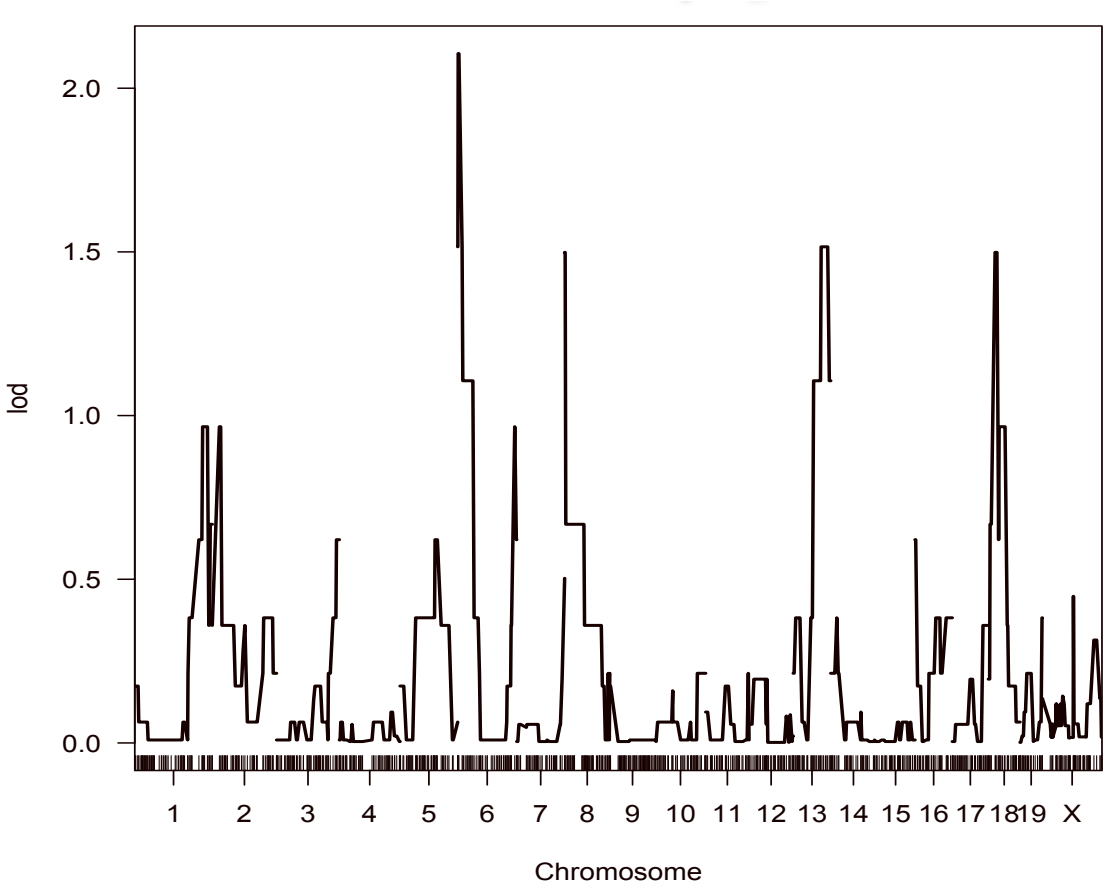

Supplementary Figure 5 Proposed mechanism by which Samd9l regulates p53. Wild-type Samd9l interacts with Stub1 and interferes with Stub1-mediated ubiquitinaton of p53. In contrast, mutation in Samd9l alters its interaction with Stub1 and promotes p53 ubiquitination and downstream proteasomal degradation.

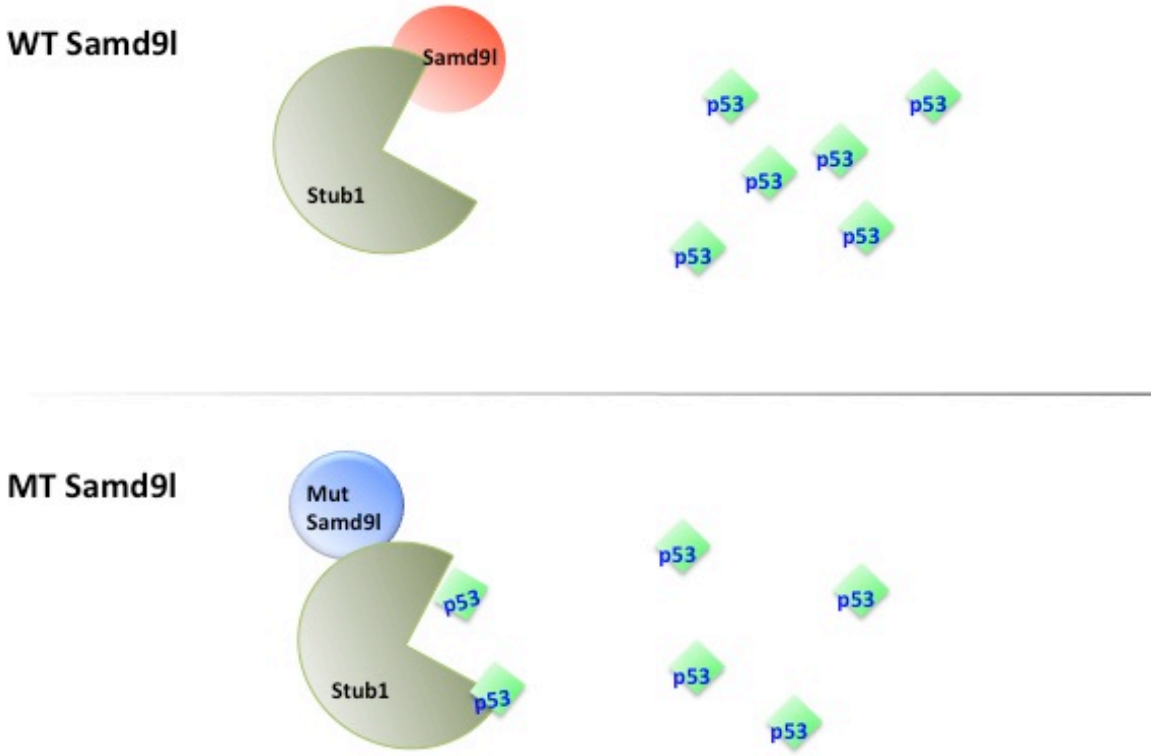

8 Reference

1. Harris PC, Torres VE. Polycystic kidney disease. Annu Rev Med. [Review]. 2009;60:321-37.
2. Pei Y. Diagnostic Approach in Autosomal Dominant Polycystic Kidney Disease. Clin J Am Soc Nephrol. 2006;1:1108-14.
3. Freedman BI, Soucie JM, Chapman A, Krisher J, McClellan WM. Racial variation in autosomal dominant polycystic kidney disease. American journal of kidney diseases : the official journal of the National Kidney Foundation. [Research Support, Non-U.S. Gov't
Research Support, U.S. Gov't, P.H.S.]. 2000 Jan;35(1):35-9.
4. United States Renal Data System. Excerpts from USRDS 2008 Annual Data Report. U.S. Department of Health and Human Services. The National Institutes of Health, National Institute of Diabetes and Digestive and Kidney Diseases. . Am J Kidney Dis. 2009;1(Suppl 1):S1.
5. Igarashi P, Somlo S. Genetics and pathogenesis of polycystic kidney disease. J Am Soc Nephrol. 2002;13(9):2384-98.
6. Torres V, Scheinman S. Genetic Diseases of the Kidney. NephSAP. 2004 January 2004;3(1):5.
7. Gresh L, Fischer E, Reimann A, Tanguy M, Garbay S, Shao X, et al. A transcriptional network in polycystic kidney disease. The EMBO journal. 2004 Apr 7;23(7):1657-68.
8. Hiesberger T, Bai Y, Shao X, McNally BT, Sinclair AM, Tian X, et al. Mutation of hepatocyte nuclear factor-1beta inhibits Pkhd1 gene expression and produces renal cysts in mice. J Clin Invest. [Research Support, Non-U.S. Gov't
Research Support, U.S. Gov't, P.H.S.]. 2004 Mar;113(6):814-25.
9. Haumaitre C, Fabre M, Cormier S, Baumann C, Delezoide AL, Cereghini S. Severe pancreas hypoplasia and multicystic renal dysplasia in two human fetuses carrying novel HNF1beta/MODY5 mutations. Human molecular genetics. [Case Reports
Research Support, Non-U.S. Gov't]. 2006 Aug 1;15(15):2363-75.
10. Iglesias CG, Torres VE, Offord KP, Holley KE, Beard CM, Kurland LT. Epidemiology of adult polycystic kidney disease, Olmsted County, Minnesota: 1935-1980. American journal of kidney diseases : the official journal of the National Kidney Foundation. [Research Support, U.S. Gov't, P.H.S.]. 1983 May;2(6):630-9.
11. Torres VE HK, Offord KP General features of autosomal dominant polycystic kidney disease. J Grantham KGE, editor. Kansas City 1985.
12. Davies F, Coles GA, Harper PS, Williams AJ, Evans C, Cochlin D. Polycystic kidney disease re-evaluated: a population-based study. Q J Med. 1991 Jun;79(290):477-85.
13. Parfrey PS, Bear JC, Morgan J, Cramer BC, McManamon PJ, Gault MH, et al. The diagnosis and prognosis of autosomal dominant polycystic kidney disease. The New England journal of medicine. [Comparative Study
Research Support, Non-U.S. Gov't]. 1990 Oct 18;323(16):1085-90.
14. Gabow PA, Johnson AM, Kaehny WD, Kimberling WJ, Lezotte DC, Duley IT, et al. Factors affecting the progression of renal disease in autosomal-dominant polycystic

kidney disease. Kidney Int. [Research Support, U.S. Gov't, P.H.S.]. 1992 May;41(5):1311-9.
15. Torres VE, Harris PC, Pirson Y. Autosomal dominant polycystic kidney disease. Lancet. [Review]. 2007 Apr 14;369(9569):1287-301.
16. Stengel B, Billon S, Van Dijk PC, Jager KJ, Dekker FW, Simpson K, et al. Trends in the incidence of renal replacement therapy for end-stage renal disease in Europe, 1990-1999. Nephrology, dialysis, transplantation : official publication of the European Dialysis and Transplant Association - European Renal Association. [Research Support, Non-U.S. Gov't]. 2003 Sep;18(9):1824-33.
17. Wakai K, Nakai S, Kikuchi K, Iseki K, Miwa N, Masakane I, et al. Trends in incidence of end-stage renal disease in Japan, 1983-2000: age-adjusted and age-specific rates by gender and cause. Nephrology, dialysis, transplantation : official publication of the European Dialysis and Transplant Association - European Renal Association. 2004 Aug;19(8):2044-52.
18. Hughes J, Ward CJ, Peral B, Aspinwall R, Clark K, San Millan JL, et al. The polycystic kidney disease 1 (PKD1) gene encodes a novel protein with multiple cell recognition domains. Nature genetics. [Comparative Study
Research Support, Non-U.S. Gov't]. 1995 Jun;10(2):151-60.
19. Ponting CP, Hofmann K, Bork P. A latrophilin/CL-1-like GPS domain in polycystin-1. Current biology : CB. [Letter]. 1999 Aug 26;9(16):R585-8.
20. Sandford R, Sgotto B, Aparicio S, Brenner S, Vaudin M, Wilson RK, et al. Comparative analysis of the polycystic kidney disease 1 (PKD1) gene reveals an integral membrane glycoprotein with multiple evolutionary conserved domains. Human molecular genetics. [Comparative Study
Research Support, Non-U.S. Gov't]. 1997 Sep;6(9):1483-9.
21. Calvet JP. Ciliary signaling goes down the tubes. Nature genetics. [Comment News]. 2003 Feb;33(2):113-4.
22. Ong AC, Harris PC. Molecular pathogenesis of ADPKD: the polycystin complex gets complex. Kidney Int. [Research Support, Non-U.S. Gov't]. 2005 Apr;67(4):1234-47.
23. Hanaoka K, Qian F, Boletta A, Bhunia AK, Piontek K, Tsiokas L, et al. Co-assembly of polycystin-1 and -2 produces unique cation-permeable currents. Nature. [Research Support, Non-U.S. Gov't
Research Support, U.S. Gov't, P.H.S.]. 2000 Dec 21-28;408(6815):990-4.
24. Torres VE, Wang X, Qian Q, Somlo S, Harris PC, Gattone VH, 2nd. Effective treatment of an orthologous model of autosomal dominant polycystic kidney disease. Nature Medicine. [Research Support, Non-U.S. Gov't
Research Support, U.S. Gov't, P.H.S.]. 2004 Apr;10(4):363-4.
25. Gonzalez-Perrett S, Kim K, Ibarra C, Damiano AE, Zotta E, Batelli M, et al. Polycystin-2, the protein mutated in autosomal dominant polycystic kidney disease (ADPKD), is a Ca2+-permeable nonselective cation channel. Proceedings of the National Academy of Sciences of the United States of America. [Research Support, Non-U.S. Gov't]. 2001 Jan 30;98(3):1182-7.
26. Yoder BK, Hou X, Guay-Woodford LM. The polycystic kidney disease proteins, polycystin-1, polycystin-2, polaris, and cystin, are co-localized in renal cilia. Journal of the American Society of Nephrology : JASN. 2002 Oct;13(10):2508-16.
27. Pazour GJ, San Agustin JT, Follit JA, Rosenbaum JL, Witman GB. Polycystin-2 localizes to kidney cilia and the ciliary level is elevated in orpk mice with polycystic kidney disease. Current biology : CB. [Letter

Research Support, Non-U.S. Gov't
Research Support, U.S. Gov't, P.H.S.]. 2002 Jun 4;12(11):R378-80.
28. Rossetti S, Consugar MB, Chapman AB, Torres VE, Guay-Woodford LM, Grantham JJ, et al. Comprehensive molecular diagnostics in autosomal dominant polycystic kidney disease. Journal of the American Society of Nephrology : JASN. [Research Support, N.I.H., Extramural]. 2007 Jul;18(7):2143-60.
29. Hateboer N, v Dijk MA, Bogdanova N, Coto E, Saggar-Malik AK, San Millan JL, et al. Comparison of phenotypes of polycystic kidney disease types 1 and 2. European PKD1-PKD2 Study Group. Lancet. [Research Support, Non-U.S. Gov't]. 1999 Jan 9;353(9147):103-7.
30. Harris PC, Bae KT, Rossetti S, Torres VE, Grantham JJ, Chapman AB, et al. Cyst number but not the rate of cystic growth is associated with the mutated gene in autosomal dominant polycystic kidney disease. Journal of the American Society of Nephrology : JASN. [Research Support, N.I.H., Extramural
Research Support, Non-U.S. Gov't]. 2006 Nov;17(11):3013-9.
31. Torres VE, Harris PC. Autosomal dominant polycystic kidney disease: the last 3 years. Kidney Int. [Review]. 2009 Jul;76(2):149-68.
32. Rossetti S, Chauveau D, Kubly V, Slezak JM, Saggar-Malik AK, Pei Y, et al. Association of mutation position in polycystic kidney disease 1 (PKD1) gene and development of a vascular phenotype. Lancet. [Multicenter Study
Research Support, Non-U.S. Gov't
Research Support, U.S. Gov't, P.H.S.]. 2003 Jun 28;361(9376):2196-201.
33. Adeva M, El-Youssef M, Rossetti S, Kamath PS, Kubly V, Consugar MB, et al. Clinical and molecular characterization defines a broadened spectrum of autosomal recessive polycystic kidney disease (ARPKD). Medicine (Baltimore). [Research Support, N.I.H., Extramural]. 2006 Jan;85(1):1-21.
34. Richards WG, Sweeney WE, Yoder BK, Wilkinson JE, Woychik RP, Avner ED. Epidermal growth factor receptor activity mediates renal cyst formation in polycystic kidney disease. J Clin Invest. [Research Support, U.S. Gov't, P.H.S.]. 1998 Mar 1;101(5):935-9.
35. Pei Y, Watnick T, He N, Wang K, Liang Y, Parfrey P, et al. Somatic PKD2 mutations in individual kidney and liver cysts support a "two-hit" model of cystogenesis in type 2 autosomal dominant polycystic kidney disease. Journal of the American Society of Nephrology : JASN. [Research Support, Non-U.S. Gov't
Research Support, U.S. Gov't, P.H.S.]. 1999 Jul;10(7):1524-9.
36. Qian F, Watnick TJ, Onuchic LF, Germino GG. The molecular basis of focal cyst formation in human autosomal dominant polycystic kidney disease type I. Cell. [Research Support, Non-U.S. Gov't
Research Support, U.S. Gov't, P.H.S.]. 1996 Dec 13;87(6):979-87.
37. Lu W, Peissel B, Babakhanlou H, Pavlova A, Geng L, Fan X, et al. Perinatal lethality with kidney and pancreas defects in mice with a targetted Pkd1 mutation. Nature genetics. [Research Support, Non-U.S. Gov't
Research Support, U.S. Gov't, P.H.S.]. 1997 Oct;17(2):179-81.
38. Lu W, Fan X, Basora N, Babakhanlou H, Law T, Rifai N, et al. Late onset of renal and hepatic cysts in Pkd1-targeted heterozygotes. Nature genetics. [Letter
Research Support, Non-U.S. Gov't
Research Support, U.S. Gov't, P.H.S.]. 1999 Feb;21(2):160-1.
39. Watnick TJ, Torres VE, Gandolph MA, Qian F, Onuchic LF, Klinger KW, et al. Somatic mutation in individual liver cysts supports a two-hit model of cystogenesis in

autosomal dominant polycystic kidney disease. Mol Cell. [Research Support, Non-U.S. Gov't
Research Support, U.S. Gov't, P.H.S.]. 1998 Aug;2(2):247-51.
40. Lantinga-van Leeuwen IS, Dauwerse JG, Baelde HJ, Leonhard WN, van de Wal A, Ward CJ, et al. Lowering of Pkd1 expression is sufficient to cause polycystic kidney disease. Human molecular genetics. [Research Support, Non-U.S. Gov't]. 2004 Dec 15;13(24):3069-77.
41. Boletta A. Emerging evidence of a link between the polycystins and the mTOR pathways. Pathogenetics. 2009;2(1):6.
42. Roos A. Polycystic Kidney: report of a case studied by reconstruction. Am J Dis Child. 1941 1941;61:116-27.
43. Bialestock D. Anaemia of renal origin, studied by micro-dissection of the kidney. Australas Ann Med. 1960 Feb;9:44-52.
44. Baxter TJ. Cysts arising in the renal corpuscle. A microdissection study. Arch Dis Child. 1965 Oct;40(213):455-63.
45. Taxy JB, Filmer RB. Glomerulocystic kidney. Report of a case. Arch Pathol Lab Med. [Case Reports]. 1976 Apr;100(4):186-8.
46. Dedeoglu IO, Fisher JE, Springate JE, Waz WR, Stapleton FB, Feld LG. Spectrum of glomerulocystic kidneys: a case report and review of the literature. Pediatr Pathol Lab Med. 1996 Nov-Dec;16(6):941-9.
47. Sharp CK, Bergman SM, Stockwin JM, Robbin ML, Galliani C, Guay-Woodford LM. Dominantly transmitted glomerulocystic kidney disease: a distinct genetic entity. J Am Soc Nephrol. 1997 Jan;8(1):77-84.
48. Bernstein J. Glomerulocystic kidney disease--nosological considerations. Pediatr Nephrol. 1993 Aug;7(4):464-70.
49. Gupta K, Vankalakunti M, Sachdeva MU. Glomerulocystic kidney disease and its rare associations: an autopsy report of two unrelated cases. Diagn Pathol. 2007;2:12.
50. Bernstein J. Renal cystic disease in the tuberous sclerosis complex. Pediatric nephrology. [Review]. 1993 Aug;7(4):490-5.
51. Bergmann C, Fliegauf M, Bruchle NO, Frank V, Olbrich H, Kirschner J, et al. Loss of nephrocystin-3 function can cause embryonic lethality, Meckel-Gruber-like syndrome, situs inversus, and renal-hepatic-pancreatic dysplasia. Am J Hum Genet. 2008 Apr;82(4):959-70.
52. Feather SA, Winyard PJ, Dodd S, Woolf AS. Oral-facial-digital syndrome type 1 is another dominant polycystic kidney disease: clinical, radiological and histopathological features of a new kindred. Nephrology, dialysis, transplantation : official publication of the European Dialysis and Transplant Association - European Renal Association. [Research Support, Non-U.S. Gov't]. 1997 Jul;12(7):1354-61.
53. Langer LO, Jr., Nishino R, Yamaguchi A, Ito Y, Ueke T, Togari H, et al. Brachymesomelia-renal syndrome. Am J Med Genet. [Case Reports]. 1983 May;15(1):57-65.
54. Montemarano H, Bulas DI, Chandra R, Tifft C. Prenatal diagnosis of glomerulocystic kidney disease in short-rib polydactyly syndrome type II, Majewski type. Pediatr Radiol. [Case Reports]. 1995;25(6):469-71.
55. Kelley RI, Datta NS, Dobyns WB, Hajra AK, Moser AB, Noetzel MJ, et al. Neonatal adrenoleukodystrophy: new cases, biochemical studies, and differentiation from Zellweger and related peroxisomal polydystrophy syndromes. Am J Med Genet. [Case Reports

Comparative Study
Research Support, Non-U.S. Gov't
Research Support, U.S. Gov't, P.H.S.
Review]. 1986 Apr;23(4):869-901.
56. Tory K, Rousset-Rouviere C, Gubler MC, Moriniere V, Pawtowski A, Becker C, et al. Mutations of NPHP2 and NPHP3 in infantile nephronophthisis. Kidney Int. [Research Support, Non-U.S. Gov't]. 2009 Apr;75(8):839-47.
57. Benetti E, Caridi G, Vella MD, Rampoldi L, Ghiggeri GM, Artifoni L, et al. Immature renal structures associated with a novel UMOD sequence variant. American journal of kidney diseases : the official journal of the National Kidney Foundation. [Case Reports]. 2009 Feb;53(2):327-31.
58. Blacque OE, Leroux MR. Bardet-Biedl syndrome: an emerging pathomechanism of intracellular transport. Cell Mol Life Sci. [Research Support, Non-U.S. Gov't Review]. 2006 Sep;63(18):2145-61.
59. Edghill EL, Bingham C, Slingerland AS, Minton JA, Noordam C, Ellard S, et al. Hepatocyte nuclear factor-1 beta mutations cause neonatal diabetes and intrauterine growth retardation: support for a critical role of HNF-1beta in human pancreatic development. Diabet Med. [Research Support, Non-U.S. Gov't]. 2006 Dec;23(12):1301-6.
60. Siroky BJ, Czyzyk-Krzeska MF, Bissler JJ. Renal involvement in tuberous sclerosis complex and von Hippel-Lindau disease: shared disease mechanisms? Nat Clin Pract Nephrol. 2009 Mar;5(3):143-56.
61. Scolari F, Caridi G, Rampoldi L, Tardanico R, Izzi C, Pirulli D, et al. Uromodulin storage diseases: clinical aspects and mechanisms. American journal of kidney diseases : the official journal of the National Kidney Foundation. [Research Support, Non-U.S. Gov't
Review]. 2004 Dec;44(6):987-99.
62. Lens XM, Banet JF, Outeda P, Barrio-Lucia V. A novel pattern of mutation in uromodulin disorders: autosomal dominant medullary cystic kidney disease type 2, familial juvenile hyperuricemic nephropathy, and autosomal dominant glomerulocystic kidney disease. American journal of kidney diseases : the official journal of the National Kidney Foundation. [Comparative Study
Research Support, Non-U.S. Gov't]. 2005 Jul;46(1):52-7.
63. Hoyer JR, Sisson SP, Vernier RL. Tamm-Horsfall glycoprotein: ultrastructural immunoperoxidase localization in rat kidney. Lab Invest. [Research Support, U.S. Gov't, P.H.S.]. 1979 Aug;41(2):168-73.
64. Choi SW, Ryu OH, Choi SJ, Song IS, Bleyer AJ, Hart TC. Mutant tamm-horsfall glycoprotein accumulation in endoplasmic reticulum induces apoptosis reversed by colchicine and sodium 4-phenylbutyrate. Journal of the American Society of Nephrology : JASN. [Research Support, N.I.H., Extramural
Research Support, U.S. Gov't, P.H.S.]. 2005 Oct;16(10):3006-14.
65. Rampoldi L, Caridi G, Santon D, Boaretto F, Bernascone I, Lamorte G, et al. Allelism of MCKD, FJHN and GCKD caused by impairment of uromodulin export dynamics. Human molecular genetics. [Research Support, Non-U.S. Gov't]. 2003 Dec 15;12(24):3369-84.
66. Bleyer AJ, Hart TC, Willingham MC, Iskandar SS, Gorry MC, Trachtman H. Clinico-pathologic findings in medullary cystic kidney disease type 2. Pediatric nephrology. [Case Reports
Research Support, N.I.H., Extramural

Research Support, U.S. Gov't, P.H.S.]. 2005 Jun;20(6):824-7.
67. Rezende-Lima W, Parreira KS, Garcia-Gonzalez M, Riveira E, Banet JF, Lens XM. Homozygosity for uromodulin disorders: FJHN and MCKD-type 2. Kidney Int. 2004 Aug;66(2):558-63.
68. Wolf MT, Hildebrandt F. Nephronophthisis. Pediatric nephrology. [Research Support, N.I.H., Extramural
Research Support, Non-U.S. Gov't
Review]. 2011 Feb;26(2):181-94.
69. Hildebrandt F, Attanasio M, Otto E. Nephronophthisis: disease mechanisms of a ciliopathy. Journal of the American Society of Nephrology : JASN. [Research Support, N.I.H., Extramural
Research Support, Non-U.S. Gov't
Review]. 2009 Jan;20(1):23-35.
70. Takahashi H, Calvet JP, Dittemore-Hoover D, Yoshida K, Grantham JJ, Gattone VH, 2nd. A hereditary model of slowly progressive polycystic kidney disease in the mouse. Journal of the American Society of Nephrology : JASN. [Research Support, Non-U.S. Gov't
Research Support, U.S. Gov't, P.H.S.]. 1991 Jan;1(7):980-9.
71. Moyer JH, Lee-Tischler MJ, Kwon HY, Schrick JJ, Avner ED, Sweeney WE, et al. Candidate gene associated with a mutation causing recessive polycystic kidney disease in mice. Science. [Research Support, U.S. Gov't, Non-P.H.S.
Research Support, U.S. Gov't, P.H.S.]. 1994 May 27;264(5163):1329-33.
72. Ferrante MI, Zullo A, Barra A, Bimonte S, Messaddeq N, Studer M, et al. Oral-facial-digital type I protein is required for primary cilia formation and left-right axis specification. Nature genetics. [Research Support, Non-U.S. Gov't]. 2006 Jan;38(1):112-7.
73. Ross AJ, May-Simera H, Eichers ER, Kai M, Hill J, Jagger DJ, et al. Disruption of Bardet-Biedl syndrome ciliary proteins perturbs planar cell polarity in vertebrates. Nature genetics. [Research Support, N.I.H., Extramural
Research Support, Non-U.S. Gov't
Research Support, U.S. Gov't, P.H.S.]. 2005 Oct;37(10):1135-40.
74. Yen HJ, Tayeh MK, Mullins RF, Stone EM, Sheffield VC, Slusarski DC. Bardet-Biedl syndrome genes are important in retrograde intracellular trafficking and Kupffer's vesicle cilia function. Human molecular genetics. [Research Support, N.I.H., Extramural
Research Support, Non-U.S. Gov't]. 2006 Mar 1;15(5):667-77.
75. Ansley SJ, Badano JL, Blacque OE, Hill J, Hoskins BE, Leitch CC, et al. Basal body dysfunction is a likely cause of pleiotropic Bardet-Biedl syndrome. Nature. [Research Support, Non-U.S. Gov't]. 2003 Oct 9;425(6958):628-33.
76. Flaherty L, Bryda EC, Collins D, Rudofsky U, Montogomery JC. New mouse model for polycystic kidney disease with both recessive and dominant gene effects. Kidney Int. 1995 Feb;47(2):552-8.
77. Birkenmeier E, P J. Role of modifier genes in PKD. Kidney International. 1994;47:715-32.
78. Watnick T, Germino G. From cilia to cyst. Nature genetics. [Comment News]. 2003 Aug;34(4):355-6.
79. Ward CJ, Hogan MC, Rossetti S, Walker D, Sneddon T, Wang X, et al. The gene mutated in autosomal recessive polycystic kidney disease encodes a large, receptor-like protein. Nature genetics. [Research Support, Non-U.S. Gov't

Research Support, U.S. Gov't, P.H.S.]. 2002 Mar;30(3):259-69.
80. Onuchic LF, Furu L, Nagasawa Y, Hou X, Eggermann T, Ren Z, et al. PKHD1, the polycystic kidney and hepatic disease 1 gene, encodes a novel large protein containing multiple immunoglobulin-like plexin-transcription-factor domains and parallel beta-helix 1 repeats. American journal of human genetics. [Research Support, Non-U.S. Gov't
Research Support, U.S. Gov't, P.H.S.]. 2002 May;70(5):1305-17.
81. Beales PL, Bland E, Tobin JL, Bacchelli C, Tuysuz B, Hill J, et al. IFT80, which encodes a conserved intraflagellar transport protein, is mutated in Jeune asphyxiating thoracic dystrophy. Nature genetics. [Comparative Study
Research Support, N.I.H., Extramural
Research Support, Non-U.S. Gov't]. 2007 Jun;39(6):727-9.
82. Romio L, Wright V, Price K, Winyard PJ, Donnai D, Porteous ME, et al. OFD1, the gene mutated in oral-facial-digital syndrome type 1, is expressed in the metanephros and in human embryonic renal mesenchymal cells. Journal of the American Society of Nephrology : JASN. [Research Support, Non-U.S. Gov't]. 2003 Mar;14(3):680-9.
83. Khaddour R, Smith U, Baala L, Martinovic J, Clavering D, Shaffiq R, et al. Spectrum of MKS1 and MKS3 mutations in Meckel syndrome: a genotype-phenotype correlation. Mutation in brief #960. Online. Hum Mutat. 2007 May;28(5):523-4.
84. DiBella LM, Park A, Sun Z. Zebrafish Tsc1 reveals functional interactions between the cilium and the TOR pathway. Human molecular genetics. [Research Support, N.I.H., Extramural
Research Support, Non-U.S. Gov't
Research Support, U.S. Gov't, Non-P.H.S.]. 2009 Feb 15;18(4):595-606.
85. Abd-El-Barr MM, Sykoudis K, Andrabi S, Eichers ER, Pennesi ME, Tan PL, et al. Impaired photoreceptor protein transport and synaptic transmission in a mouse model of Bardet-Biedl syndrome. Vision Res. [Research Support, N.I.H., Extramural Research Support, Non-U.S. Gov't]. 2007 Dec;47(27):3394-407.
86. Pazour GJ, Dickert BL, Vucica Y, Seeley ES, Rosenbaum JL, Witman GB, et al. Chlamydomonas IFT88 and its mouse homologue, polycystic kidney disease gene tg737, are required for assembly of cilia and flagella. The Journal of cell biology. [Research Support, Non-U.S. Gov't
Research Support, U.S. Gov't, P.H.S.]. 2000 Oct 30;151(3):709-18.
87. Shao X, Johnson JE, Richardson JA, Hiesberger T, Igarashi P. A minimal Ksp-cadherin promoter linked to a green fluorescent protein reporter gene exhibits tissue-specific expression in the developing kidney and genitourinary tract. Journal of the American Society of Nephrology : JASN. [Research Support, Non-U.S. Gov't
Research Support, U.S. Gov't, P.H.S.]. 2002 Jul;13(7):1824-36.
88. Lin F, Hiesberger T, Cordes K, Sinclair AM, Goldstein LS, Somlo S, et al. Kidney-specific inactivation of the KIF3A subunit of kinesin-II inhibits renal ciliogenesis and produces polycystic kidney disease. Proceedings of the National Academy of Sciences of the United States of America. [Research Support, U.S. Gov't, P.H.S.]. 2003 Apr 29;100(9):5286-91.
89. Hossain Z, Ali SM, Ko HL, Xu J, Ng CP, Guo K, et al. Glomerulocystic kidney disease in mice with a targeted inactivation of Wwtr1. Proceedings of the National Academy of Sciences of the United States of America. [Research Support, Non-U.S. Gov't]. 2007 Jan 30;104(5):1631-6.

90. Kang HS, Beak JY, Kim YS, Herbert R, Jetten AM. Glis3 is associated with primary cilia and Wwtr1/TAZ and implicated in polycystic kidney disease. Molecular and cellular biology. [Research Support, N.I.H., Intramural]. 2009 May;29(10):2556-69.
91. Pritchard L, Sloane-Stanley JA, Sharpe JA, Aspinwall R, Lu W, Buckle V, et al. A human PKD1 transgene generates functional polycystin-1 in mice and is associated with a cystic phenotype. Human molecular genetics. [Research Support, Non-U.S. Gov't]. 2000 Nov 1;9(18):2617-27.
92. Wheatley DN. Primary cilia in normal and pathological tissues. Pathobiology. [Research Support, Non-U.S. Gov't
Review]. 1995;63(4):222-38.
93. Berbari NF, O'Connor AK, Haycraft CJ, Yoder BK. The primary cilium as a complex signaling center. Current biology : CB. [Research Support, N.I.H., Extramural Review]. 2009 Jul 14;19(13):R526-35.
94. Reinsch S, Karsenti E. Orientation of spindle axis and distribution of plasma membrane proteins during cell division in polarized MDCKII cells. The Journal of cell biology. [Research Support, Non-U.S. Gov't
Research Support, U.S. Gov't, P.H.S.]. 1994 Sep;126(6):1509-26.
95. Rosenbaum JL, Witman GB. Intraflagellar transport. Nat Rev Mol Cell Biol. [Research Support, Non-U.S. Gov't
Research Support, U.S. Gov't, P.H.S.
Review]. 2002 Nov;3(11):813-25.
96. Scholey JM. Intraflagellar transport motors in cilia: moving along the cell's antenna. The Journal of cell biology. [Research Support, N.I.H., Extramural Review]. 2008 Jan 14;180(1):23-9.
97. Flood PR, Totland GK. Substructure of solitary cilia in mouse kidney. Cell Tissue Res. 1977 Sep 26;183(2):281-90.
98. Pfaller W, Klima J. A critical reevaluation of the structure of the rat uriniferous tubule as revealed by scanning electron microscopy. Cell Tissue Res. 1976 Feb 6;166(1):91-100.
99. Veland IR, Awan A, Pedersen LB, Yoder BK, Christensen ST. Primary cilia and signaling pathways in mammalian development, health and disease. Nephron Physiol. [Research Support, N.I.H., Extramural
Research Support, Non-U.S. Gov't
Review]. 2009;111(3):p39-53.
100. Bernstein J, and Gilbert-Barness,E. Congenital malformation of the kidney. Brenner B, editor. Philadelphia, Pennsylvania, USA.: J.B. Lippincott Co.; 1994.
101. Lubarsky B, Krasnow MA. Tube morphogenesis: making and shaping biological tubes. Cell. [Research Support, Non-U.S. Gov't
Research Support, U.S. Gov't, Non-P.H.S.
Review]. 2003 Jan 10;112(1):19-28.
102. Nauli SM, Alenghat FJ, Luo Y, Williams E, Vassilev P, Li X, et al. Polycystins 1 and 2 mediate mechanosensation in the primary cilium of kidney cells. Nature genetics. [Comparative Study
Research Support, Non-U.S. Gov't
Research Support, U.S. Gov't, Non-P.H.S.
Research Support, U.S. Gov't, P.H.S.]. 2003 Feb;33(2):129-37.
103. Praetorius HA, Spring KR. Bending the MDCK cell primary cilium increases intracellular calcium. J Membr Biol. 2001 Nov 1;184(1):71-9.

104. Davenport JR, Watts AJ, Roper VC, Croyle MJ, van Groen T, Wyss JM, et al. Disruption of intraflagellar transport in adult mice leads to obesity and slow-onset cystic kidney disease. Current biology : CB. [Research Support, N.I.H., Extramural Research Support, Non-U.S. Gov't]. 2007 Sep 18;17(18):1586-94.
105. Piontek K, Menezes LF, Garcia-Gonzalez MA, Huso DL, Germino GG. A critical developmental switch defines the kinetics of kidney cyst formation after loss of Pkd1. Nature Medicine. [Research Support, N.I.H., Extramural Research Support, Non-U.S. Gov't]. 2007 Dec;13(12):1490-5.
106. Fischer E, Legue E, Doyen A, Nato F, Nicolas JF, Torres V, et al. Defective planar cell polarity in polycystic kidney disease. Nature genetics. [Research Support, Non-U.S. Gov't]. 2006 Jan;38(1):21-3.
107. Hildebrandt F, Benzing T, Katsanis N. Ciliopathies. The New England journal of medicine. [Research Support, Non-U.S. Gov't Review]. 2011 Apr 21;364(16):1533-43.
108. Essner JJ, Vogan KJ, Wagner MK, Tabin CJ, Yost HJ, Brueckner M. Conserved function for embryonic nodal cilia. Nature. 2002 Jul 4;418(6893):37-8.
109. Strutt D. Organ shape: controlling oriented cell division. Current biology : CB. [Comment Review]. 2005 Sep 20;15(18):R758-9.
110. Baena-Lopez LA, Baonza A, Garcia-Bellido A. The orientation of cell divisions determines the shape of Drosophila organs. Current biology : CB. [Comparative Study Research Support, Non-U.S. Gov't]. 2005 Sep 20;15(18):1640-4.
111. Klein TJ, Mlodzik M. Planar cell polarization: an emerging model points in the right direction. Annu Rev Cell Dev Biol. [Research Support, N.I.H., Extramural Review]. 2005;21:155-76.
112. McNeill H. Planar cell polarity: keeping hairs straight is not so simple. Cold Spring Harb Perspect Biol. [Review]. 2010 Feb;2(2):a003376.
113. Vladar EK, Antic D, Axelrod JD. Planar cell polarity signaling: the developing cell's compass. Cold Spring Harb Perspect Biol. [Research Support, N.I.H., Extramural Review]. 2009 Sep;1(3):a002964.
114. Boutros M, Mlodzik M. Dishevelled: at the crossroads of divergent intracellular signaling pathways. Mech Dev. [Review]. 1999 May;83(1-2):27-37.
115. Yamanaka H, Moriguchi T, Masuyama N, Kusakabe M, Hanafusa H, Takada R, et al. JNK functions in the non-canonical Wnt pathway to regulate convergent extension movements in vertebrates. EMBO Rep. [Research Support, Non-U.S. Gov't]. 2002 Jan;3(1):69-75.
116. Benzing T, Simons M, Walz G. Wnt signaling in polycystic kidney disease. Journal of the American Society of Nephrology : JASN. [Review]. 2007 May;18(5):1389-98.
117. Murdoch JN, Henderson DJ, Doudney K, Gaston-Massuet C, Phillips HM, Paternotte C, et al. Disruption of scribble (Scrb1) causes severe neural tube defects in the circletail mouse. Human molecular genetics. [Research Support, Non-U.S. Gov't]. 2003 Jan 15;12(2):87-98.
118. Montcouquiol M, Sans N, Huss D, Kach J, Dickman JD, Forge A, et al. Asymmetric localization of Vangl2 and Fz3 indicate novel mechanisms for planar cell polarity in mammals. J Neurosci. [Research Support, N.I.H., Extramural Research Support, N.I.H., Intramural Research Support, Non-U.S. Gov't]. 2006 May 10;26(19):5265-75.

119. Bacallao R, Antony C, Dotti C, Karsenti E, Stelzer EH, Simons K. The subcellular organization of Madin-Darby canine kidney cells during the formation of a polarized epithelium. The Journal of cell biology. [Research Support, Non-U.S. Gov't Research Support, U.S. Gov't, P.H.S.]. 1989 Dec;109(6 Pt 1):2817-32.
120. Suzuki A, Ohno S. The PAR-aPKC system: lessons in polarity. J Cell Sci. [Review]. 2006 Mar 15;119(Pt 6):979-87.
121. Fukata M, Nakagawa M, Kaibuchi K. Roles of Rho-family GTPases in cell polarisation and directional migration. Curr Opin Cell Biol. [Research Support, Non-U.S. Gov't
Review]. 2003 Oct;15(5):590-7.
122. Jaffe AB, Hall A. Rho GTPases: biochemistry and biology. Annu Rev Cell Dev Biol. [Research Support, Non-U.S. Gov't
Review]. 2005;21:247-69.
123. Fan S, Hurd TW, Liu CJ, Straight SW, Weimbs T, Hurd EA, et al. Polarity proteins control ciliogenesis via kinesin motor interactions. Current biology : CB. [Comparative Study
Research Support, Non-U.S. Gov't]. 2004 Aug 24;14(16):1451-61.
124. Schluter MA, Margolis B. Apicobasal polarity in the kidney. Exp Cell Res. [Research Support, N.I.H., Extramural
Research Support, Non-U.S. Gov't
Review]. 2012 May 15;318(9):1033-9.
125. Roh MH, Margolis B. Composition and function of PDZ protein complexes during cell polarization. American journal of physiology Renal physiology. [Research Support, U.S. Gov't, P.H.S.
Review]. 2003 Sep;285(3):F377-87.
126. Karner C, Wharton KA, Carroll TJ. Apical-basal polarity, Wnt signaling and vertebrate organogenesis. Semin Cell Dev Biol. [Review]. 2006 Apr;17(2):214-22.
127. Schermer B, Ghenoiu C, Bartram M, Muller RU, Kotsis F, Hohne M, et al. The von Hippel-Lindau tumor suppressor protein controls ciliogenesis by orienting microtubule growth. The Journal of cell biology. [Research Support, Non-U.S. Gov't]. 2006 Nov 20;175(4):547-54.
128. Dollar GL, Weber U, Mlodzik M, Sokol SY. Regulation of Lethal giant larvae by Dishevelled. Nature. [Research Support, N.I.H., Extramural
Research Support, U.S. Gov't, P.H.S.]. 2005 Oct 27;437(7063):1376-80.
129. Park TJ, Mitchell BJ, Abitua PB, Kintner C, Wallingford JB. Dishevelled controls apical docking and planar polarization of basal bodies in ciliated epithelial cells. Nature genetics. [Research Support, N.I.H., Extramural]. 2008 Jul;40(7):871-9.
130. Park TJ, Haigo SL, Wallingford JB. Ciliogenesis defects in embryos lacking inturned or fuzzy function are associated with failure of planar cell polarity and Hedgehog signaling. Nature genetics. [Research Support, N.I.H., Extramural Research Support, Non-U.S. Gov't]. 2006 Mar;38(3):303-11.
131. Okada Y, Takeda S, Tanaka Y, Izpisua Belmonte JC, Hirokawa N. Mechanism of nodal flow: a conserved symmetry breaking event in left-right axis determination. Cell. [Research Support, Non-U.S. Gov't]. 2005 May 20;121(4):633-44.
132. Saburi S, Hester I, Fischer E, Pontoglio M, Eremina V, Gessler M, et al. Loss of Fat4 disrupts PCP signaling and oriented cell division and leads to cystic kidney disease. Nat Genet. 2008 Aug;40(8):1010-5.

133. Ross AJ, May-Simera H, Eichers ER, Kai M, Hill J, Jagger DJ, et al. Disruption of Bardet-Biedl syndrome ciliary proteins perturbs planar cell polarity in vertebrates. Nat Genet. 2005 Oct;37(10):1135-40.
134. Ferrante MI, Romio L, Castro S, Collins JE, Goulding DA, Stemple DL, et al. Convergent extension movements and ciliary function are mediated by ofd1, a zebrafish orthologue of the human oral-facial-digital type 1 syndrome gene. Human molecular genetics. [Research Support, Non-U.S. Gov't]. 2009 Jan 15;18(2):289-303.
135. Simons M, Gloy J, Ganner A, Bullerkotte A, Bashkurov M, Kronig C, et al. Inversin, the gene product mutated in nephronophthisis type II, functions as a molecular switch between Wnt signaling pathways. Nature genetics. [Research Support, Non-U.S. Gov't]. 2005 May;37(5):537-43.
136. Gong Y, Mo C, Fraser SE. Planar cell polarity signalling controls cell division orientation during zebrafish gastrulation. Nature. 2004 Aug 5;430(7000):689-93.
137. Karner CM, Chirumamilla R, Aoki S, Igarashi P, Wallingford JB, Carroll TJ. Wnt9b signaling regulates planar cell polarity and kidney tubule morphogenesis. Nature genetics. [Research Support, N.I.H., Extramural
Research Support, Non-U.S. Gov't]. 2009 Jul;41(7):793-9.
138. Du J, Wilson PD. Abnormal polarization of EGF receptors and autocrine stimulation of cyst epithelial growth in human ADPKD. Am J Physiol. [Research Support, U.S. Gov't, P.H.S.]. 1995 Aug;269(2 Pt 1):C487-95.
139. Avner ED, Sweeney, W.E. Apical epidermal growth factor receptor expression defines a distinct cystic tubular epithelial phenotype in autosomal recessive polycystic kidney disease. Pediatr Res. 1995;37:359A.
140. Orellana SA, Sweeney WE, Neff CD, Avner ED. Epidermal growth factor receptor expression is abnormal in murine polycystic kidney. Kidney Int. [Research Support, U.S. Gov't, P.H.S.]. 1995 Feb;47(2):490-9.
141. Wilson PD, Du J, Norman JT. Autocrine, endocrine and paracrine regulation of growth abnormalities in autosomal dominant polycystic kidney disease. Eur J Cell Biol. [Research Support, U.S. Gov't, P.H.S.]. 1993 Jun;61(1):131-8.
142. Sweeney WE, Jr., Avner ED. Functional activity of epidermal growth factor receptors in autosomal recessive polycystic kidney disease. Am J Physiol. [Research Support, Non-U.S. Gov't
Research Support, U.S. Gov't, P.H.S.]. 1998 Sep;275(3 Pt 2):F387-94.
143. Cadigan KM, Liu YI. Wnt signaling: complexity at the surface. J Cell Sci. [Research Support, N.I.H., Extramural
Research Support, Non-U.S. Gov't
Review]. 2006 Feb 1;119(Pt 3):395-402.
144. Lancaster MA, Gleeson JG. Cystic kidney disease: the role of Wnt signaling. Trends Mol Med. [Review]. 2010 Aug;16(8):349-60.
145. Cong F, Schweizer L, Varmus H. Wnt signals across the plasma membrane to activate the beta-catenin pathway by forming oligomers containing its receptors, Frizzled and LRP. Development. [Research Support, Non-U.S. Gov't]. 2004 Oct;131(20):5103-15.
146. Tolwinski NS, Wehrli M, Rives A, Erdeniz N, DiNardo S, Wieschaus E. Wg/Wnt signal can be transmitted through arrow/LRP5,6 and Axin independently of Zw3/Gsk3beta activity. Dev Cell. [Research Support, Non-U.S. Gov't
Research Support, U.S. Gov't, Non-P.H.S.
Research Support, U.S. Gov't, P.H.S.]. 2003 Mar;4(3):407-18.

147. Zeng X, Tamai K, Doble B, Li S, Huang H, Habas R, et al. A dual-kinase mechanism for Wnt co-receptor phosphorylation and activation. Nature. [Research Support, N.I.H., Extramural
Research Support, Non-U.S. Gov't]. 2005 Dec 8;438(7069):873-7.
148. Hart M, Concordet JP, Lassot I, Albert I, del los Santos R, Durand H, et al. The F-box protein beta-TrCP associates with phosphorylated beta-catenin and regulates its activity in the cell. Current biology : CB. [Research Support, Non-U.S. Gov't
Research Support, U.S. Gov't, P.H.S.]. 1999 Feb 25;9(4):207-10.
149. Behrens J, von Kries JP, Kuhl M, Bruhn L, Wedlich D, Grosschedl R, et al. Functional interaction of beta-catenin with the transcription factor LEF-1. Nature. [Research Support, Non-U.S. Gov't]. 1996 Aug 15;382(6592):638-42.
150. Molenaar M, van de Wetering M, Oosterwegel M, Peterson-Maduro J, Godsave S, Korinek V, et al. XTcf-3 transcription factor mediates beta-catenin-induced axis formation in Xenopus embryos. Cell. [Research Support, Non-U.S. Gov't]. 1996 Aug 9;86(3):391-9.
151. Jones KJ, Korb E, Kundel MA, Kochanek AR, Kabraji S, McEvoy M, et al. CPEB1 regulates beta-catenin mRNA translation and cell migration in astrocytes. Glia. [Comparative Study
Research Support, N.I.H., Extramural
Research Support, Non-U.S. Gov't]. 2008 Oct;56(13):1401-13.
152. Ebert MP, Fei G, Kahmann S, Muller O, Yu J, Sung JJ, et al. Increased beta-catenin mRNA levels and mutational alterations of the APC and beta-catenin gene are present in intestinal-type gastric cancer. Carcinogenesis. [Research Support, Non-U.S. Gov't]. 2002 Jan;23(1):87-91.
153. Saito T, Oda Y, Kawaguchi K, Tanaka K, Matsuda S, Tamiya S, et al. Possible association between higher beta-catenin mRNA expression and mutated beta-catenin in sporadic desmoid tumors: real-time semiquantitative assay by TaqMan polymerase chain reaction. Lab Invest. [Research Support, Non-U.S. Gov't]. 2002 Jan;82(1):97-103.
154. El-Rifai W, Frierson HF, Jr., Harper JC, Powell SM, Knuutila S. Expression profiling of gastric adenocarcinoma using cDNA array. International journal of cancer Journal international du cancer. [Research Support, Non-U.S. Gov't
Research Support, U.S. Gov't, P.H.S.]. 2001 Jun 15;92(6):832-8.
155. Gherzi R, Trabucchi M, Ponassi M, Ruggiero T, Corte G, Moroni C, et al. The RNA-binding protein KSRP promotes decay of beta-catenin mRNA and is inactivated by PI3K-AKT signaling. PLoS Biol. [Research Support, Non-U.S. Gov't]. 2006 Dec;5(1):e5.
156. Herzlinger D, Qiao J, Cohen D, Ramakrishna N, Brown AM. Induction of kidney epithelial morphogenesis by cells expressing Wnt-1. Dev Biol. [Research Support, Non-U.S. Gov't
Research Support, U.S. Gov't, P.H.S.]. 1994 Dec;166(2):815-8.
157. Stark K, Vainio S, Vassileva G, McMahon AP. Epithelial transformation of metanephric mesenchyme in the developing kidney regulated by Wnt-4. Nature. [Research Support, Non-U.S. Gov't
Research Support, U.S. Gov't, P.H.S.]. 1994 Dec 15;372(6507):679-83.
158. Pepicelli CV, Kispert A, Rowitch DH, McMahon AP. GDNF induces branching and increased cell proliferation in the ureter of the mouse. Dev Biol. [Research Support, Non-U.S. Gov't
Research Support, U.S. Gov't, P.H.S.]. 1997 Dec 1;192(1):193-8.

159. Kim E, Arnould T, Sellin LK, Benzing T, Fan MJ, Gruning W, et al. The polycystic kidney disease 1 gene product modulates Wnt signaling. J Biol Chem. [Research Support, U.S. Gov't, P.H.S.]. 1999 Feb 19;274(8):4947-53.
160. Saadi-Kheddouci S, Berrebi D, Romagnolo B, Cluzeaud F, Peuchmaur M, Kahn A, et al. Early development of polycystic kidney disease in transgenic mice expressing an activated mutant of the beta-catenin gene. Oncogene. [Research Support, Non-U.S. Gov't]. 2001 Sep 20;20(42):5972-81.
161. Qian CN, Knol J, Igarashi P, Lin F, Zylstra U, Teh BT, et al. Cystic renal neoplasia following conditional inactivation of apc in mouse renal tubular epithelium. J Biol Chem. [Research Support, Non-U.S. Gov't
Research Support, U.S. Gov't, P.H.S.]. 2005 Feb 4;280(5):3938-45.
162. Pinson KI, Brennan J, Monkley S, Avery BJ, Skarnes WC. An LDL-receptor-related protein mediates Wnt signalling in mice. Nature. [Research Support, Non-U.S. Gov't]. 2000 Sep 28;407(6803):535-8.
163. Kim I, Ding T, Fu Y, Li C, Cui L, Li A, et al. Conditional mutation of Pkd2 causes cystogenesis and upregulates beta-catenin. Journal of the American Society of Nephrology : JASN. [Research Support, N.I.H., Extramural
Research Support, Non-U.S. Gov't]. 2009 Dec;20(12):2556-69.
164. Thivierge C, Kurbegovic A, Couillard M, Guillaume R, Cote O, Trudel M. Overexpression of PKD1 causes polycystic kidney disease. Molecular and cellular biology. [Research Support, Non-U.S. Gov't]. 2006 Feb;26(4):1538-48.
165. Lancaster MA, Louie CM, Silhavy JL, Sintasath L, Decambre M, Nigam SK, et al. Impaired Wnt-beta-catenin signaling disrupts adult renal homeostasis and leads to cystic kidney ciliopathy. Nature Medicine. [Research Support, N.I.H., Extramural Research Support, Non-U.S. Gov't]. 2009 Sep;15(9):1046-54.
166. Pei Y. Of mice and men: therapeutic mTOR inhibition in polycystic kidney disease. Journal of the American Society of Nephrology : JASN. [Comment Editorial
Research Support, Non-U.S. Gov't]. 2010 Mar;21(3):390-1.
167. Lieberthal W, Levine JS. Mammalian target of rapamycin and the kidney. I. The signaling pathway. American journal of physiology Renal physiology. [Review]. 2012 Jul 1;303(1):F1-10.
168. Kleymenova E, Ibraghimov-Beskrovnaya O, Kugoh H, Everitt J, Xu H, Kiguchi K, et al. Tuberin-dependent membrane localization of polycystin-1: a functional link between polycystic kidney disease and the TSC2 tumor suppressor gene. Mol Cell. [Research Support, U.S. Gov't, Non-P.H.S.
Research Support, U.S. Gov't, P.H.S.]. 2001 Apr;7(4):823-32.
169. Zhou J, Brugarolas J, Parada LF. Loss of Tsc1, but not Pten, in renal tubular cells causes polycystic kidney disease by activating mTORC1. Human molecular genetics. [Research Support, Non-U.S. Gov't]. 2009 Nov 15;18(22):4428-41.
170. Curatolo P, Bombardieri R, Jozwiak S. Tuberous sclerosis. Lancet. [Review]. 2008 Aug 23;372(9639):657-68.
171. Sampson JR, Maheshwar MM, Aspinwall R, Thompson P, Cheadle JP, Ravine D, et al. Renal cystic disease in tuberous sclerosis: role of the polycystic kidney disease 1 gene. American journal of human genetics. [Research Support, Non-U.S. Gov't]. 1997 Oct;61(4):843-51.
172. Brook-Carter PT, Peral B, Ward CJ, Thompson P, Hughes J, Maheshwar MM, et al. Deletion of the TSC2 and PKD1 genes associated with severe infantile polycystic

kidney disease--a contiguous gene syndrome. Nature genetics. [Research Support, Non-U.S. Gov't]. 1994 Dec;8(4):328-32.
173. Shillingford JM, Murcia NS, Larson CH, Low SH, Hedgepeth R, Brown N, et al. The mTOR pathway is regulated by polycystin-1, and its inhibition reverses renal cystogenesis in polycystic kidney disease. Proceedings of the National Academy of Sciences of the United States of America. [Research Support, N.I.H., Extramural Research Support, Non-U.S. Gov't]. 2006 Apr 4;103(14):5466-71.
174. Dere R, Wilson PD, Sandford RN, Walker CL. Carboxy terminal tail of polycystin-1 regulates localization of TSC2 to repress mTOR. PLoS One. [Research Support, N.I.H., Extramural
Research Support, Non-U.S. Gov't]. 2010;5(2):e9239.
175. Distefano G, Boca M, Rowe I, Wodarczyk C, Ma L, Piontek KB, et al. Polycystin-1 regulates extracellular signal-regulated kinase-dependent phosphorylation of tuberin to control cell size through mTOR and its downstream effectors S6K and 4EBP1. Molecular and cellular biology. [Research Support, N.I.H., Extramural
Research Support, Non-U.S. Gov't]. 2009 May;29(9):2359-71.
176. Ma L, Chen Z, Erdjument-Bromage H, Tempst P, Pandolfi PP. Phosphorylation and functional inactivation of TSC2 by Erk implications for tuberous sclerosis and cancer pathogenesis. Cell. [In Vitro
Research Support, U.S. Gov't, P.H.S.]. 2005 Apr 22;121(2):179-93.
177. Canaud G, Knebelmann B, Harris PC, Vrtovsnik F, Correas JM, Pallet N, et al. Therapeutic mTOR inhibition in autosomal dominant polycystic kidney disease: What is the appropriate serum level? Am J Transplant. [Case Reports]. 2010 Jul;10(7):1701-6.
178. Shillingford JM, Piontek KB, Germino GG, Weimbs T. Rapamycin ameliorates PKD resulting from conditional inactivation of Pkd1. Journal of the American Society of Nephrology : JASN. [Research Support, N.I.H., Extramural
Research Support, Non-U.S. Gov't]. 2010 Mar;21(3):489-97.
179. Tao Y, Kim J, Schrier RW, Edelstein CL. Rapamycin markedly slows disease progression in a rat model of polycystic kidney disease. Journal of the American Society of Nephrology : JASN. [Research Support, N.I.H., Extramural
Research Support, U.S. Gov't, P.H.S.]. 2005 Jan;16(1):46-51.
180. Wahl PR, Le Hir M, Vogetseder A, Arcaro A, Starke A, Waeckerle-Men Y, et al. Mitotic activation of Akt signalling pathway in Han:SPRD rats with polycystic kidney disease. Nephrology (Carlton). [Research Support, Non-U.S. Gov't]. 2007 Aug;12(4):357-63.
181. Wahl PR, Serra AL, Le Hir M, Molle KD, Hall MN, Wuthrich RP. Inhibition of mTOR with sirolimus slows disease progression in Han:SPRD rats with autosomal dominant polycystic kidney disease (ADPKD). Nephrology, dialysis, transplantation : official publication of the European Dialysis and Transplant Association - European Renal Association. [Comparative Study
Research Support, Non-U.S. Gov't]. 2006 Mar;21(3):598-604.
182. Natoli TA, Husson H, Rogers KA, Smith LA, Wang B, Budman Y, et al. Loss of GM3 synthase gene, but not sphingosine kinase 1, is protective against murine nephronophthisis-related polycystic kidney disease. Human molecular genetics. [Research Support, Non-U.S. Gov't]. 2012 Aug 1;21(15):3397-407.
183. Zafar I, Ravichandran K, Belibi FA, Doctor RB, Edelstein CL. Sirolimus attenuates disease progression in an orthologous mouse model of human autosomal dominant polycystic kidney disease. Kidney Int. [Research Support, N.I.H., Extramural Research Support, Non-U.S. Gov't]. 2010 Oct;78(8):754-61.

184. Reichardt W, Romaker D, Becker A, Buechert M, Walz G, von Elverfeldt D. Monitoring kidney and renal cyst volumes applying MR approaches on a rapamycin treated mouse model of ADPKD. Magma. 2009 Jun;22(3):143-9.
185. Gattone VH, 2nd, Sinders RM, Hornberger TA, Robling AG. Late progression of renal pathology and cyst enlargement is reduced by rapamycin in a mouse model of nephronophthisis. Kidney Int. 2009 Jul;76(2):178-82.
186. Renken C, Fischer DC, Kundt G, Gretz N, Haffner D. Inhibition of mTOR with sirolimus does not attenuate progression of liver and kidney disease in PCK rats. Nephrology, dialysis, transplantation : official publication of the European Dialysis and Transplant Association - European Renal Association. [Research Support, Non-U.S. Gov't]. 2011 Jan;26(1):92-100.
187. Qian Q, Du H, King BF, Kumar S, Dean PG, Cosio FG, et al. Sirolimus reduces polycystic liver volume in ADPKD patients. Journal of the American Society of Nephrology : JASN. [Comparative Study
Randomized Controlled Trial
Research Support, N.I.H., Extramural
Research Support, Non-U.S. Gov't]. 2008 Mar;19(3):631-8.
188. Perico N, Antiga L, Caroli A, Ruggenenti P, Fasolini G, Cafaro M, et al. Sirolimus therapy to halt the progression of ADPKD. Journal of the American Society of Nephrology : JASN. [Randomized Controlled Trial]. 2010 Jun;21(6):1031-40.
189. Walz G, Budde K, Mannaa M, Nurnberger J, Wanner C, Sommerer C, et al. Everolimus in patients with autosomal dominant polycystic kidney disease. The New England journal of medicine. [Multicenter Study
Randomized Controlled Trial
Research Support, Non-U.S. Gov't]. 2010 Aug 26;363(9):830-40.
190. Serra AL, Poster D, Kistler AD, Krauer F, Raina S, Young J, et al. Sirolimus and kidney growth in autosomal dominant polycystic kidney disease. The New England journal of medicine. [Randomized Controlled Trial
Research Support, Non-U.S. Gov't]. 2010 Aug 26;363(9):820-9.
191. Hartman TR, Liu D, Zilfou JT, Robb V, Morrison T, Watnick T, et al. The tuberous sclerosis proteins regulate formation of the primary cilium via a rapamycin-insensitive and polycystin 1-independent pathway. Human molecular genetics. [Research Support, N.I.H., Extramural
Research Support, Non-U.S. Gov't]. 2009 Jan 1;18(1):151-63.
192. Boehlke C, Kotsis F, Patel V, Braeg S, Voelker H, Bredt S, et al. Primary cilia regulate mTORC1 activity and cell size through Lkb1. Nature cell biology. [Research Support, N.I.H., Extramural
Research Support, Non-U.S. Gov't]. 2010 Nov;12(11):1115-22.
193. Jacoby M, Cox JJ, Gayral S, Hampshire DJ, Ayub M, Blockmans M, et al. INPP5E mutations cause primary cilium signaling defects, ciliary instability and ciliopathies in human and mouse. Nature genetics. [Research Support, N.I.H., Extramural
Research Support, Non-U.S. Gov't]. 2009 Sep;41(9):1027-31.
194. Hampshire DJ, Ayub M, Springell K, Roberts E, Jafri H, Rashid Y, et al. MORM syndrome (mental retardation, truncal obesity, retinal dystrophy and micropenis), a new autosomal recessive disorder, links to 9q34. Eur J Hum Genet. [Research Support, Non-U.S. Gov't]. 2006 May;14(5):543-8.

195. Goetz SC, Anderson KV. The primary cilium: a signalling centre during vertebrate development. Nature reviews Genetics. [Research Support, N.I.H., Extramural
Research Support, Non-U.S. Gov't
Review]. 2010 May;11(5):331-44.
196. Lum L, Beachy PA. The Hedgehog response network: sensors, switches, and routers. Science. [Research Support, Non-U.S. Gov't
Research Support, U.S. Gov't, P.H.S.
Review]. 2004 Jun 18;304(5678):1755-9.
197. Zhang F, Jetten AM. Genomic structure of the gene encoding the human GLI-related, Kruppel-like zinc finger protein GLIS2. Gene. 2001 Dec 12;280(1-2):49-57.
198. Haycraft CJ, Banizs B, Aydin-Son Y, Zhang Q, Michaud EJ, Yoder BK. Gli2 and Gli3 localize to cilia and require the intraflagellar transport protein polaris for processing and function. PLoS Genet. [Research Support, N.I.H., Extramural
Research Support, Non-U.S. Gov't
Research Support, U.S. Gov't, Non-P.H.S.]. 2005 Oct;1(4):e53.
199. Attanasio M, Uhlenhaut NH, Sousa VH, O'Toole JF, Otto E, Anlag K, et al. Loss of GLIS2 causes nephronophthisis in humans and mice by increased apoptosis and fibrosis. Nature genetics. [Research Support, N.I.H., Extramural
Research Support, Non-U.S. Gov't]. 2007 Aug;39(8):1018-24.
200. Zhang F, Nakanishi G, Kurebayashi S, Yoshino K, Perantoni A, Kim YS, et al. Characterization of Glis2, a novel gene encoding a Gli-related, Kruppel-like transcription factor with transactivation and repressor functions. Roles in kidney development and neurogenesis. J Biol Chem. 2002 Mar 22;277(12):10139-49.
201. Li B, Rauhauser AA, Dai J, Sakthivel R, Igarashi P, Jetten AM, et al. Increased hedgehog signaling in postnatal kidney results in aberrant activation of nephron developmental programs. Human molecular genetics. [Research Support, N.I.H., Extramural
Research Support, Non-U.S. Gov't]. 2011 Nov 1;20(21):4155-66.
202. Dafinger C, Liebau MC, Elsayed SM, Hellenbroich Y, Boltshauser E, Korenke GC, et al. Mutations in KIF7 link Joubert syndrome with Sonic Hedgehog signaling and microtubule dynamics. J Clin Invest. [Research Support, Non-U.S. Gov't]. 2011 Jul;121(7):2662-7.
203. Brancati F, Dallapiccola B, Valente EM. Joubert Syndrome and related disorders. Orphanet J Rare Dis. [Research Support, Non-U.S. Gov't
Review]. 2010;5:20.
204. Duldulao NA, Lee S, Sun Z. Cilia localization is essential for in vivo functions of the Joubert syndrome protein Arl13b/Scorpion. Development. [Research Support, N.I.H., Extramural
Research Support, Non-U.S. Gov't]. 2009 Dec;136(23):4033-42.
205. Macca M, Franco B. The molecular basis of oral-facial-digital syndrome, type 1. Am J Med Genet C Semin Med Genet. [Research Support, Non-U.S. Gov't
Review]. 2009 Nov 15;151C(4):318-25.
206. Justice MJ, Noveroske JK, Weber JS, Zheng B, Bradley A. Mouse ENU mutagenesis. Human molecular genetics. [Research Support, Non-U.S. Gov't
Research Support, U.S. Gov't, P.H.S.
Review]. 1999;8(10):1955-63.
207. Soewarto D, Klaften M, Rubio-Aliaga I. Features and strategies of ENU mouse mutagenesis. Curr Pharm Biotechnol. [Review]. 2009 Feb;10(2):198-213.

208. Jun JE, Wilson LE, Vinuesa CG, Lesage S, Blery M, Miosge LA, et al. Identifying the MAGUK protein Carma-1 as a central regulator of humoral immune responses and atopy by genome-wide mouse mutagenesis. Immunity. 2003 Jun;18(6):751-62.
209. Eremina V, Wong MA, Cui S, Schwartz L, Quaggin SE. Glomerular-specific gene excision in vivo. J Am Soc Nephrol. 2002 Mar;13(3):788-93.
210. Schmittgen TD, Livak KJ. Analyzing real-time PCR data by the comparative C(T) method. Nat Protoc. 2008;3(6):1101-8.
211. Bernstein J. Glomerulocystic kidney disease--nosological considerations. Pediatric nephrology. [Review]. 1993 Aug;7(4):464-70.
212. Bingham C, Bulman MP, Ellard S, Allen LI, Lipkin GW, Hoff WG, et al. Mutations in the hepatocyte nuclear factor-1beta gene are associated with familial hypoplastic glomerulocystic kidney disease. Am J Hum Genet. 2001 Jan;68(1):219-24.
213. Sun Z, Hopkins N. vhnf1, the MODY5 and familial GCKD-associated gene, regulates regional specification of the zebrafish gut, pronephros, and hindbrain. Genes & development. 2001 Dec 1;15(23):3217-29.
214. Silver LM. Mouse genetics: Concepts and applications. New York: Oxford University Press; 1994.
215. Harismendy O, Ng PC, Strausberg RL, Wang X, Stockwell TB, Beeson KY, et al. Evaluation of next generation sequencing platforms for population targeted sequencing studies. Genome Biol. [Evaluation Studies
Research Support, N.I.H., Extramural]. 2009;10(3):R32.
216. Ogborn MR, Sareen S, Tomobe K, Takahashi H, Crocker JF. Renal tubule Na,K-ATPase polarity in different animal models of polycystic kidney disease. J Histochem Cytochem. [Research Support, Non-U.S. Gov't]. 1995 Aug;43(8):785-90.
217. Yu J, Carroll TJ, Rajagopal J, Kobayashi A, Ren Q, McMahon AP. A Wnt7b-dependent pathway regulates the orientation of epithelial cell division and establishes the cortico-medullary axis of the mammalian kidney. Development. [Research Support, N.I.H., Extramural
Research Support, Non-U.S. Gov't]. 2009 Jan;136(1):161-71.
218. Veikkolainen V, Naillat F, Railo A, Chi L, Manninen A, Hohenstein P, et al. ErbB4 modulates tubular cell polarity and lumen diameter during kidney development. Journal of the American Society of Nephrology : JASN. [Research Support, Non-U.S. Gov't]. 2012 Jan;23(1):112-22.
219. Goto H, Tomono Y, Ajiro K, Kosako H, Fujita M, Sakurai M, et al. Identification of a novel phosphorylation site on histone H3 coupled with mitotic chromosome condensation. J Biol Chem. [Research Support, Non-U.S. Gov't]. 1999 Sep 3;274(36):25543-9.
220. Phillips HM, Rhee HJ, Murdoch JN, Hildreth V, Peat JD, Anderson RH, et al. Disruption of planar cell polarity signaling results in congenital heart defects and cardiomyopathy attributable to early cardiomyocyte disorganization. Circ Res. [Research Support, Non-U.S. Gov't]. 2007 Jul 20;101(2):137-45.
221. Saburi S, Hester I, Fischer E, Pontoglio M, Eremina V, Gessler M, et al. Loss of Fat4 disrupts PCP signaling and oriented cell division and leads to cystic kidney disease. Nature genetics. [Research Support, Non-U.S. Gov't]. 2008 Aug;40(8):1010-5.
222. Stanier P, Henson JN, Eddleston J, Moore GE, Copp AJ. Genetic basis of neural tube defects: the mouse gene loop-tail maps to a region of chromosome 1 syntenic with human 1q21-q23. Genomics. [Research Support, Non-U.S. Gov't]. 1995 Apr 10;26(3):473-8.

223. Underhill DA, Vogan KJ, Kibar Z, Morrison J, Rommens J, Gros P. Transcription mapping and expression analysis of candidate genes in the vicinity of the mouse Loop-tail mutation. Mammalian genome : official journal of the International Mammalian Genome Society. [Research Support, Non-U.S. Gov't]. 2000 Aug;11(8):633-8.
224. Peterson AJ, Kyba M, Bornemann D, Morgan K, Brock HW, Simon J. A domain shared by the Polycomb group proteins Scm and ph mediates heterotypic and homotypic interactions. Molecular and cellular biology. [Research Support, Non-U.S. Gov't
Research Support, U.S. Gov't, Non-P.H.S.
Research Support, U.S. Gov't, P.H.S.]. 1997 Nov;17(11):6683-92.
225. Li CF, MacDonald JR, Wei RY, Ray J, Lau K, Kandel C, et al. Human sterile alpha motif domain 9, a novel gene identified as down-regulated in aggressive fibromatosis, is absent in the mouse. BMC Genomics. [Research Support, Non-U.S. Gov't]. 2007;8:92.
226. Jiang Q, Quaynor B, Sun A, Li Q, Matsui H, Honda H, et al. The Samd9L gene: transcriptional regulation and tissue-specific expression in mouse development. The Journal of investigative dermatology. [Research Support, N.I.H., Extramural
Research Support, Non-U.S. Gov't]. 2011 Jul;131(7):1428-34.
227. Schultz J, Ponting CP, Hofmann K, Bork P. SAM as a protein interaction domain involved in developmental regulation. Protein Sci. 1997 Jan;6(1):249-53.
228. Kim CA, Bowie JU. SAM domains: uniform structure, diversity of function. Trends Biochem Sci. [Research Support, Non-U.S. Gov't
Research Support, U.S. Gov't, P.H.S.]. 2003 Dec;28(12):625-8.
229. Thanos CD, Goodwill KE, Bowie JU. Oligomeric structure of the human EphB2 receptor SAM domain. Science. [Research Support, U.S. Gov't, Non-P.H.S.
Research Support, U.S. Gov't, P.H.S.]. 1999 Feb 5;283(5403):833-6.
230. Chefetz I, Ben Amitai D, Browning S, Skorecki K, Adir N, Thomas MG, et al. Normophosphatemic familial tumoral calcinosis is caused by deleterious mutations in SAMD9, encoding a TNF-alpha responsive protein. The Journal of investigative dermatology. [Research Support, N.I.H., Extramural
Research Support, Non-U.S. Gov't]. 2008 Jun;128(6):1423-9.
231. Hoff S, Halbritter J, Epting D, Frank V, Nguyen TM, van Reeuwijk J, et al. ANKS6 is a central component of a nephronophthisis module linking NEK8 to INVS and NPHP3. Nature genetics. 2013 Aug;45(8):951-6.
232. Asou H, Matsui H, Ozaki Y, Nagamachi A, Nakamura M, Aki D, et al. Identification of a common microdeletion cluster in 7q21.3 subband among patients with myeloid leukemia and myelodysplastic syndrome. Biochem Biophys Res Commun. [Research Support, Non-U.S. Gov't]. 2009 May 29;383(2):245-51.
233. Topaz O, Indelman M, Chefetz I, Geiger D, Metzker A, Altschuler Y, et al. A deleterious mutation in SAMD9 causes normophosphatemic familial tumoral calcinosis. American journal of human genetics. [Research Support, N.I.H., Extramural
Research Support, Non-U.S. Gov't]. 2006 Oct;79(4):759-64.
234. Hershkovitz D, Gross Y, Nahum S, Yehezkel S, Sarig O, Uitto J, et al. Functional characterization of SAMD9, a protein deficient in normophosphatemic familial tumoral calcinosis. The Journal of investigative dermatology. [Research Support, N.I.H., Extramural]. 2011 Mar;131(3):662-9.
235. Schmitz F, Heit A, Guggemoos S, Krug A, Mages J, Schiemann M, et al. Interferon-regulatory-factor 1 controls Toll-like receptor 9-mediated IFN-beta production

in myeloid dendritic cells. Eur J Immunol. [Research Support, Non-U.S. Gov't]. 2007 Feb;37(2):315-27.
236. Gao J, Senthil M, Ren B, Yan J, Xing Q, Yu J, et al. IRF-1 transcriptionally upregulates PUMA, which mediates the mitochondrial apoptotic pathway in IRF-1-induced apoptosis in cancer cells. Cell Death Differ. [Research Support, N.I.H., Extramural
Research Support, Non-U.S. Gov't]. 2010 Apr;17(4):699-709.
237. Wang Y, Liu DP, Chen PP, Koeffler HP, Tong XJ, Xie D. Involvement of IFN regulatory factor (IRF)-1 and IRF-2 in the formation and progression of human esophageal cancers. Cancer research. [Research Support, Non-U.S. Gov't]. 2007 Mar 15;67(6):2535-43.
238. Zekri AR, Moharram RA, Mohamed WS, Bahnassy AA, Alam El-Din HM, Abo-Shadi MM, et al. Disease progression from chronic hepatitis C to cirrhosis and hepatocellular carcinoma is associated with repression of interferon regulatory factor-1. Eur J Gastroenterol Hepatol. 2010 Apr;22(4):450-6.
239. Liebermann DA, Hoffman B. Interferon regulatory factor-1 myelodysplasia and leukemia. Leuk Res. [Editorial
Review]. 2006 Sep;30(9):1069-71.
240. Li Q, Guo H, Matsui H, Honda H, Inaba T, Sundberg JP, et al. Mouse Samd9l is not a functional paralogue of the human SAMD9, the gene mutated in normophosphataemic familial tumoral calcinosis. Exp Dermatol. [Letter
Research Support, N.I.H., Extramural]. 2012 Jul;21(7):554-6.
241. Gallant-Behm CL, Ramsey MR, Bensard CL, Nojek I, Tran J, Liu M, et al. {Delta}Np63alpha represses anti-proliferative genes via H2A.Z deposition. Genes & development. 2012 Sep 26.
242. Yang A, Kaghad M, Wang Y, Gillett E, Fleming MD, Dotsch V, et al. p63, a p53 homolog at 3q27-29, encodes multiple products with transactivating, death-inducing, and dominant-negative activities. Mol Cell. [Research Support, Non-U.S. Gov't
Research Support, U.S. Gov't, Non-P.H.S.
Research Support, U.S. Gov't, P.H.S.]. 1998 Sep;2(3):305-16.
243. Senoo M, Pinto F, Crum CP, McKeon F. p63 Is essential for the proliferative potential of stem cells in stratified epithelia. Cell. [Research Support, N.I.H., Extramural
Research Support, Non-U.S. Gov't
Research Support, U.S. Gov't, Non-P.H.S.]. 2007 May 4;129(3):523-36.
244. Yang A, Schweitzer R, Sun D, Kaghad M, Walker N, Bronson RT, et al. p63 is essential for regenerative proliferation in limb, craniofacial and epithelial development. Nature. [Research Support, U.S. Gov't, P.H.S.]. 1999 Apr 22;398(6729):714-8.
245. Parsa R, Yang A, McKeon F, Green H. Association of p63 with proliferative potential in normal and neoplastic human keratinocytes. The Journal of investigative dermatology. [Research Support, U.S. Gov't, P.H.S.]. 1999 Dec;113(6):1099-105.
246. Rocco JW, Leong CO, Kuperwasser N, DeYoung MP, Ellisen LW. p63 mediates survival in squamous cell carcinoma by suppression of p73-dependent apoptosis. Cancer Cell. [Research Support, N.I.H., Extramural
Research Support, Non-U.S. Gov't]. 2006 Jan;9(1):45-56.
247. Westfall MD, Mays DJ, Sniezek JC, Pietenpol JA. The Delta Np63 alpha phosphoprotein binds the p21 and 14-3-3 sigma promoters in vivo and has transcriptional repressor activity that is reduced by Hay-Wells syndrome-derived mutations. Molecular and cellular biology. [Research Support, Non-U.S. Gov't
Research Support, U.S. Gov't, Non-P.H.S.

Research Support, U.S. Gov't, P.H.S.]. 2003 Apr;23(7):2264-76.
248. Marques M, Laflamme L, Gervais AL, Gaudreau L. Reconciling the positive and negative roles of histone H2A.Z in gene transcription. Epigenetics. [Review]. 2010 May 16;5(4):267-72.
249. Gevry N, Chan HM, Laflamme L, Livingston DM, Gaudreau L. p21 transcription is regulated by differential localization of histone H2A.Z. Genes & development. [Research Support, N.I.H., Extramural
Research Support, Non-U.S. Gov't]. 2007 Aug 1;21(15):1869-81.
250. Ballinger CA, Connell P, Wu Y, Hu Z, Thompson LJ, Yin LY, et al. Identification of CHIP, a novel tetratricopeptide repeat-containing protein that interacts with heat shock proteins and negatively regulates chaperone functions. Molecular and cellular biology. [Research Support, Non-U.S. Gov't
Research Support, U.S. Gov't, P.H.S.]. 1999 Jun;19(6):4535-45.
251. Peng HM, Morishima Y, Jenkins GJ, Dunbar AY, Lau M, Patterson C, et al. Ubiquitylation of neuronal nitric-oxide synthase by CHIP, a chaperone-dependent E3 ligase. J Biol Chem. [Research Support, U.S. Gov't, P.H.S.]. 2004 Dec 17;279(51):52970-7.
252. McClellan AJ, Tam S, Kaganovich D, Frydman J. Protein quality control: chaperones culling corrupt conformations. Nature cell biology. 2005 Aug;7(8):736-41.
253. Seeger-Nukpezah T, Proia DA, Egleston BL, Nikonova AS, Kent T, Cai KQ, et al. Inhibiting the HSP90 chaperone slows cyst growth in a mouse model of autosomal dominant polycystic kidney disease. Proceedings of the National Academy of Sciences of the United States of America. 2013 Jul 30;110(31):12786-91.
254. Sha Y, Pandit L, Zeng S, Eissa NT. A critical role for CHIP in the aggresome pathway. Molecular and cellular biology. [Research Support, N.I.H., Extramural Research Support, Non-U.S. Gov't]. 2009 Jan;29(1):116-28.
255. Naito AT, Okada S, Minamino T, Iwanaga K, Liu ML, Sumida T, et al. Promotion of CHIP-mediated p53 degradation protects the heart from ischemic injury. Circ Res. [Research Support, Non-U.S. Gov't]. 2010 Jun 11;106(11):1692-702.
256. Tripathi V, Ali A, Bhat R, Pati U. CHIP chaperones wild type p53 tumor suppressor protein. J Biol Chem. [Research Support, Non-U.S. Gov't]. 2007 Sep 28;282(39):28441-54.
257. Esser C, Scheffner M, Hohfeld J. The chaperone-associated ubiquitin ligase CHIP is able to target p53 for proteasomal degradation. J Biol Chem. 2005 Jul 22;280(29):27443-8.
258. Hirayama S, Yamazaki Y, Kitamura A, Oda Y, Morito D, Okawa K, et al. MKKS is a centrosome-shuttling protein degraded by disease-causing mutations via CHIP-mediated ubiquitination. Mol Biol Cell. [Research Support, Non-U.S. Gov't]. 2008 Mar;19(3):899-911.
259. Shang Y, Zhao X, Xu X, Xin H, Li X, Zhai Y, et al. CHIP functions an E3 ubiquitin ligase of Runx1. Biochem Biophys Res Commun. [Research Support, Non-U.S. Gov't]. 2009 Aug 14;386(1):242-6.
260. McDonough H, Charles PC, Hilliard EG, Qian SB, Min JN, Portbury A, et al. Stress-dependent Daxx-CHIP interaction suppresses the p53 apoptotic program. J Biol Chem. [Research Support, N.I.H., Extramural
Research Support, Non-U.S. Gov't]. 2009 Jul 31;284(31):20649-59.
261. Ogawa E, Maruyama M, Kagoshima H, Inuzuka M, Lu J, Satake M, et al. PEBP2/PEA2 represents a family of transcription factors homologous to the products

of the Drosophila runt gene and the human AML1 gene. Proceedings of the National Academy of Sciences of the United States of America. [Comparative Study Research Support, Non-U.S. Gov't]. 1993 Jul 15;90(14):6859-63.
262. Speck NA, Gilliland DG. Core-binding factors in haematopoiesis and leukaemia. Nat Rev Cancer. [Review]. 2002 Jul;2(7):502-13.
263. Niini T, Kanerva J, Vettenranta K, Saarinen-Pihkala UM, Knuutila S. AML1 gene amplification: a novel finding in childhood acute lymphoblastic leukemia. Haematologica. 2000 Apr;85(4):362-6.
264. Foy RL, Chitalia VC, Panchenko MV, Zeng L, Lopez D, Lee JW, et al. Polycystin-1 regulates the stability and ubiquitination of transcription factor Jade-1. Human molecular genetics. 2012 Oct 5.
265. Bhunia AK, Piontek K, Boletta A, Liu L, Qian F, Xu PN, et al. PKD1 induces p21(waf1) and regulation of the cell cycle via direct activation of the JAK-STAT signaling pathway in a process requiring PKD2. Cell. [Research Support, Non-U.S. Gov't
Research Support, U.S. Gov't, P.H.S.]. 2002 Apr 19;109(2):157-68.
266. Nishio S, Hatano M, Nagata M, Horie S, Koike T, Tokuhisa T, et al. Pkd1 regulates immortalized proliferation of renal tubular epithelial cells through p53 induction and JNK activation. J Clin Invest. [Research Support, Non-U.S. Gov't]. 2005 Apr;115(4):910-8.
267. Kim H, Bae Y, Jeong W, Ahn C, Kang S. Depletion of PKD1 by an antisense oligodeoxynucleotide induces premature G1/S-phase transition. Eur J Hum Genet. [Research Support, Non-U.S. Gov't]. 2004 Jun;12(6):433-40.
268. Lanoix J, D'Agati V, Szabolcs M, Trudel M. Dysregulation of cellular proliferation and apoptosis mediates human autosomal dominant polycystic kidney disease (ADPKD). Oncogene. [Research Support, Non-U.S. Gov't
Research Support, U.S. Gov't, P.H.S.]. 1996 Sep 19;13(6):1153-60.
269. Gartel AL, Tyner AL. Transcriptional regulation of the p21((WAF1/CIP1)) gene. Exp Cell Res. [Research Support, Non-U.S. Gov't
Research Support, U.S. Gov't, P.H.S.
Review]. 1999 Feb 1;246(2):280-9.
270. Nadasdy T, Laszik Z, Lajoie G, Blick KE, Wheeler DE, Silva FG. Proliferative activity of cyst epithelium in human renal cystic diseases. Journal of the American Society of Nephrology : JASN. [Comparative Study]. 1995 Jan;5(7):1462-8.
271. Woo D. Apoptosis and loss of renal tissue in polycystic kidney diseases. The New England journal of medicine. [Research Support, U.S. Gov't, P.H.S.]. 1995 Jul 6;333(1):18-25.
272. Li X, Luo Y, Starremans PG, McNamara CA, Pei Y, Zhou J. Polycystin-1 and polycystin-2 regulate the cell cycle through the helix-loop-helix inhibitor Id2. Nature cell biology. [Research Support, N.I.H., Extramural
Research Support, Non-U.S. Gov't]. 2005 Dec;7(12):1202-12.
273. Grantham JJ, Ye M, Gattone VH, 2nd, Sullivan LP. In vitro fluid secretion by epithelium from polycystic kidneys. J Clin Invest. [In Vitro
Research Support, Non-U.S. Gov't
Research Support, U.S. Gov't, P.H.S.]. 1995 Jan;95(1):195-202.
274. Babich V, Zeng WZ, Yeh BI, Ibraghimov-Beskrovnaya O, Cai Y, Somlo S, et al. The N-terminal extracellular domain is required for polycystin-1-dependent channel activity. J Biol Chem. [Research Support, Non-U.S. Gov't
Research Support, U.S. Gov't, P.H.S.]. 2004 Jun 11;279(24):25582-9.

275. Koulen P, Cai Y, Geng L, Maeda Y, Nishimura S, Witzgall R, et al. Polycystin-2 is an intracellular calcium release channel. Nature cell biology. [In Vitro
Research Support, Non-U.S. Gov't
Research Support, U.S. Gov't, P.H.S.]. 2002 Mar;4(3):191-7.
276. Calvet JP, Grantham JJ. The genetics and physiology of polycystic kidney disease. Semin Nephrol. [Research Support, Non-U.S. Gov't
Research Support, U.S. Gov't, P.H.S.
Review]. 2001 Mar;21(2):107-23.
277. Yamaguchi T, Wallace DP, Magenheimer BS, Hempson SJ, Grantham JJ, Calvet JP. Calcium restriction allows cAMP activation of the B-Raf/ERK pathway, switching cells to a cAMP-dependent growth-stimulated phenotype. J Biol Chem. [Research Support, U.S. Gov't, P.H.S.]. 2004 Sep 24;279(39):40419-30.